

4-

Structure determination of solids

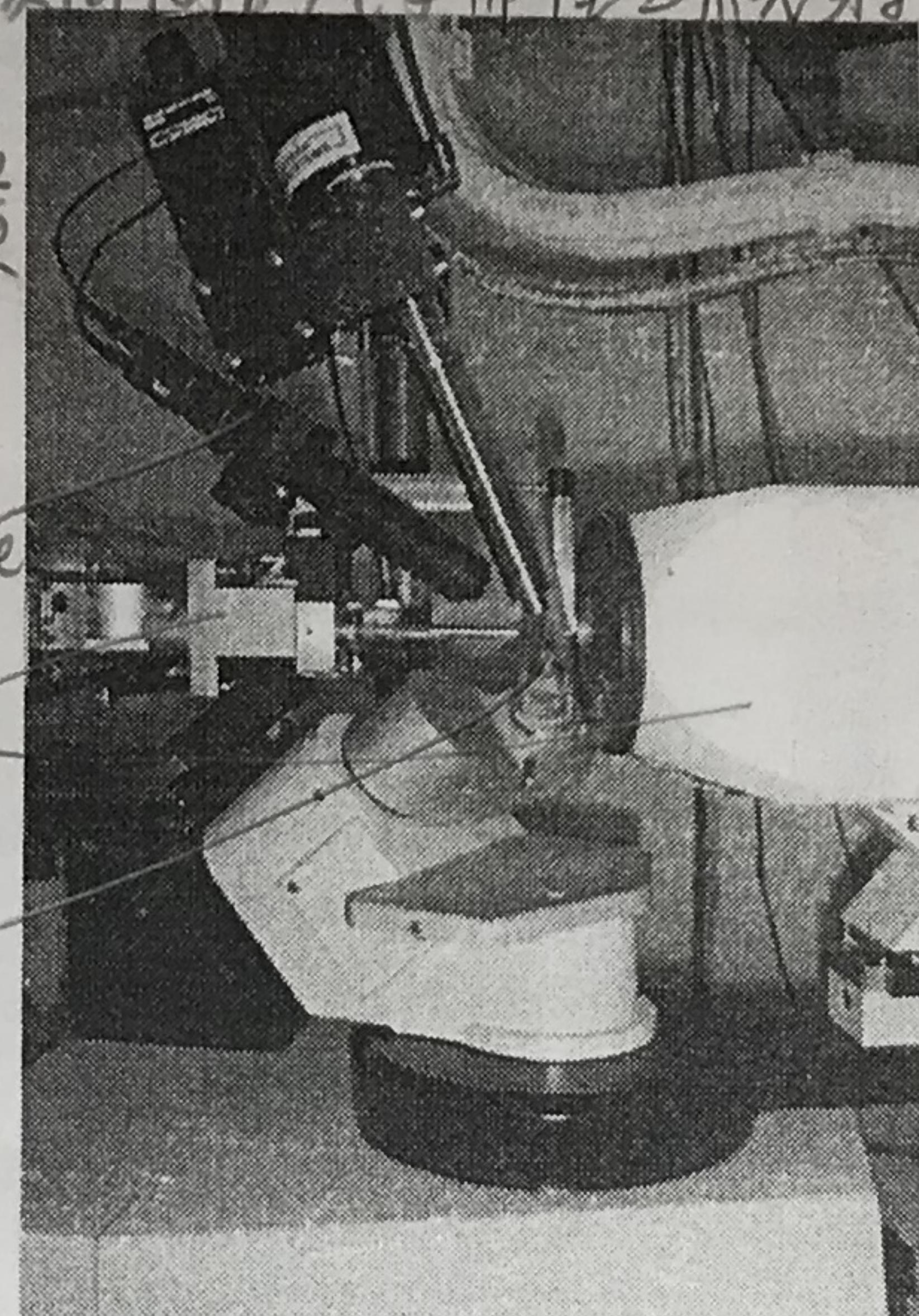
In X-ray diffraction (XRD), X-rays are diffracted by electrons surrounding the nuclei in atoms in a crystalline or polycrystalline solid.

X-ray 細過結晶或多晶固体中原子核周圍的電子而產生繞射。

A Kappa-CCD diffractometer equipped with a nitrogen gas, low-temperature cryostat (upper centre in the photograph). The X-ray source and the detector are on the left- and right-hand sides of the photograph, respectively. The crystal is mounted on the goniometer head (centre). The black "tube" shown at the upper left is a microscope.

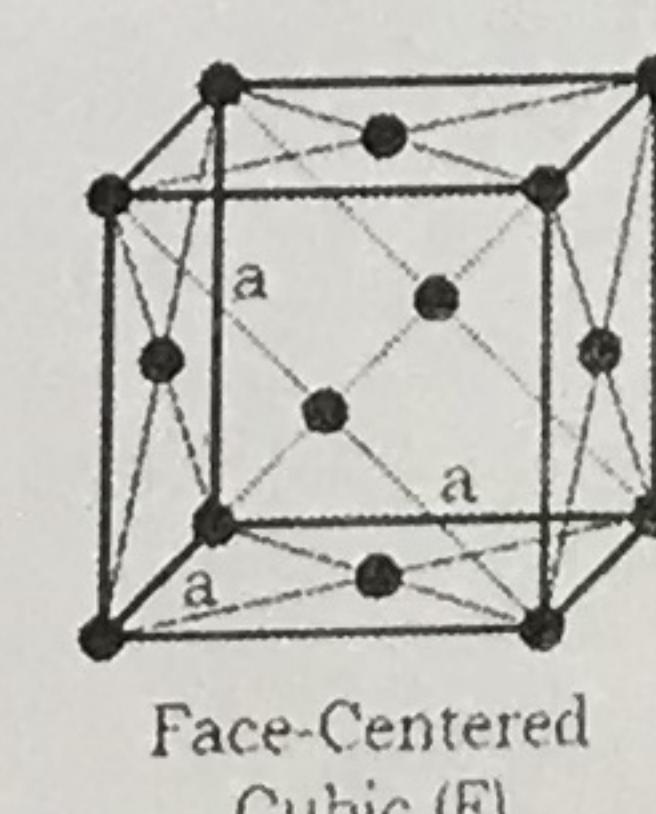
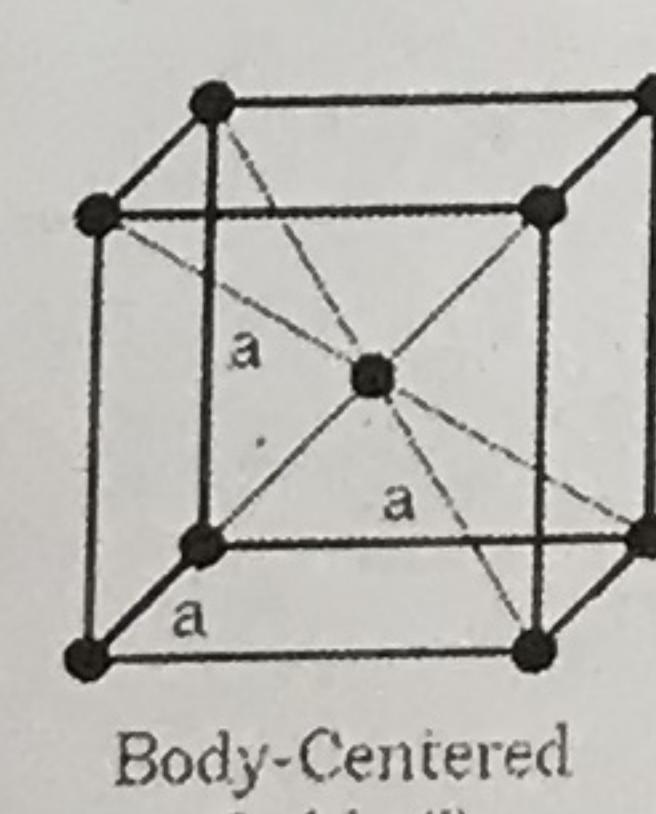
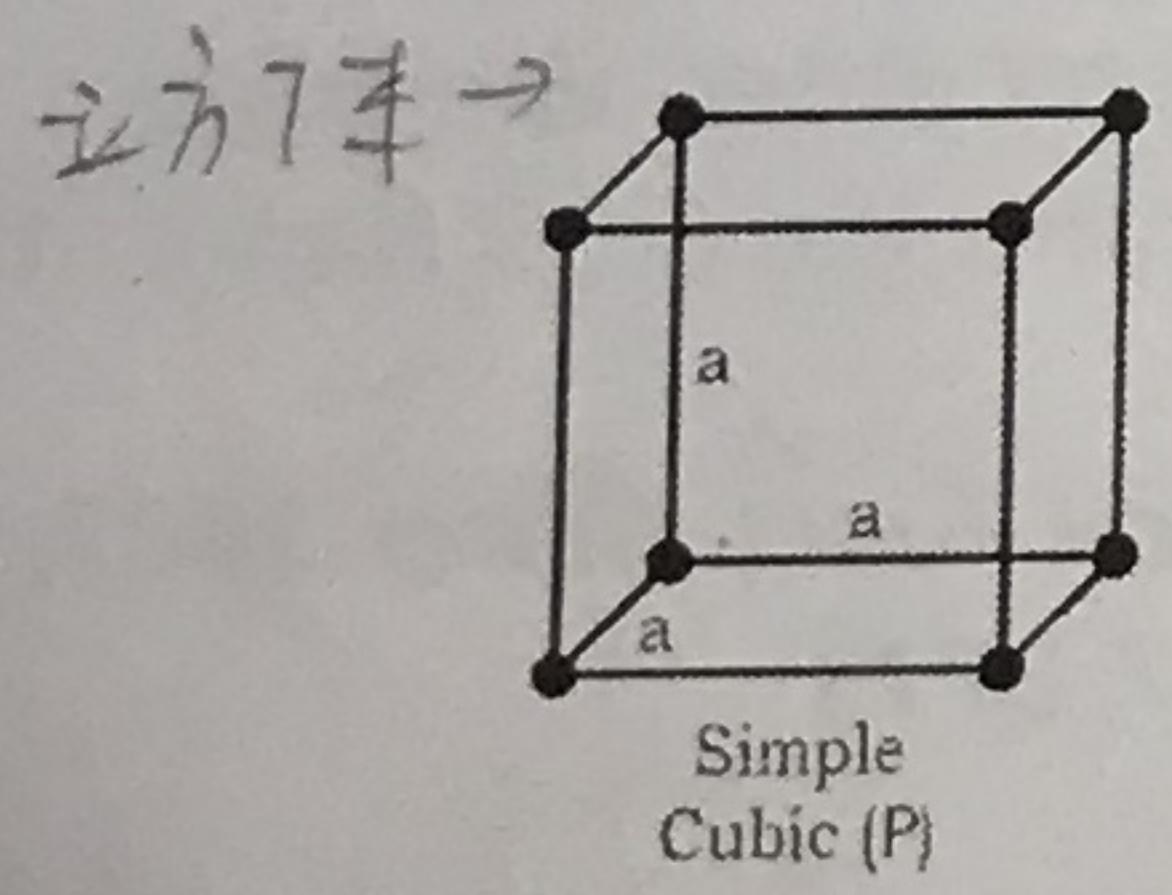
測角儀
X-ray resources
and detector.

crystal 放置處

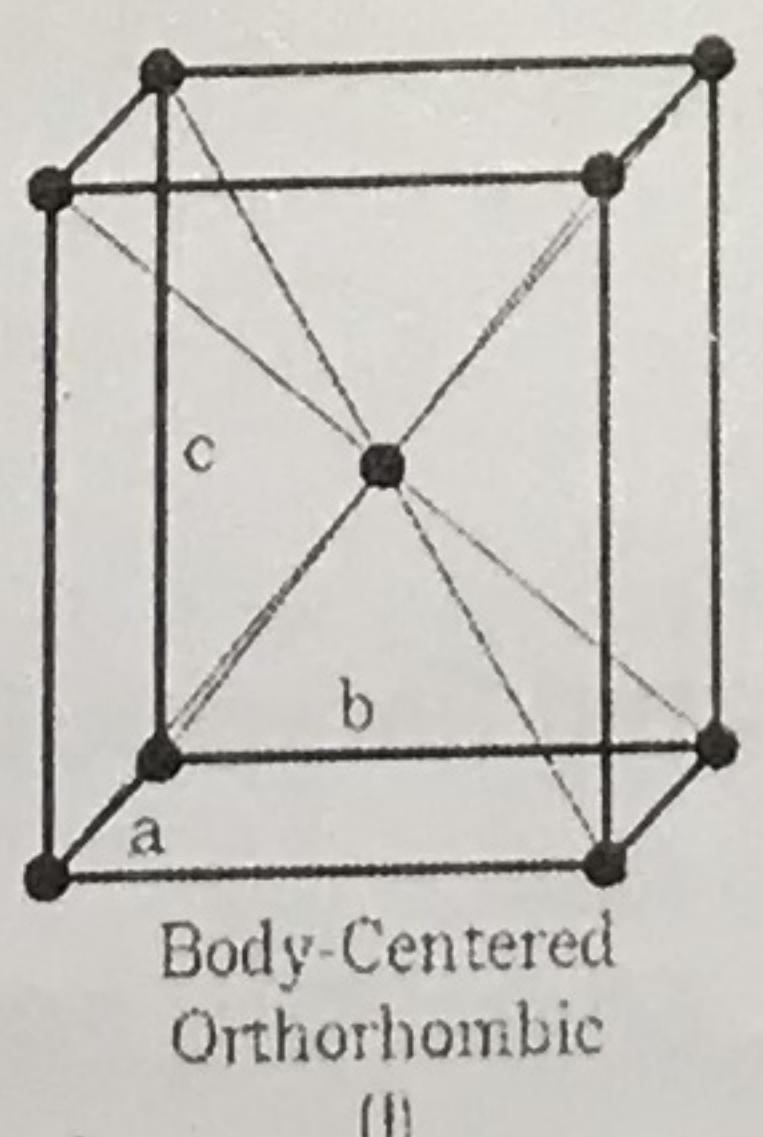
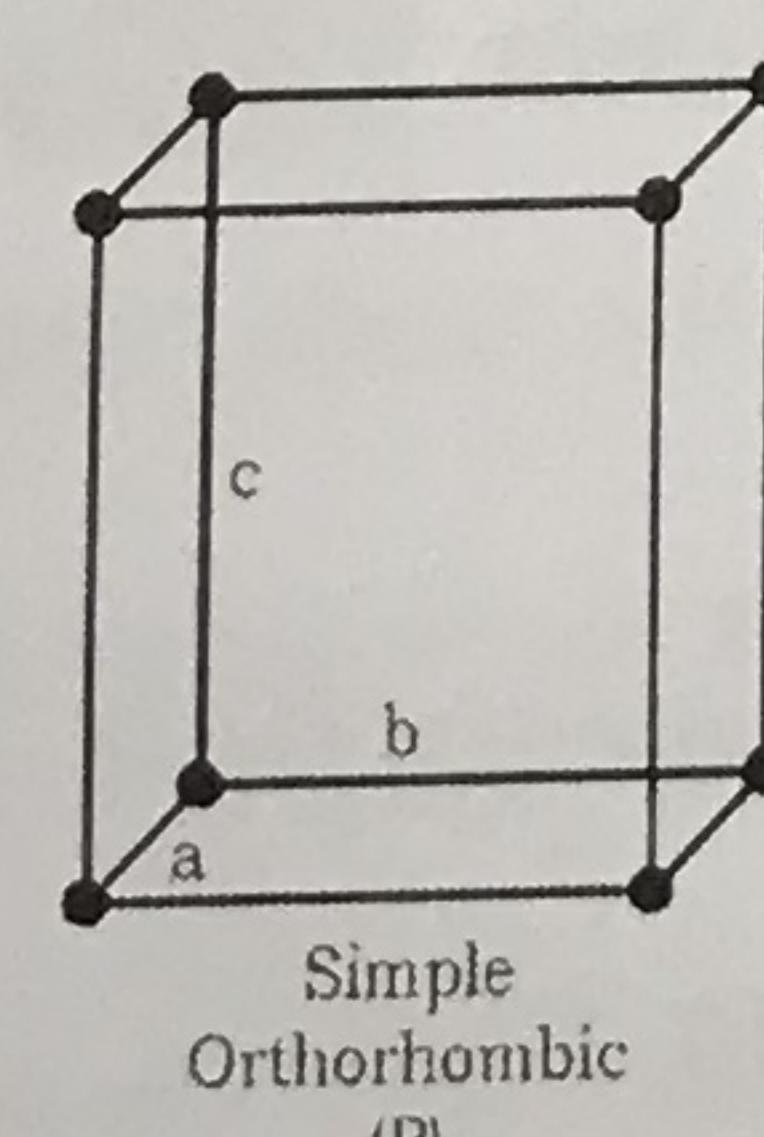
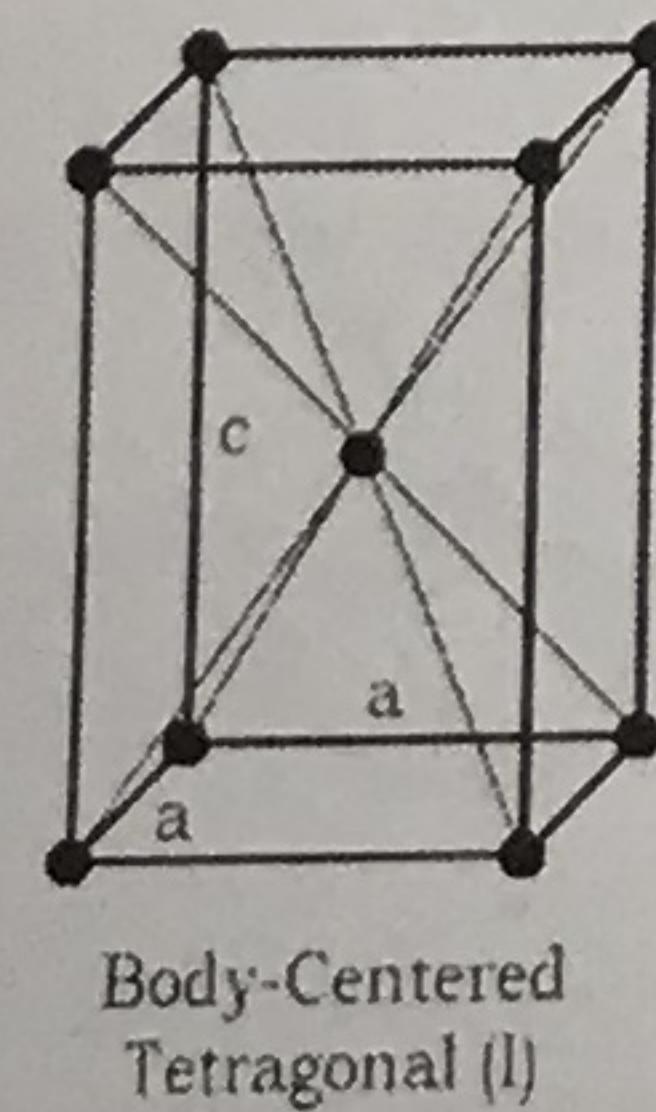
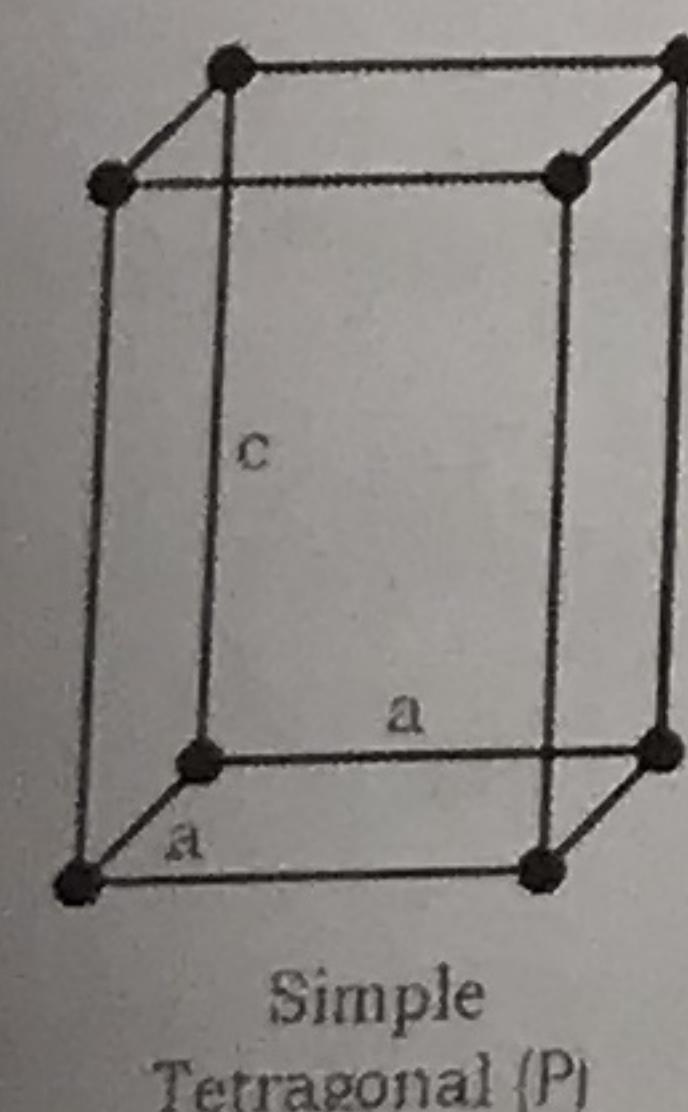


Bravais Lattices

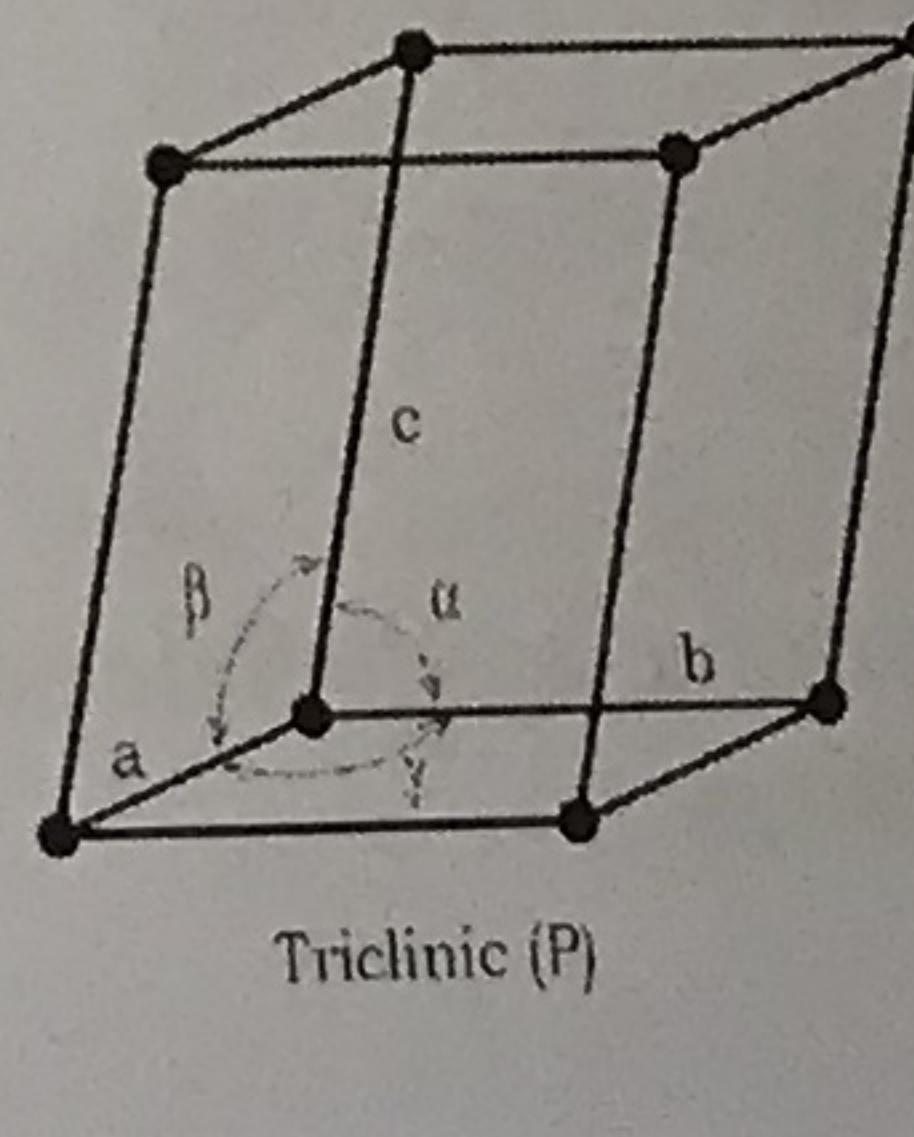
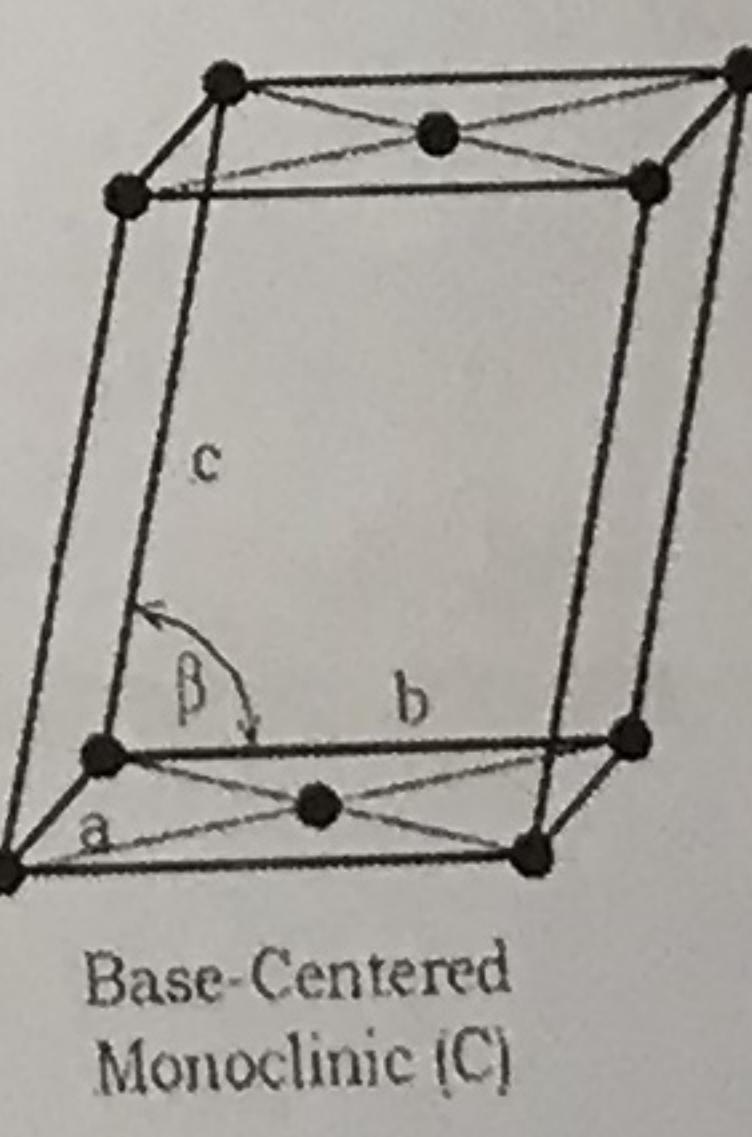
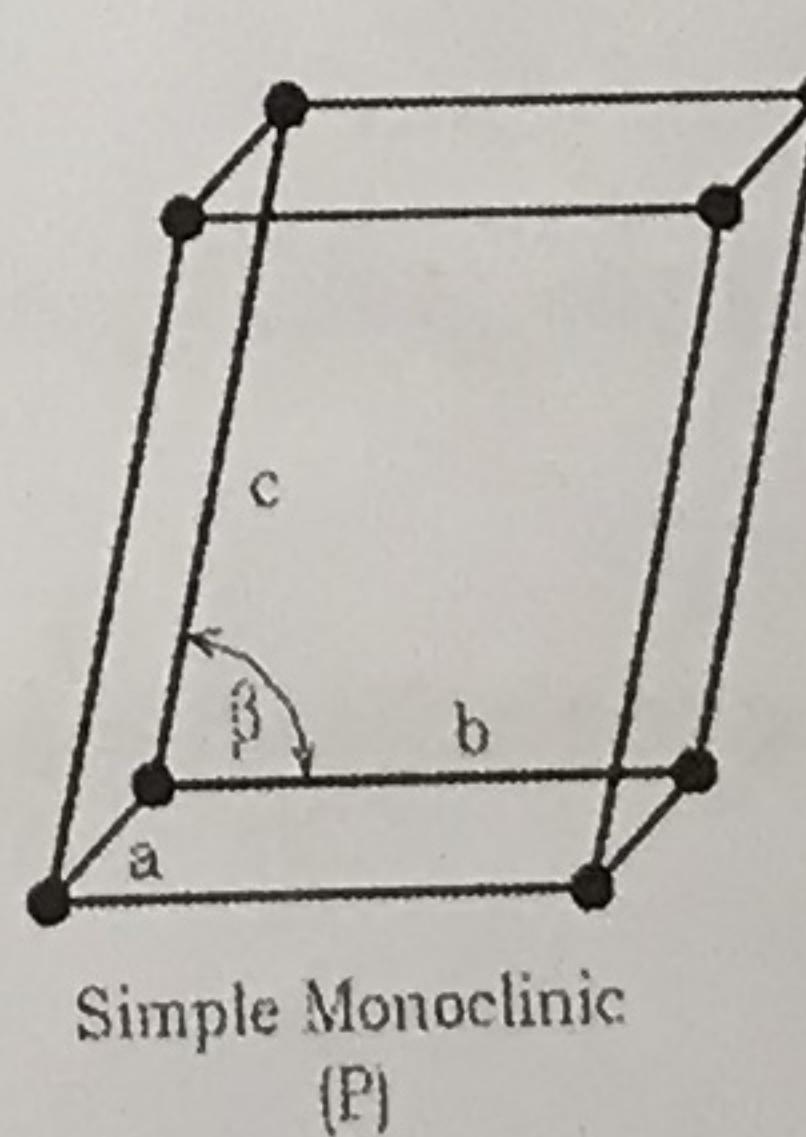
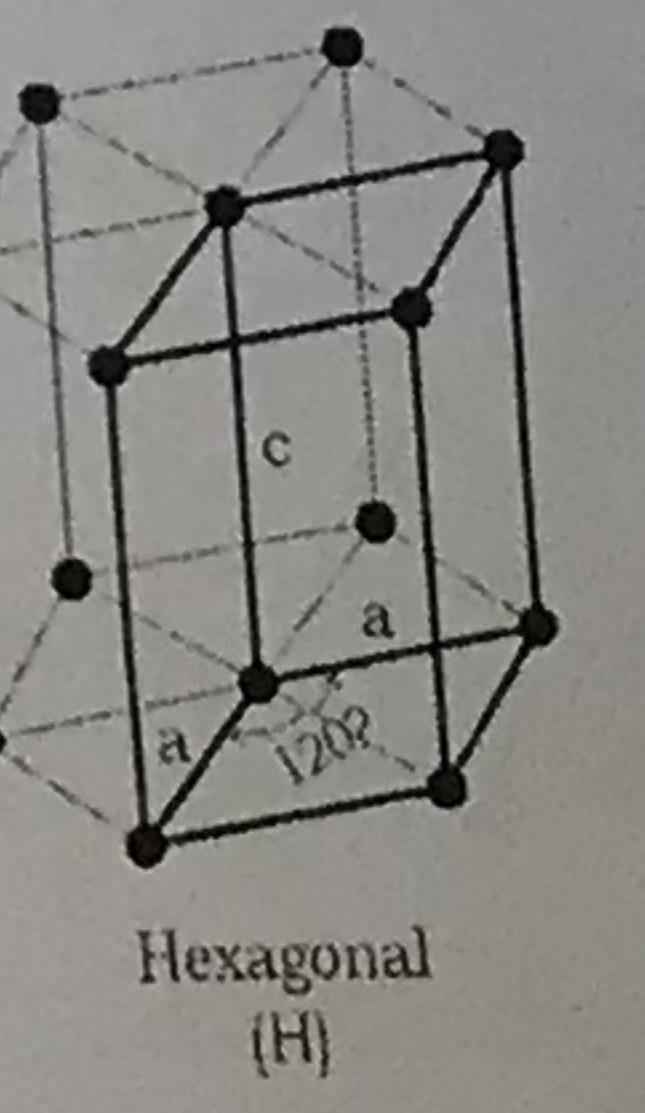
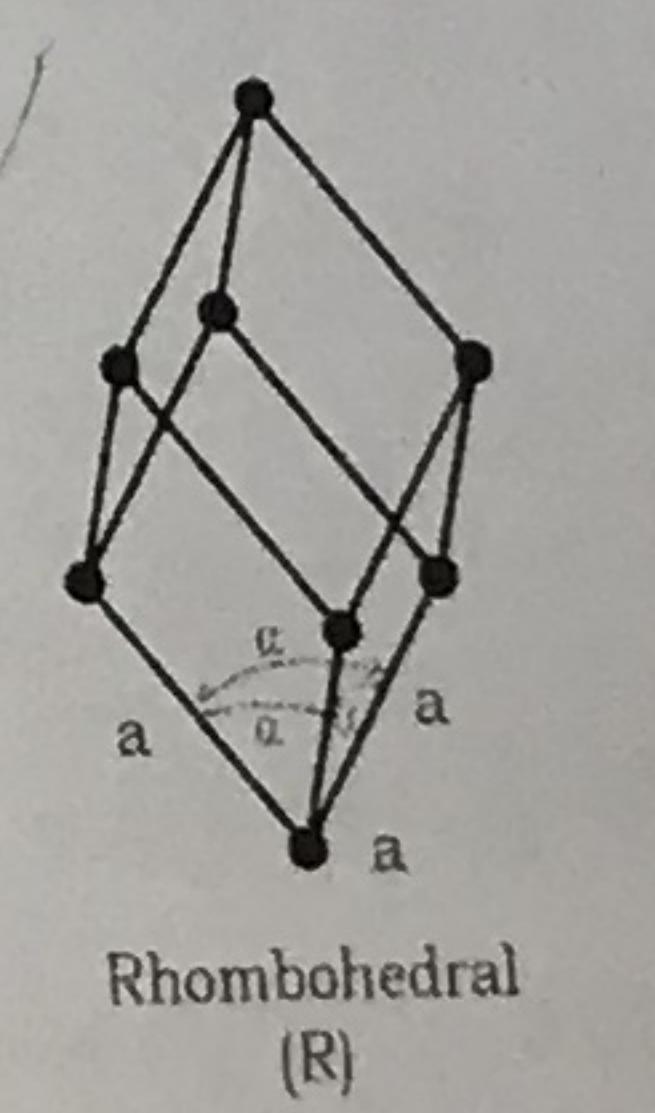
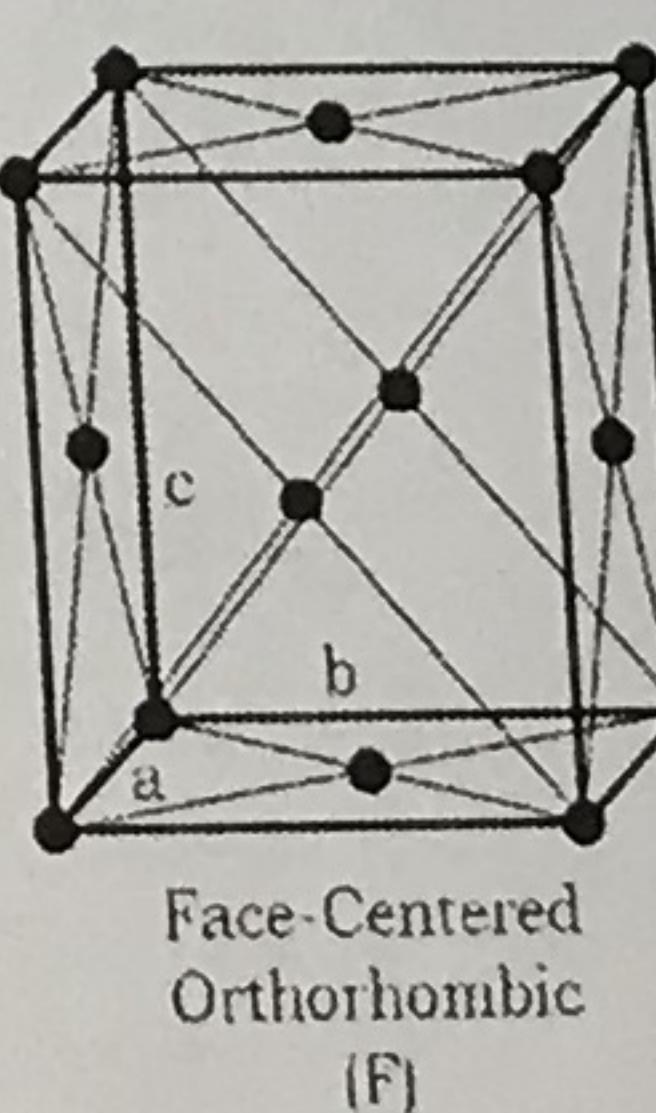
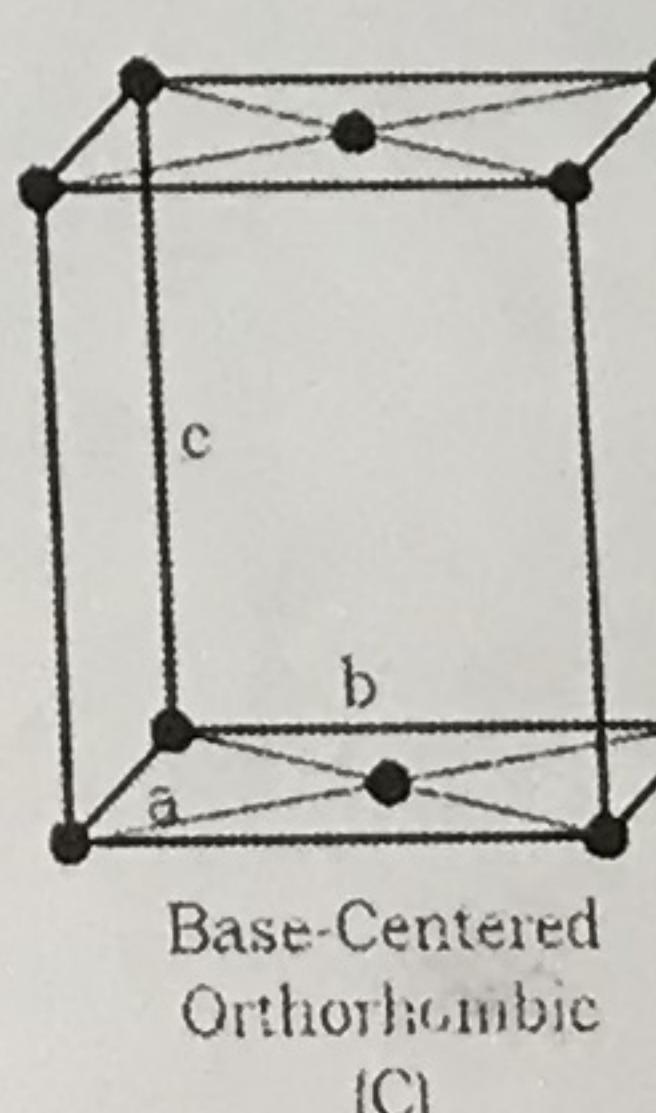
晶格結構



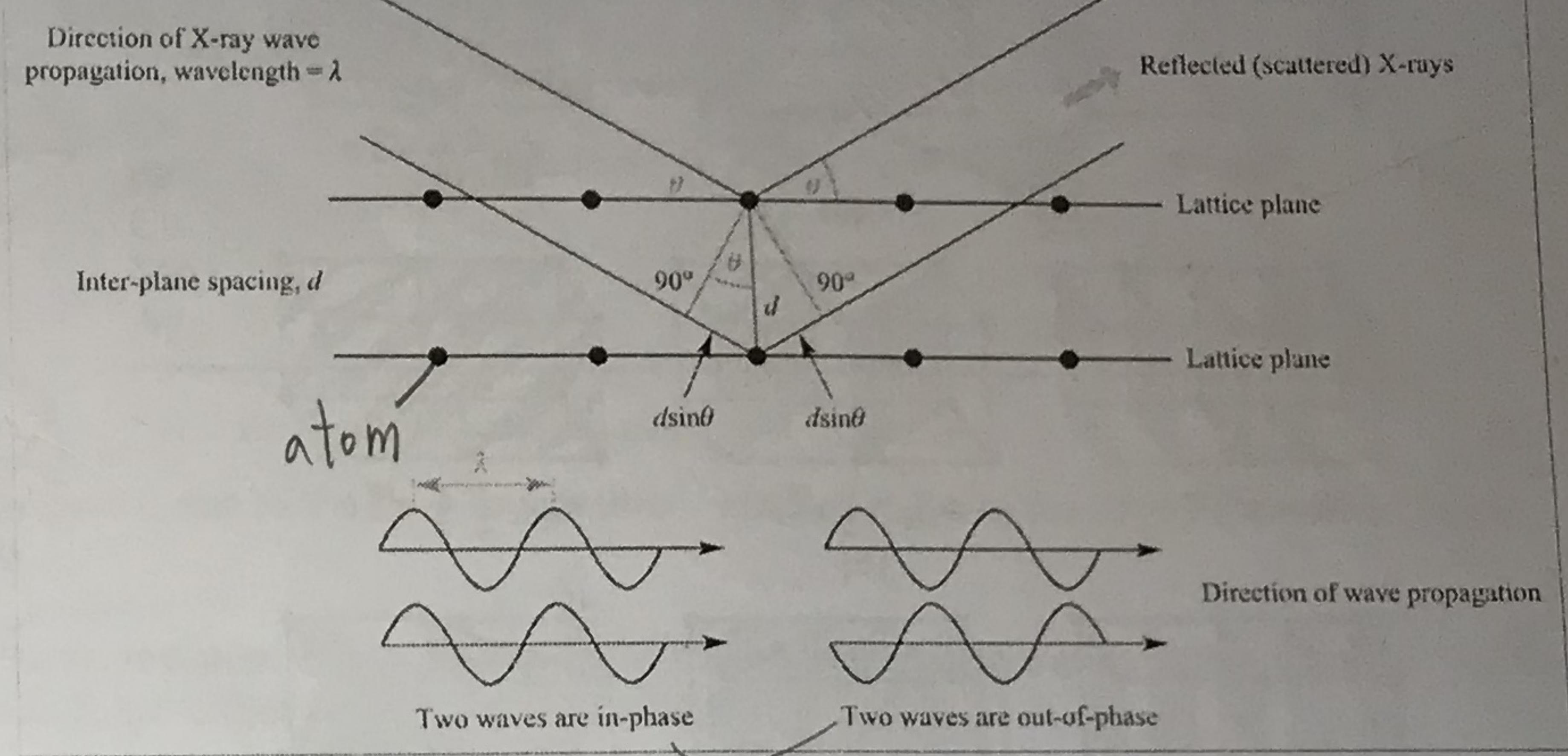
正方



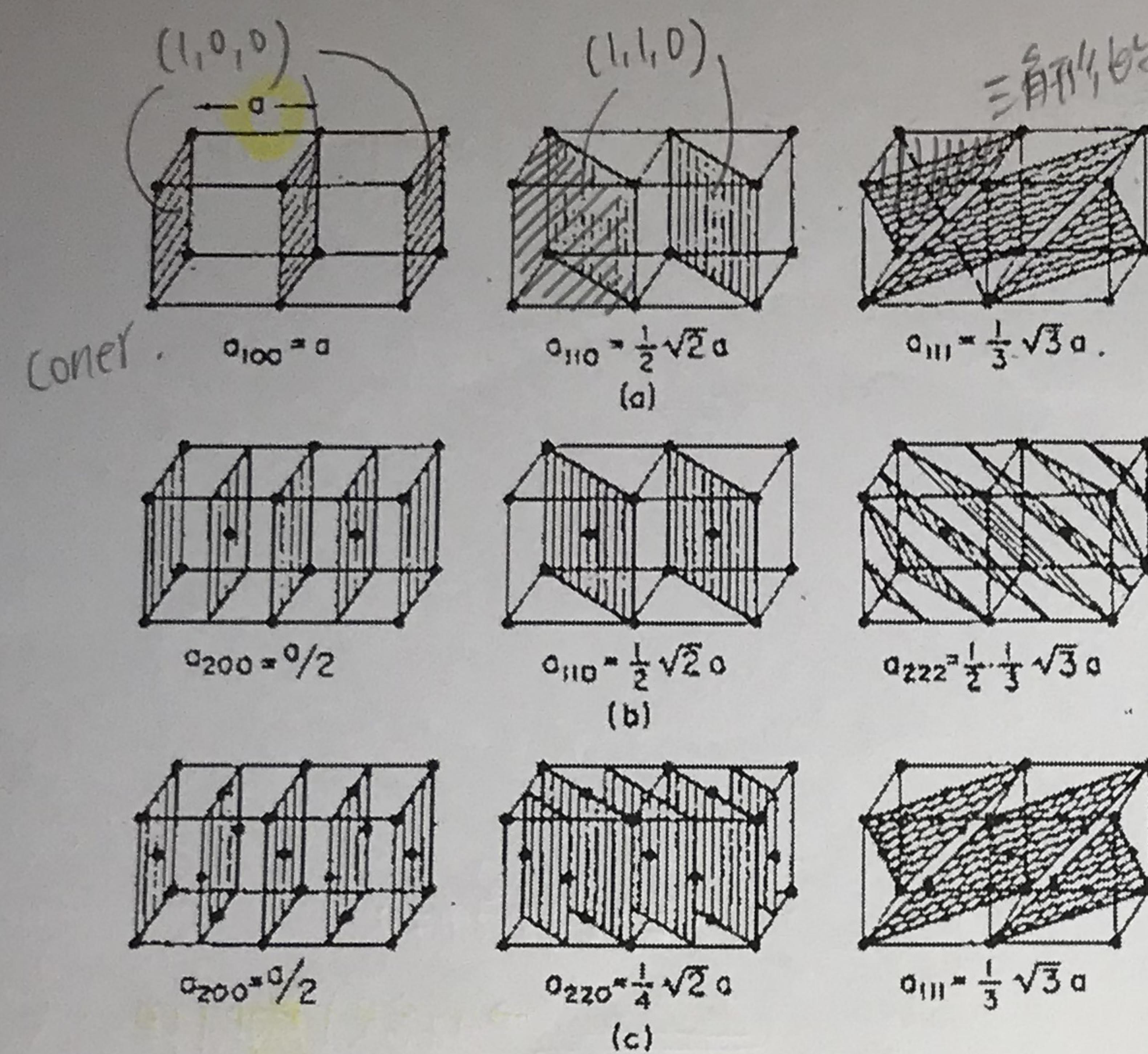
Bravais Lattices



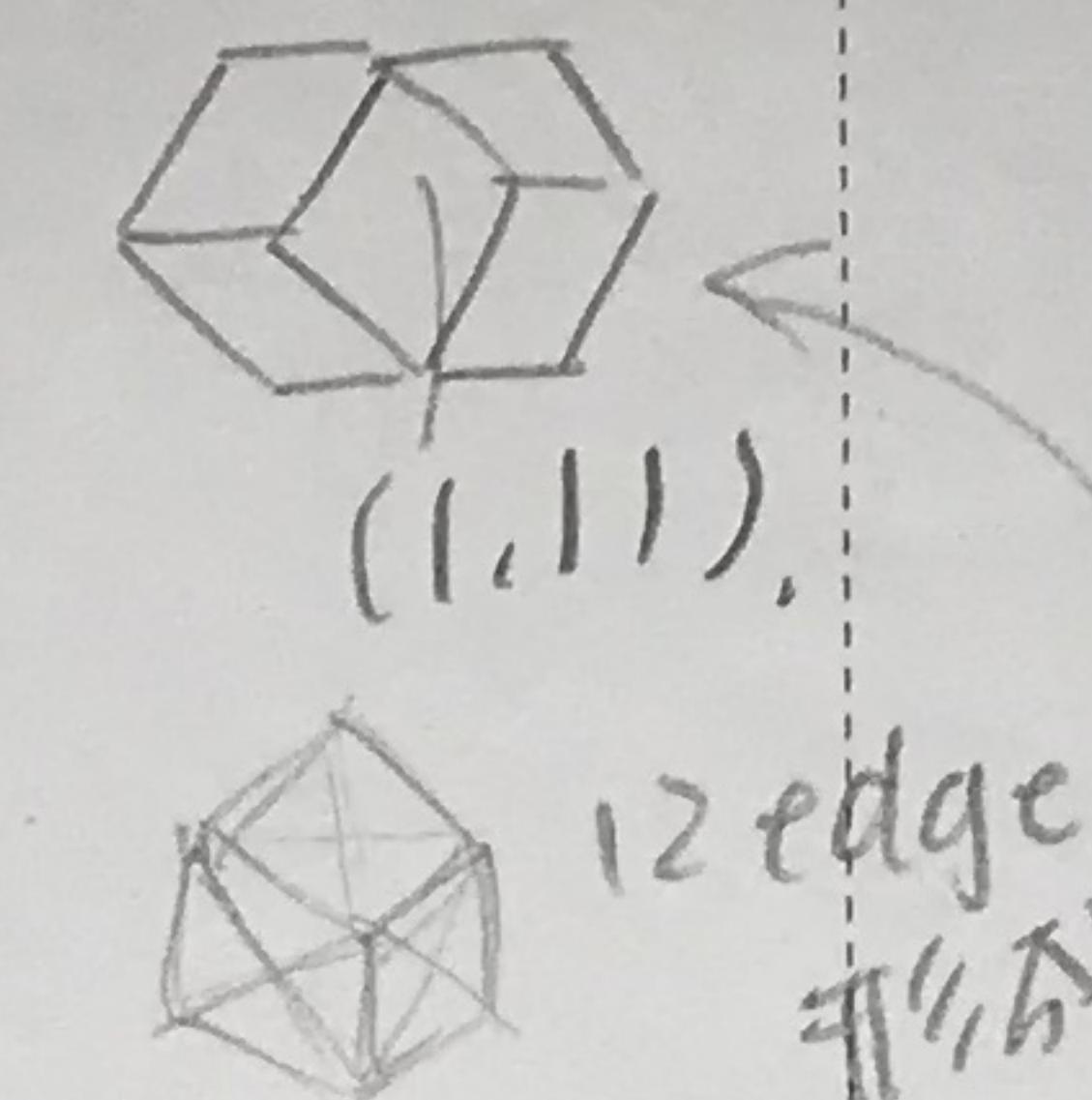
X-ray 繞射圖 $2ds\sin\theta = n\lambda$. Bragg's equation.



(反射的時候)
Schematic representation of the interaction of X-rays with layers of atoms in a crystal. This leads to the derivation of Bragg's equation $2ds\sin\theta = n\lambda \rightarrow$ 符合則同相.



Spacings in cubic lattices: (a) simple cubic; (b) body-centered cubic; (c) face-centered cubic.



d-spacing formula (see p. 447)

晶面間距，2個晶面的垂直距離。

The value of d , the perpendicular distance between adjacent planes in the set (hkl) , may be calculated using the formulae:

Cubic

$$\frac{1}{d^2} = \frac{h^2 + k^2 + l^2}{a^2} \Rightarrow \text{對照 } (1,0,0).$$

Tetragonal

$$\frac{1}{d^2} = \frac{h^2 + k^2}{a^2} + \frac{l^2}{c^2} \quad \text{但指教的晶面其面間距較大}$$

Orthorhombic

$$\frac{1}{d^2} = \frac{h^2}{a^2} + \frac{k^2}{b^2} + \frac{l^2}{c^2} \quad (1,0,0) \text{ 間距最大} \quad \leftarrow \text{對照左边的圖}$$

Hexagonal

$$\frac{1}{d^2} = \frac{4}{3} \left(\frac{h^2 + hk + k^2}{a^2} \right) + \frac{l^2}{c^2}$$

Monoclinic

$$\frac{1}{d^2} = \frac{1}{\sin^2 \beta} \left(\frac{h^2}{a^2} + \frac{k^2 \sin^2 \beta}{b^2} + \frac{l^2}{c^2} - \frac{2hl \cos \beta}{ac} \right)$$

晶面間距越小其陣列越稀疏。

Indices of Directions

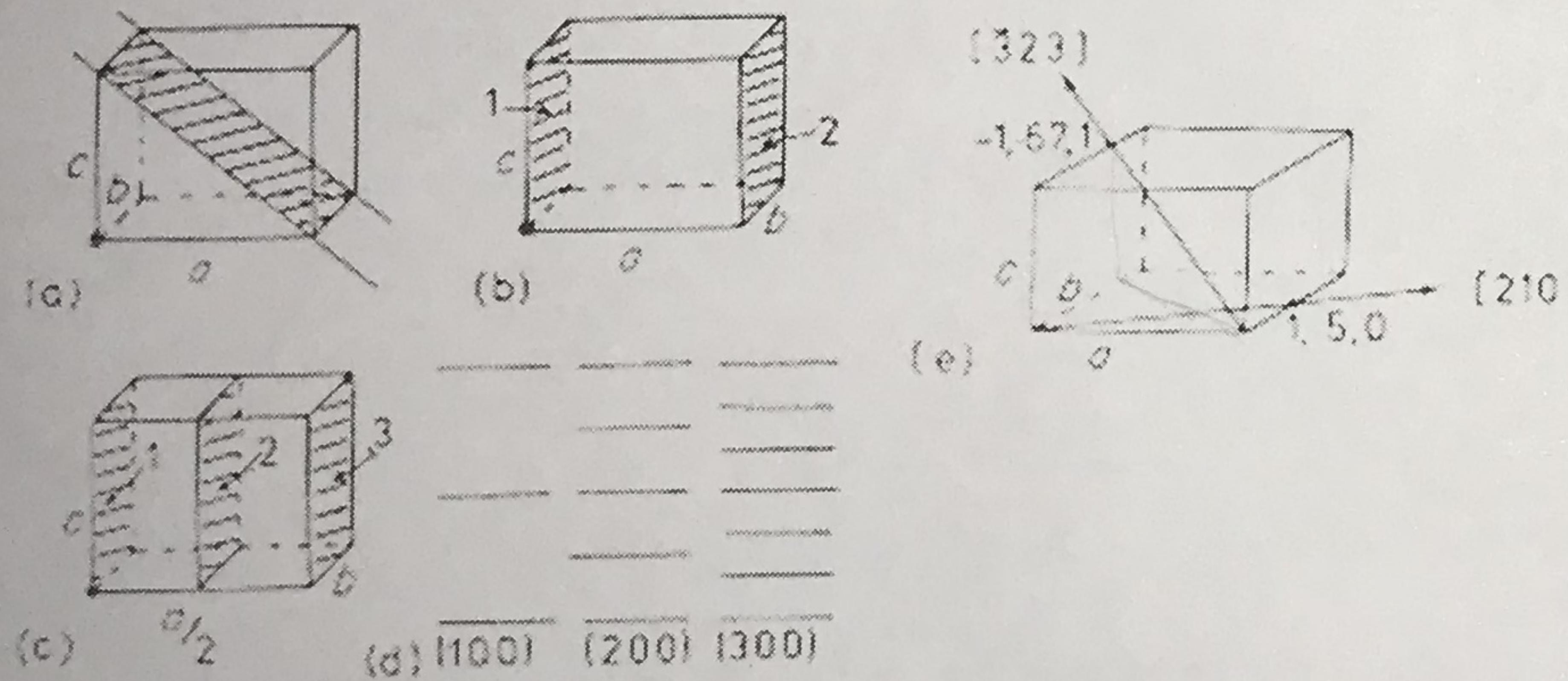
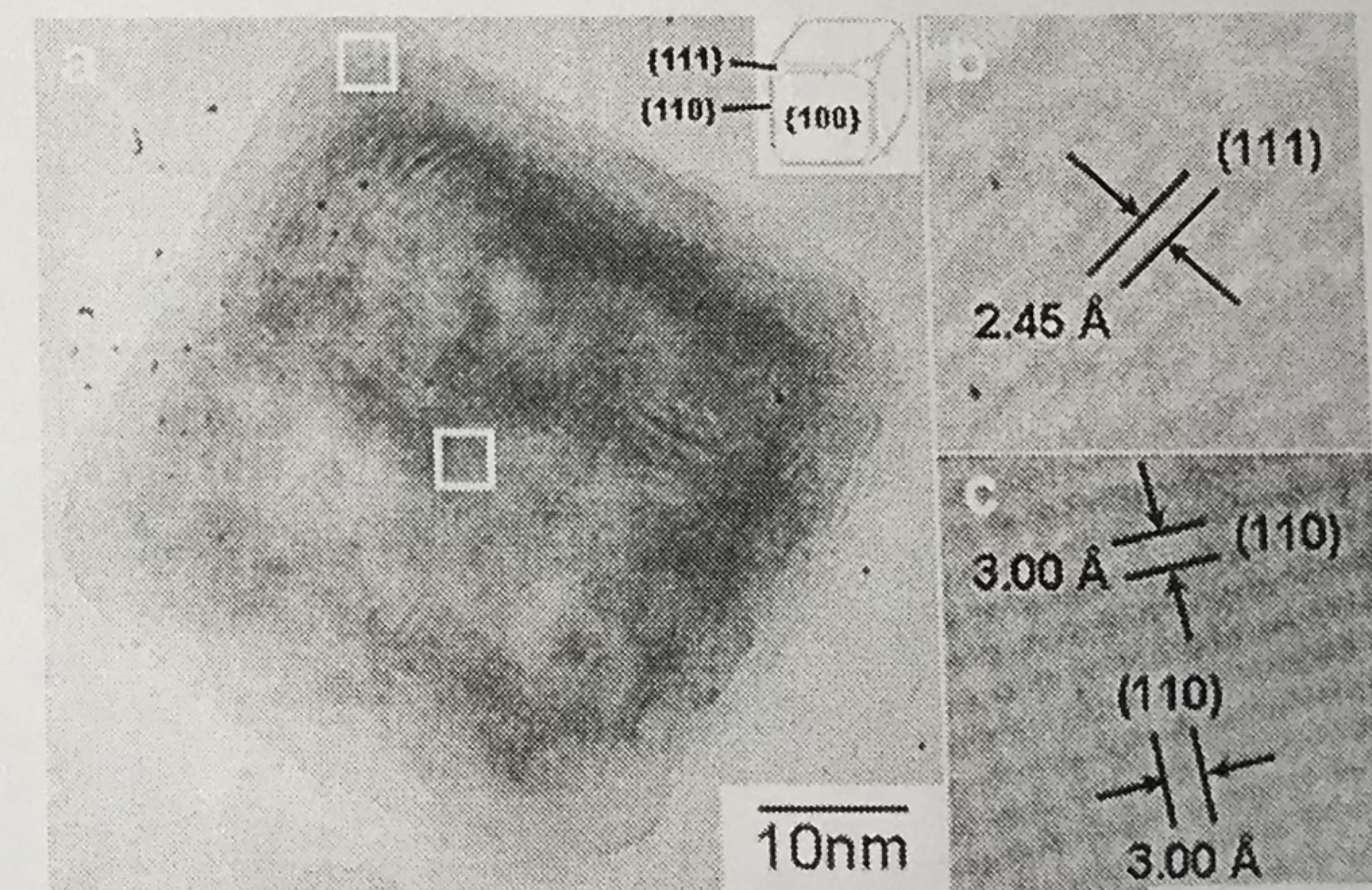


Fig. 1.11 Examples of Miller indices: (a) $\langle 101 \rangle$; (b) $\langle 100 \rangle$; (c) $\langle 200 \rangle$; (d) $\langle 300 \rangle$; (e) indices of directions $\langle 323 \rangle$ and $\langle 210 \rangle$

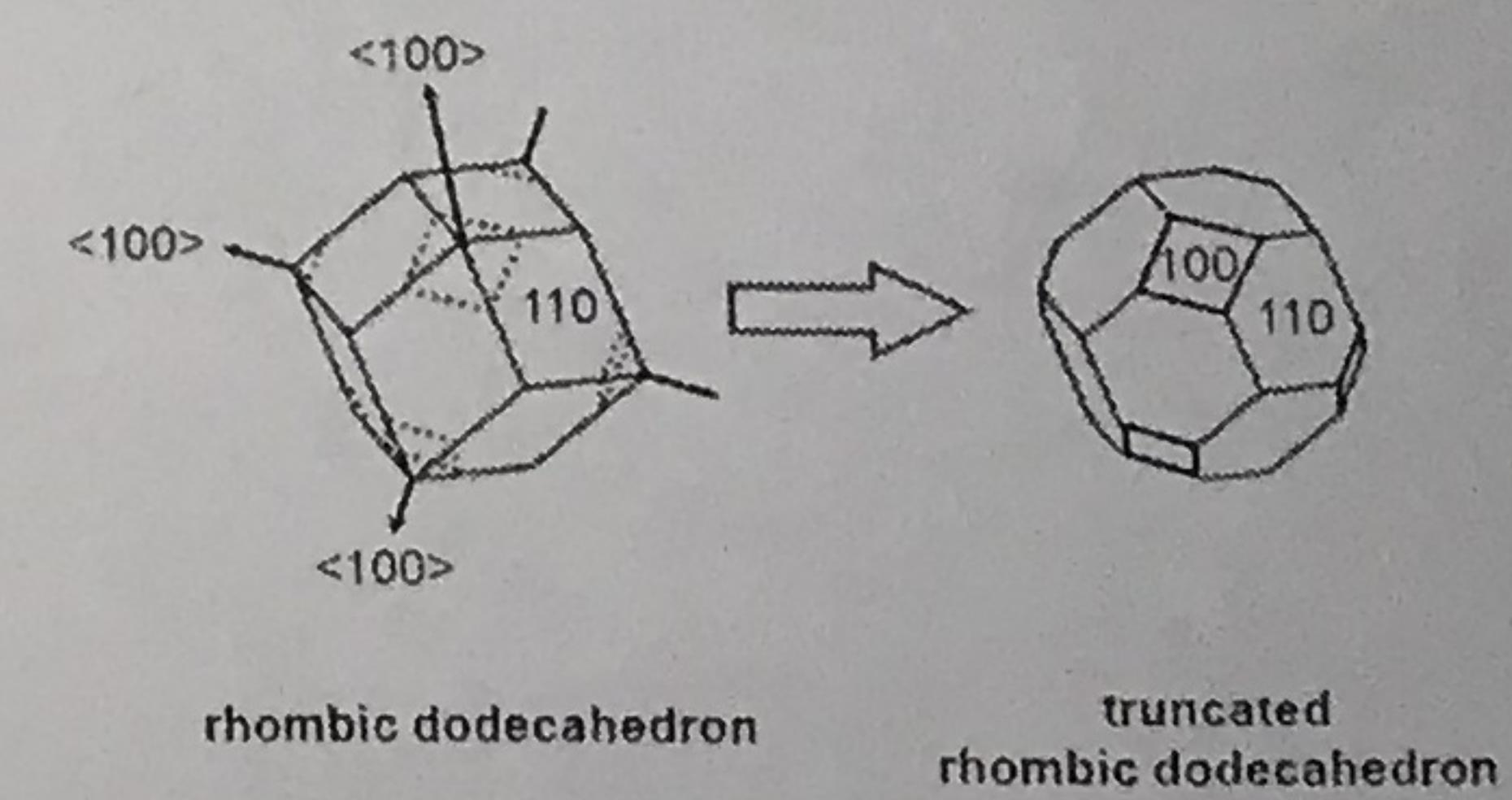
For cubic systems, an $[hkl]$ direction is always perpendicular to the (hkl) plane of the same indices.

Miller Indices of Crystal Faces



Adv. Funct. Mater. 2007,
17, 3773

Truncated Rhombic Dodecahedral Cu_2O Nanocages
J. Am. Chem. Soc. 2008, 130, 12815



粉末X射線衍射原理

- fingerprint characterization of crystalline materials
- determination of their structure

Generation of X-rays

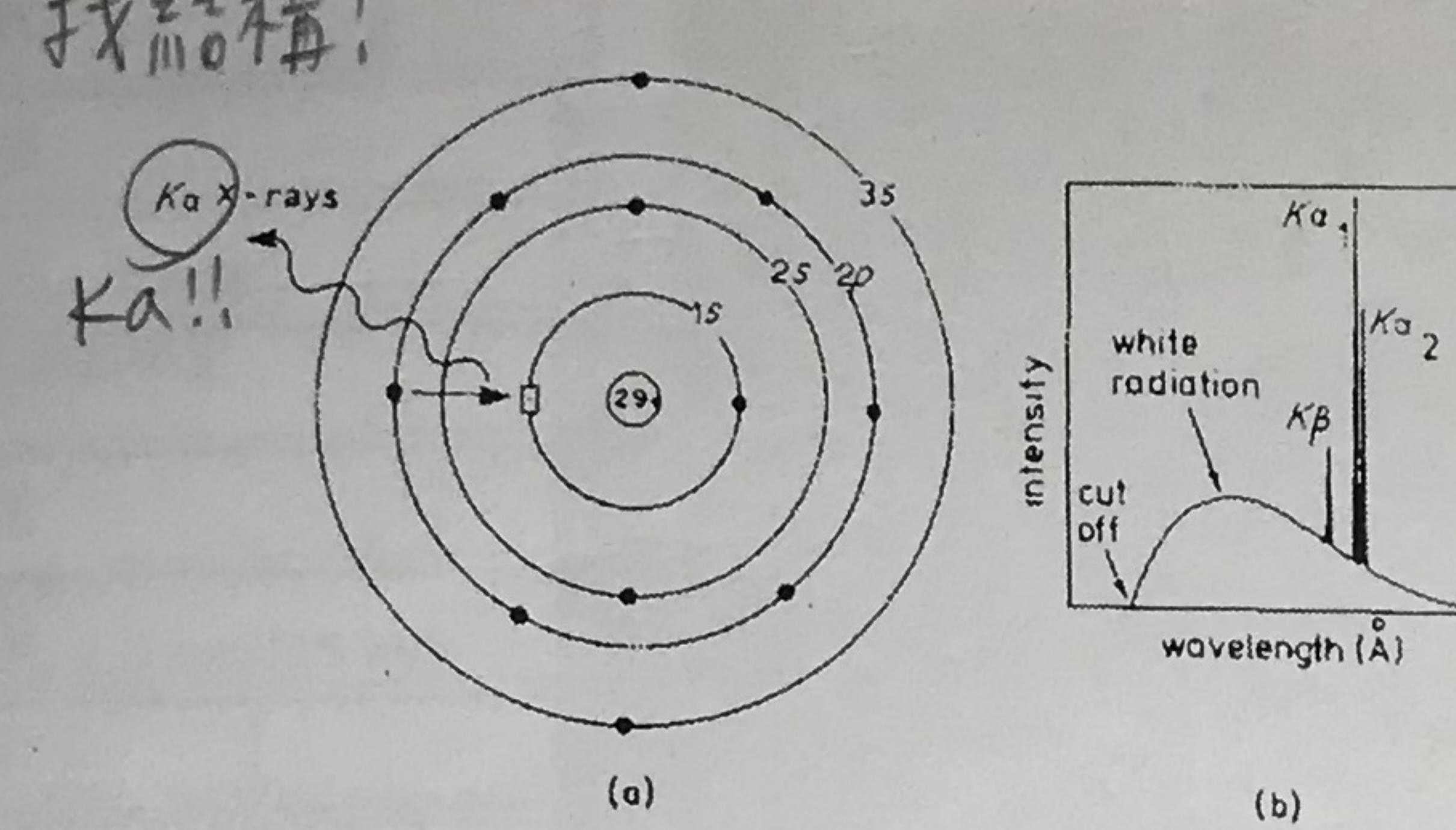
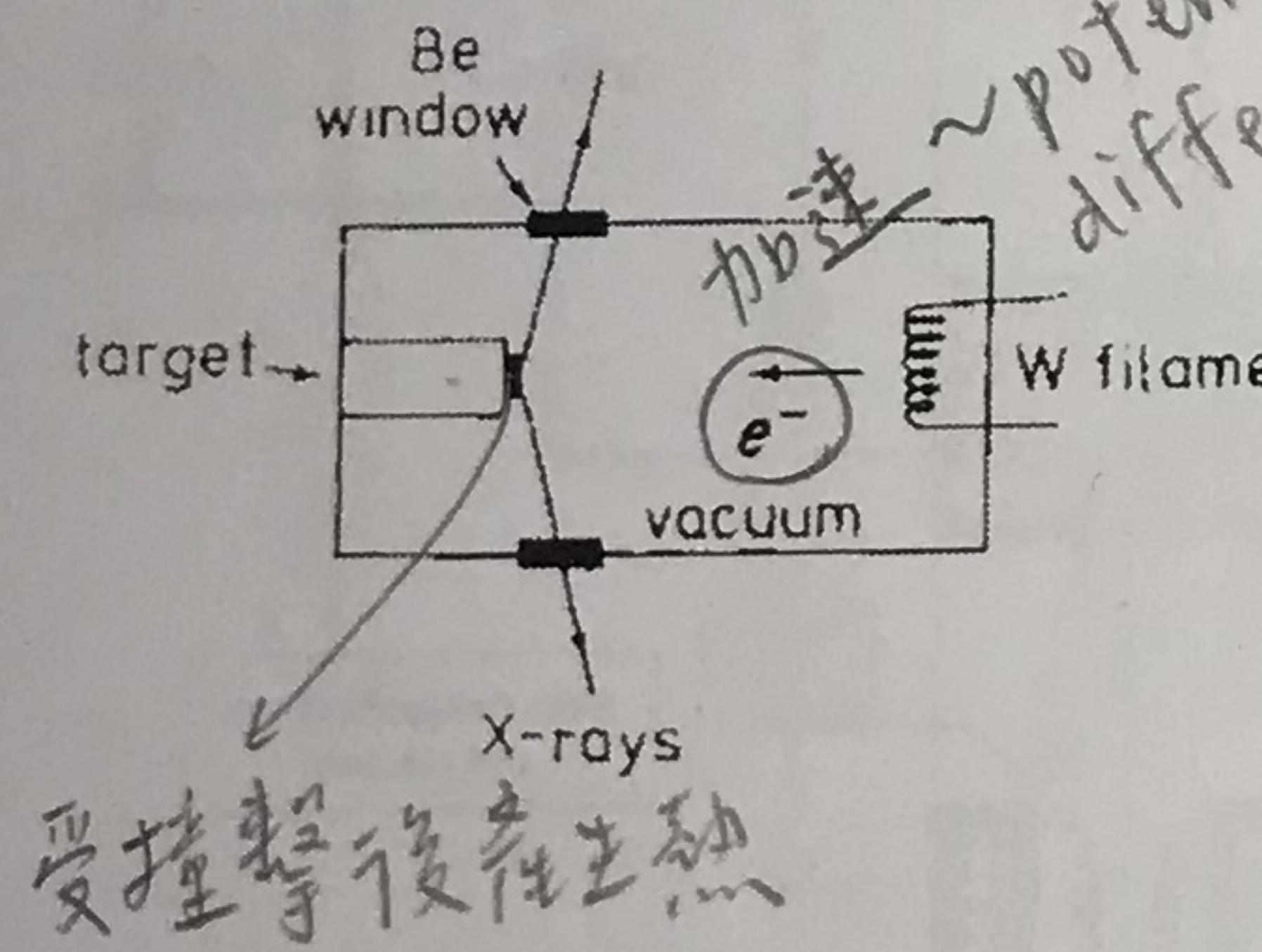


Fig. 3.1 (a) Generation of Cu K_α X-rays. A 1s electron is ionized; a 2p electron falls into the empty 1s level (□) and the excess energy is released as X-rays. (b) X-ray emission spectrum of Cu

White radiation arises when the electrons are slowed down or stopped by the collision and some of their lost energy is converted into electromagnetic radiation. The lower wavelength cut off occurs when all the kinetic energy of the incident particles is converted into X-rays.

→ 电子受到阻碍或撞擊 → 失去能量 → 電磁輻射
當入射粒子的所有動能 → X-ray → 產生較短的波長

Schematic design of a filament X-ray tube



The electron beam is provided by a heated tungsten filament.

Electrons accelerate through a potential difference of ~30 kV. The electrons strike the target, a piece of Cu fixed to the anode.

Need to cool anode. Most of the striking electron energy is converted to heat.

X-ray 線輻射 data

Table 3.2 X-ray wavelengths (Å) of commonly used target materials

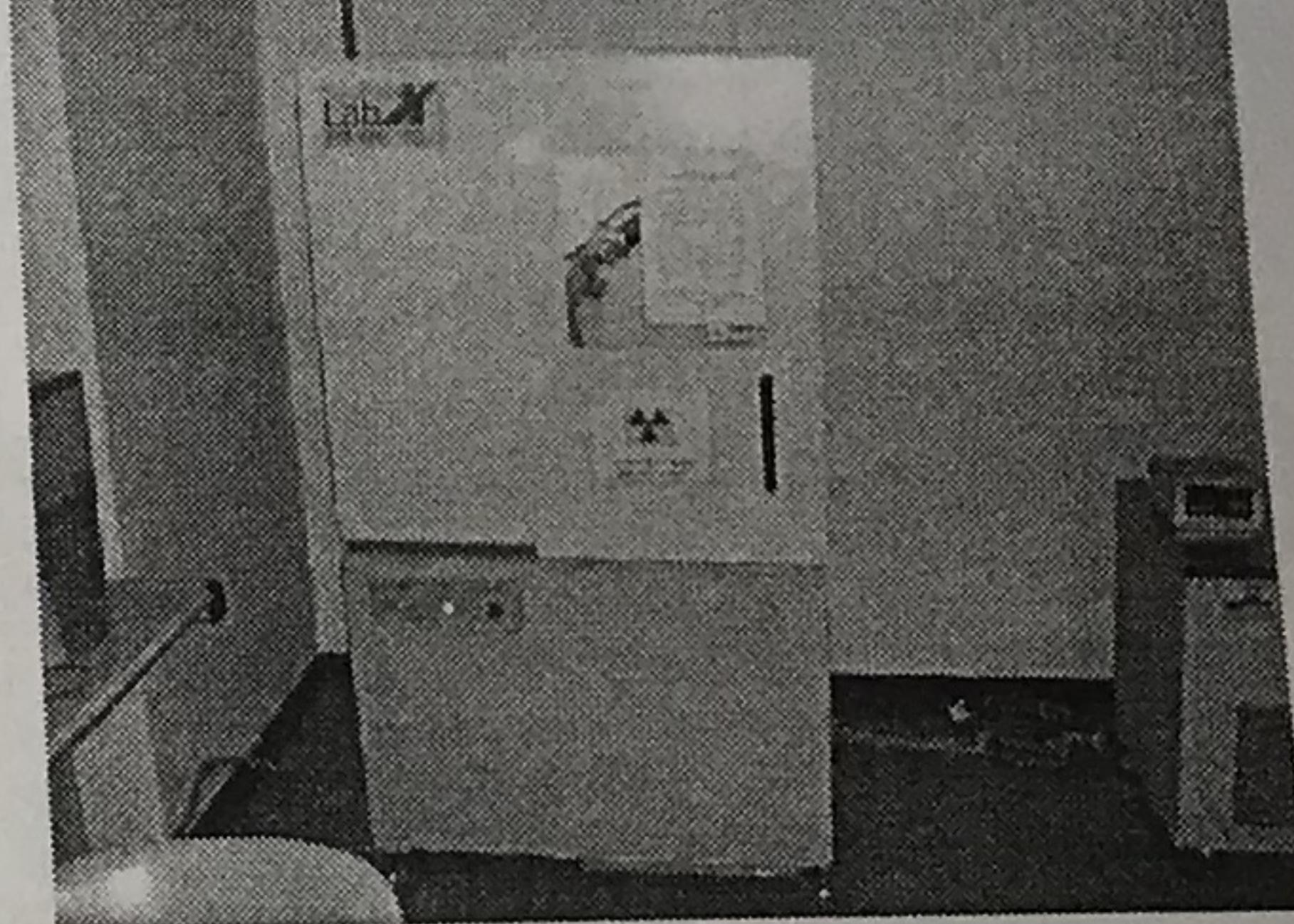
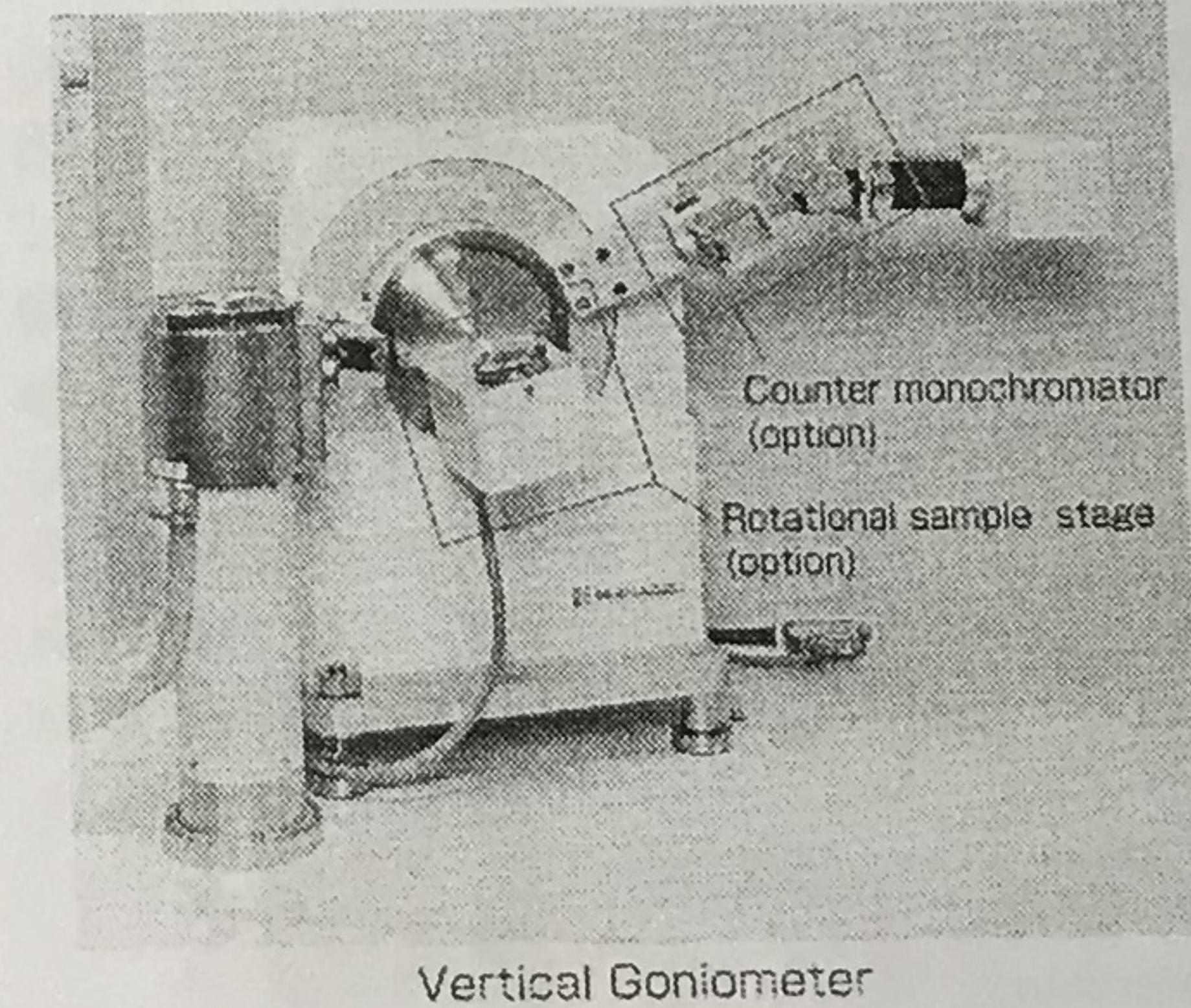
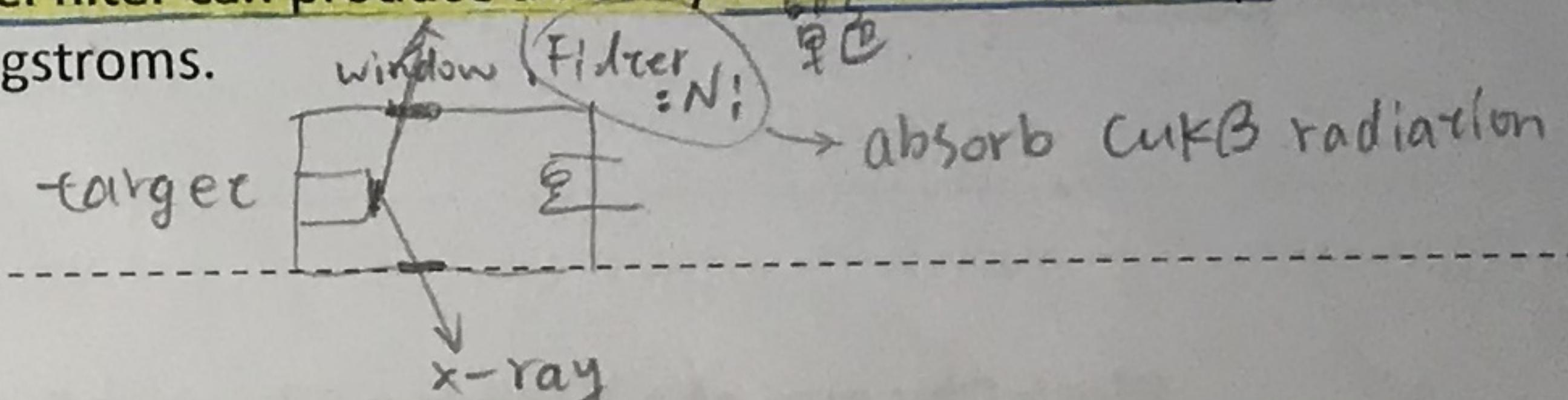
Target	K _{α1}	K _{α2}	K _{ᾱ} *	Filter
Cr	2.2896	2.2935	2.2909	V
Fe	1.9360	1.9399	1.9373	Mn
Cu	1.5405	1.5443	1.5418	Ni
Mo	0.7093	0.7135	0.7107	Nb
Ag	0.5594	0.5638	0.5608	Pd

* $\bar{\alpha}$ is the intensity-weighted average of α_1 and α_2 .

K_α peak is due to the $2p \rightarrow 1s$ transition. K_β peak is due to the $3p \rightarrow 1s$ transition (1.392 Å).

The K_α radiation is a doublet, because the transition has a slightly different energy for the two possible spin states of the 2p electron.

The energy required to ionize 1s electrons of Ni corresponds to a wavelength of 1.488 Å, which lies between the values for the K_α and K_β lines of the Cu emission spectrum. Cu K_β radiation has sufficient energy to ionize Ni 1s electrons but Cu K_α radiation does not. Ni foil is effective in absorbing the Cu K_β radiation and most of the white radiation. Thus, a copper x-ray source with a nickel filter can produce a nearly monochromatic x-ray beam with photons of mostly 1.54 angstroms.



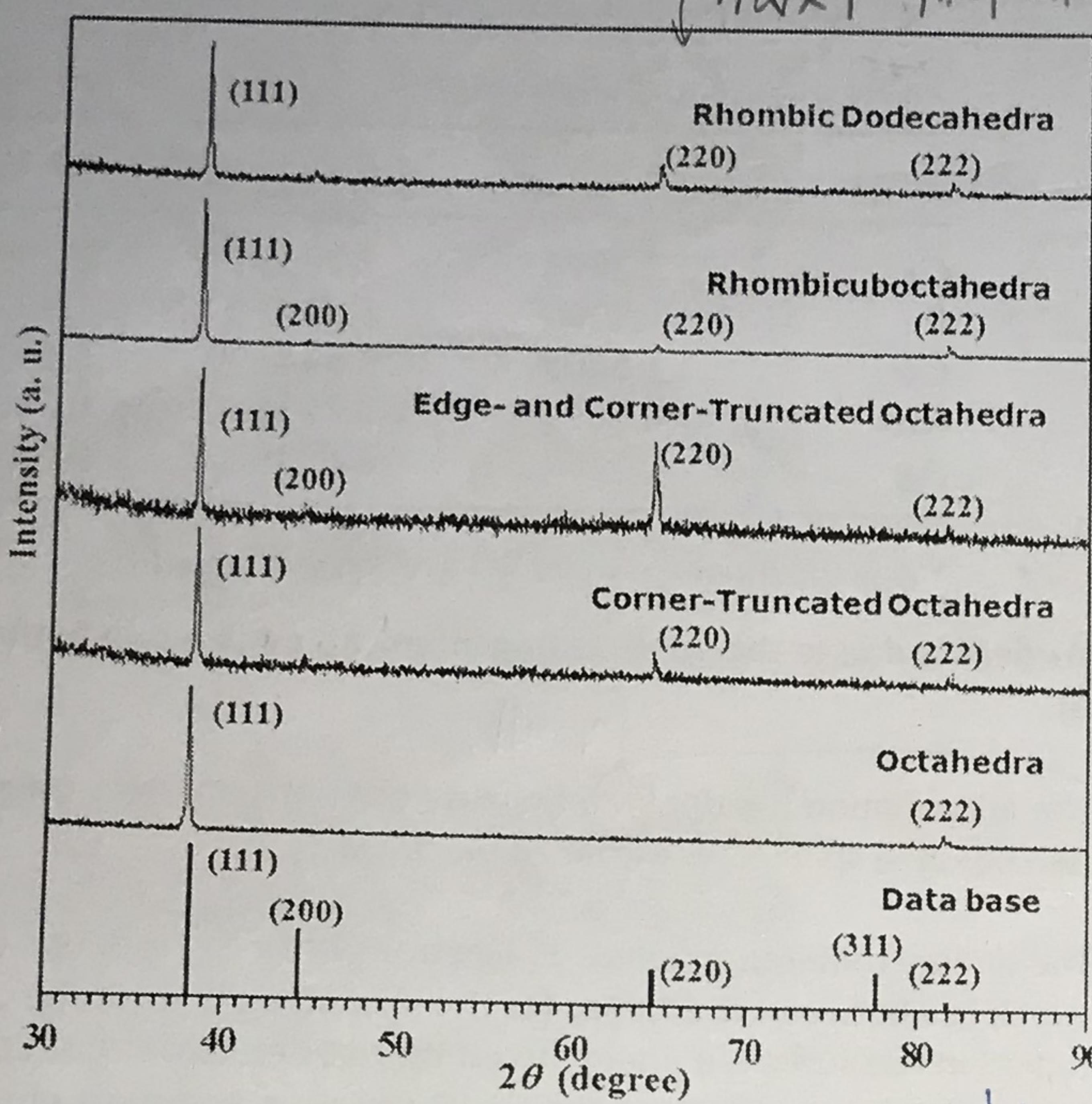
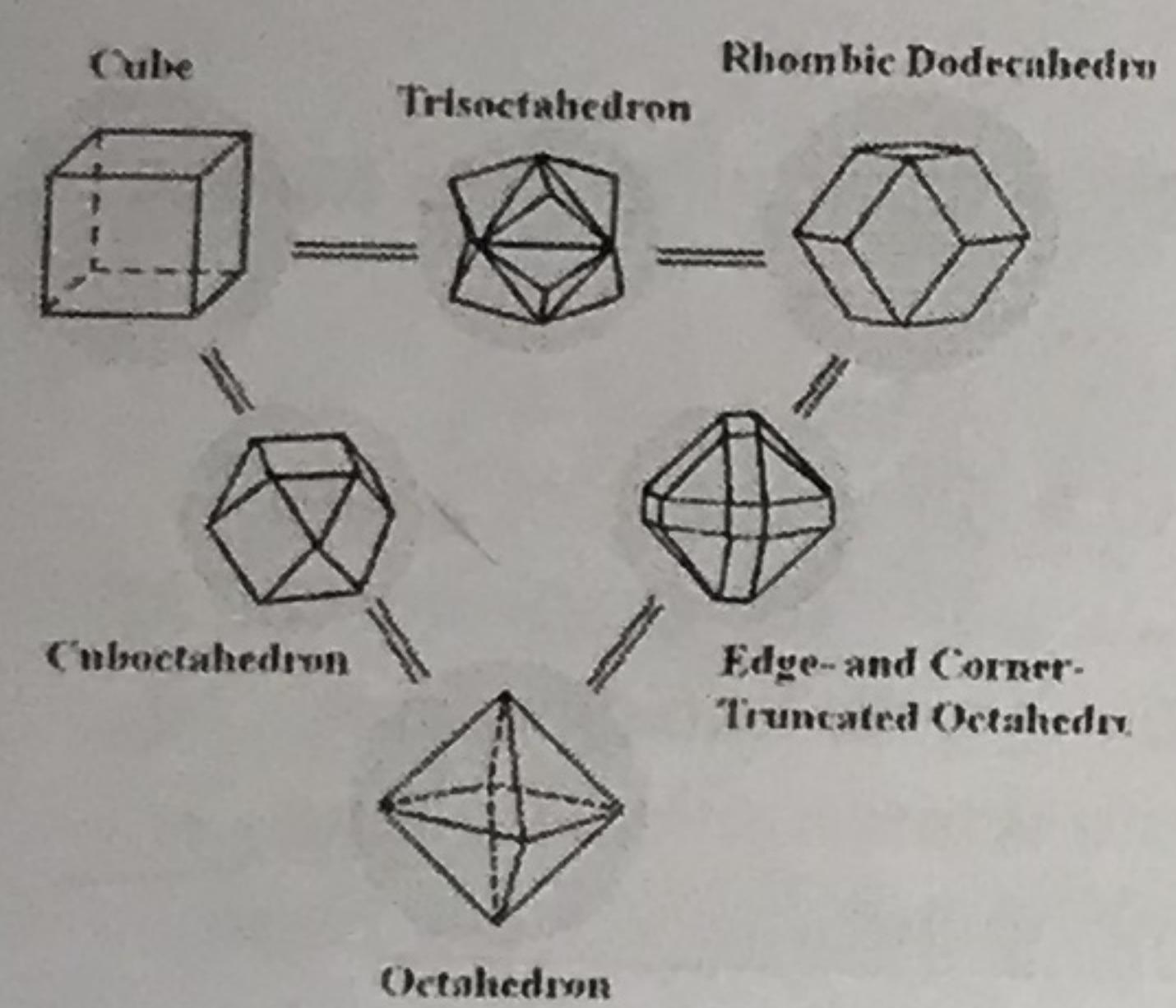
Face-Centered Cubic – h, k, l must be either all odd or all even

$$h^2 + k^2 + l^2 \rightarrow 3 \quad 4 \quad 8 \quad 11 \quad 12 \quad 16 \quad 19 \quad 20$$

(111) (200) (220) (311) (222) (400) (331) (420)

全單數 or 全奇數!

XRD patterns of Au
Rhombic Dodecahedra
to Octahedra

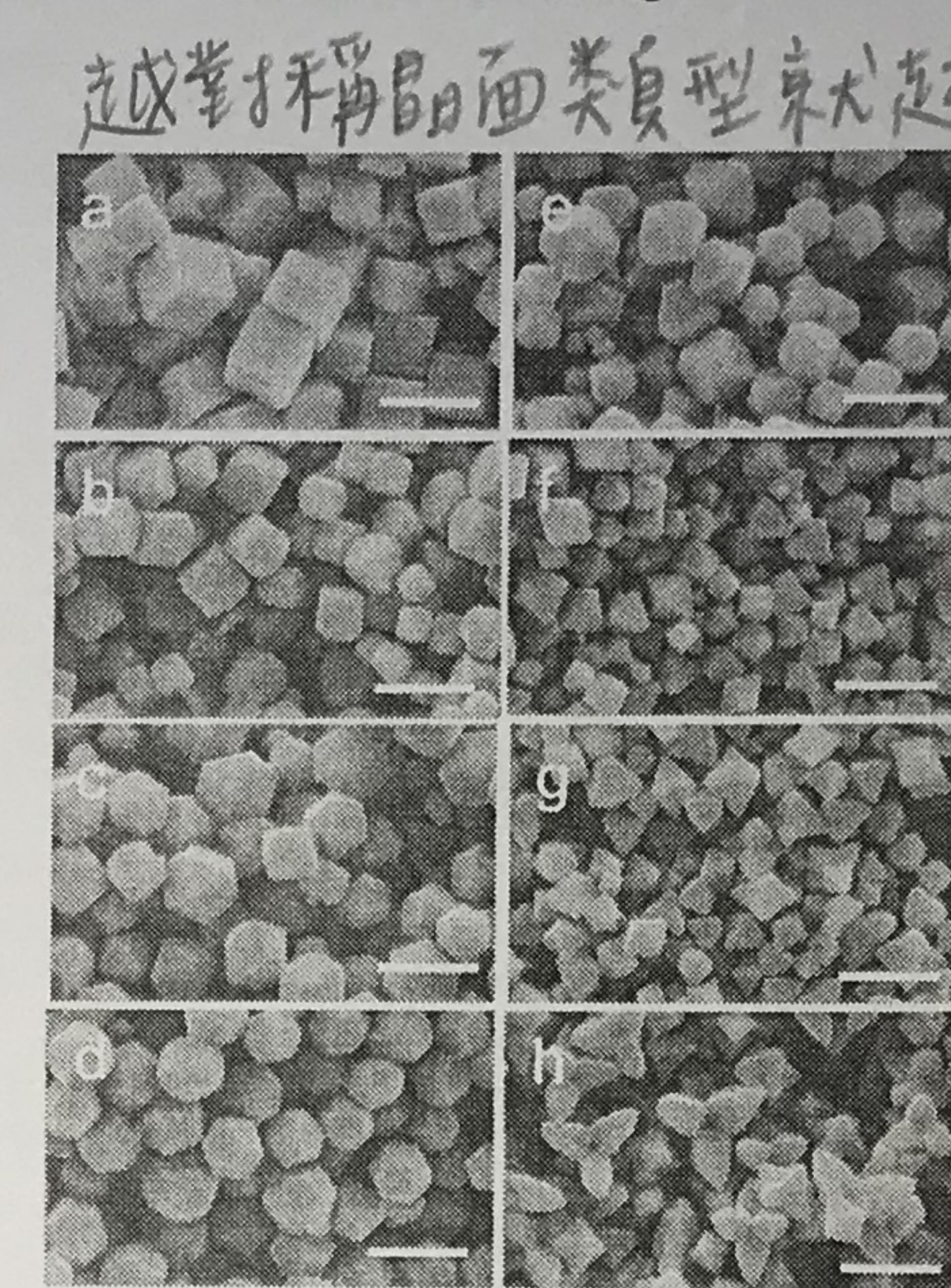


Chem.-Eur. J. 2011, 17, 9746

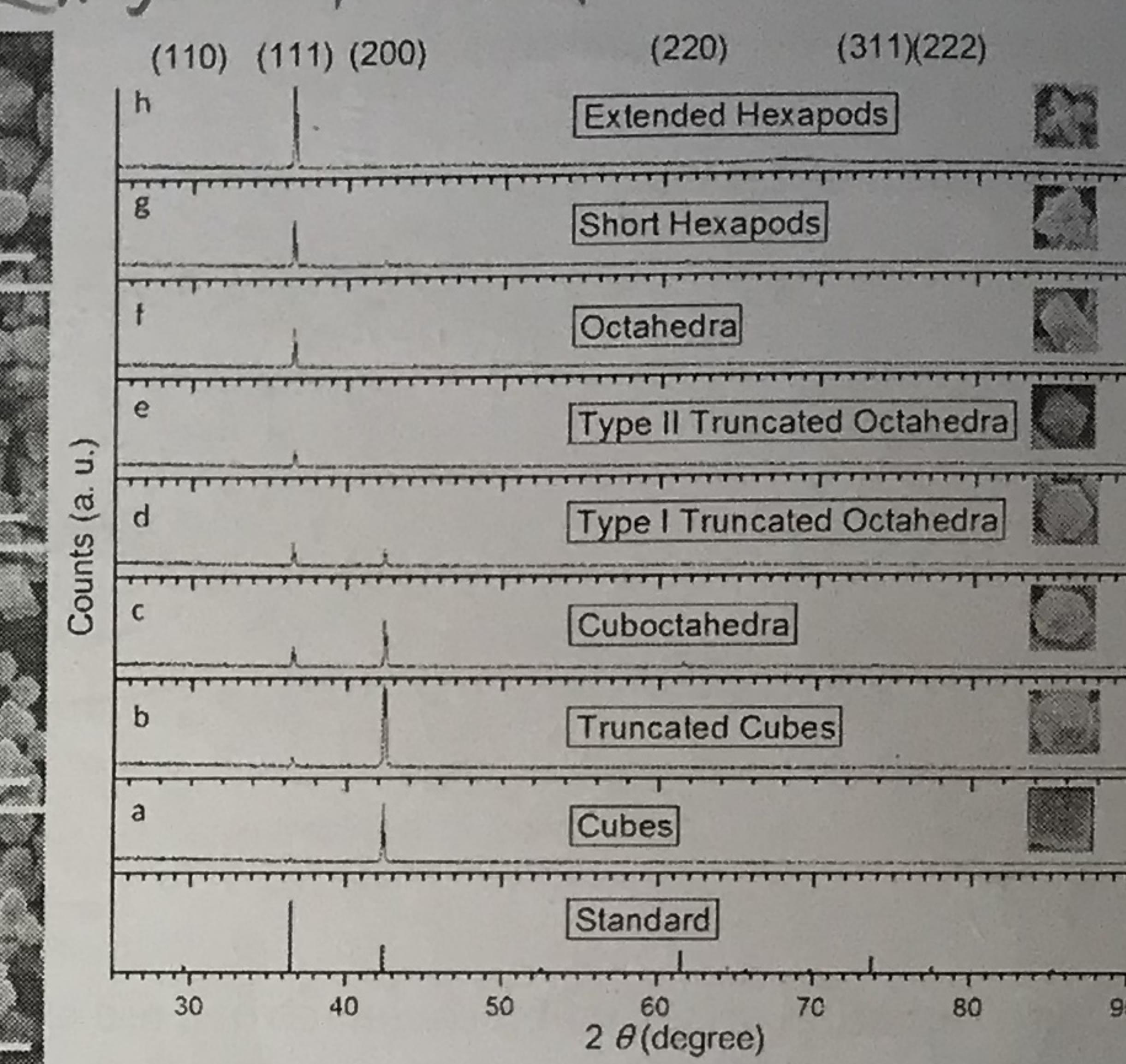
$$2d \sin\theta = n\lambda$$

濃度不一樣 peak 大小不同

Confirmation of High Particle Shape Uniformity by XRD Patterns

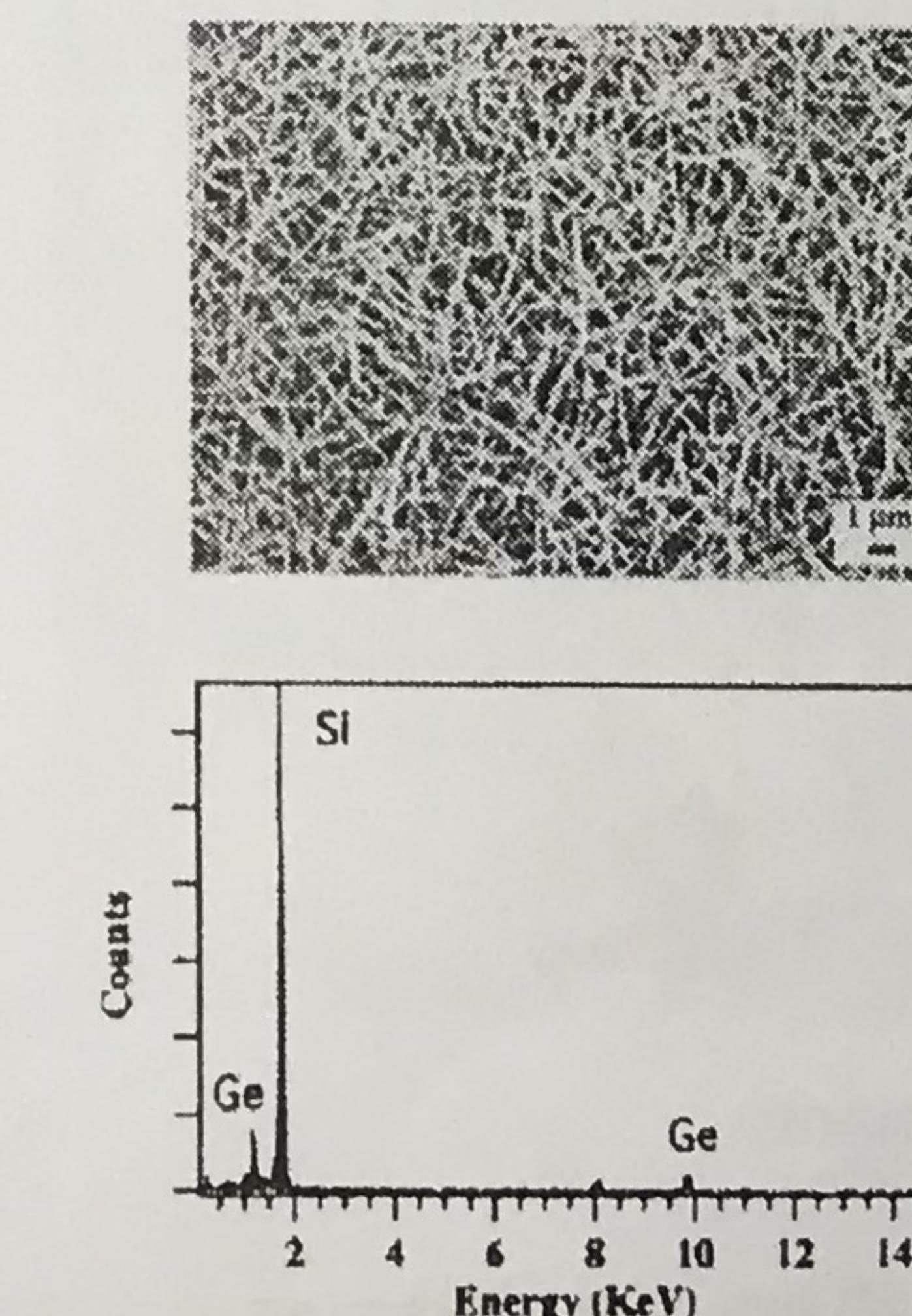


Cu₂O Cubes to Hexapods J. Phys. Chem. C 2009, 113, 14159



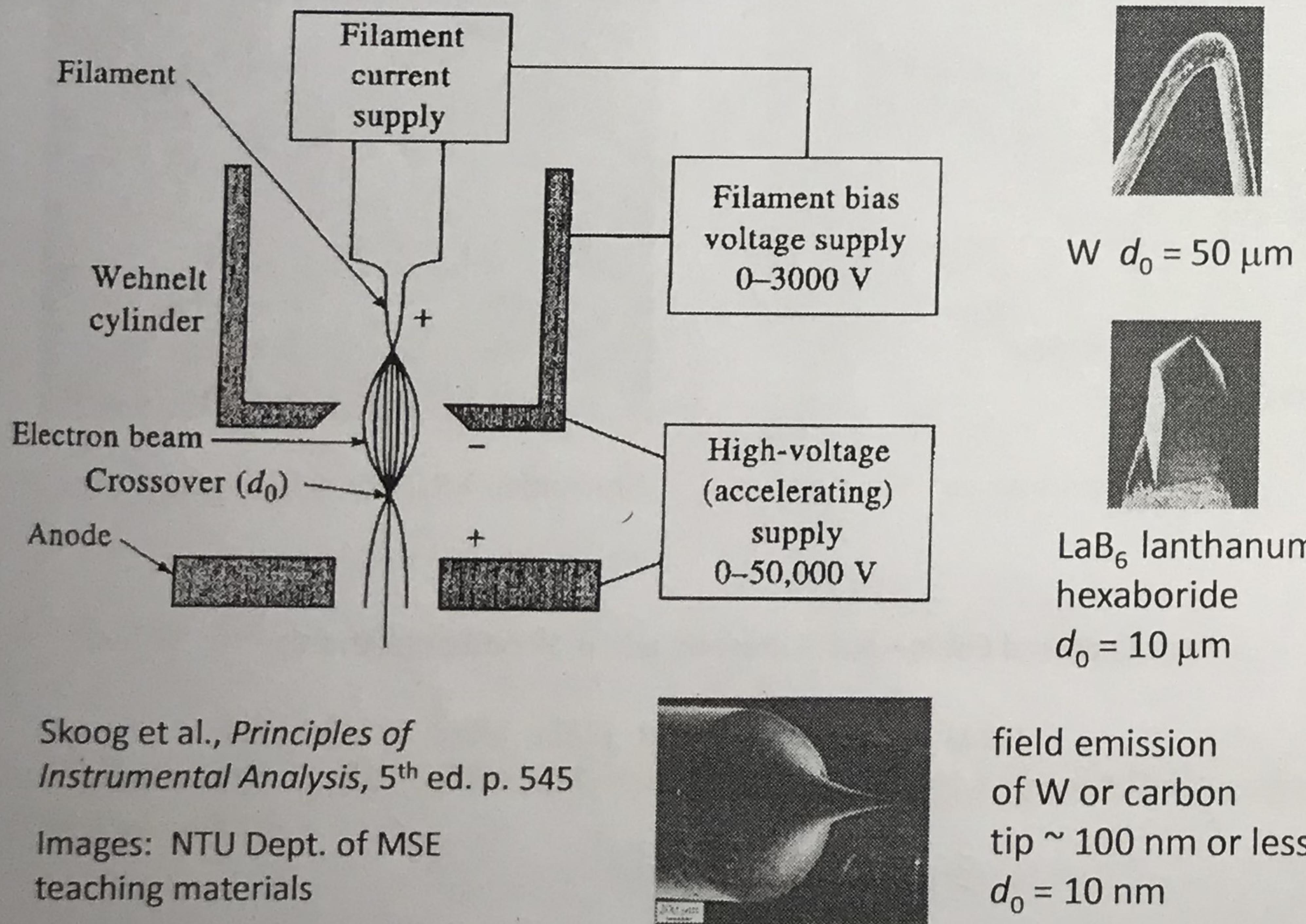
能見色散 X-ray

Schematic of SEM and EDS



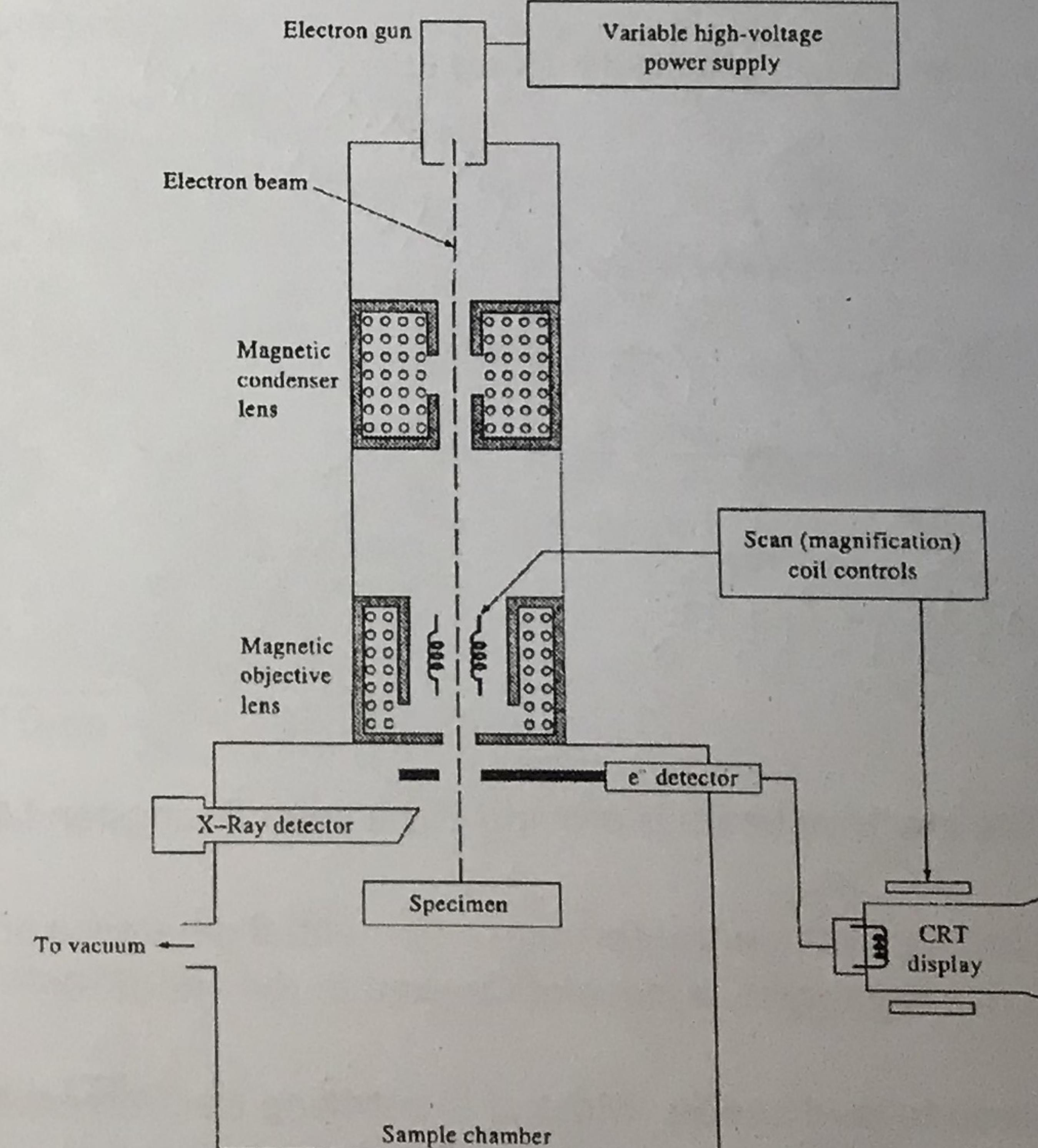
Skoog et al, Principles of
Instrumental Analysis, 5th ed. p. 551

Block Diagram of a Tungsten Filament Source for SEM (原理)



Skoog et al., Principles of
Instrumental Analysis, 5th ed. p. 545

Images: NTU Dept. of MSE
teaching materials



- 儀器中文名稱：熱場發射掃描式電子顯微鏡
- 儀器英文名稱：Thermal Type Field Emission Scanning Electron Microscope

● 儀器英文簡稱：FESEM

● 儀器背景說明：

儀器購置年月：2007年4月

儀器經費來源：教育部

廠牌及型號：日本JEOL，JSM-7000F

放置地點：清華大學化學館B24室

重要規格：

加速電壓：0.5 to 30 kV

放大倍率：30 to 250000

解像力：1.2 nm (30 kV), 1.5 nm (15 kV)

and 3.0 nm (1 kV)

電子槍：熱游離式Schottky ZrO/W gun ;

試片載台：X-Y: 70 × 50 mm, WD: 4 to

40 mm, Rotation: 360° Tilting: -5 to 70°

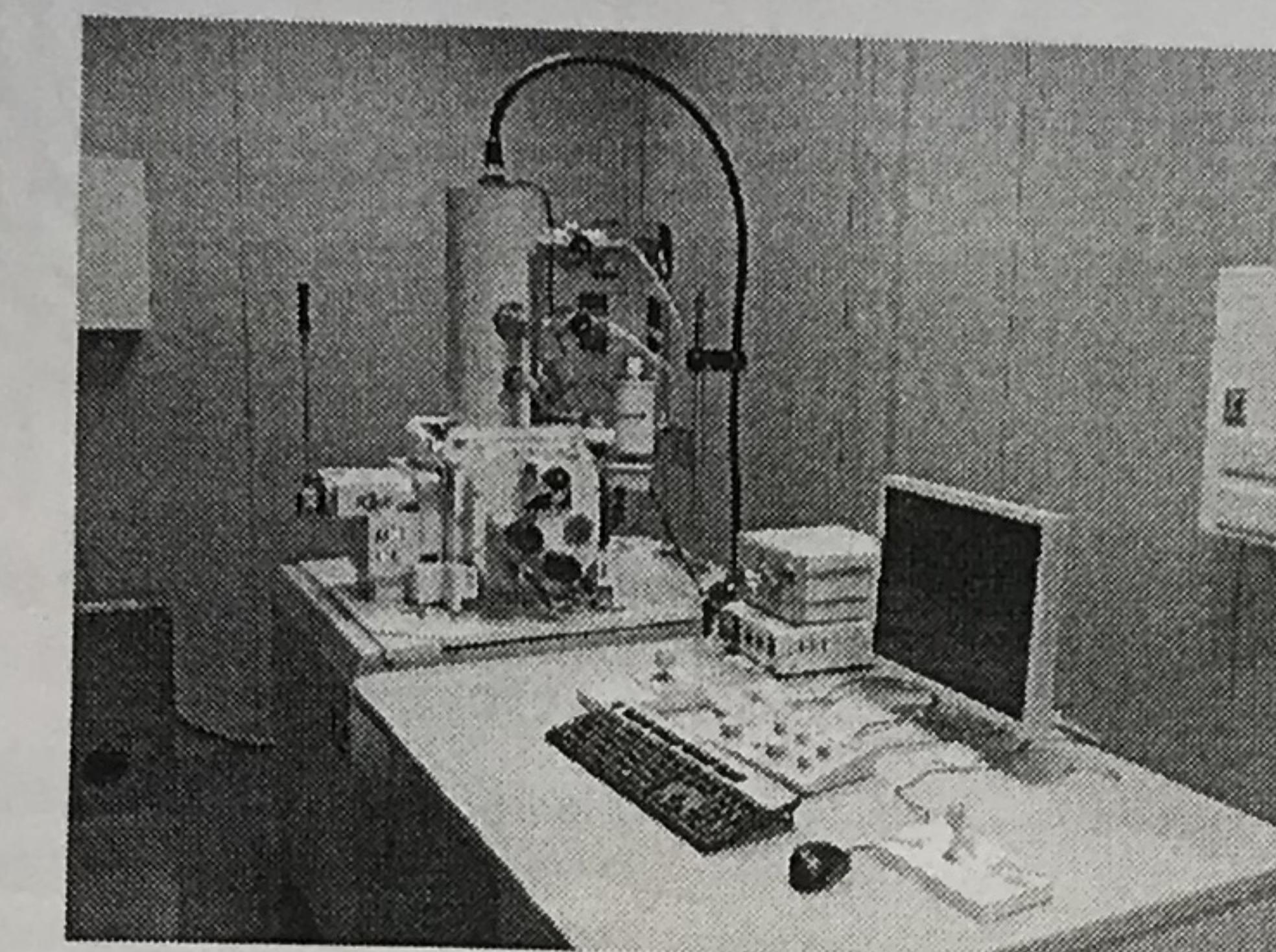
主要附件：

EDX (化學元素定性、定量和分佈影像分析)。

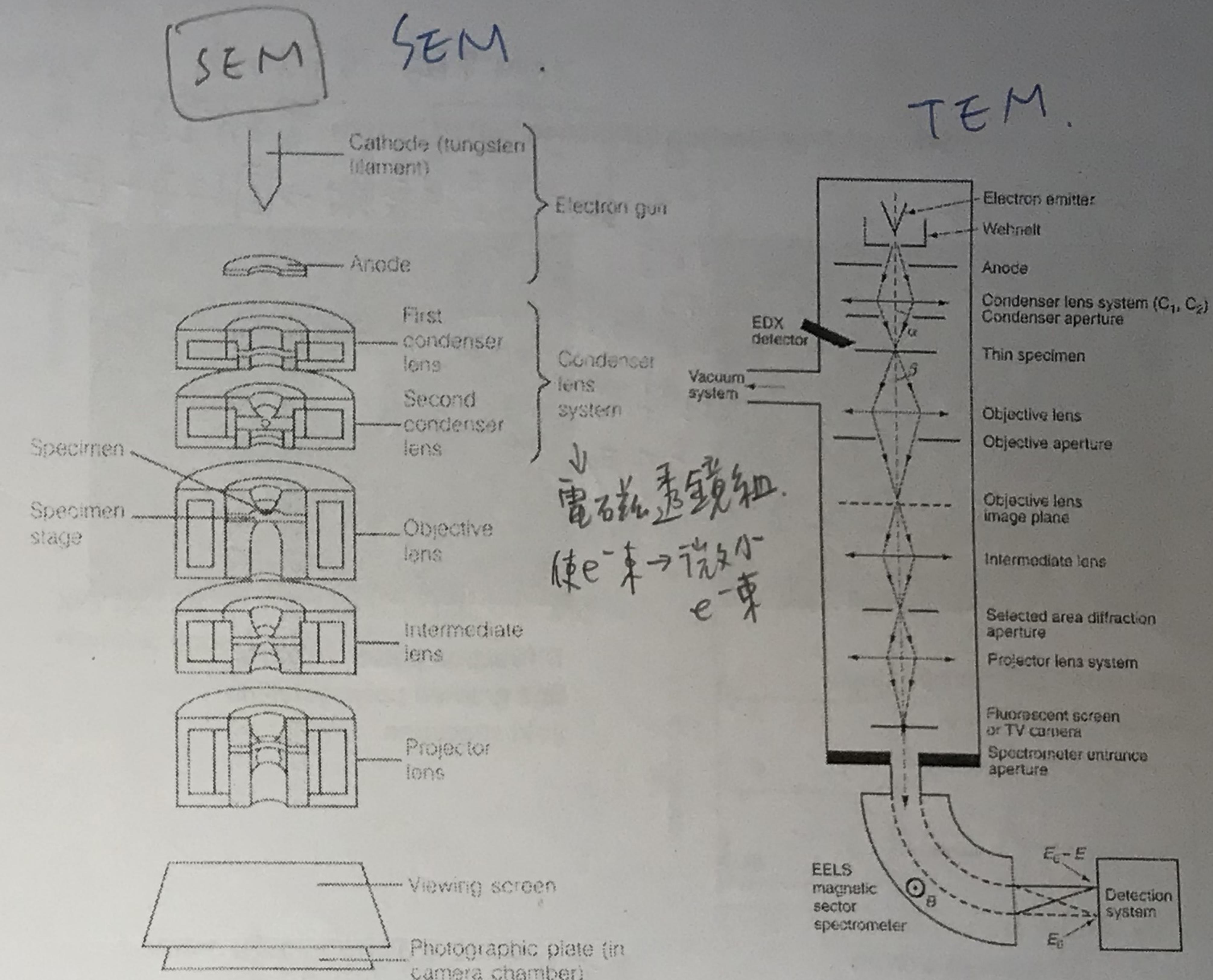
真空蒸鍍器 (Pt evaporator)。

擴充功能：1. EBSP 2. EB-writer 3.

Cathodoluminescence system



高能e-束+二次電子、背向散射e-



TEM

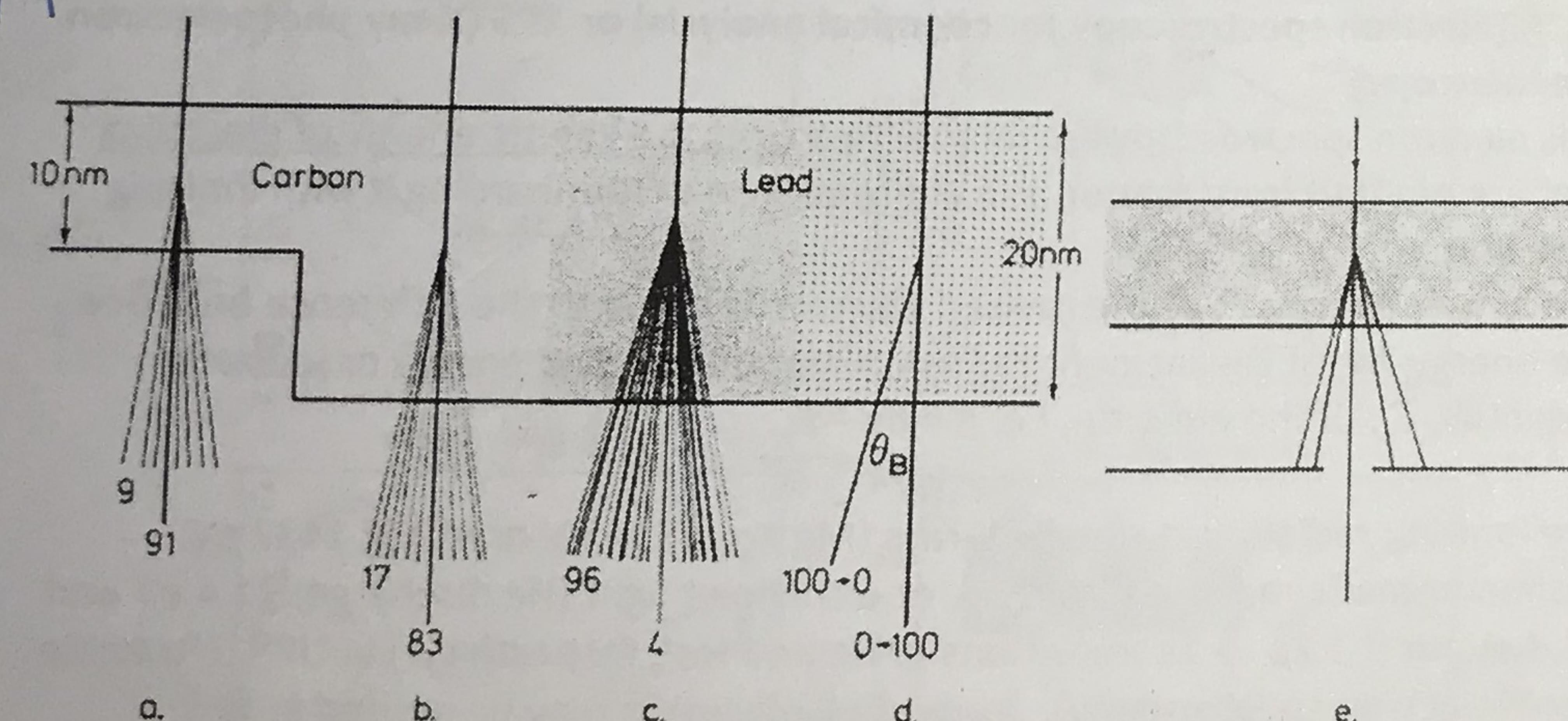


Fig. 1. The fate of 100 electrons falling on four different regions of a hypothetical specimen. The numbers shown are those scattered through more than 0.5° and those unscattered. The regions are as follows: (a) 10 nm of amorphous carbon; (b) 20 nm of amorphous carbon; (c) 20 nm of amorphous lead; (d) 20 nm of crystalline lead; (e) the effect of inserting an objective aperture to stop all electrons scattered through more than about 0.5°.

Brightness ratios of a, b and c = 91 : 83 : 4

The Operation of Transmission Electron Microscope, Dawn Chescoe and Peter J. Goodhew
Royal Microscopical Society Microscopy Handbooks 02

儀器中文名稱：高解析穿透式電子顯微鏡

- 儀器英文名稱：High Resolution Transmission Electron Microscope

● 儀器英文簡稱：HRTEM

● 儀器背景說明：

儀器購置年月：2007年4月

儀器經費來源：教育部

廠牌及型號：日本JEOL，JEM-2100

放置地點：清華大學化學館B24室

重要規格：

加速電壓：80–200 KV

放大倍率： $\times 2000$ – $1,500,000$

解像力：point image: 0.23 nm ,
Lattice image: 0.14 nm

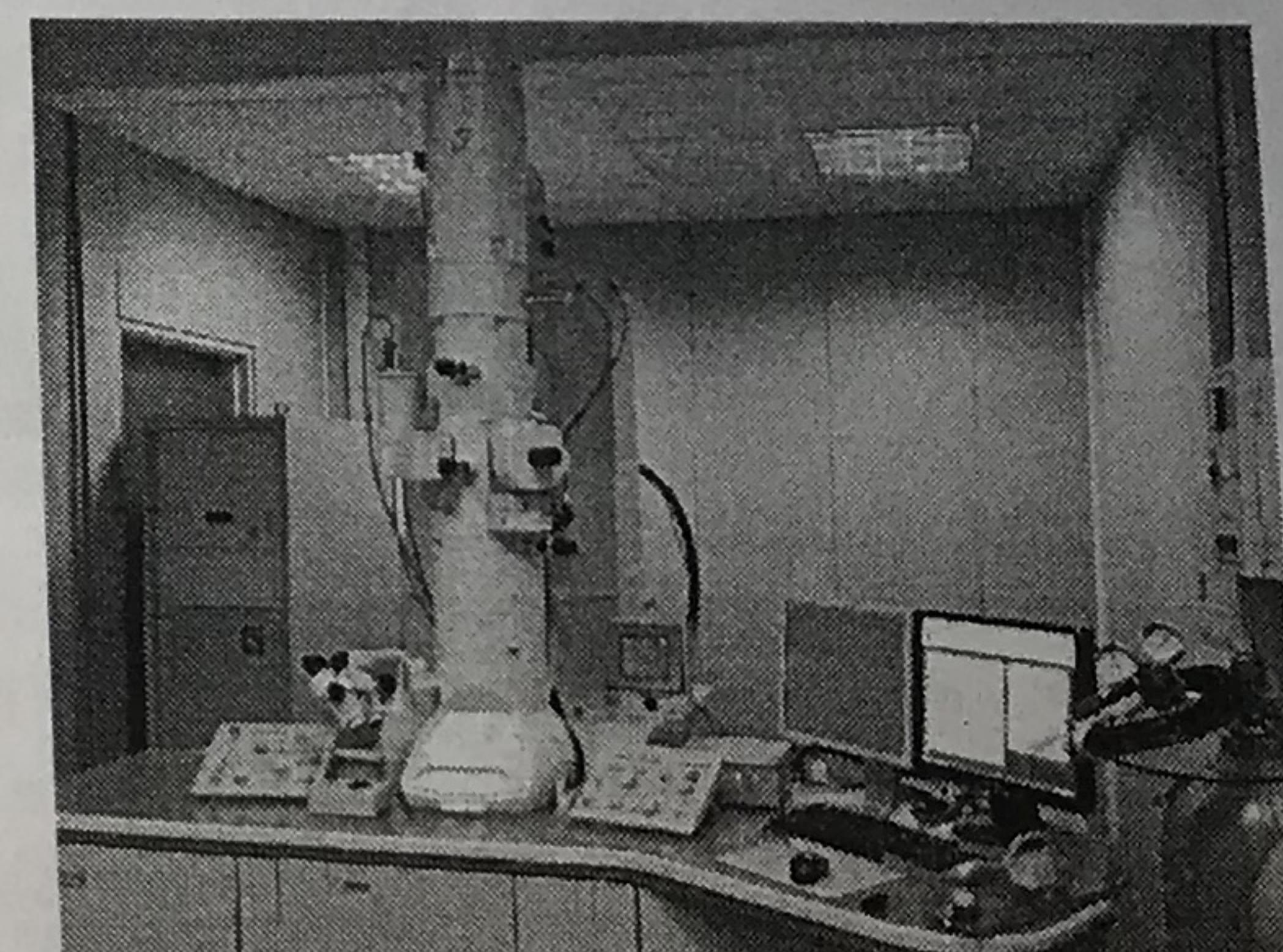
雙傾斜基座：X軸 $\pm 30^\circ$ ；Y軸 $\pm 30^\circ$ 。

主要附件：

Gatan CCD 832 digital detector
double、single tilt specimen
holder

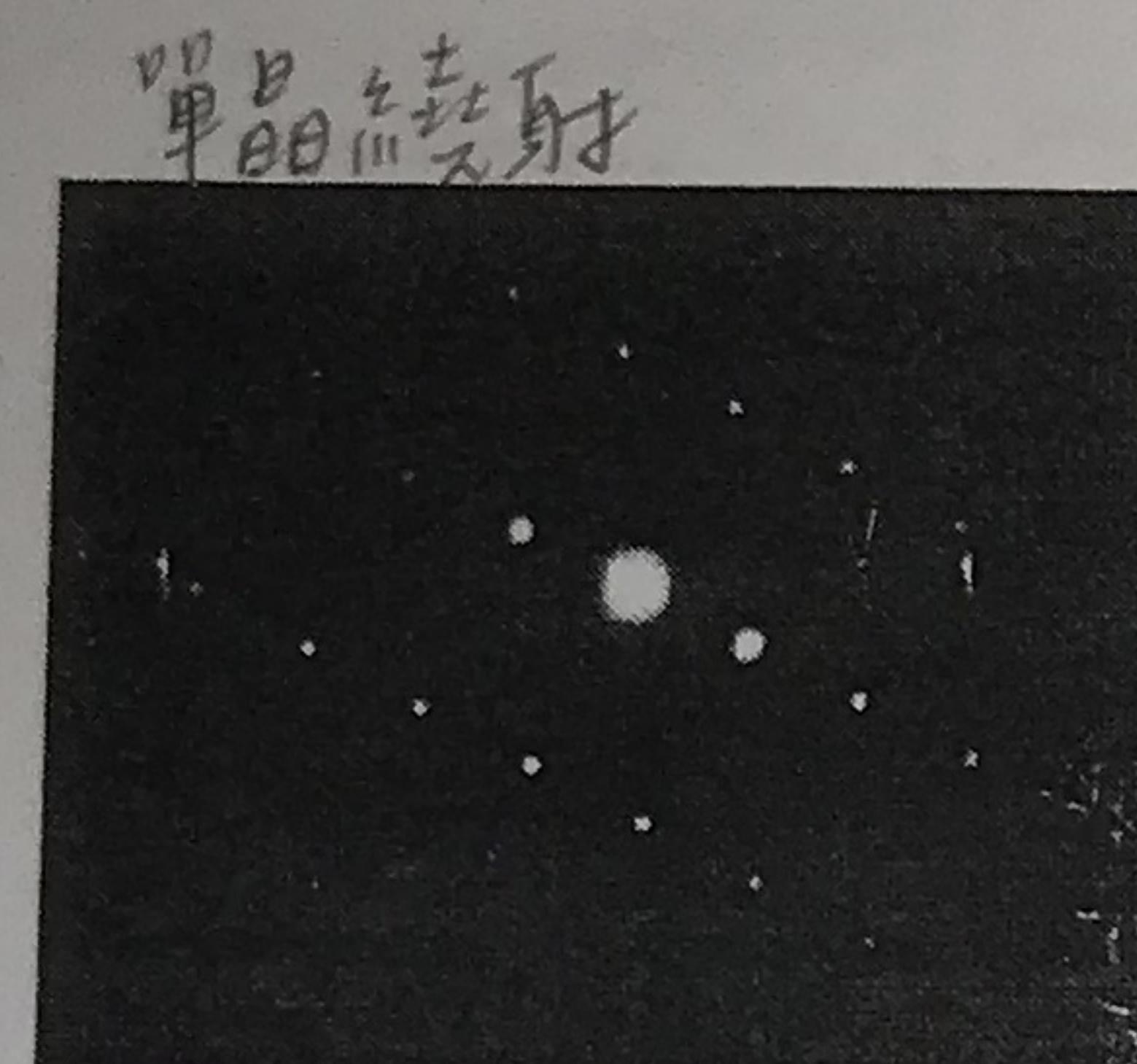
儀器性能：

材料試片表面組構(morphology)、斷面、
微細組織、晶體結構、缺陷觀察。

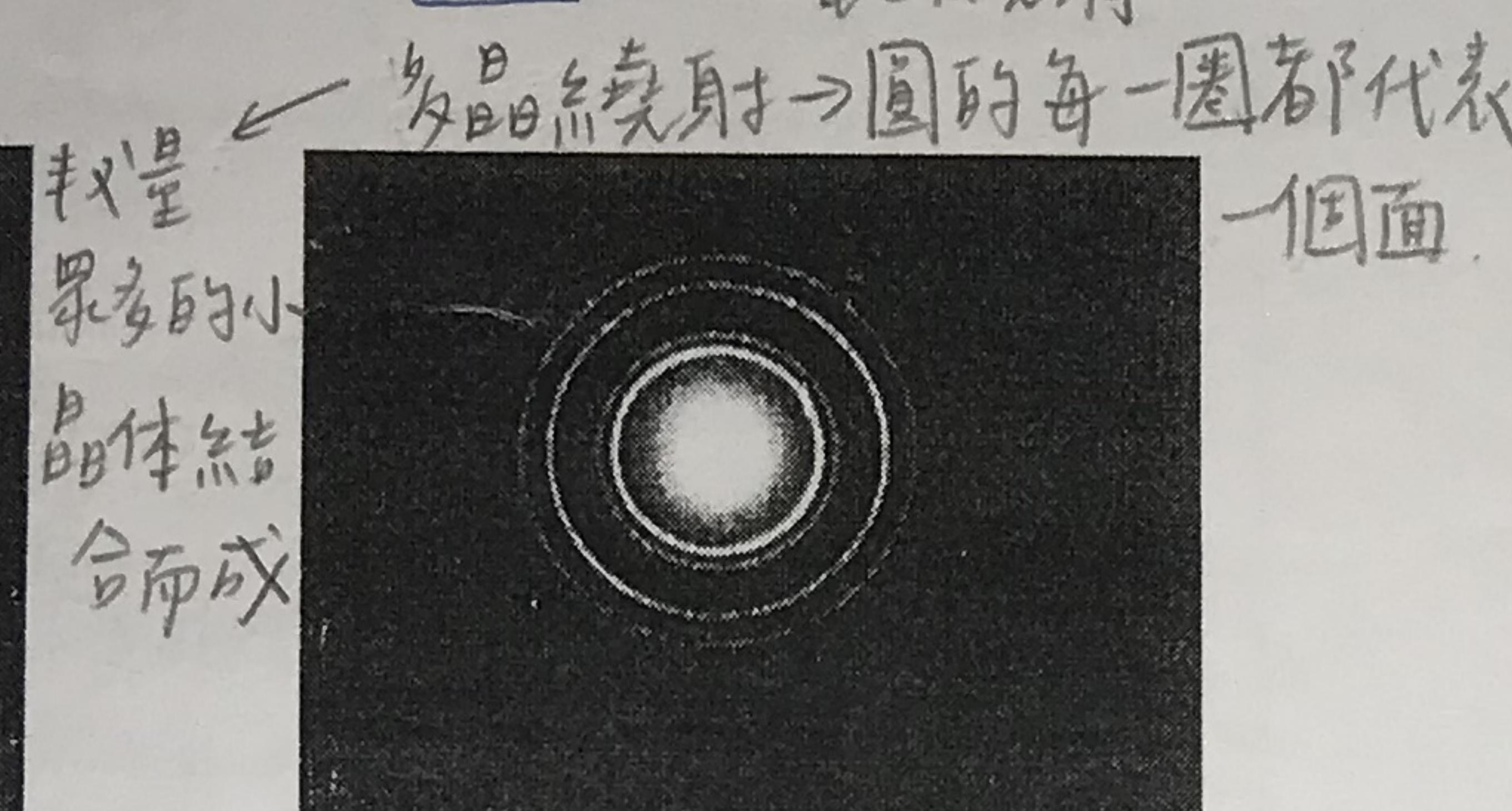


TEM 中的一项分析方法

Selected-Area Electron Diffraction (SAED) Pattern 電子繞射.

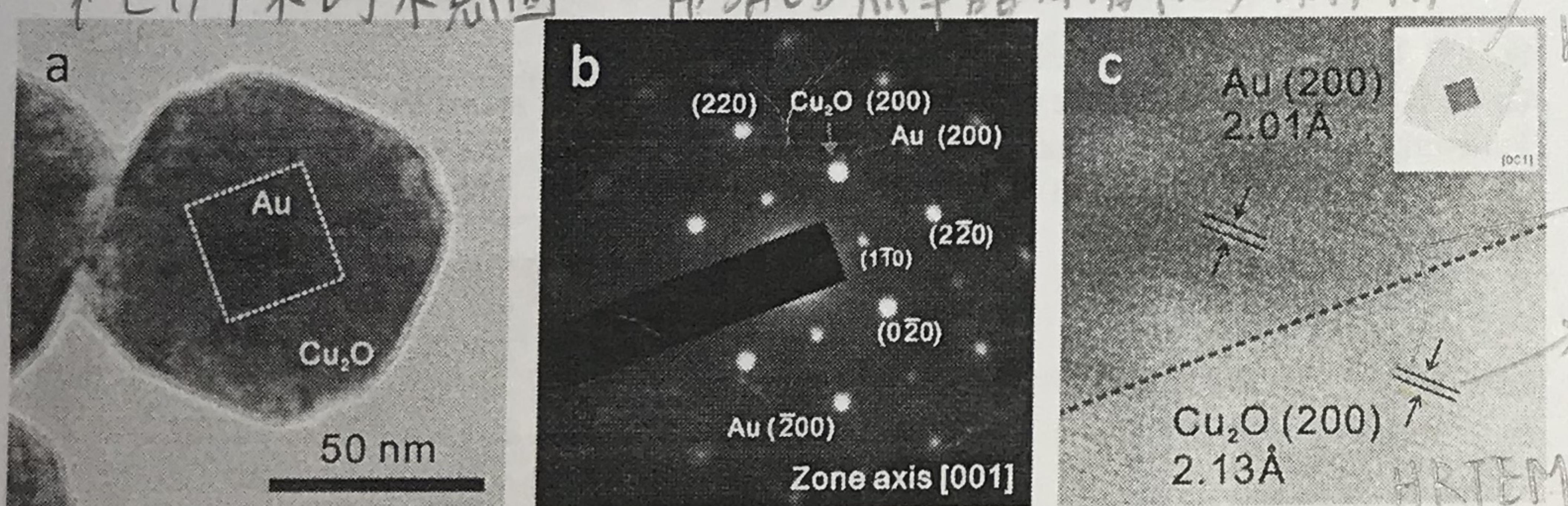


Diffraction pattern of a single crystal of aluminum



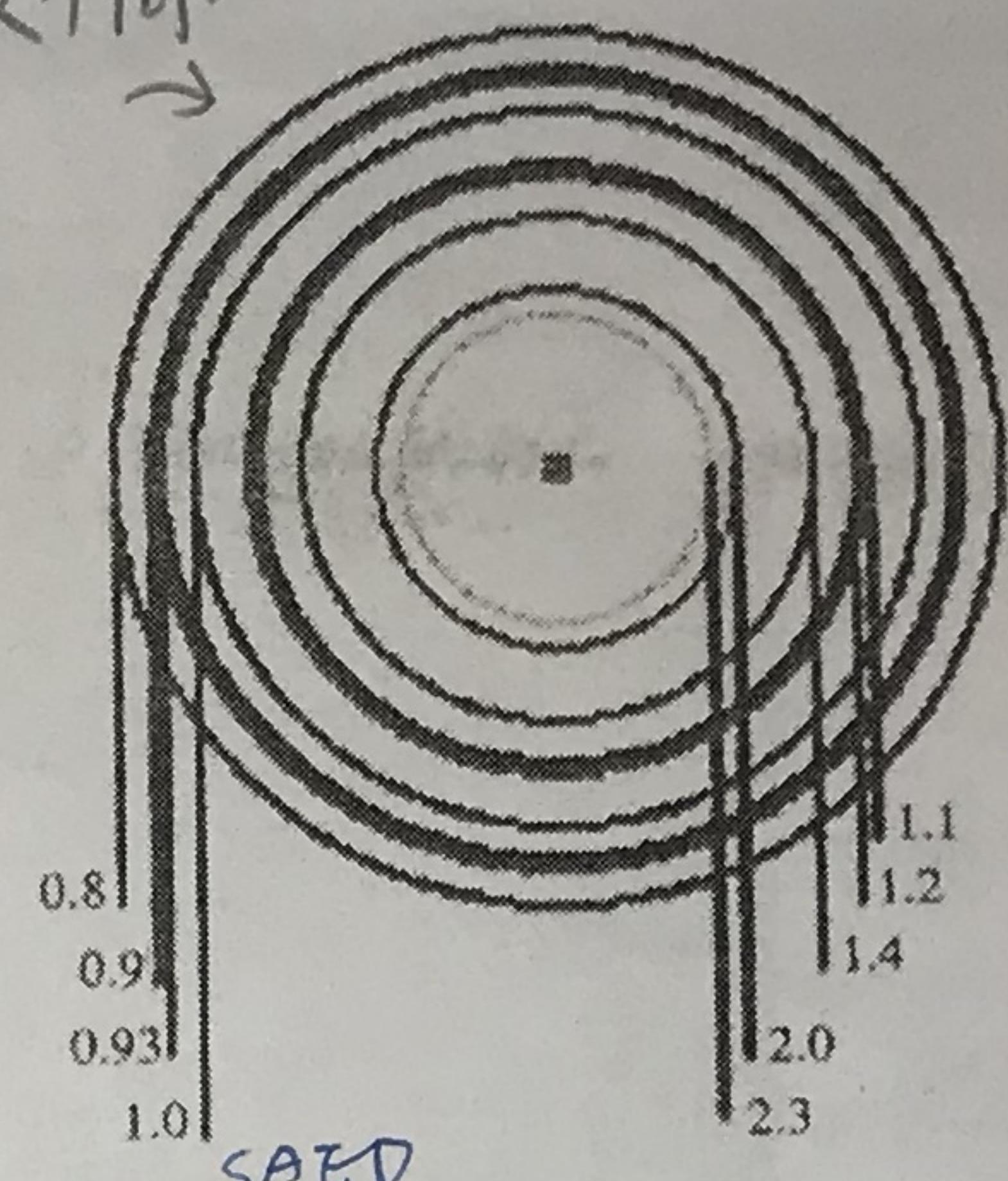
Diffraction pattern from a fine grained polycrystalline gold specimen

包在外面 → 照出來較亮
延(1,0,0)方向可看見 Au , Cu_2O . 大的是 Cu_2O , 小的是 Au .
↑ ETD 下來的示意圖
用 SAED 見單晶體有很多不同方向.



TEM analysis of a single $\text{Au}-\text{Cu}_2\text{O}$ core-shell nanocube. (a) TEM image of a $\text{Au}-\text{Cu}_2\text{O}$ nanocube viewed along the $[100]$ direction. The white dotted line indicates the outline of the octahedral Au nanocrystal core. (b) SAED pattern of this nanocube giving both Au and Cu_2O diffraction spots. (c) High-resolution TEM image of the red square region. The red dotted line marks the interfacial region between Au and Cu_2O . The Au (200) and Cu_2O (200) lattice planes are aligned along the same direction and parallel to the $\{100\}$ faces of the Cu_2O shell. Insets gives a schematic drawing the particle viewed along the $[001]$ zone axis.

繞射角度不同.



HKL	d (Å)
(111)	2.33
(002)	2.02
(220)	1.43
(311)	1.22
(222)	1.16
(004)	1.01
(313)	0.92
(042)	0.90
(422)	0.82

最佳圓的距離值
不同 \rightarrow 不同面

Figure 2.47 Selected-area electron diffraction pattern obtained from a polycrystalline aluminium specimen. Since the average aluminium grain size is much smaller than the selected area, a 'ring' pattern is formed. The measured d -spacings of the rings are indicated on the pattern, and a table of d -spacings for different planes in aluminium is also given.

To calculate d , use $r d = L \lambda$ where r is the radius distance, L is the camera length, λ is the electron wavelength ($L \lambda$ = camera constant)

$$rd = \text{Const.}$$

polycrystalline

core cell 結構 才能看到邊界.

ESCA (electron spectroscopy for chemical analysis) or XPS (X-ray photoelectron spectroscopy)

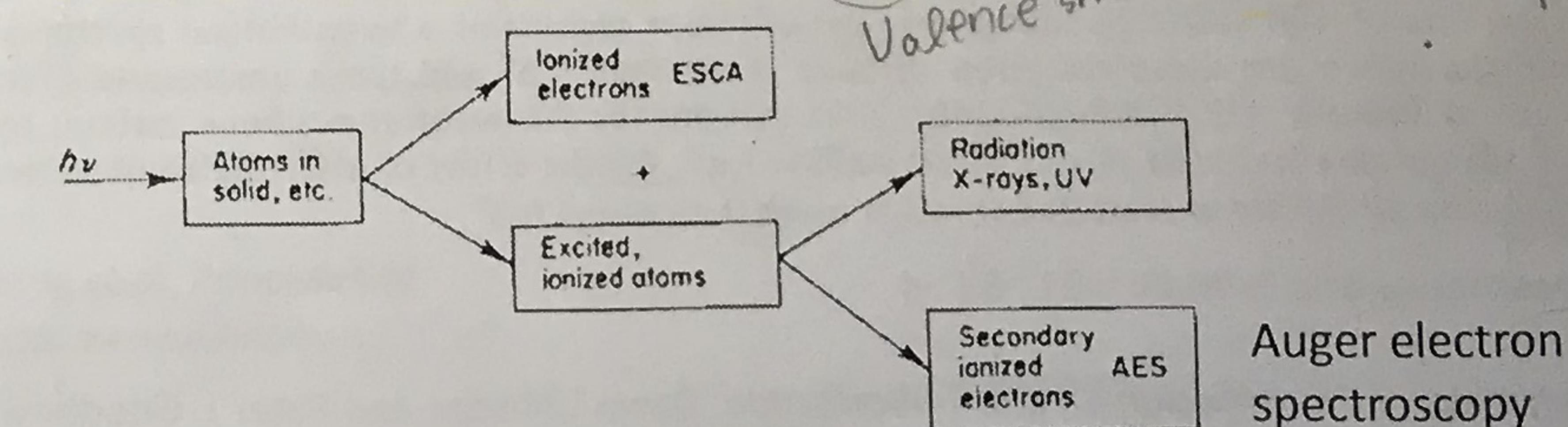
This electron spectroscopy technique measures the kinetic energy of electrons that are emitted from matter as a consequence of bombarding it with ionizing radiation.

The kinetic energy, E , of the ionized electron is equal to the difference between the energy, hv , of the incident radiation and the binding energy or ionization potential, E_b , of the electron, i.e. $E = hv - E_b$.

轉移能.

The ionizing radiation is usually X-rays (Mg $K\alpha$, 1254 eV or Al $K\alpha$, 1487 eV monochromatic radiation) for XPS, or ultraviolet light (He discharge, 21.4 eV and 40.8 eV for the $2p \rightarrow 1s$ transitions in He and He^+ , respectively) in UPS (ultraviolet photoelectron spectroscopy). Inner shell electrons may be ionized in XPS.

Valence shell electrons may be ejected in UPS.



Auger electron spectroscopy

Figure 6.5 Two layers of close-packed atoms shown (a) with the spheres touching, and (b) with the sizes of the spheres reduced. octahedral tetrahedral
lines are visible. In (b), the tetrahedral and

Chemical state
Cu metal
Cu (I) oxide
Cu (II) oxide
Cu (II) carbonate dihydroxide

ESCA

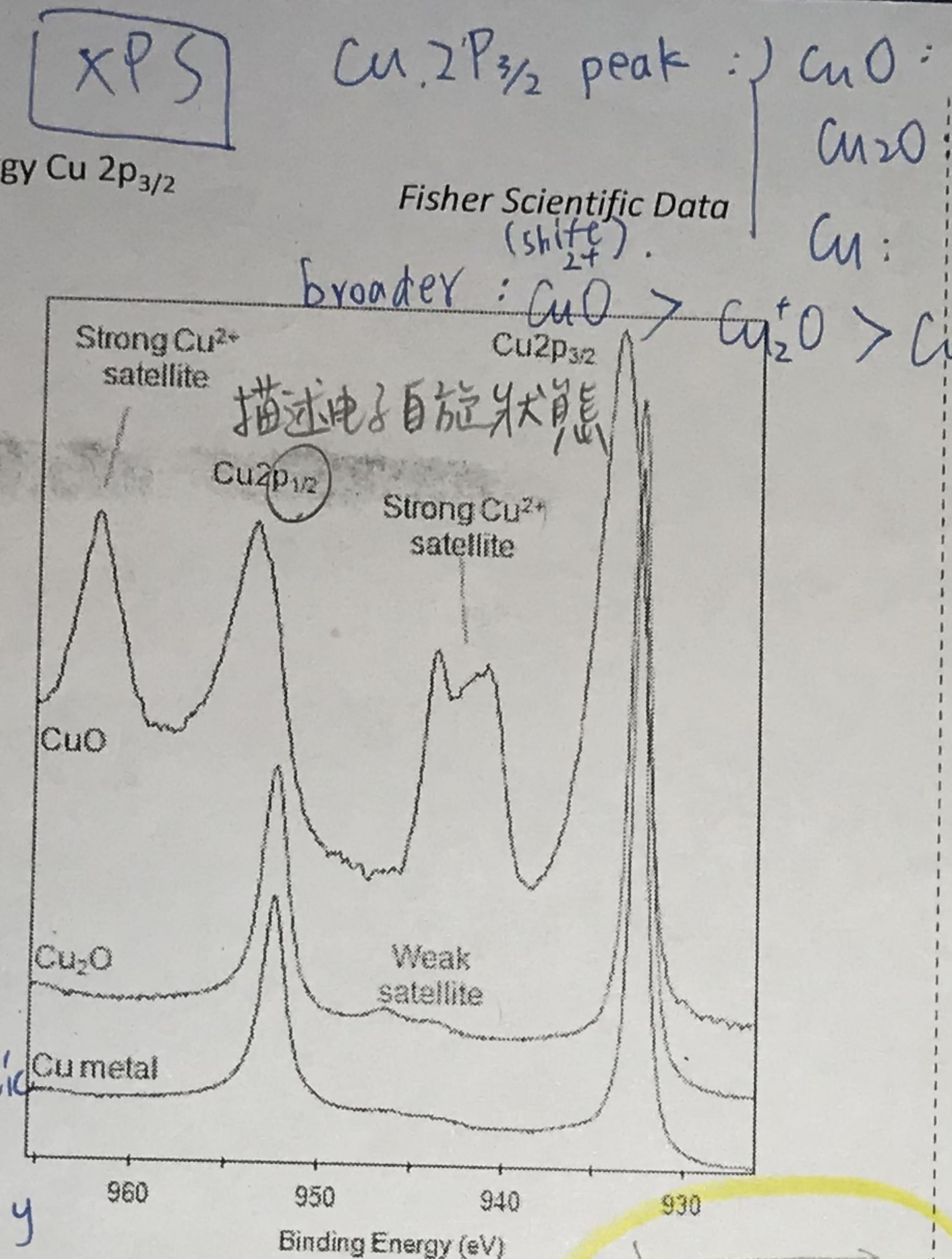
Interpretation of XPS spectra
It is possible to distinguish Cu oxidation states using satellite features of Cu 2p.

Cu (II) has observable collection of satellite features at ~ 943 eV.
Cu 2p_{3/2} peak in Cu (II) oxide is shifted and is much broader compared to Cu (I) oxide. In Cu (I) oxide, there is only a very weak satellite at 945 eV.

Cu 2p_{3/2} peak in Cu (I) oxide is NOT shifted but is broader compared to Cu metal.

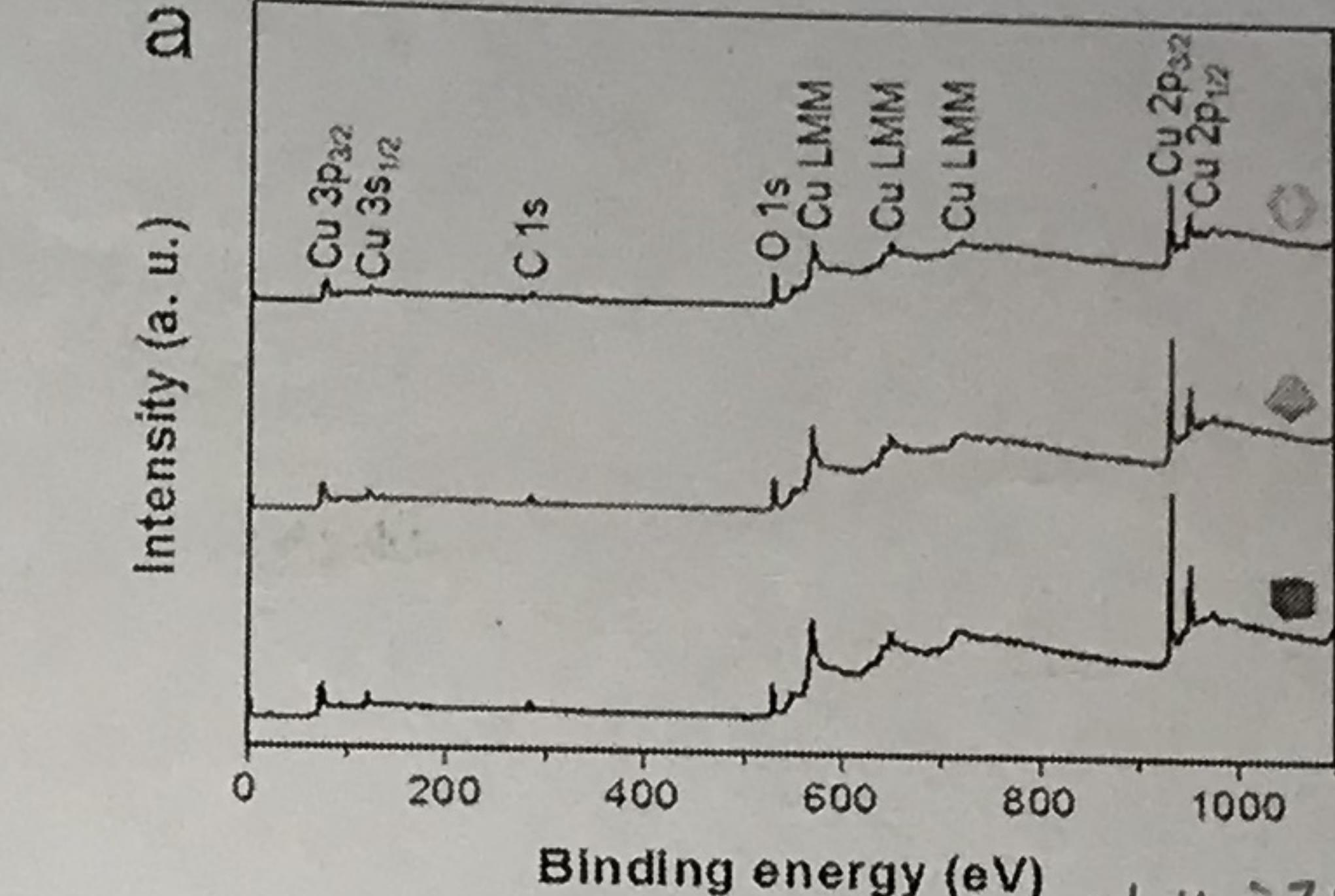
core ionization energies have characteristic values for a given element.

can be applied for the detection of any element except for hydrogen, also be used to differentiate between oxidation states of an element.

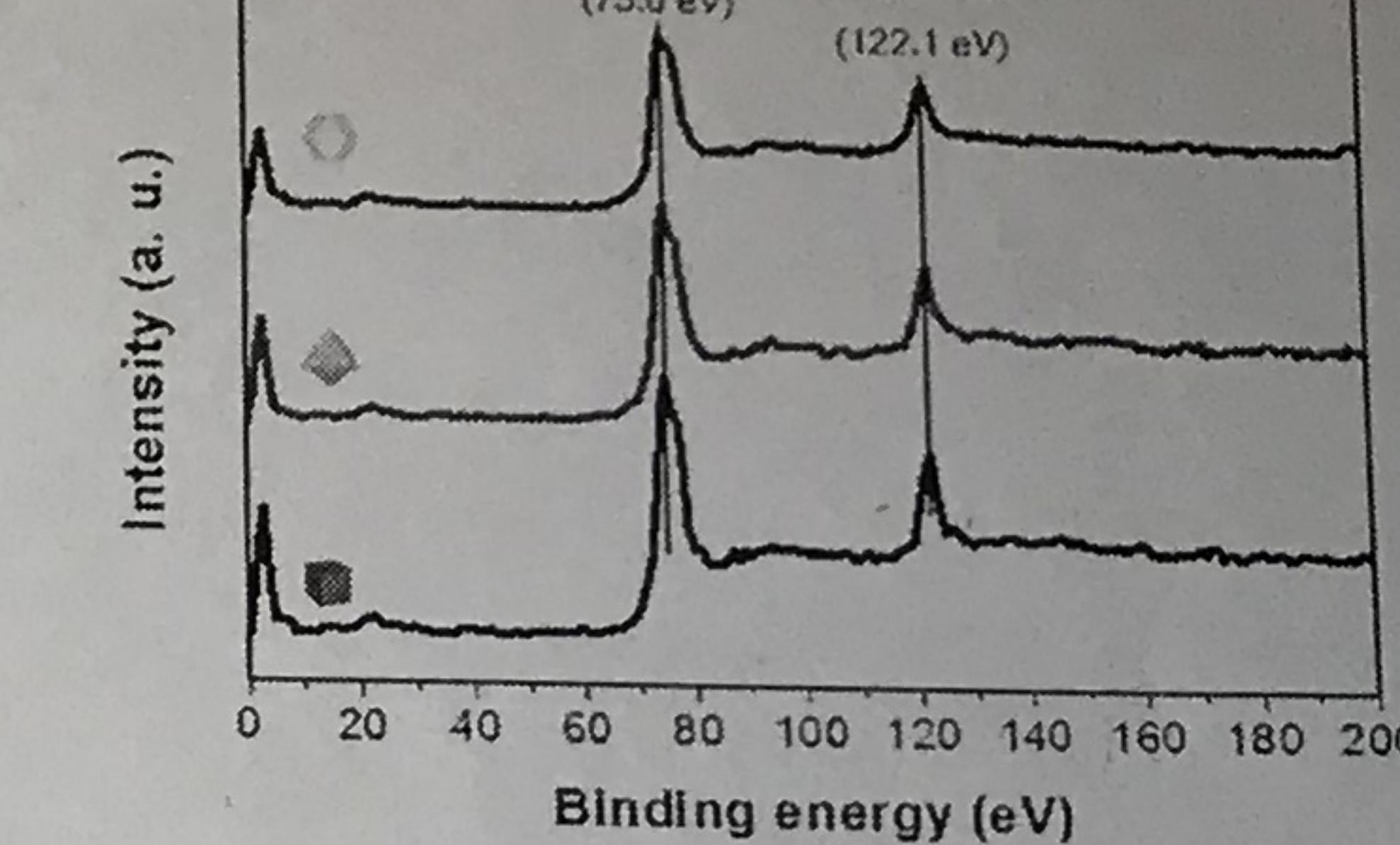
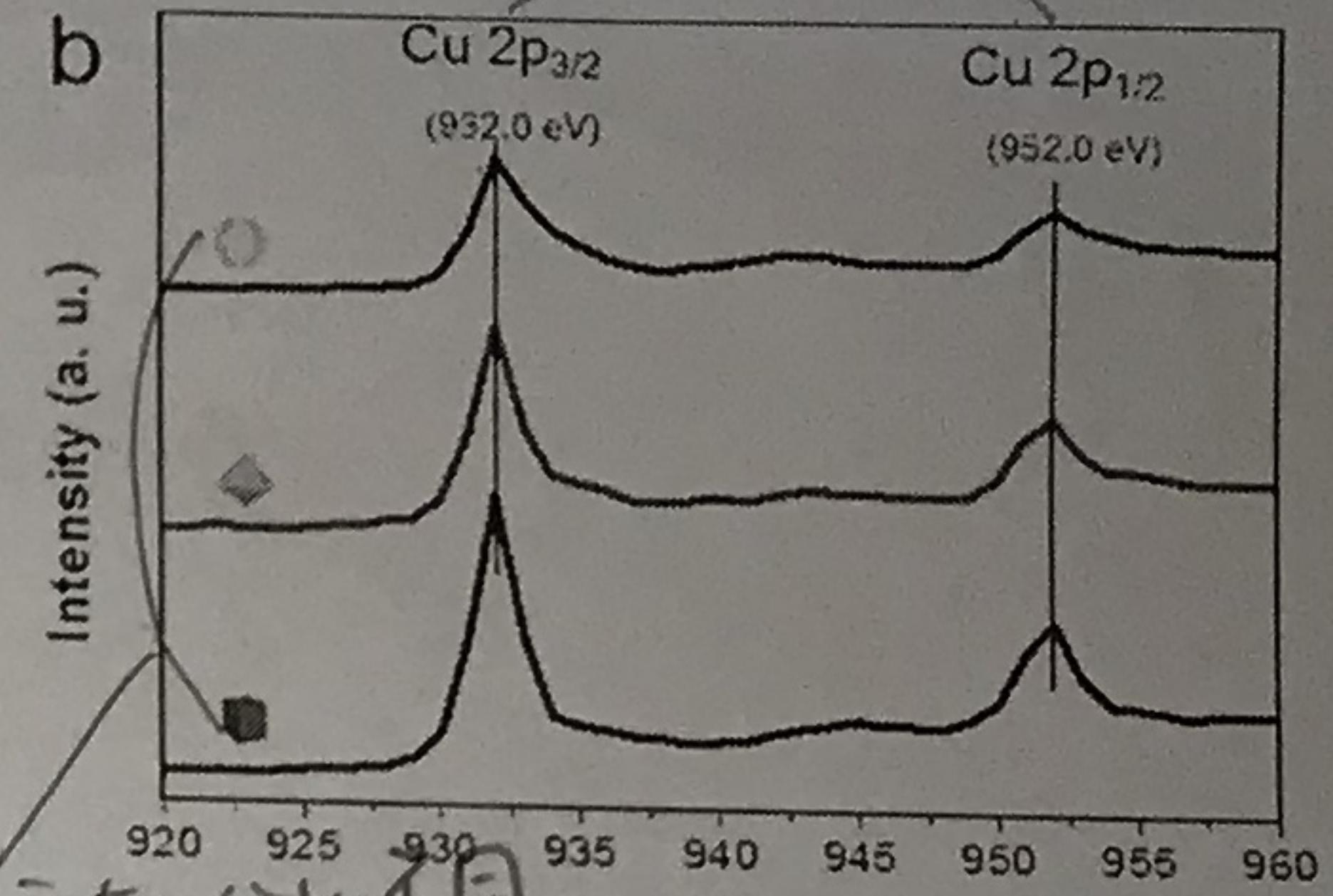


CuO : shift much broader
Cu₂O : broader
Cu :

a



XPS spectra of Cu₂O cubes, octahedra, and rhombic dodecahedra.



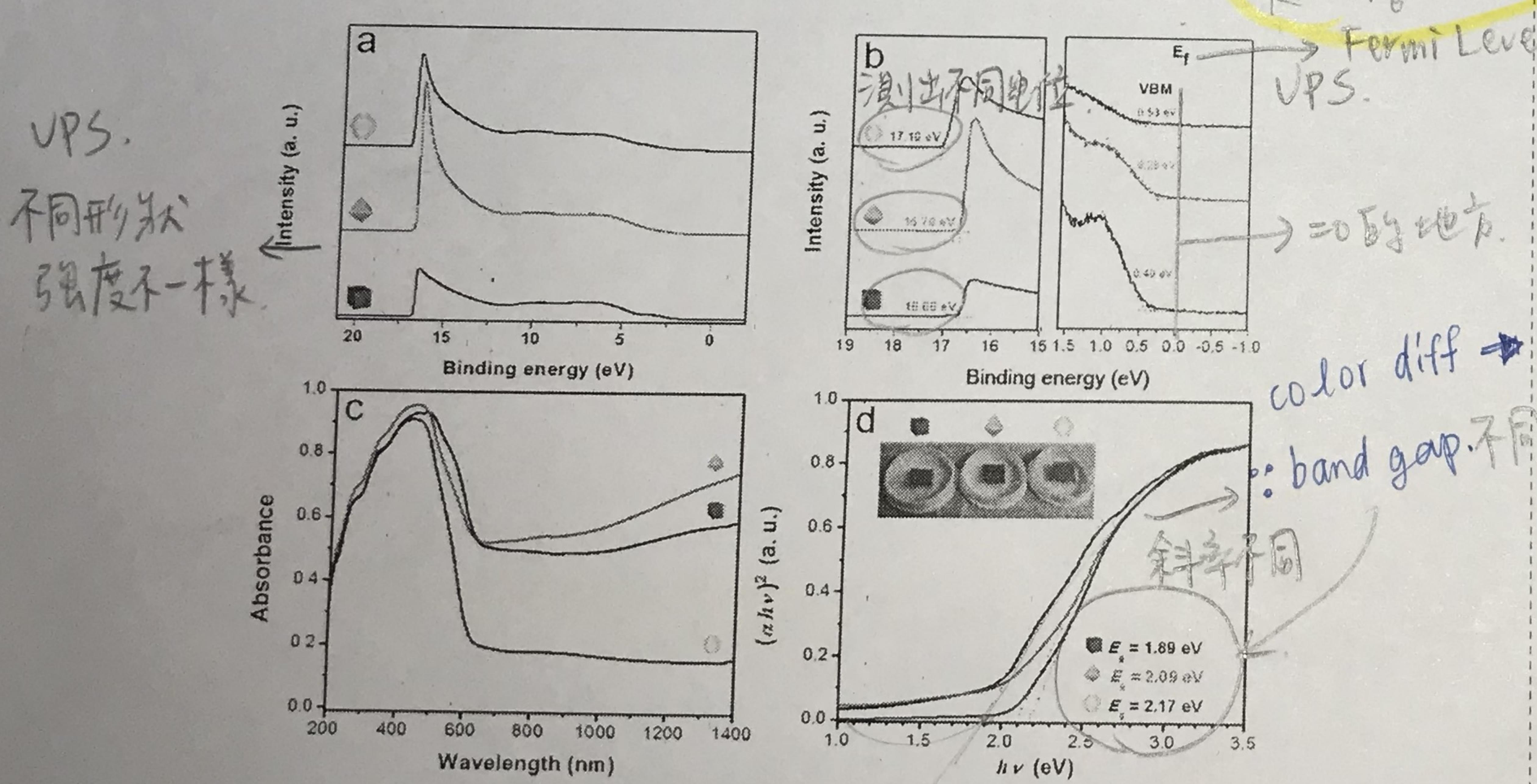
J. Mater. Chem. A 2017, 5, 15116.

下面三個

都是 Cu₂O → Fermi level 相同.

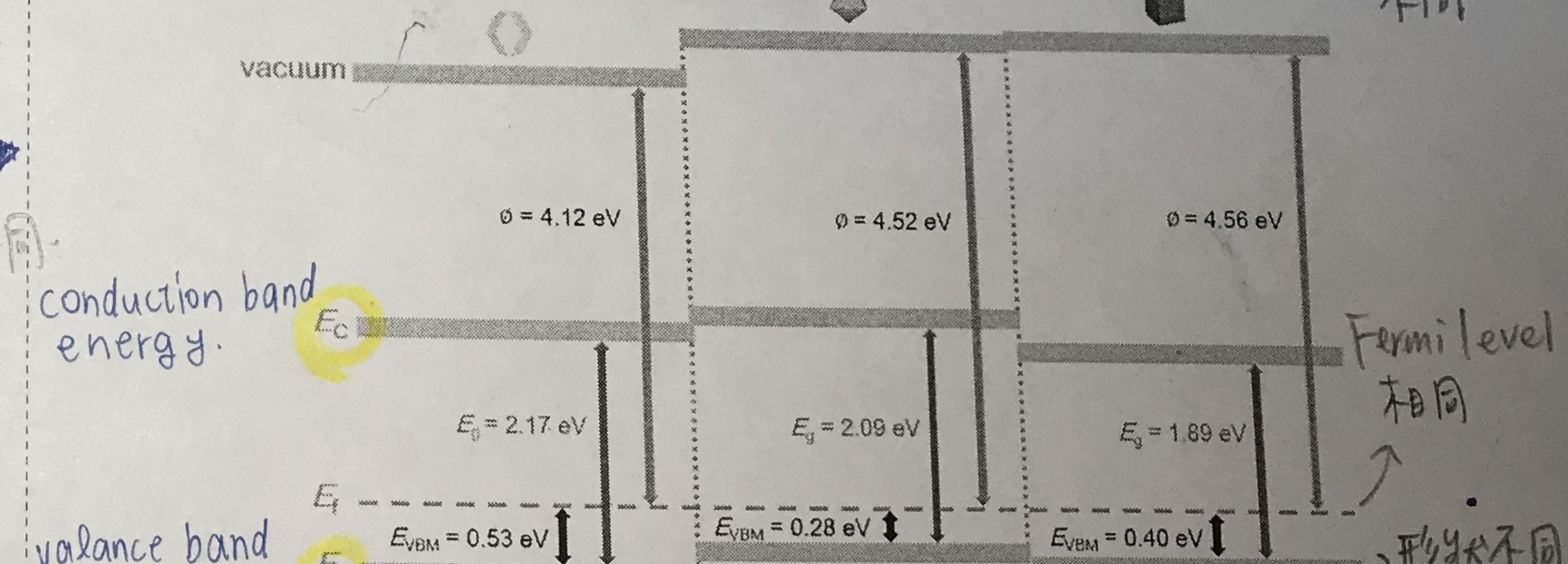
Band diagrams for different Cu₂O crystal shapes constructed using UPS and UV-vis spectroscopic data. The Fermi level is set to have the same energy with the consideration of crystals having two or three crystal faces.

↑ 形狀不同 → band gap 不同 → vibration 不同



(a) UPS spectra of the synthesized Cu₂O cubes, octahedra, and rhombic dodecahedra used for the determination of valence band maximum energies and semiconductor work function. (b) Expanded UPS spectra. (c) Reflectance spectra of these Cu₂O crystals. Absorbance is presented. (d) Tauc plot for the determination of Cu₂O band gaps. The photograph shows a film of these Cu₂O cubes, octahedra, and rhombic dodecahedra on a silicon substrate to display their colors. They have different colors.

can find band gap



Since 0 eV is regarded as the Fermi level energy, these values (e.g. 0.40 eV) correspond to the energy difference between VBM (valence band maximum) and the Fermi level (E_F). The work function (ϕ), or energy difference between vacuum level and E_F , can be calculated from the difference in the photon energy of the Helium I light source at 21.22 eV and the cut-off energy ($E_{cut-off}$) obtained from the left side of panel b in the previous slide (e.g. 21.22 – 16.66).

→ VB 下降

4-2

What we have learned about semiconductors?

$$R = \rho \frac{L}{A}$$

電導率 $\sigma = \frac{1}{\rho}$

Electrical conductivity (inverse of resistivity) σ 是電阻率的倒數

$$Si = 1.56 \times 10^{-3} S/m$$

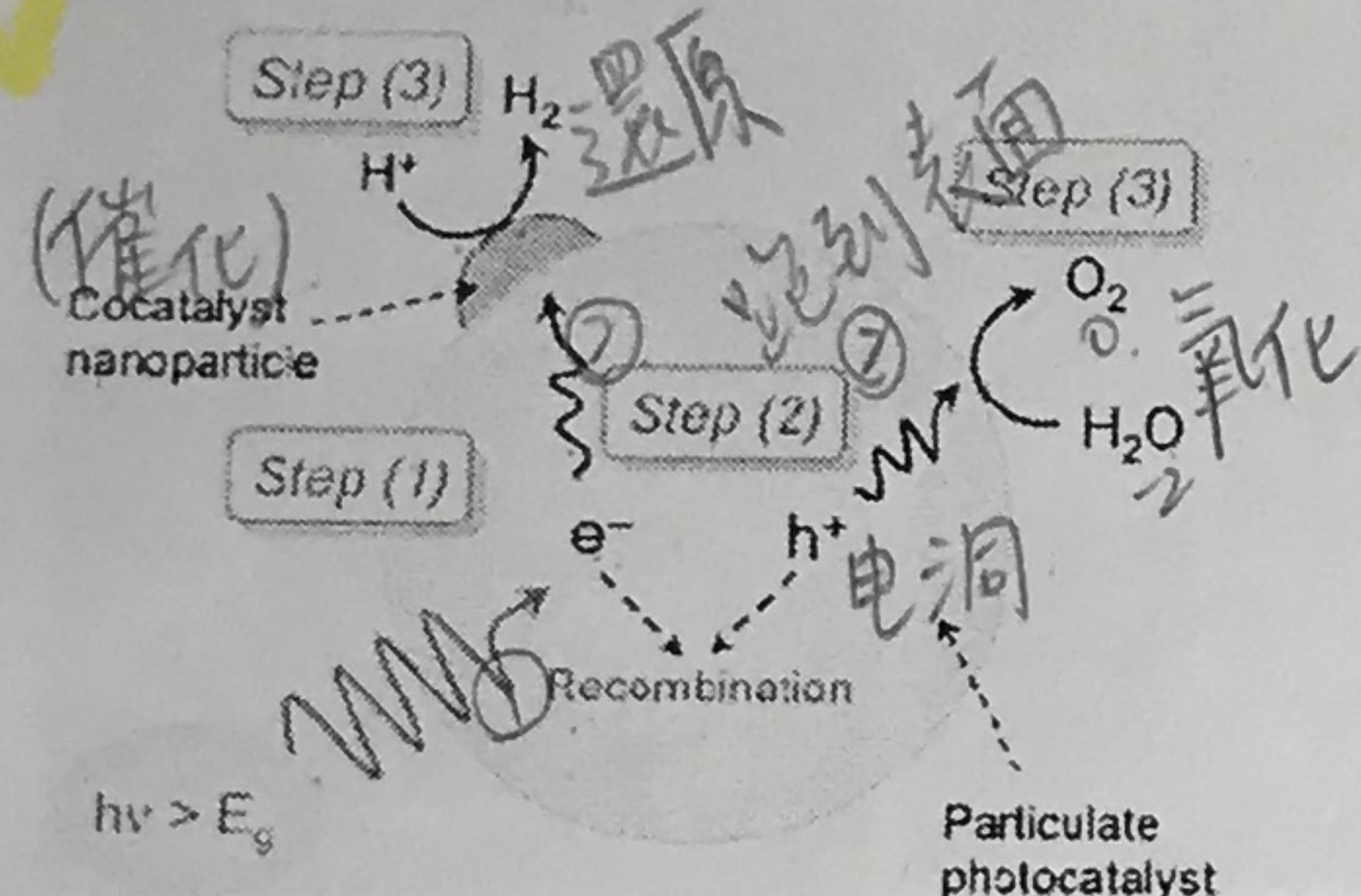
$$GaAs = 1.00 \times 10^{-8} \sim 10^3 S/m$$

是-一個範圍 \downarrow doping

$$\text{graphite } 2.00 \times 10^5 \text{ to } 3.00 \times 10^5 S/m // \text{ basal plane } 3.30 \times 10^2 S/m \perp \text{ basal plane}$$

Photoexcited electrons and holes should migrate to the surface or recombine regardless of crystal facets. And surface-deposited cocatalyst should improve photocatalytic activity of the semiconductor nanostructures.

Optical properties of metal oxide nanocrystals being facet-dependent is unheard of.

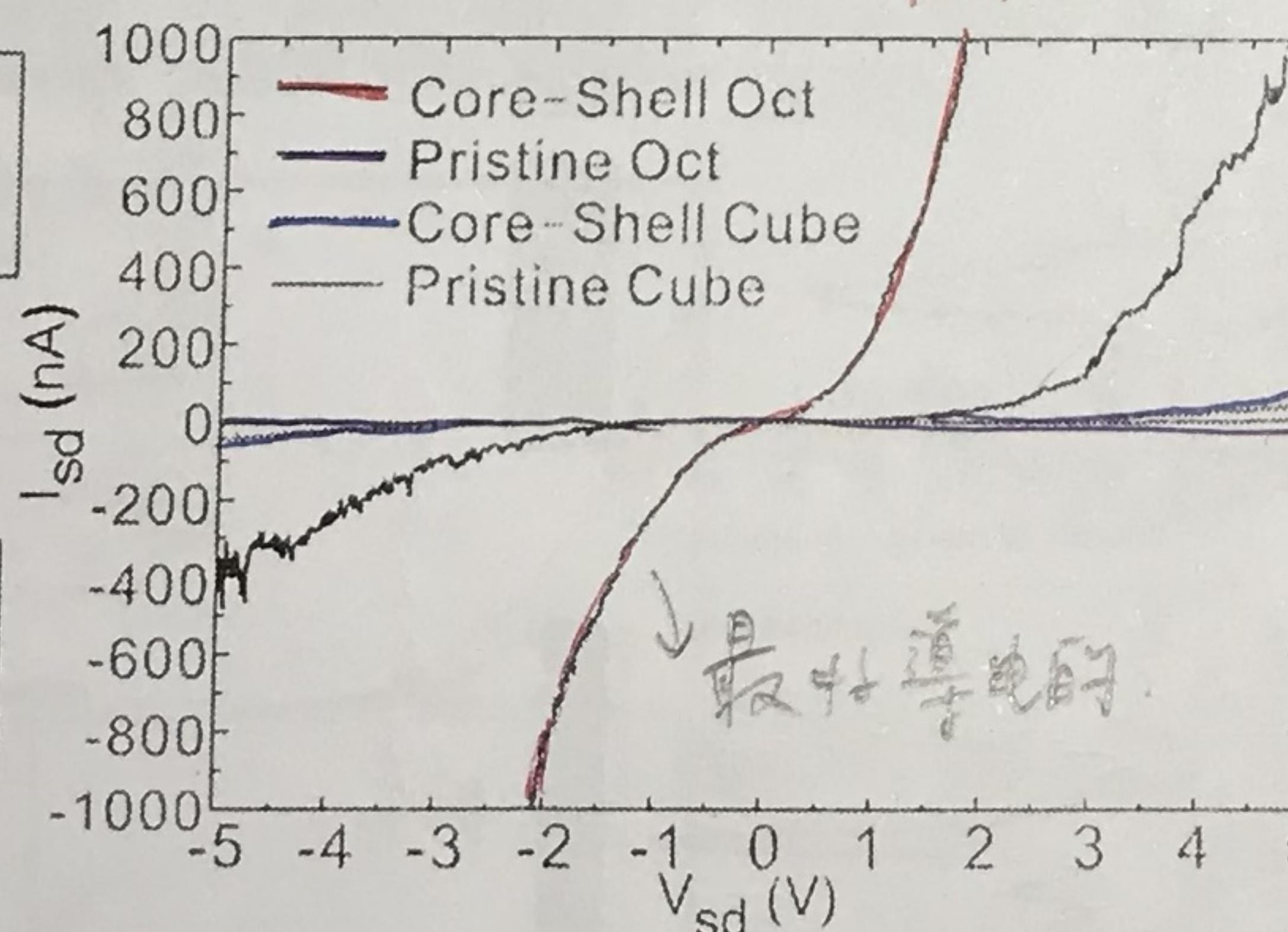
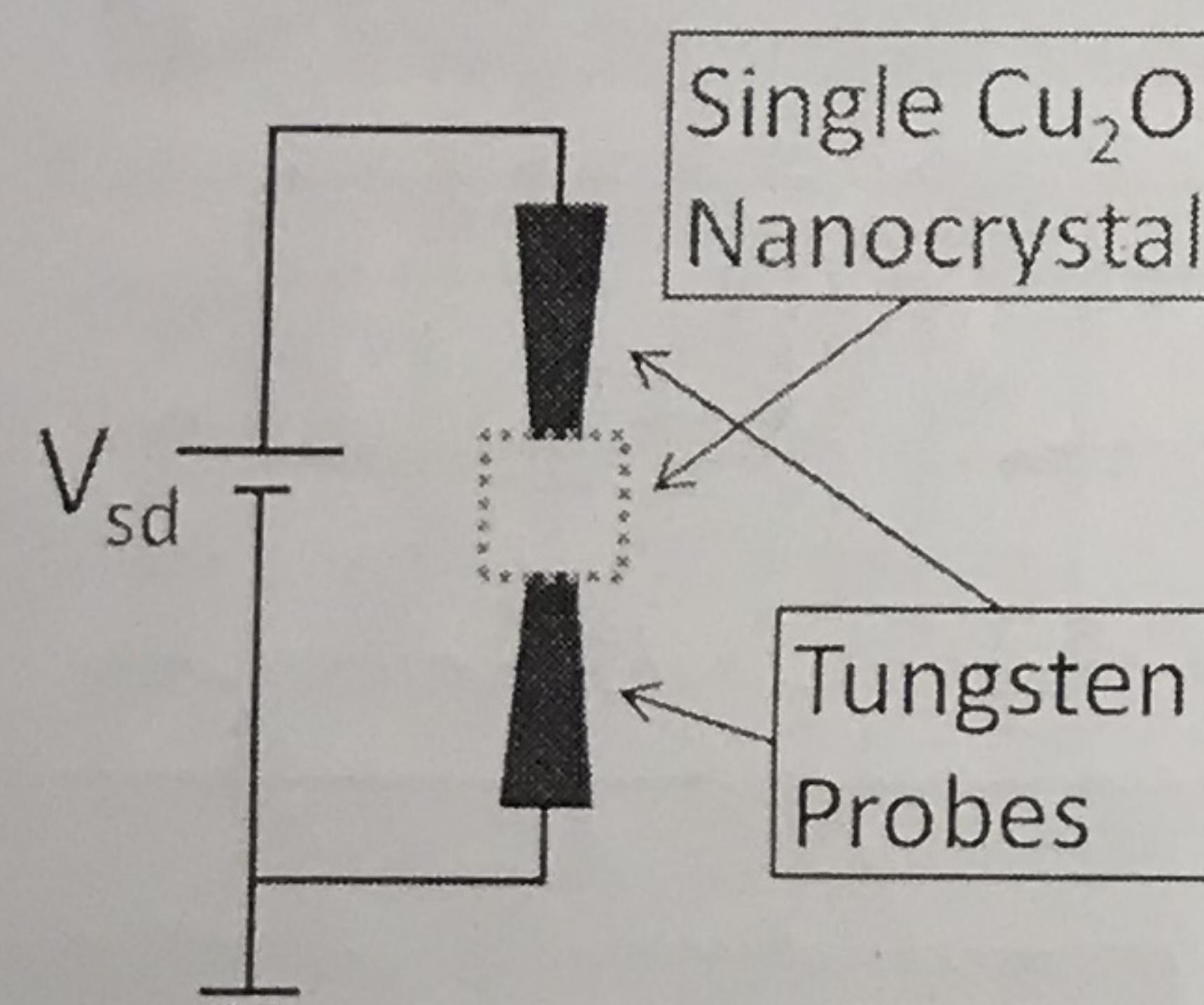


Our idea:

This thin layer changes everything.

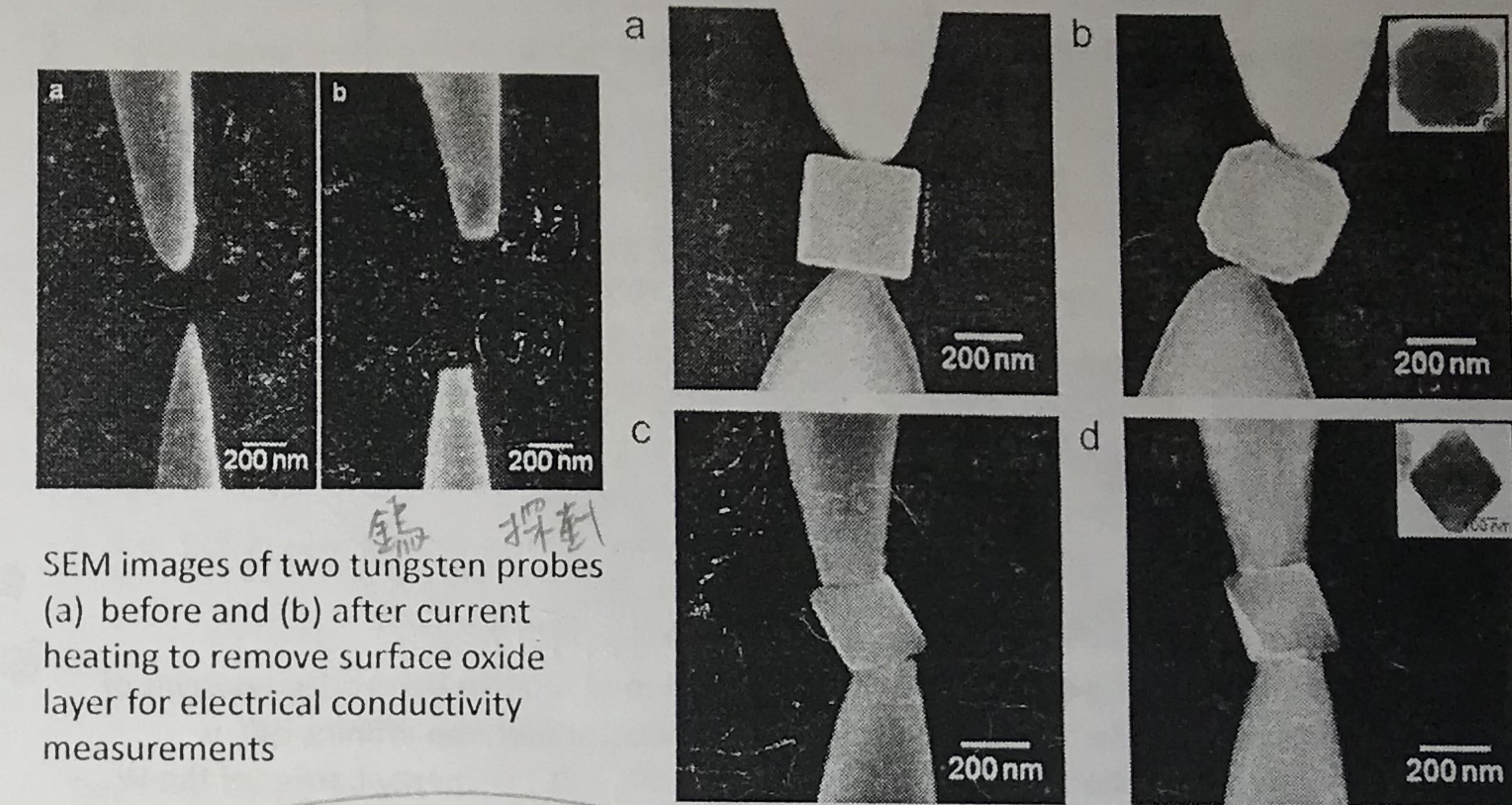
表達導體、半導體、絕緣體用的

I-V Measurements Using the Same Sets of Tungsten Probes



✓ I

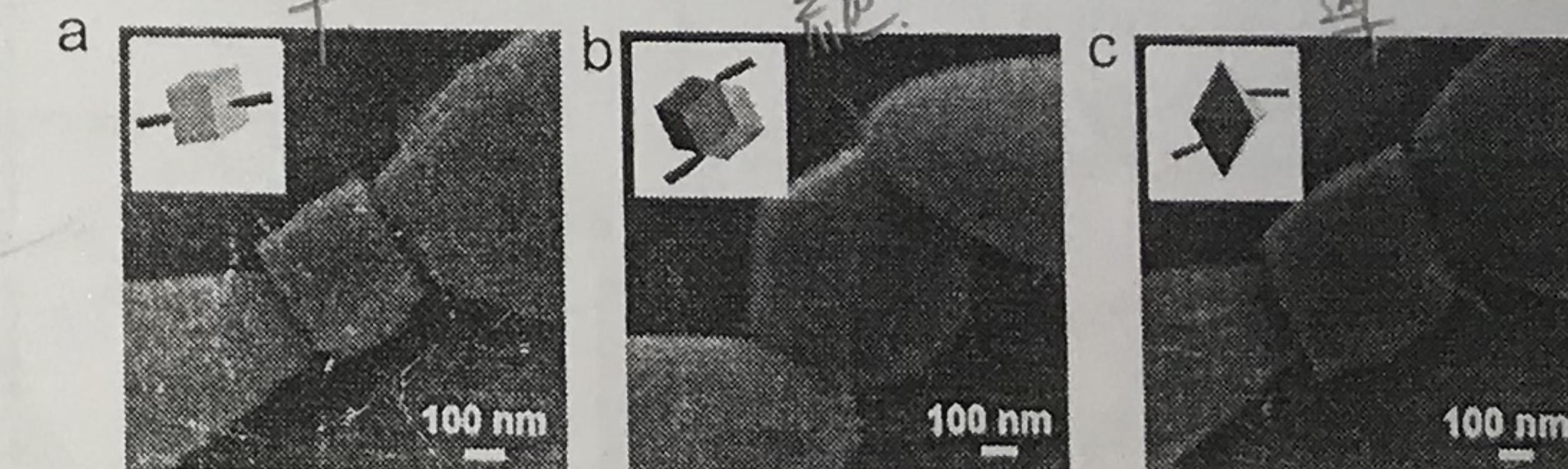
Facet-Dependent and Au-Enhanced Electrical and Photocatalytic Activity of Au-Cu₂O Core-Shell Nanocrystals



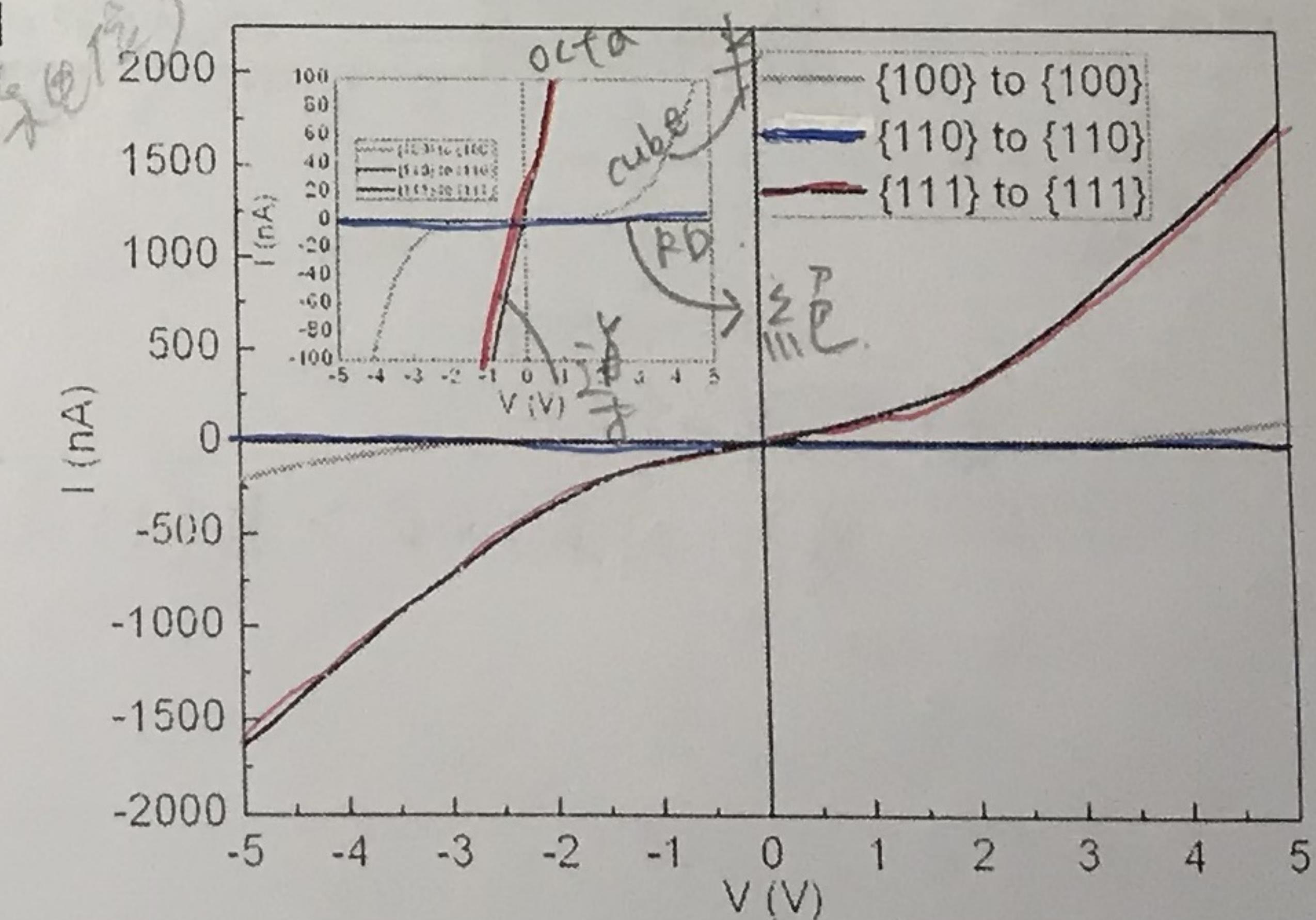
Kuo, C.-H.; Yang, Y.-C.; Gwo, S.; Huang, M. H. J. Am. Chem. Soc. 2011, 133, 1052

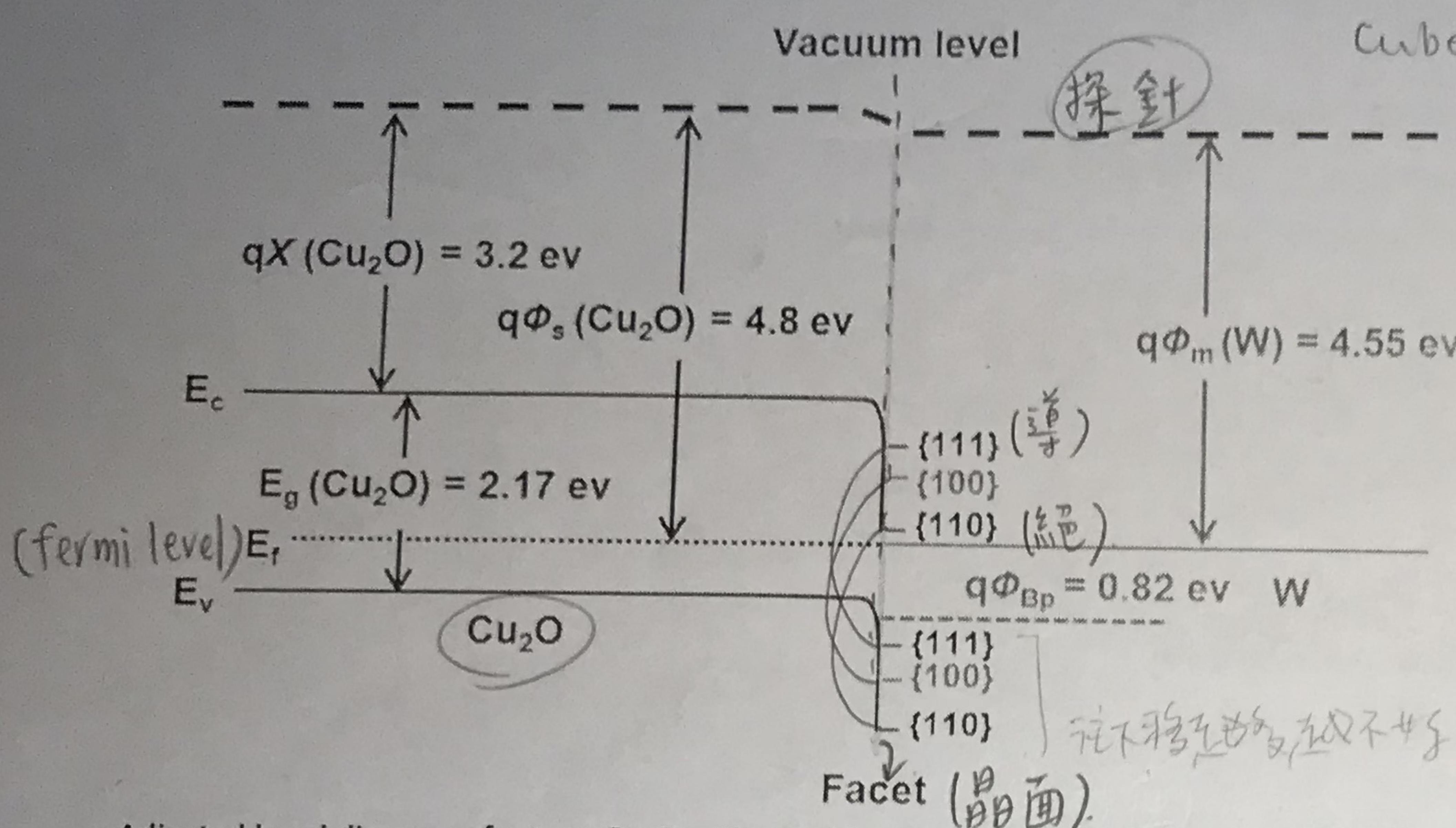
Facet-Dependent Electrical Conductivity Properties of Cu₂O Crystals

Tan, C.-S.; Hsu, S.-C.; Ke, W.-H.; Chen, L.-J.; Huang, M. H. Nano Lett. 2015, 15, 2155-2160



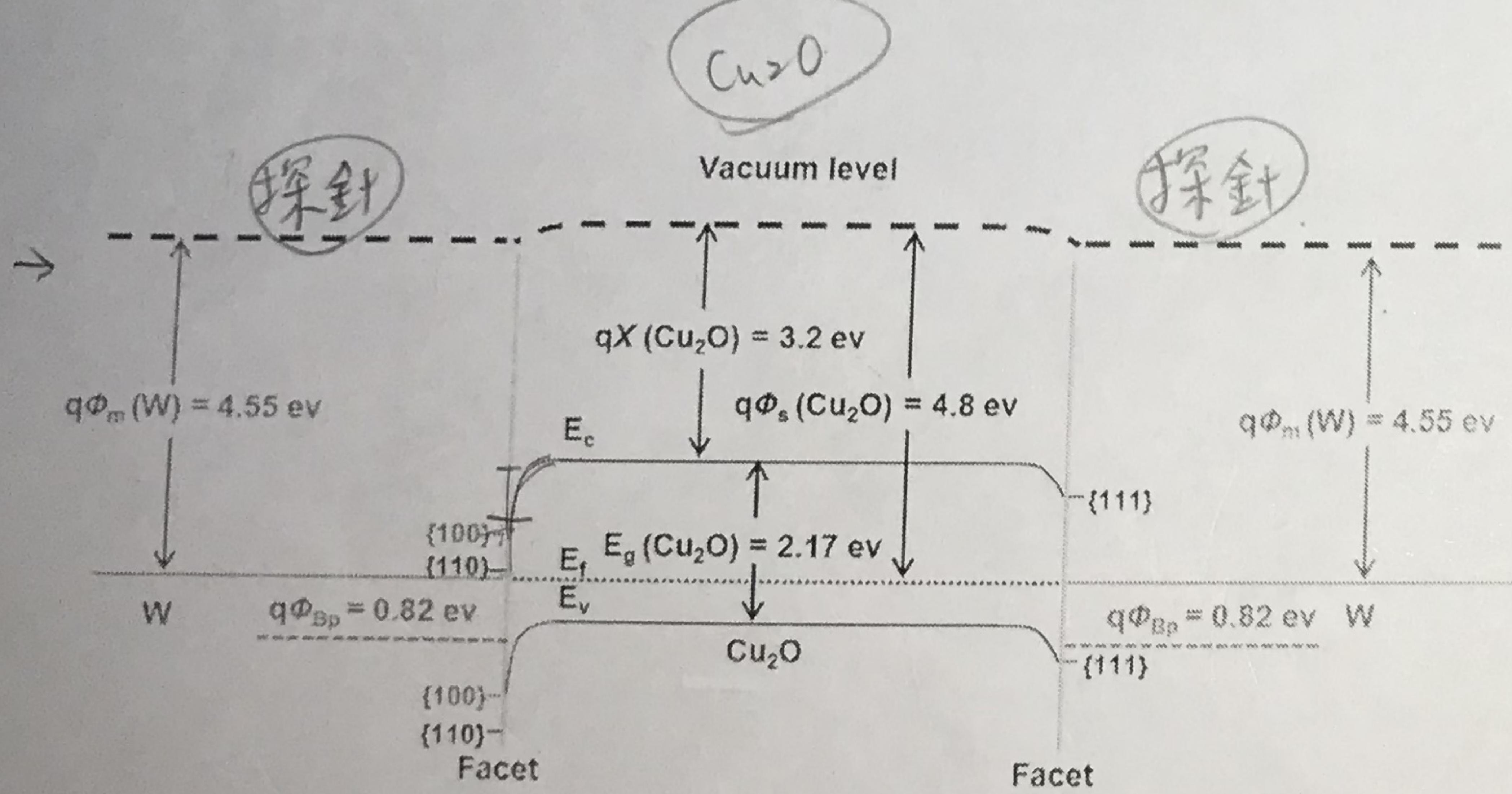
最好: 111
最差: 110





Adjusted band diagram of p-type Cu_2O with consideration of relative band edge energies of different crystal surfaces. In the diagram, qX is semiconductor electron affinity, $q\Phi_s$ is semiconductor work function, $q\Phi_m$ is metal work function, $q\Phi_{Bp}$ is energy barrier of the W and Cu_2O contact, E_c is conduction band energy, E_v is valence band energy, & E_f is Fermi level.

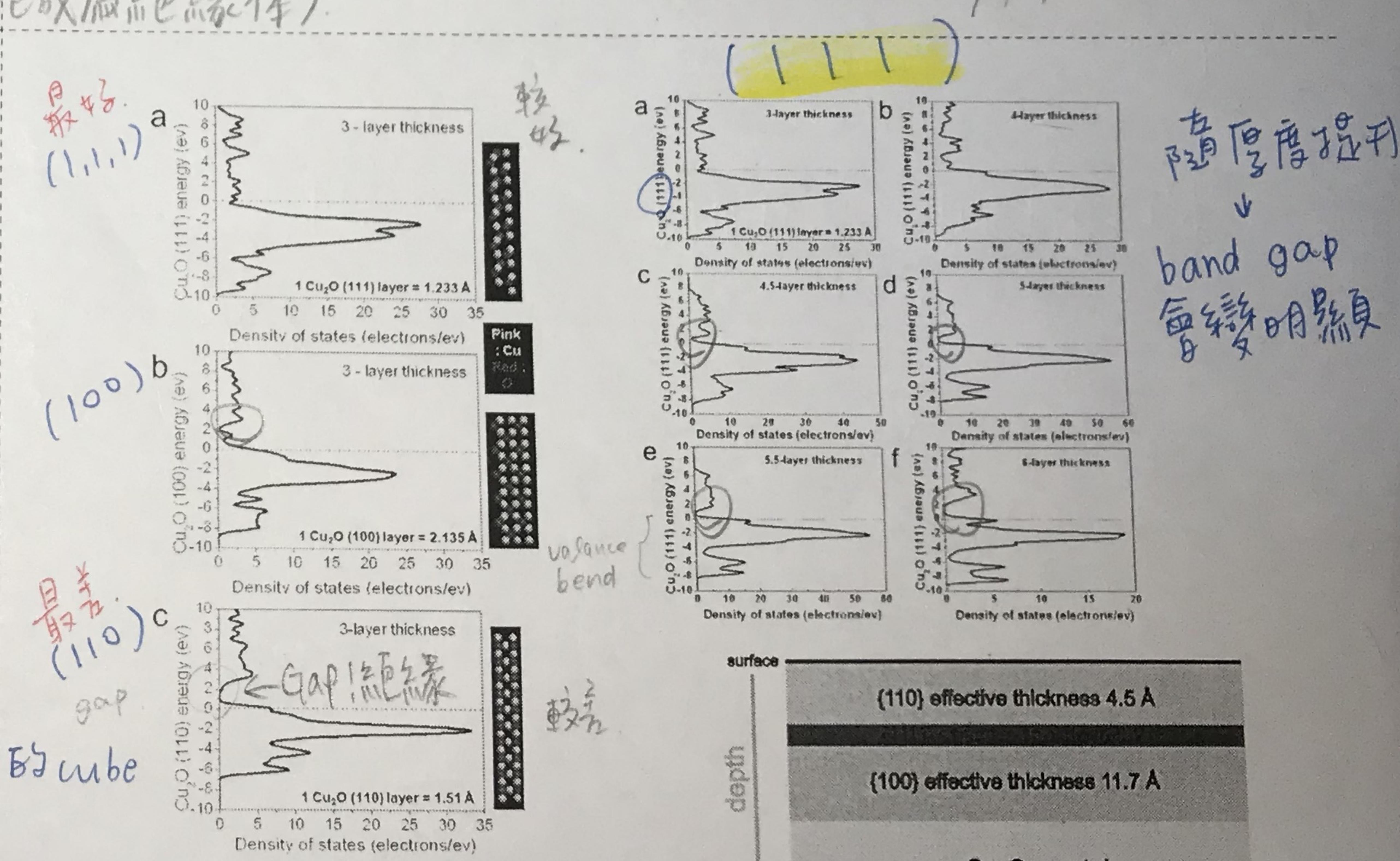
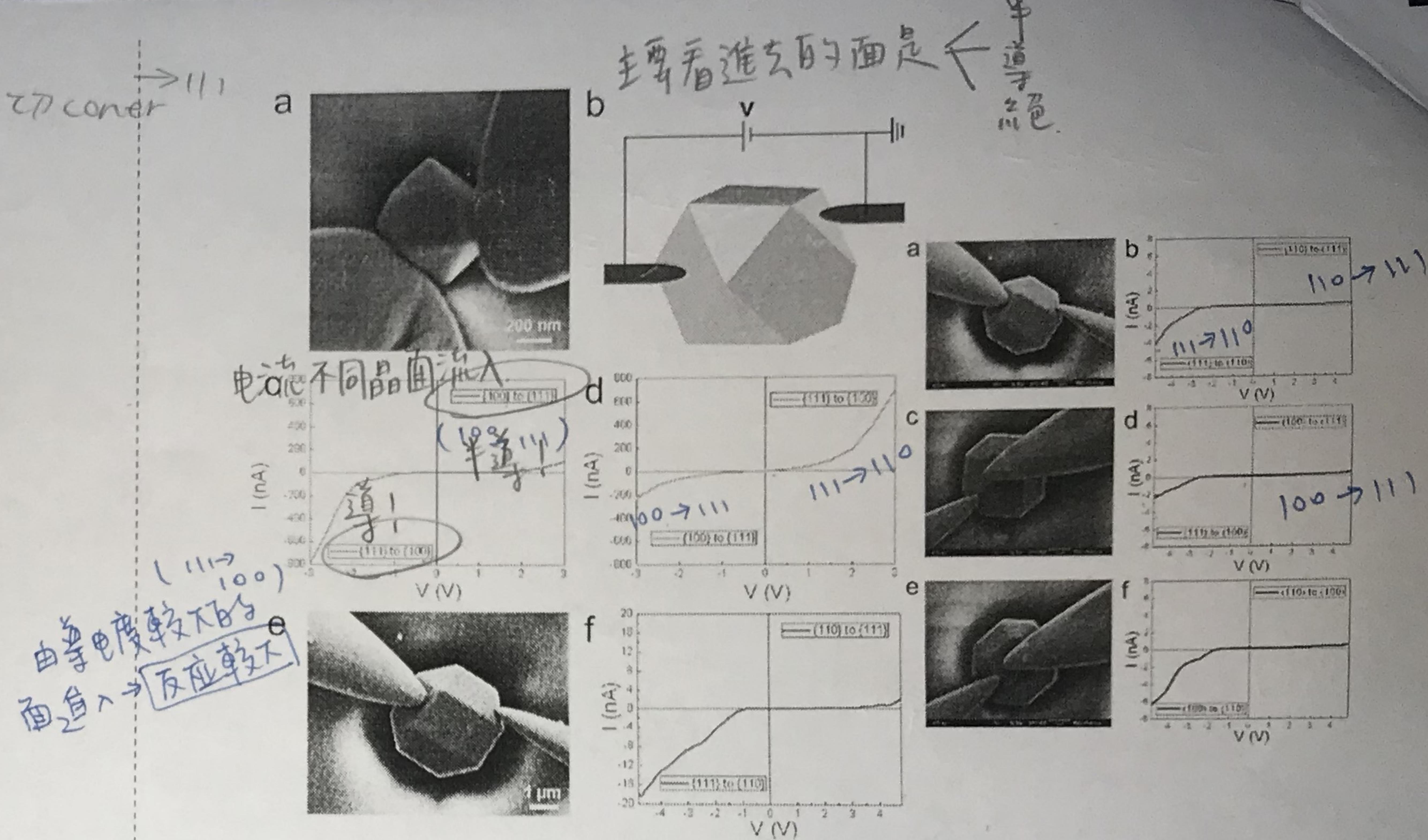
晶面效应：在晶面上的CB、VB能量都会弯曲（弯曲越明显有可能成为绝缘体）。



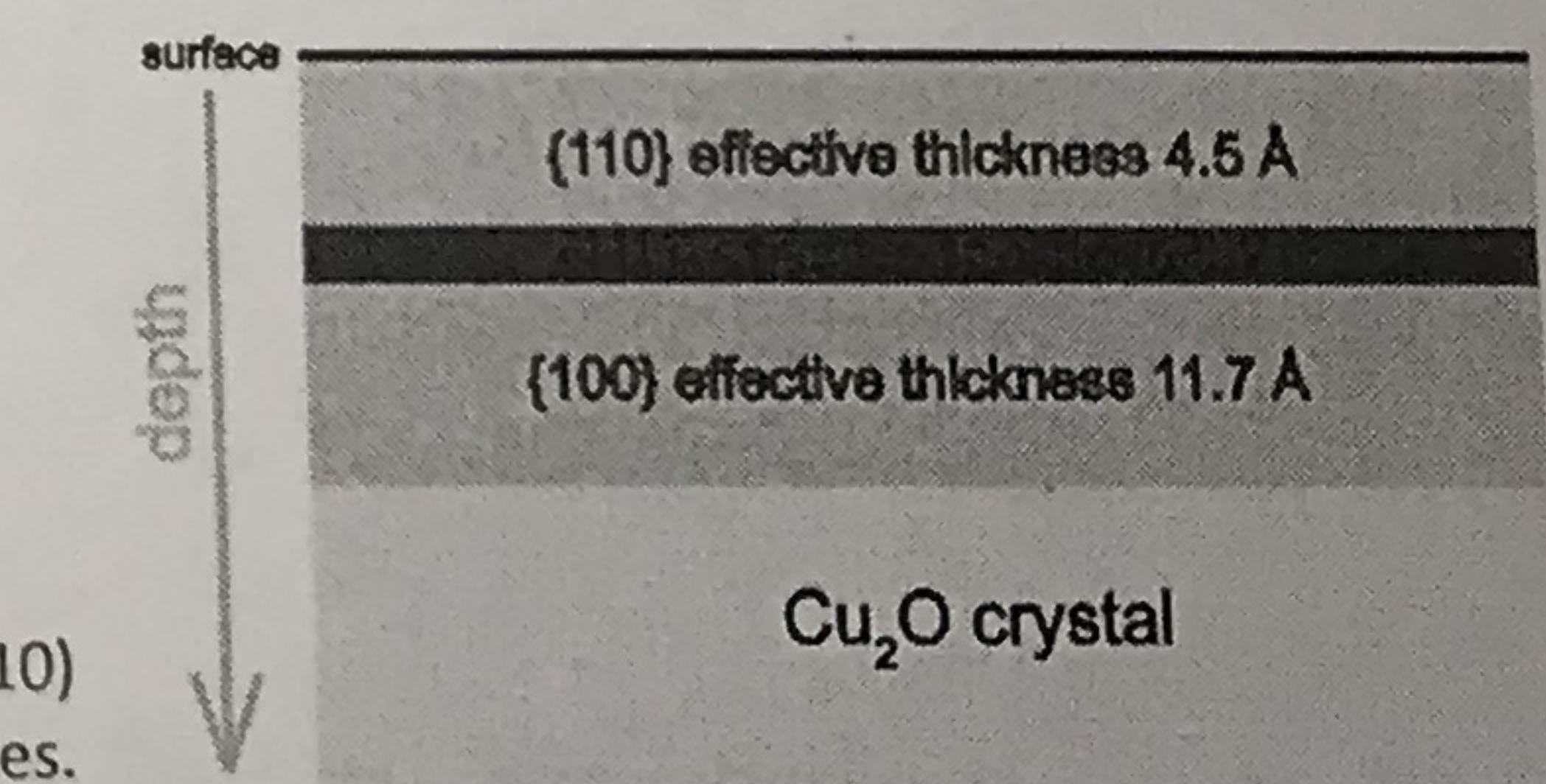
DAY

光降解角：

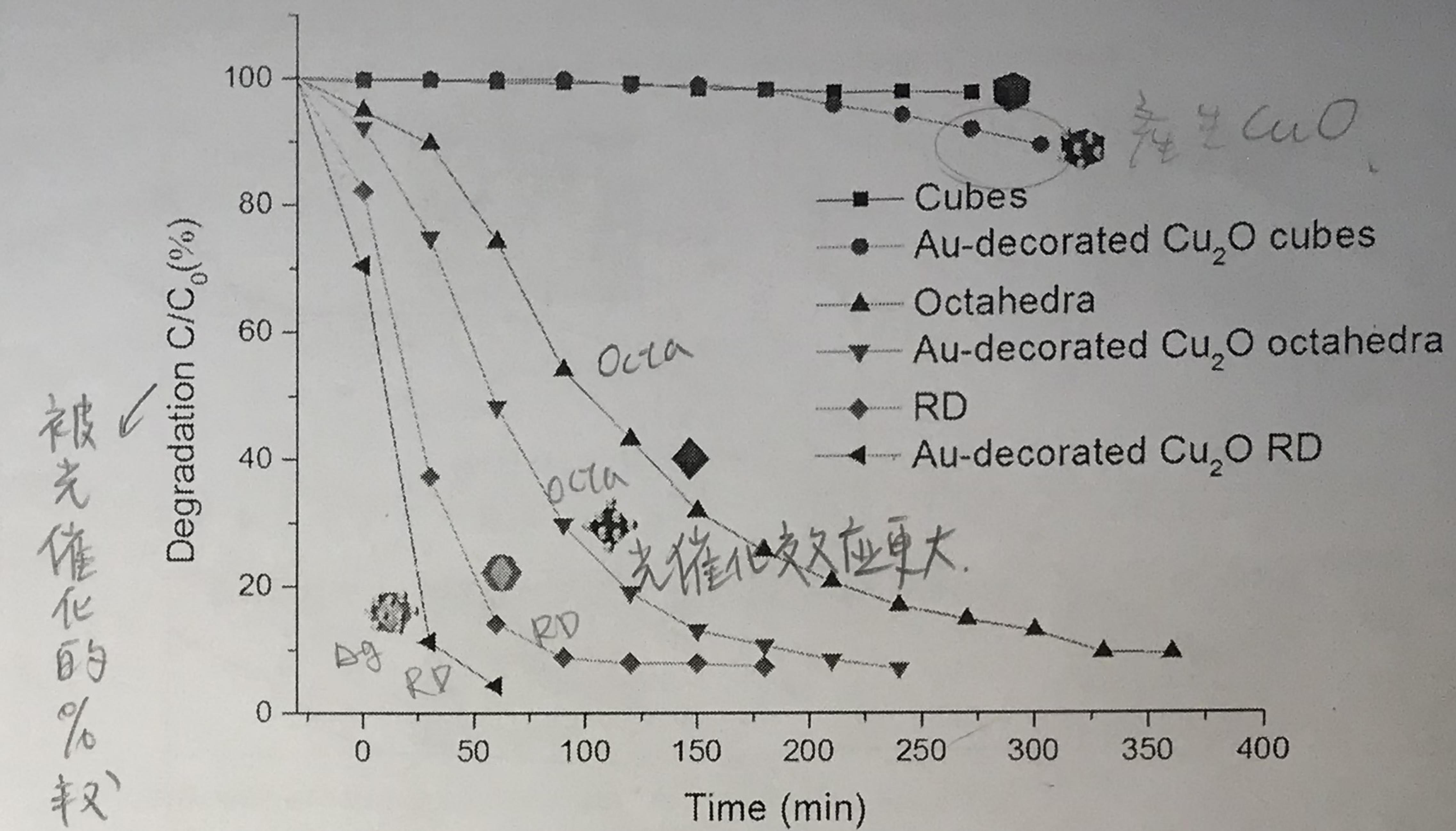
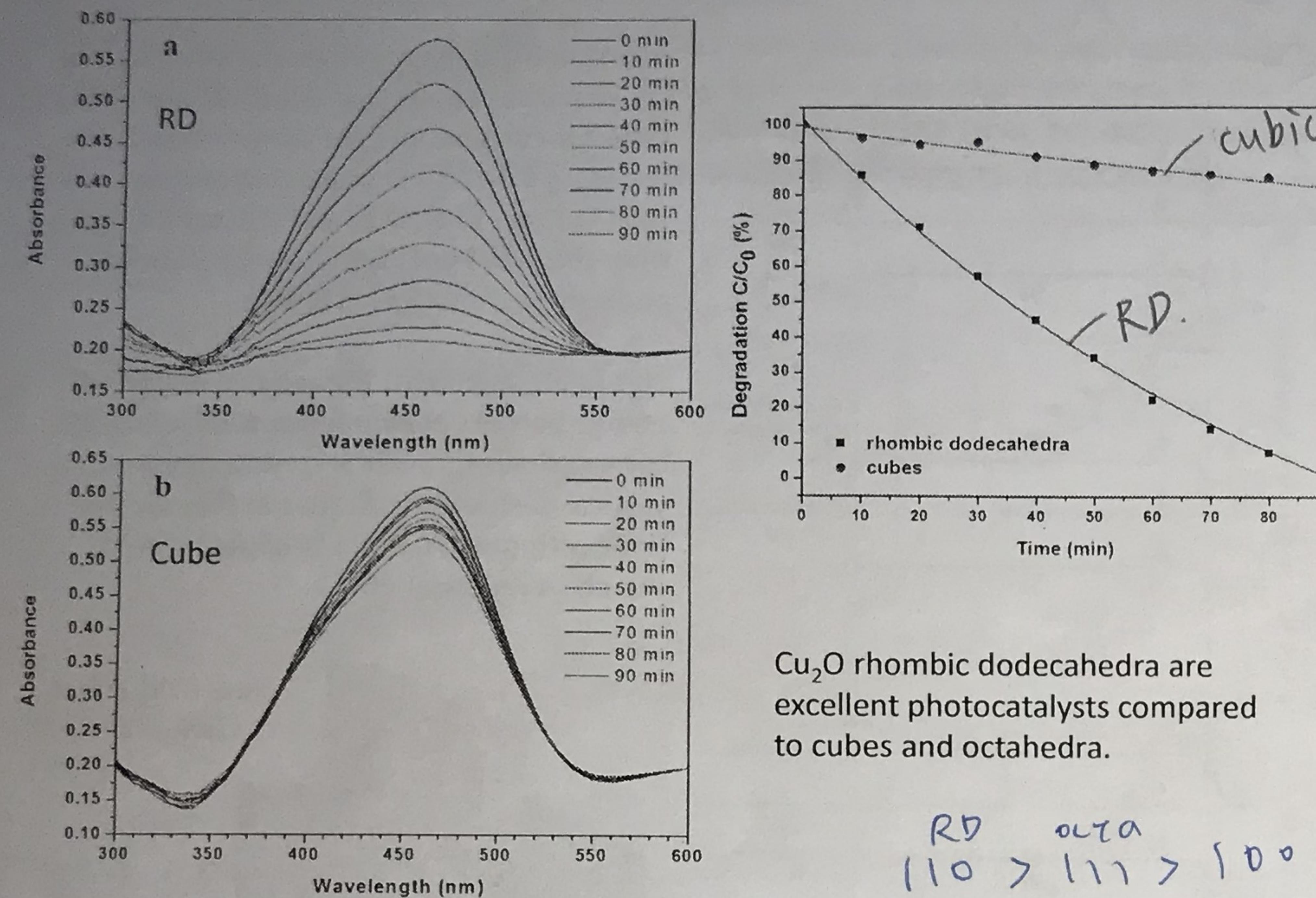
具(110)的RD > 具(111)的Ota > 具(100)的cube



Density of states plots for the (111), (100), and (110) planes of Cu_2O consisting of 3 layers of these planes.

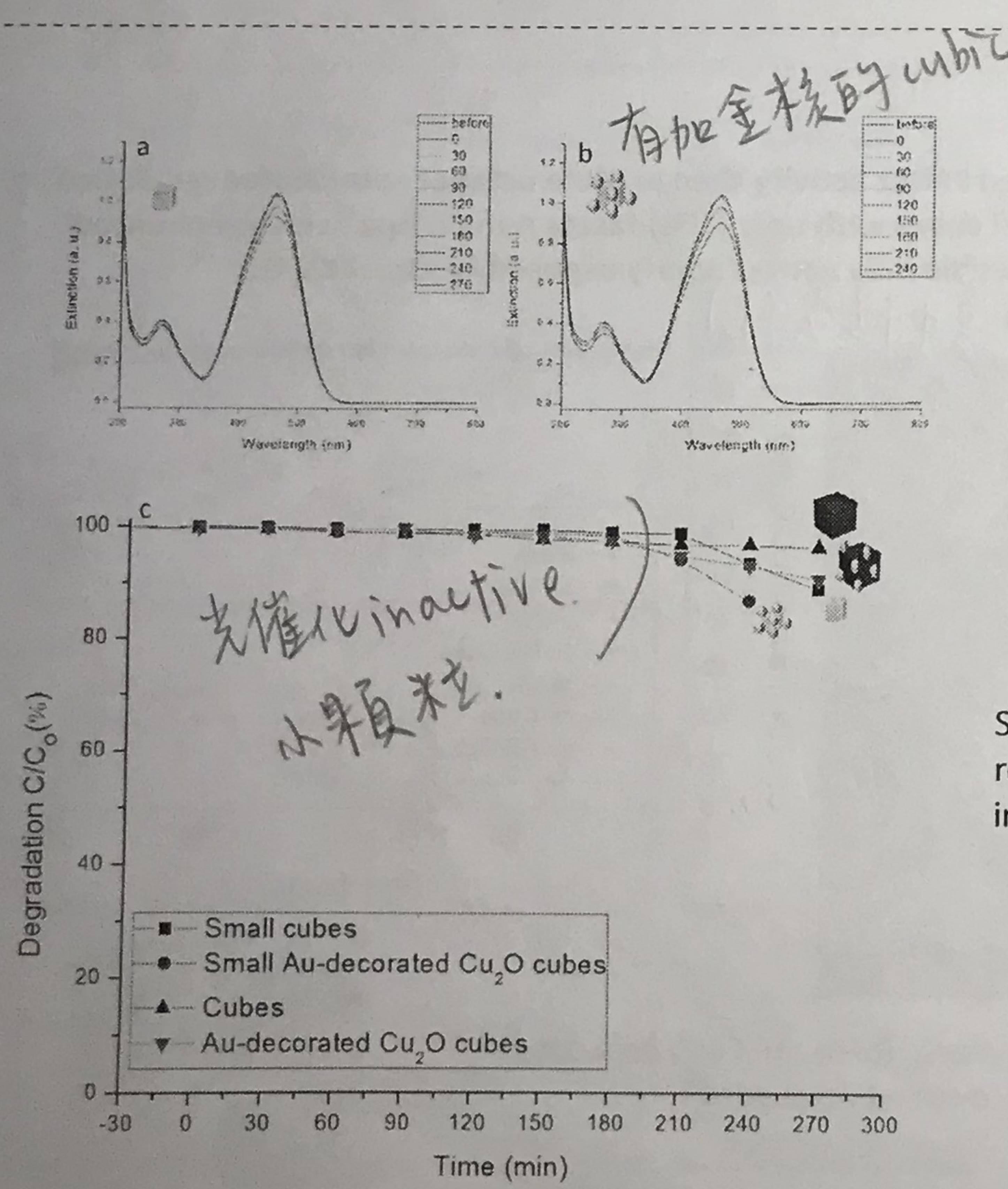


放越久 shell \rightarrow 厚 \rightarrow 吸收度会下降

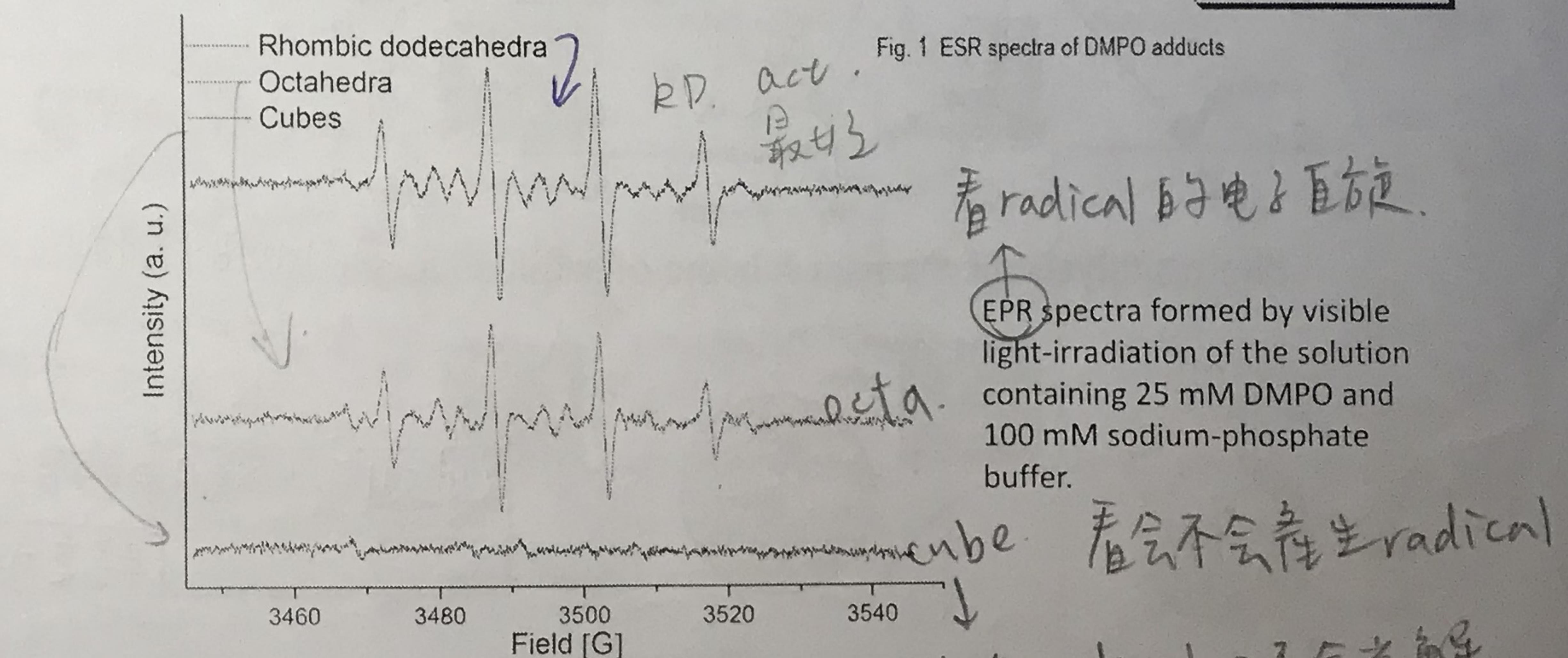


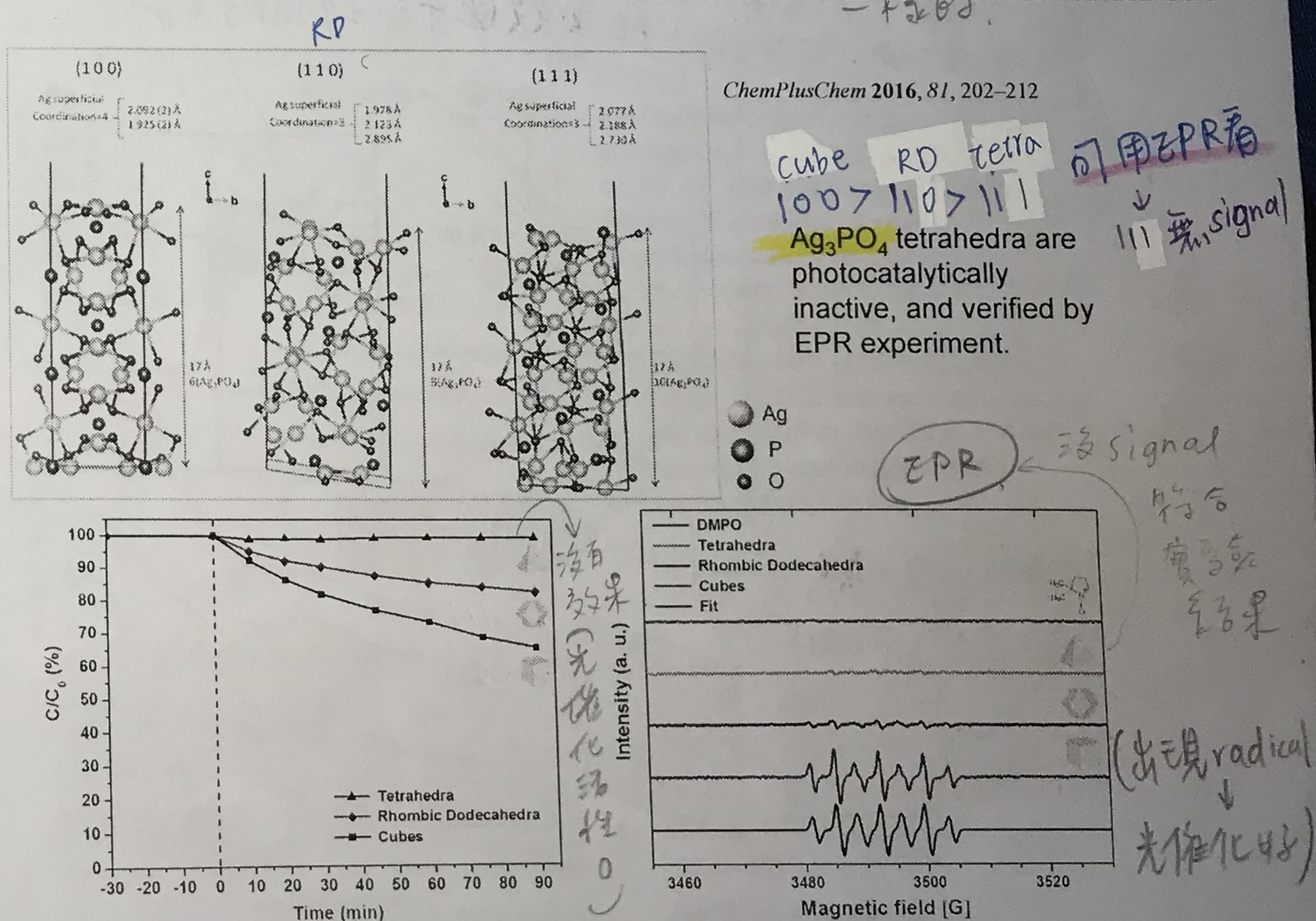
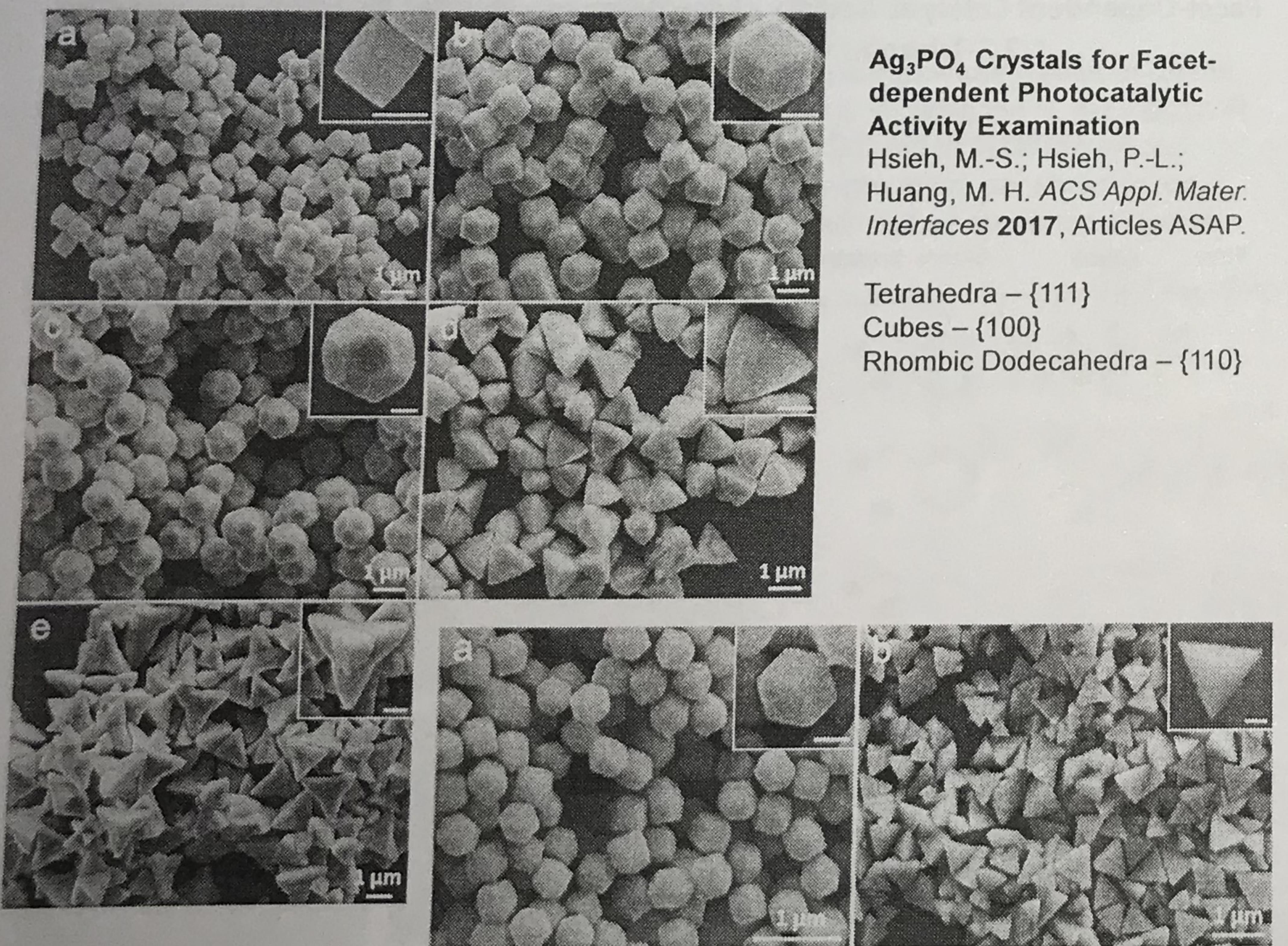
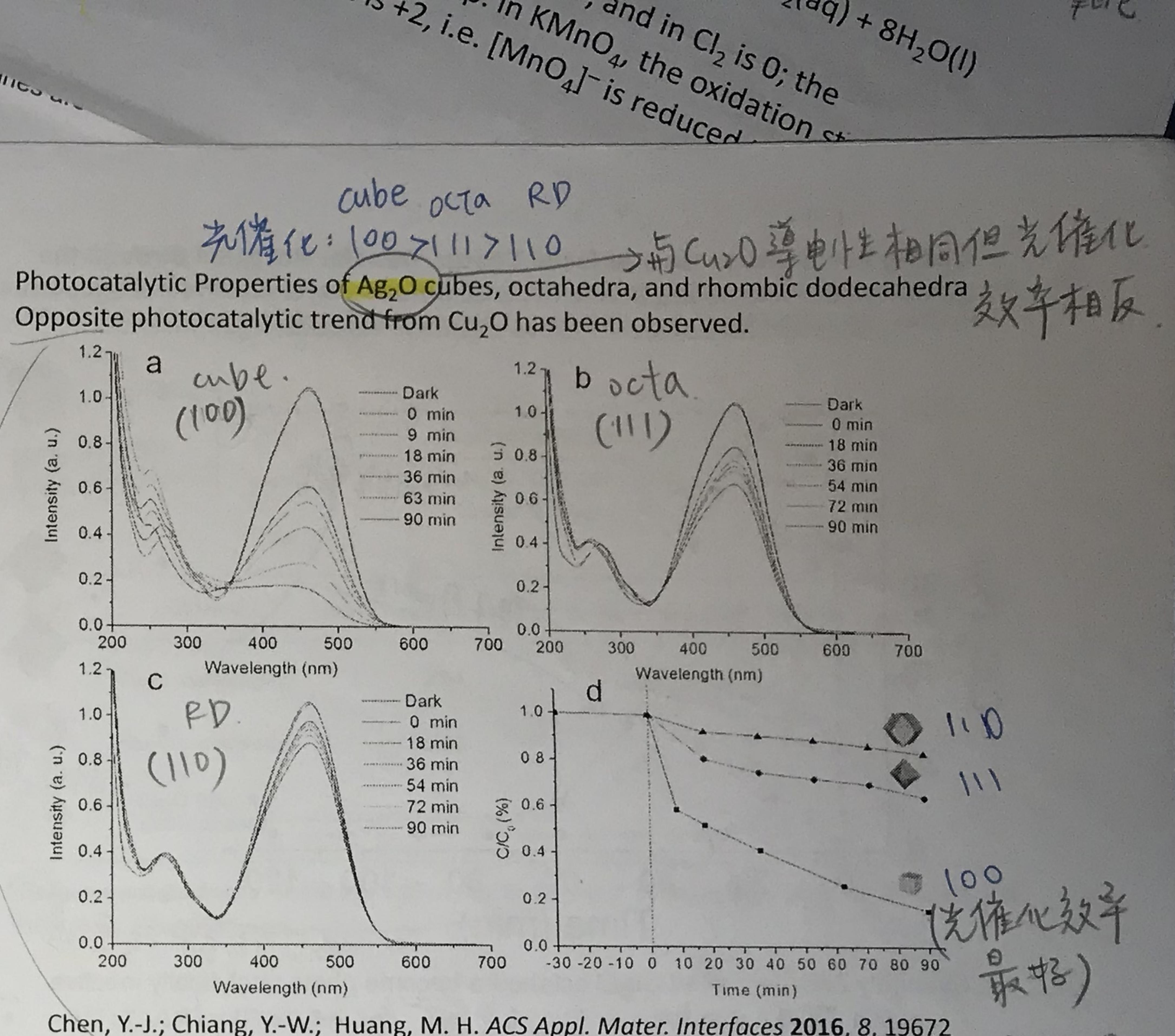
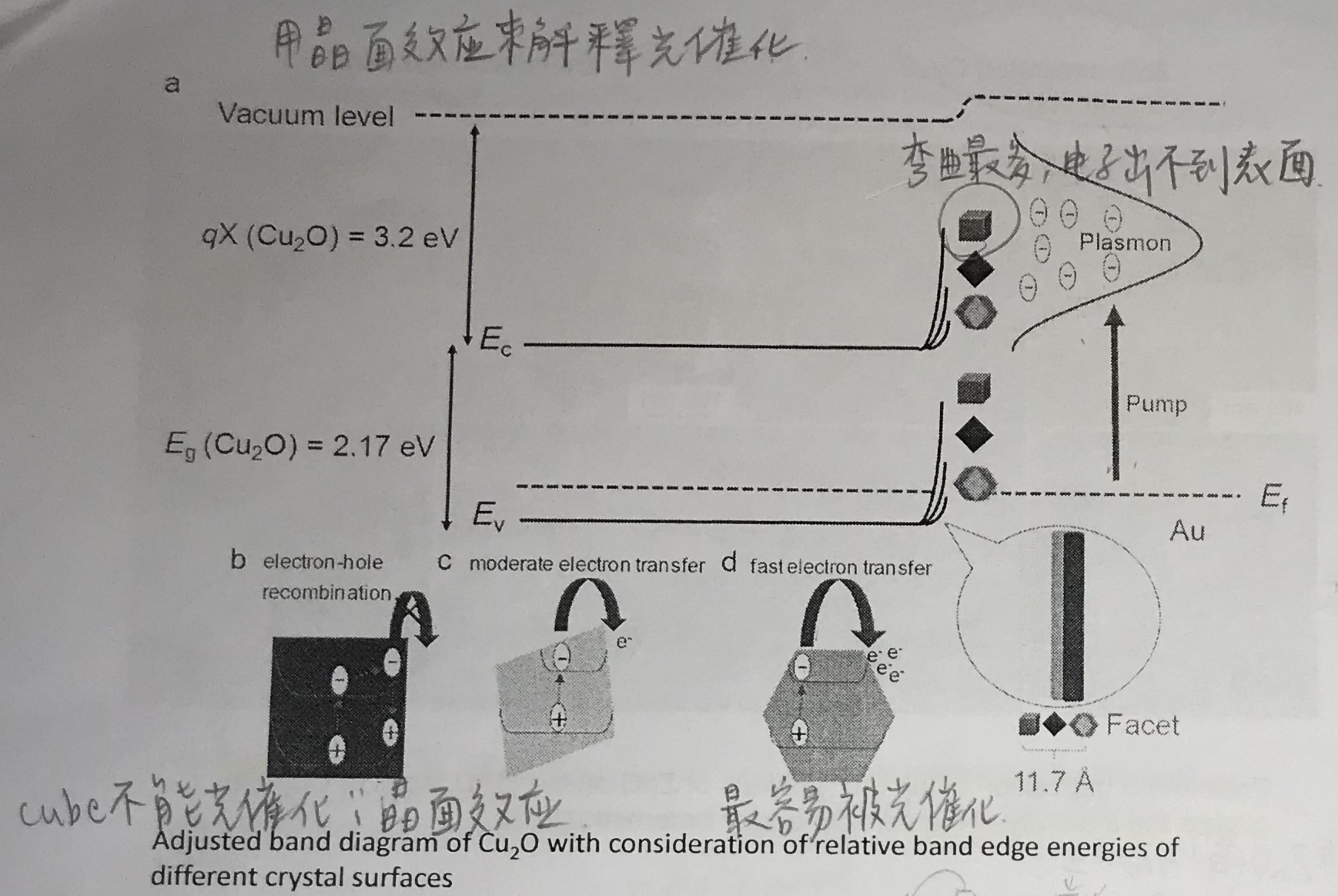
Au-decorated Cu₂O cubes remain photocatalytically inactive because hydroxyl radicals were not produced.

Yuan, G.-Z. et al. *Chem. Eur. J.*
2016, 22, 12548

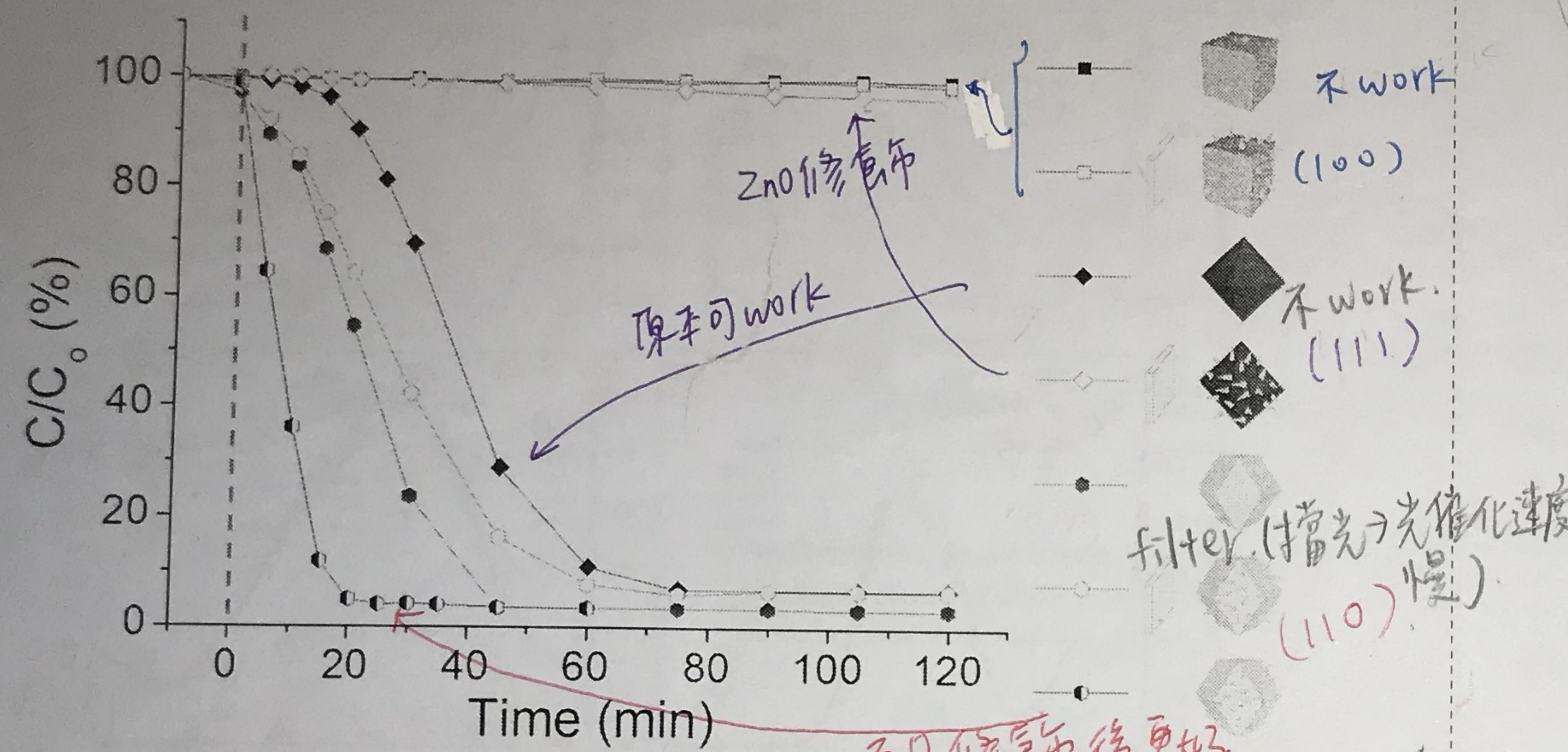


Small Cu₂O nanocubes remain photocatalytically inactive.



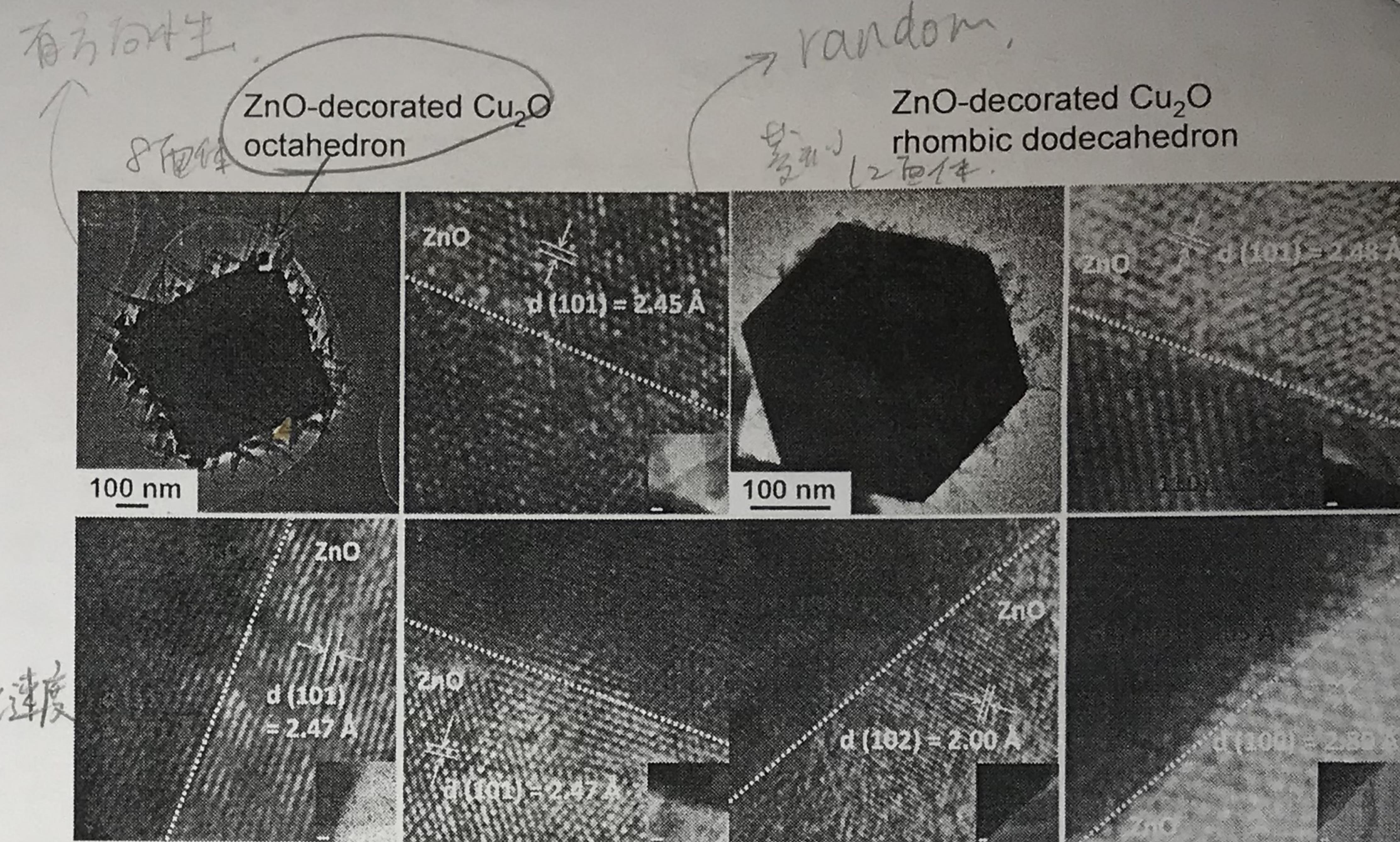
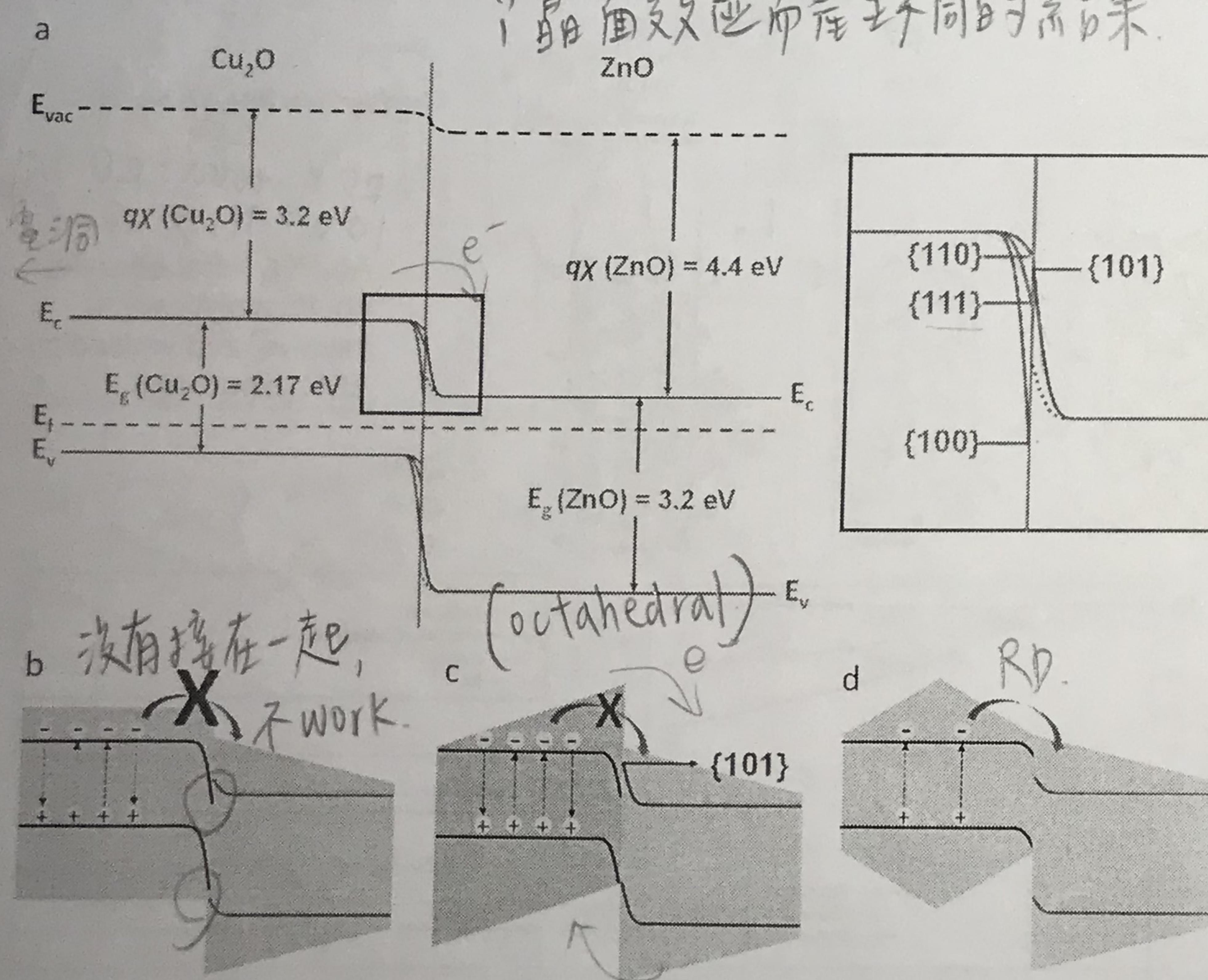


Strong Facet Effects on Interfacial Charge Transfer Revealed through the Examination of Photocatalytic Activities of Various Cu₂O-ZnO Heterostructures
Szu-Chieh Wu, Chih-Shan Tan, and Michael H. Huang, *Adv. Funct. Mater.* 2017, 27, 1604635



Strangely ZnO-decorated Cu₂O octahedra become photocatalytically inactive.

Octa 原本 active, ZnO像飾後 → Octa Inactive ; 生長在 Cu₂O 上的 ZnO 有方向性.
→ RD more active. 生長在 Cu₂O 上的 ZnO 是 random 的



Preferential deposition of the (101) planes of ZnO on the {111} faces of Cu₂O may explain the inactivity of the semiconductor heterostructures.

有机催化反应

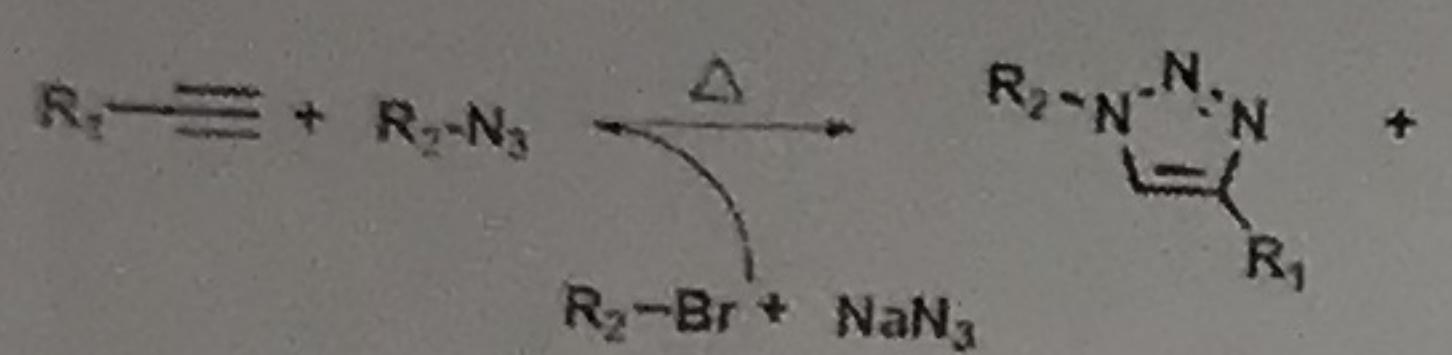
Facet-Dependent Catalytic Activity of Cu₂O Nanocrystals for One-Pot Synthesis of 1,2,3-Triazoles via Multicomponent Click Reactions

Entry	Alkyne	Organic halides	Product	Time (h)/Yield ^b	Time (h)/Yield ^b	Time (h)/Yield ^b
				(RD)	(OH)	(Cube)
1	1a	2a	3a	1/96	4.5/90	7/88
2	1c	2a	3c	1.5/92	5/88	7/80
3	1b OH	2c	3n	2/90	5.5/90	8/77

^a Reagents and conditions: 1 (0.25 mmol), 2 (0.25 mmol), Na₃ (0.38 mmol) in EtOH (3 mL) at 55 °C

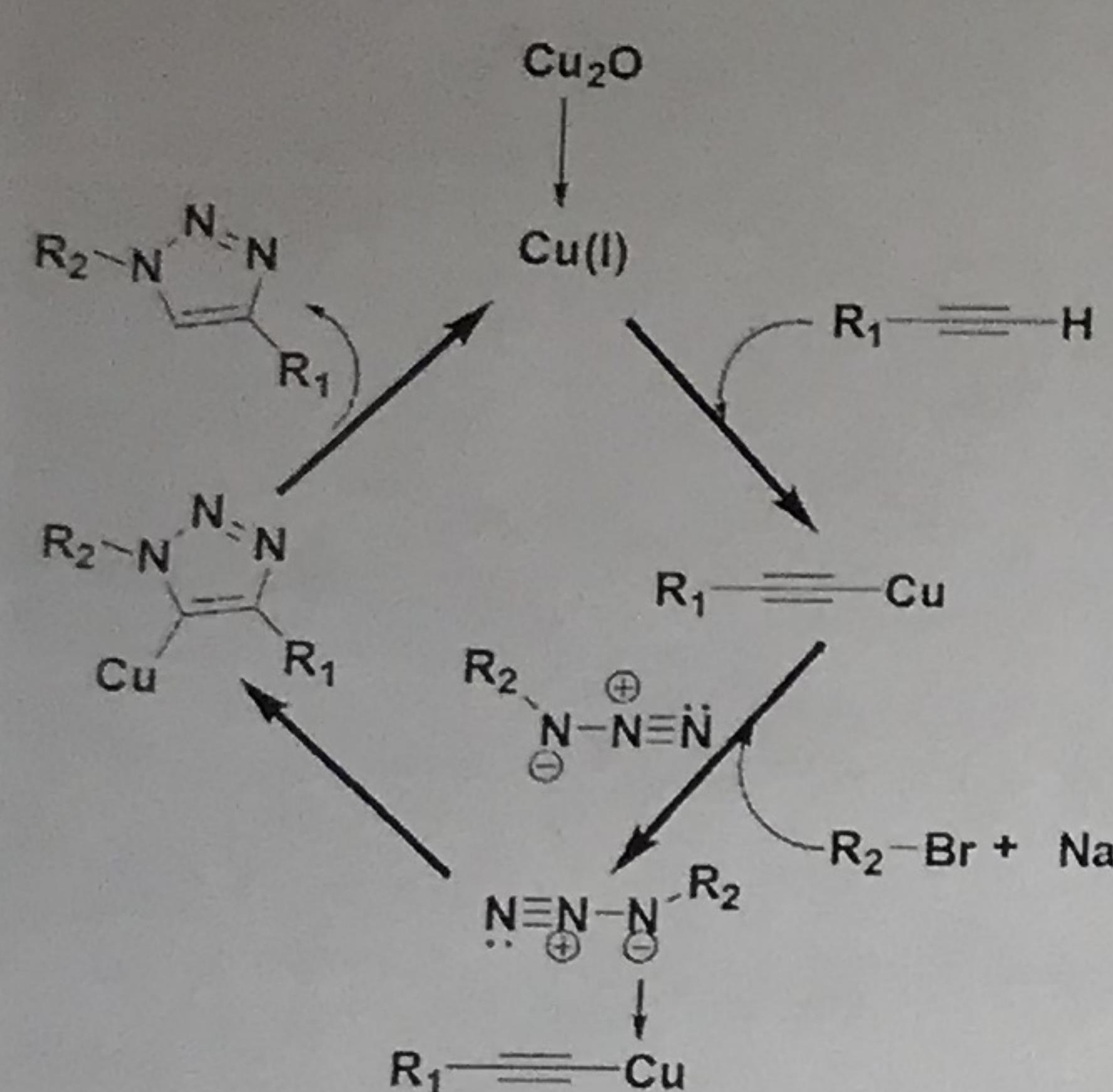
^b Isolated yields

Commercially available Cu₂O powder with the same surface area gives a yield of only 80% after 5 h of reaction (for Entry 1 reaction).

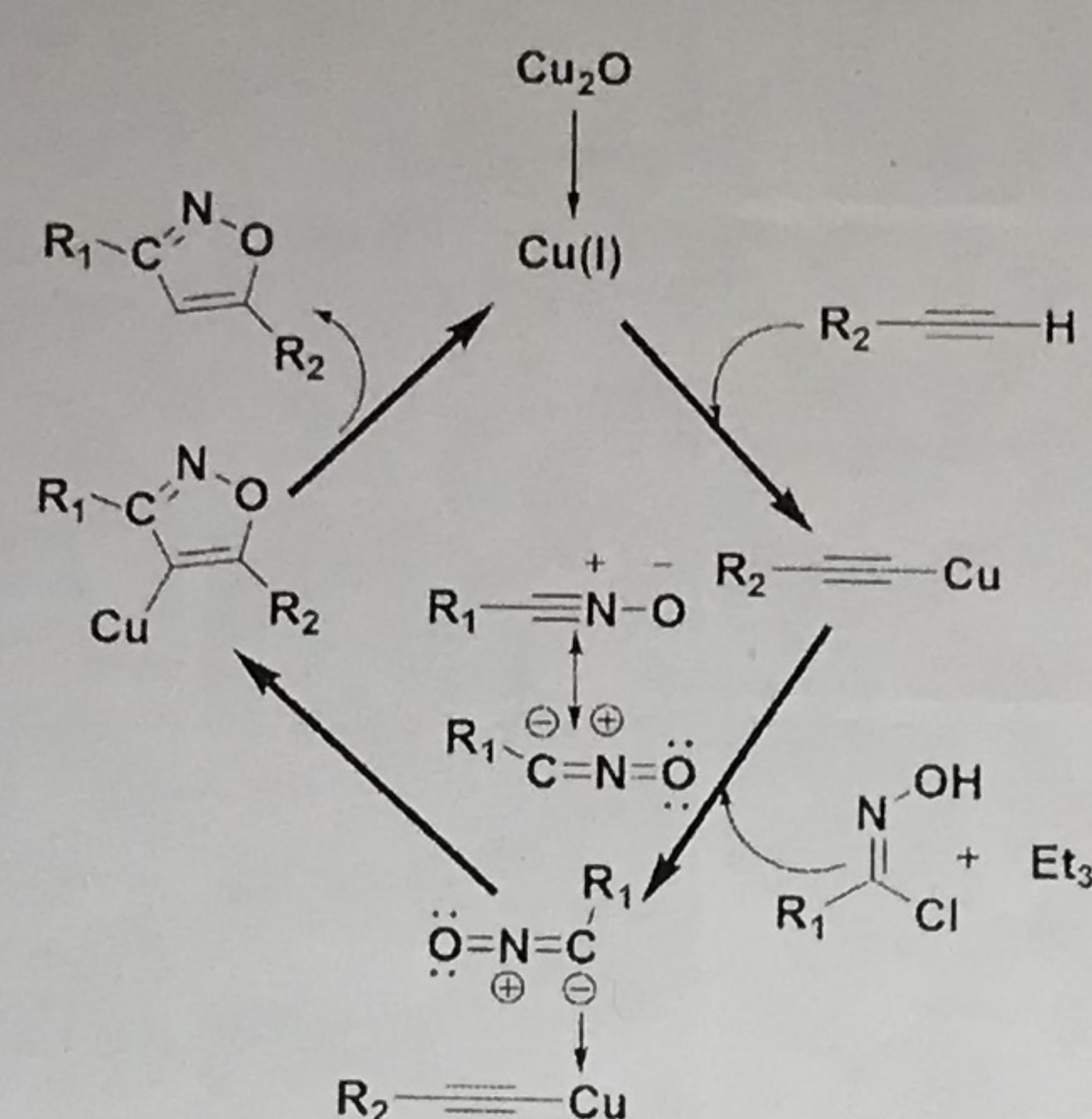


立体選擇性

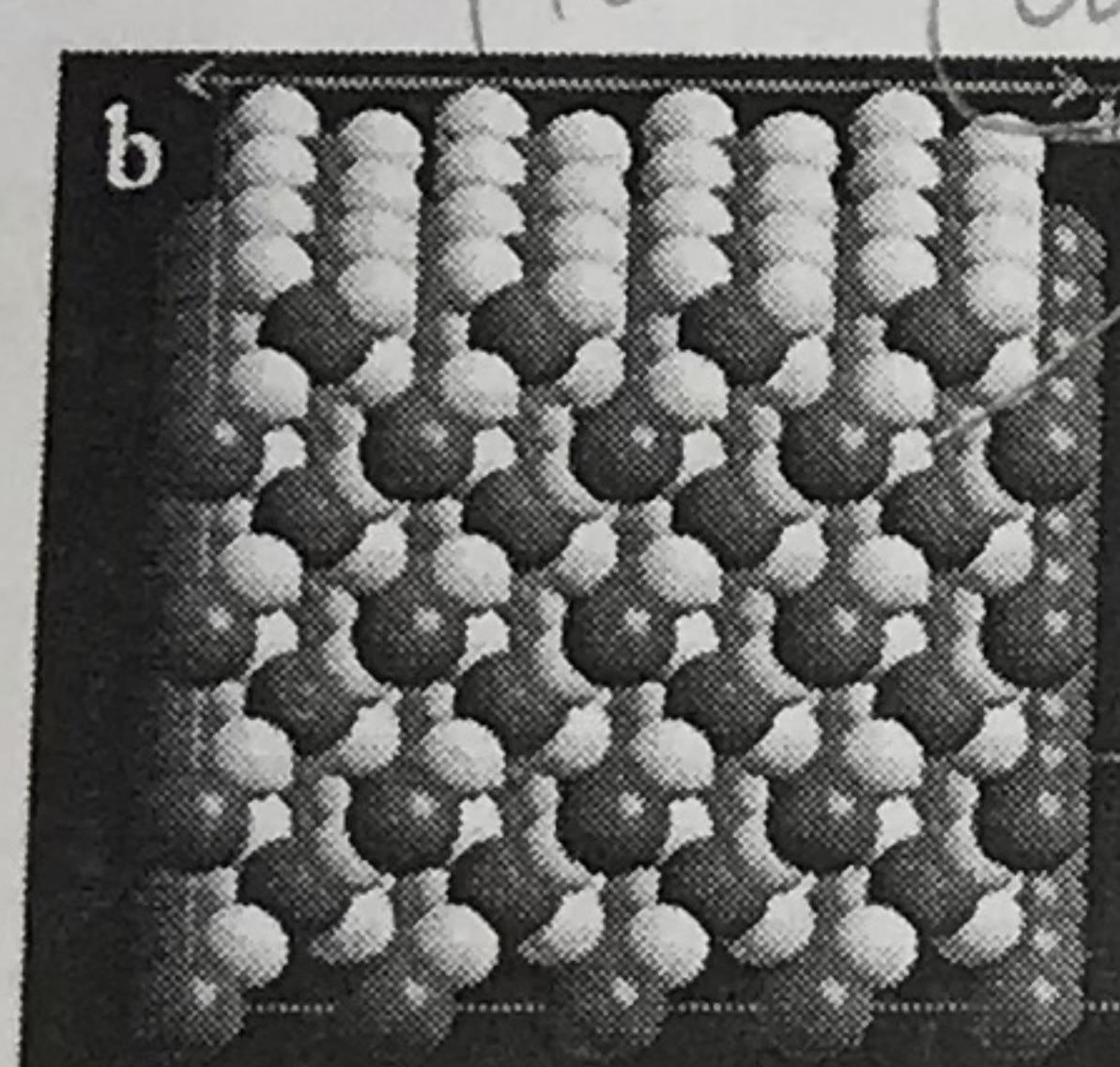
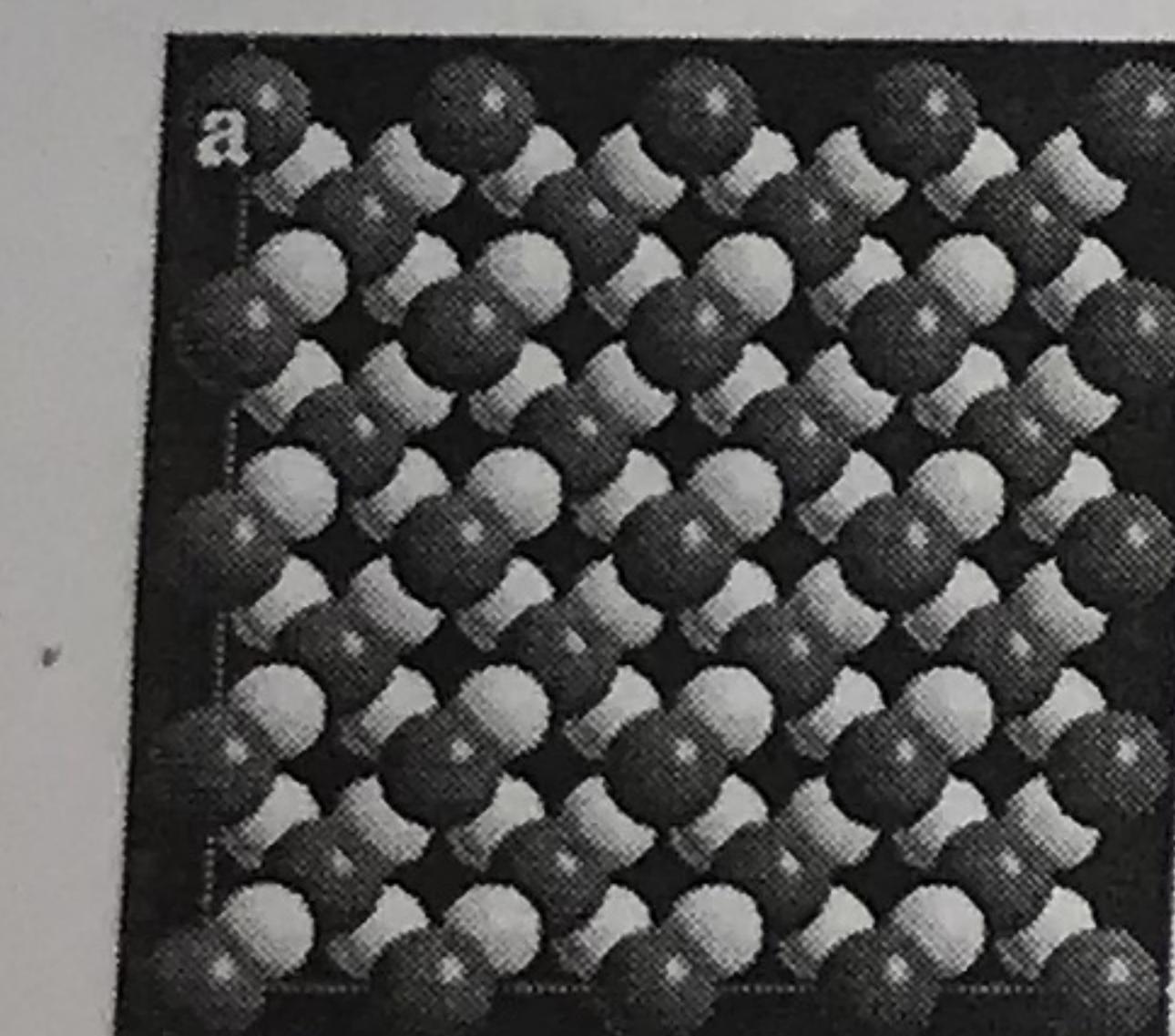
A typical click reaction involves first the preparation of an alkyl or aromatic azide, followed by its reaction with an alkyne to obtain the product.



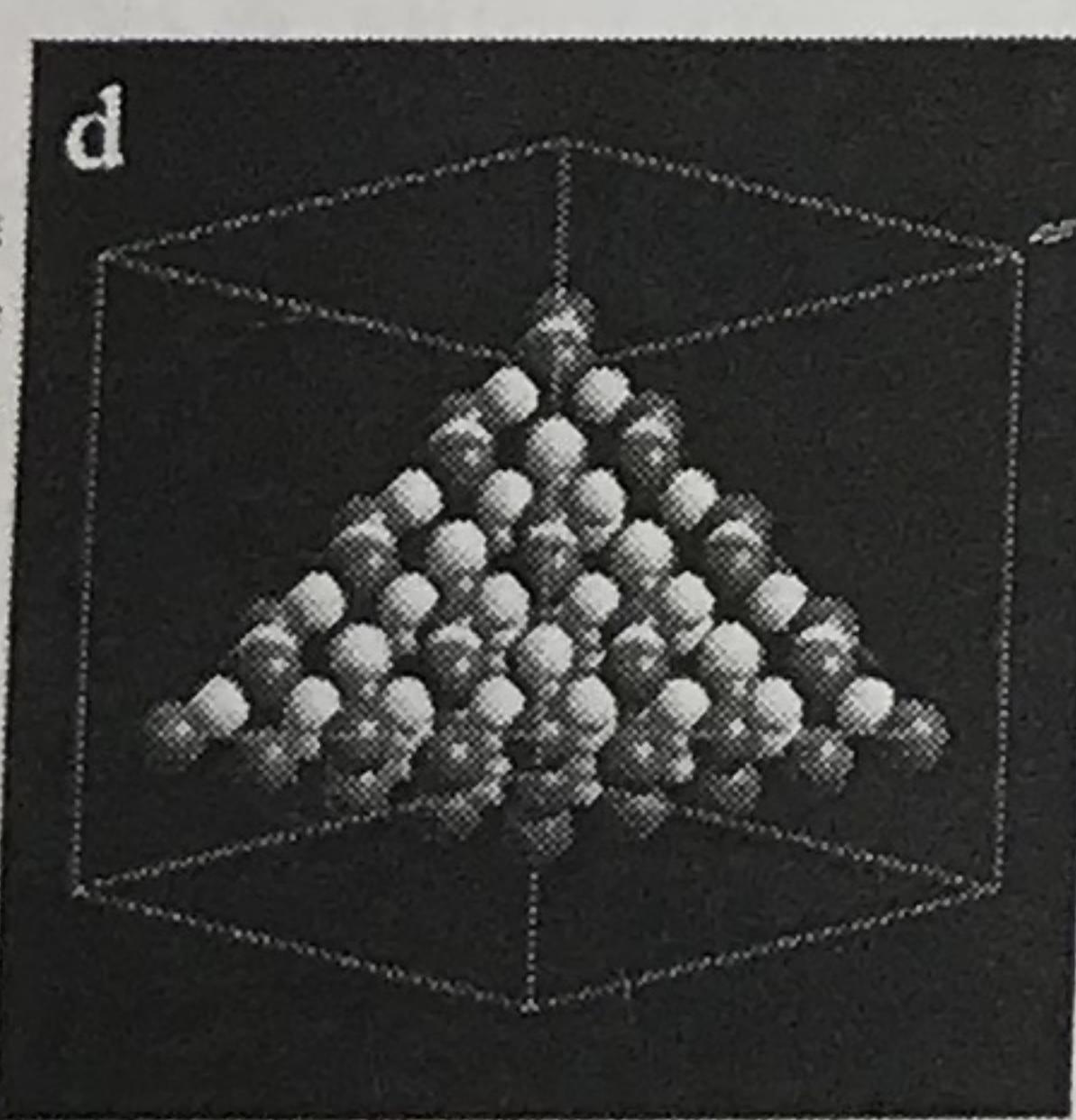
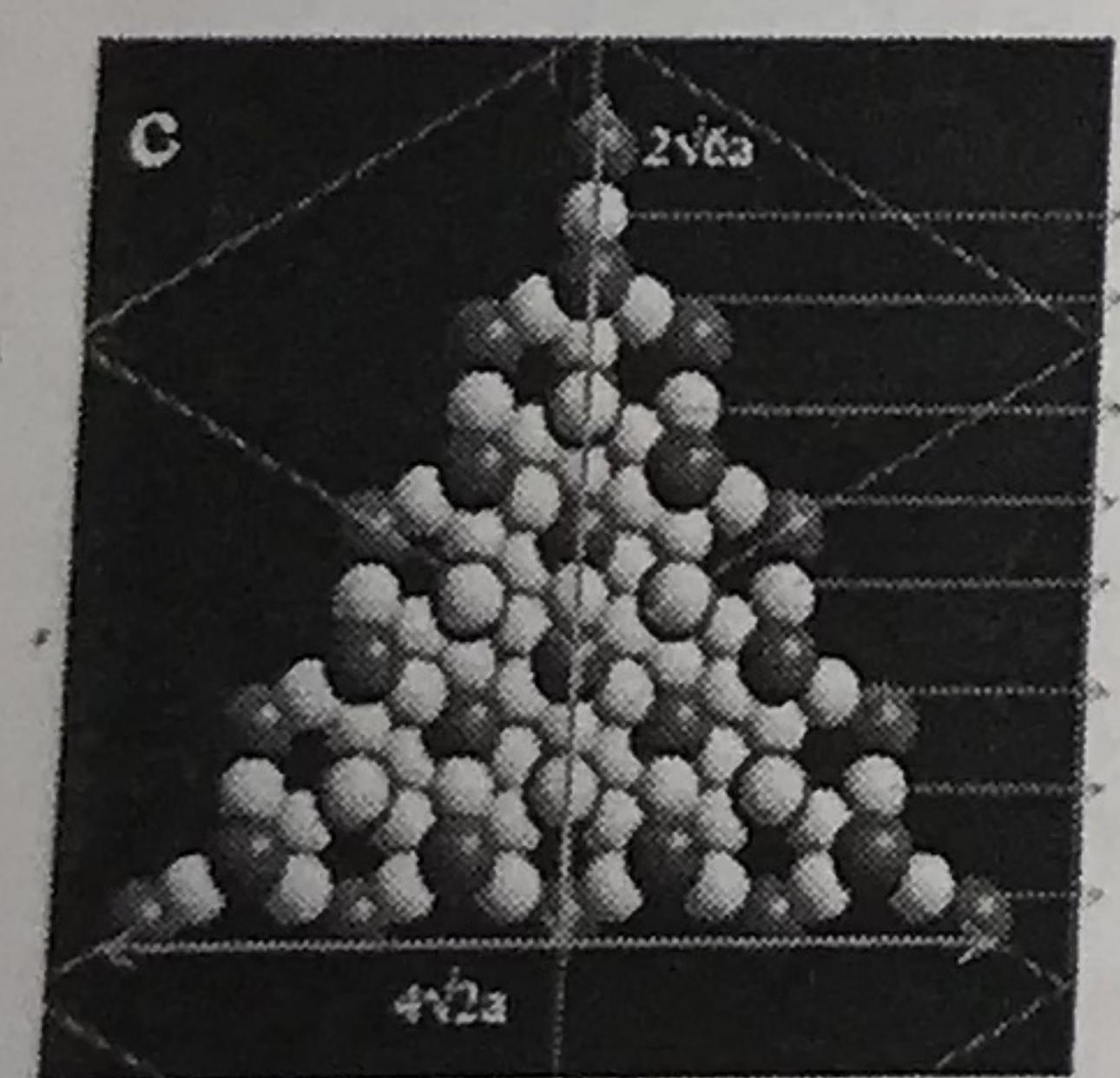
Possible mechanism for the Cu_2O -catalyzed [3 + 2] cycloaddition addition via click chemistry to form triazole.



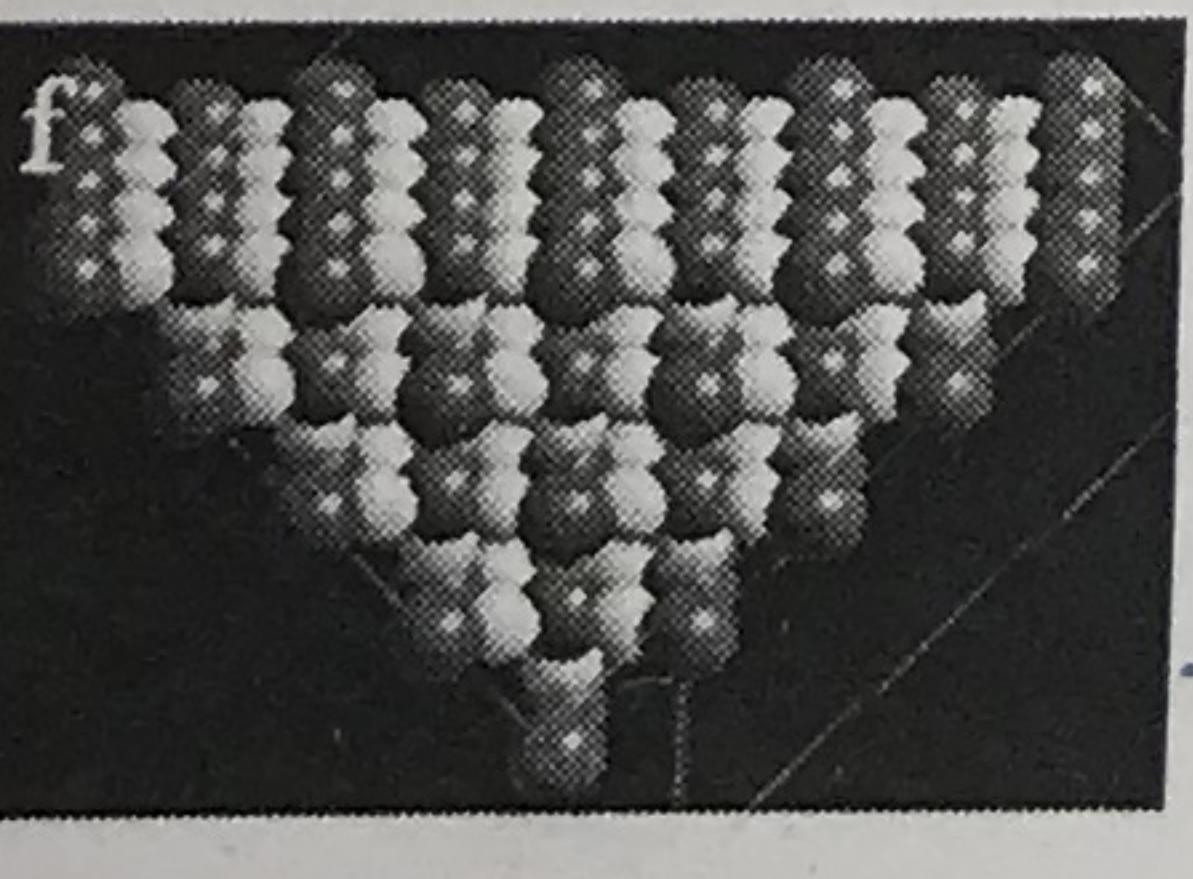
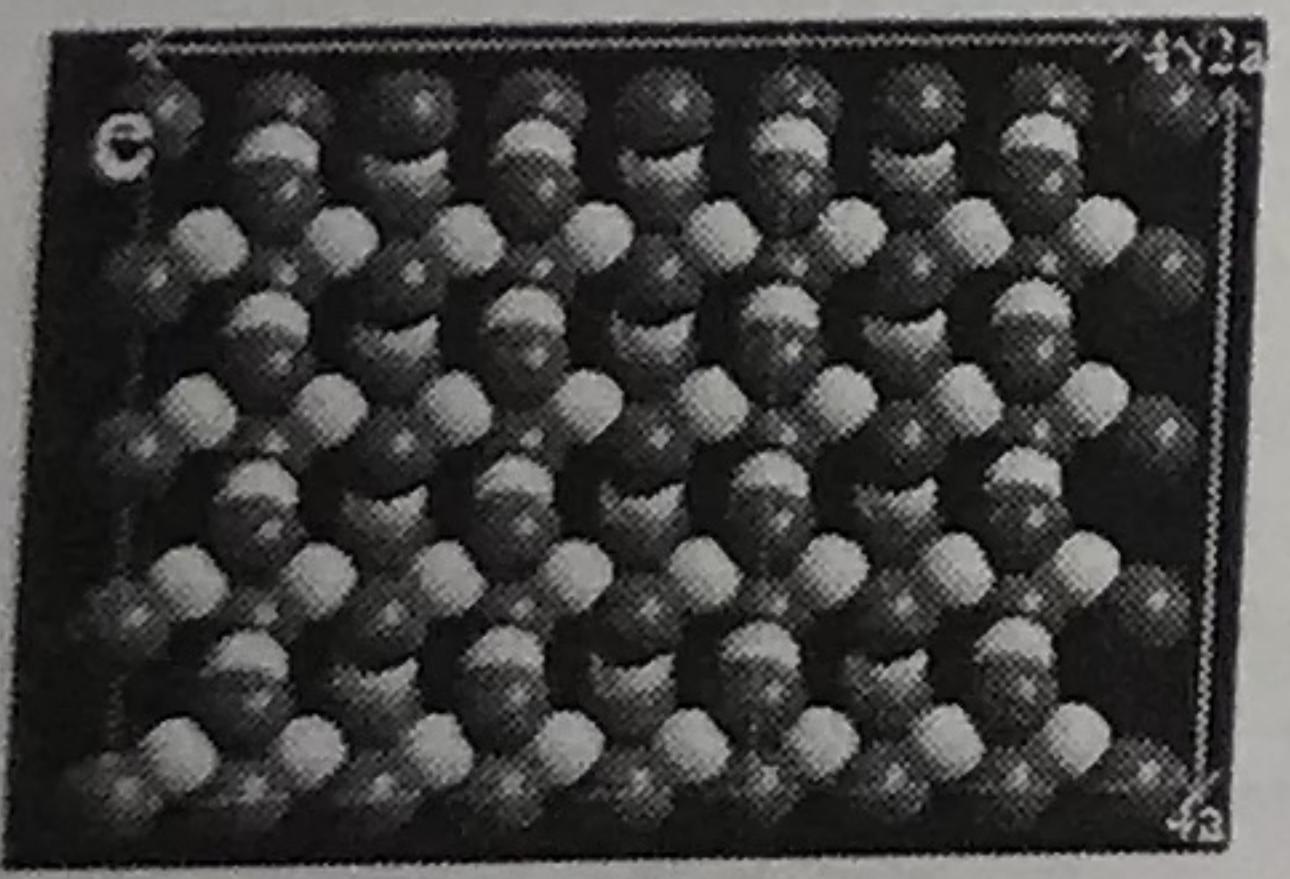
Possible mechanism for the Cu_2O -catalyzed [3 + 2] cycloaddition addition to form isoxazole.



cube.



Octa.



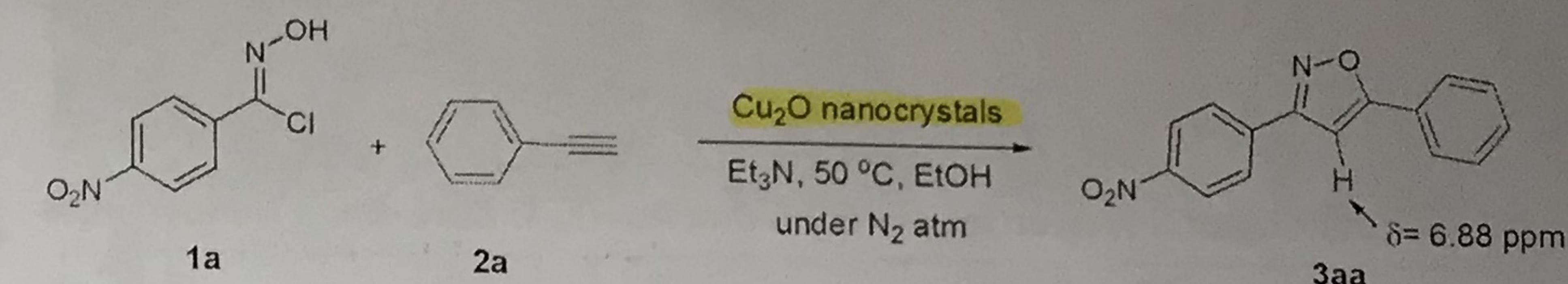
Rd.
110.

Copper atoms are fully exposed on (110) plane, leading to its best catalytic activity.

Chanda, K.; Rej, S.; Huang, M. H. *Chem.-Eur. J.* 2013, 18, 16036

\hookrightarrow Cu atoms are fully exposed.
 \downarrow 易找上 ligand \Rightarrow 光催化活性!

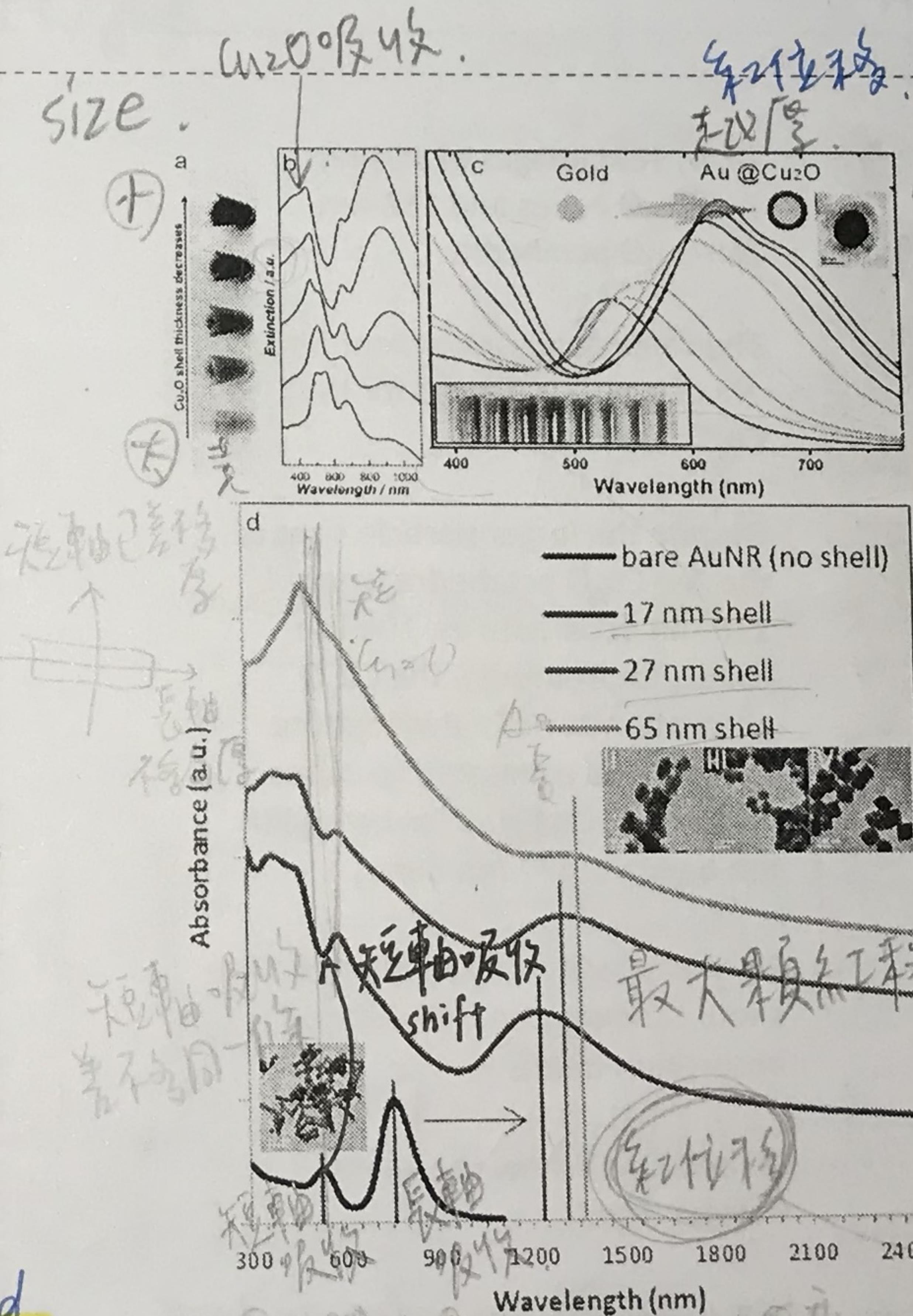
Investigation of Facet Effects on the Catalytic Activity of Cu_2O Nanocrystals for Efficient Regioselective Synthesis of 3,5-Disubstituted Isoxazoles



Entry	Catalyst	BET Surface area/m ² g ⁻¹	Amount used (mg)	Time (h)	Yield ^b
1	Cu_2O (nanocubes)	2.84	1	③ 7	82
2	Cu_2O (octahedra)	0.56	5	② 5	89
3	Cu_2O (rhombic dodecahedra)	1.35	2	① 2	95

^a Reagents and conditions: 1a (50 mg, 0.25 mmol), 2a (26 mg, 0.25 mmol), Et_3N (75 mg, 0.75 mmol), and EtOH (3 mL). ^b Isolated yields

Chanda, K.; Rej, S.; Huang, M. H. *Nanoscale* 2013, 5, 12494

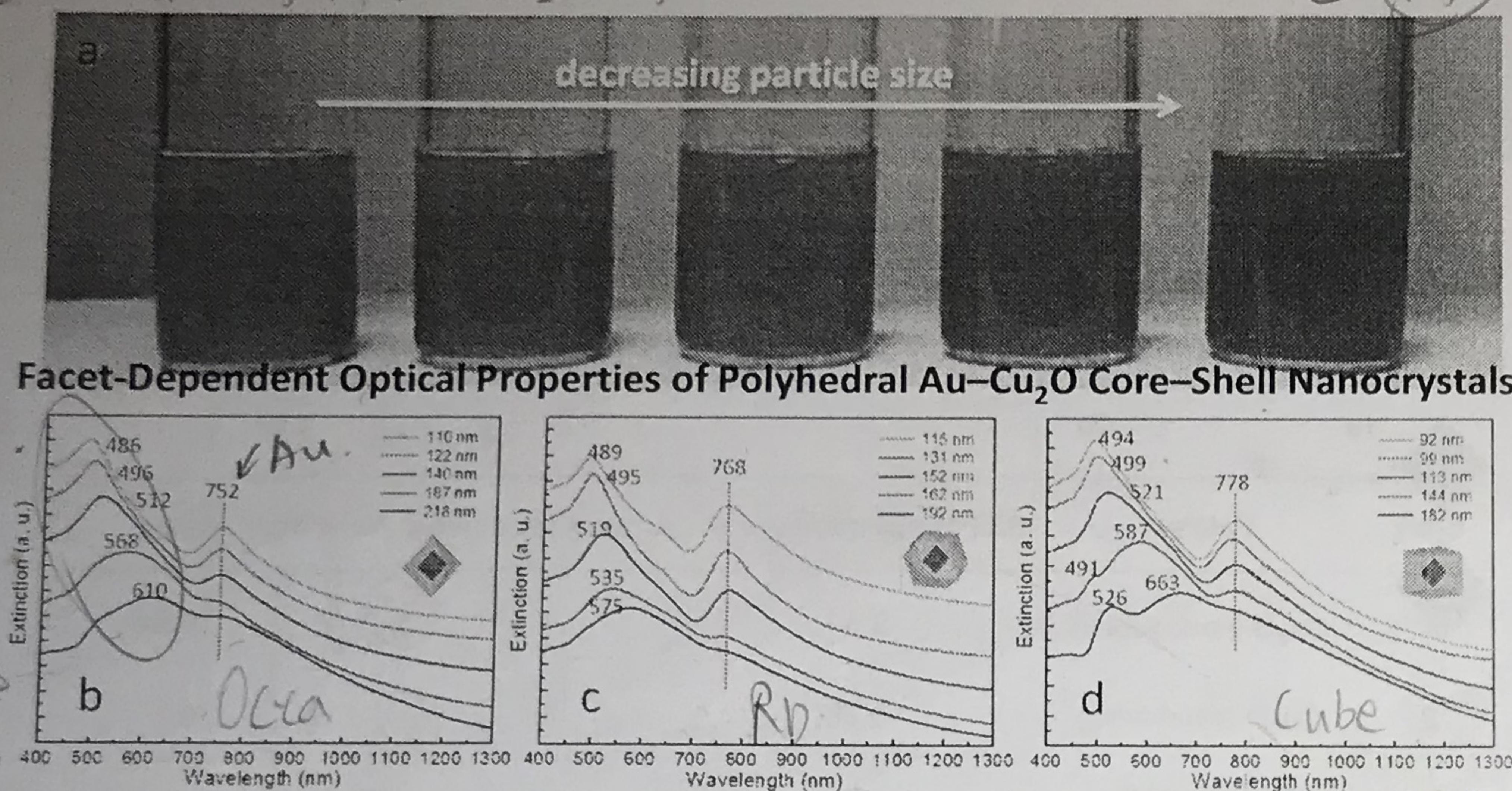


$\text{Au}-\text{Cu}_2\text{O}$ core-shell nanoparticles with average Cu_2O shell thicknesses of 35, 47, 67, 97, and 120 nm (from top to bottom) and measured extinction spectra of the five colloidal samples. (c) Photograph, TEM image and UV-vis spectra of $\text{Au}-\text{Cu}_2\text{O}$ nanoparticles with increasing shell thickness. (d) TEM images and UV-vis spectra of Au nanorods and Au nanorod- Cu_2O nanocrystals with different shell thicknesses.

Huang, M. H.; Rej, S.; Chiu, C.-Y. *Small* 2015, 11, 2716

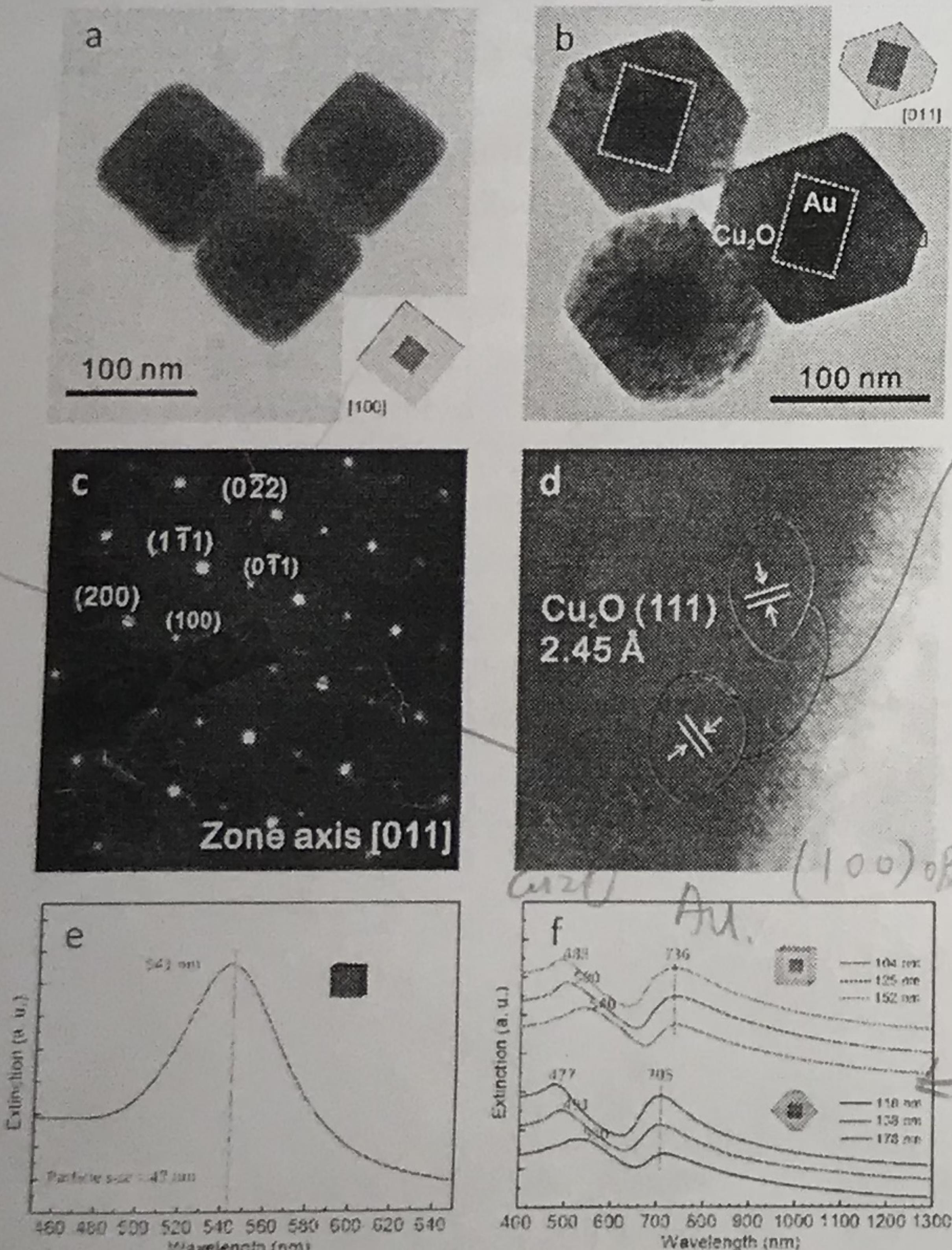
光學有晶面效應

(w)O会紅移但Au位置不變
(大小一樣)



Using 50-nm octahedral Au cores to make Au–Cu₂O core–shell octahedra, cuboctahedra, and cubes of different shell thicknesses, the Au SPR band is fixed despite changes in the shell thickness, but is dependent on the exposed surfaces of Cu₂O.

Yang, Y.-C.; Wang, H.-J.; Whang, J.; Huang, J.-S.; Lyu, L.-M.; Lin, P.-H.; Gwo, S.;
Huang, M. H. *Nanoscale* **2014**, *6*, 4316.



(a, b) TEM images of 104-nm Au–Cu₂O cubes and 118-nm Au–Cu₃O octahedra.

The same facet-dependent optical effect is also observed for the Cu₂O shell.

Despite the larger particle sizes of the Au–Cu₂O octahedra (panel f, 118-nm octahedra vs. 104-nm cubes, for example), the Cu₂O absorption band is always more blue-shifted compared to cubes with somewhat smaller sizes (488 nm band vs. 477 nm band).

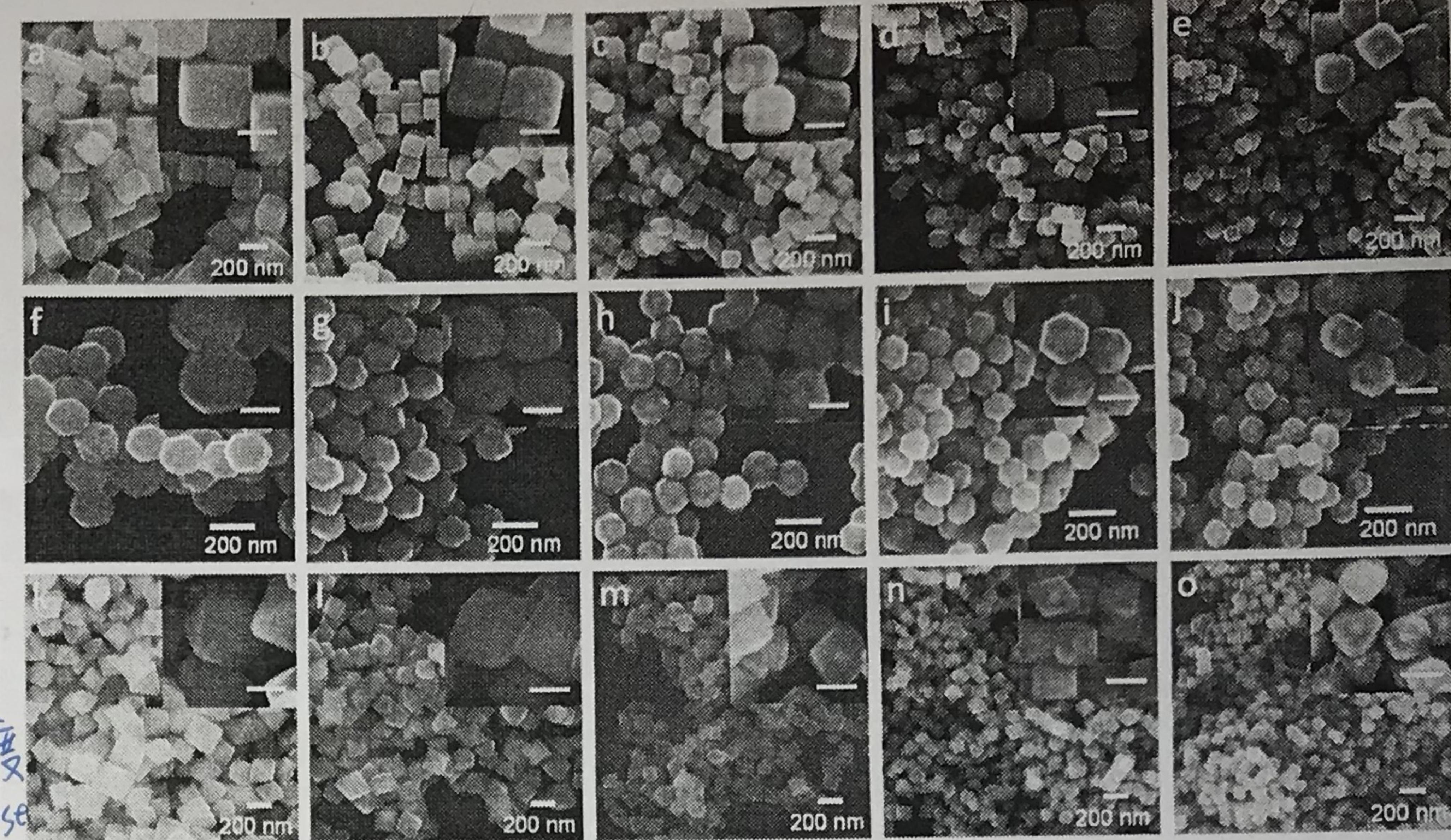
Normally larger Cu_2O particles should show more red-shifted absorption band.

Au and Cu₂O show the same shifting trend.

For Cu_2O shell:

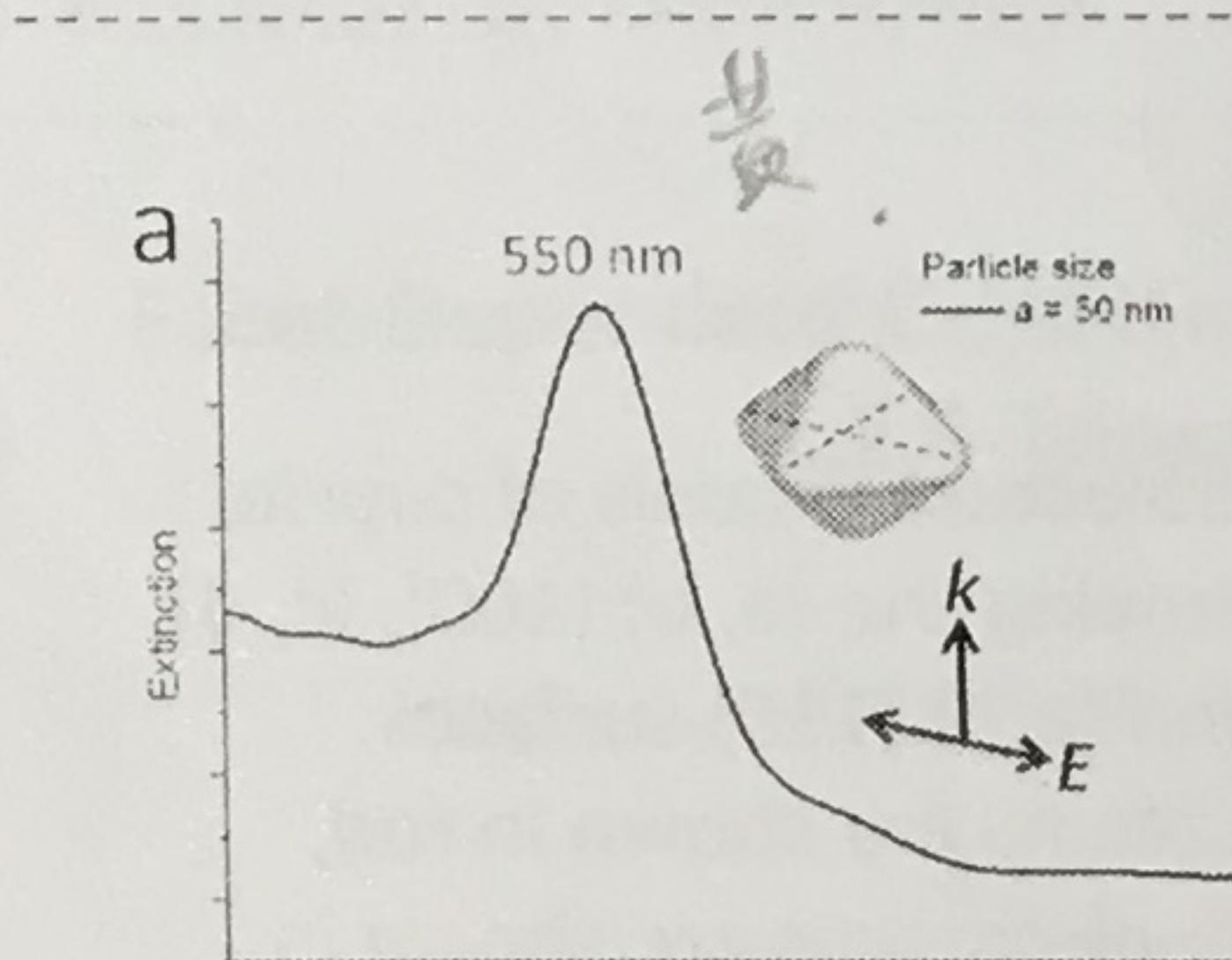
cube 軟 octa 硬面
(100) * facet-dependent
optical effect

sendent. 比較為高。



SEM images of the synthesized Au–Cu₂O core–shell nanocrystals. The particle morphologies are (a–e) cubic, (f–j) cuboctahedral, and (k–o) octahedral in shape. Particle sizes decrease from left to right. The octahedral gold cores have an average size of 50 nm.

Audi-英語



(a) Normalized extinction spectrum of the bare octahedral cores. (b and c) Simulation results for the UV–vis absorption spectra of cubooctahedral and cubic $\text{Au}-\text{Cu}_x\text{O}$ core–shell nanocrystal solutions with different particle sizes.

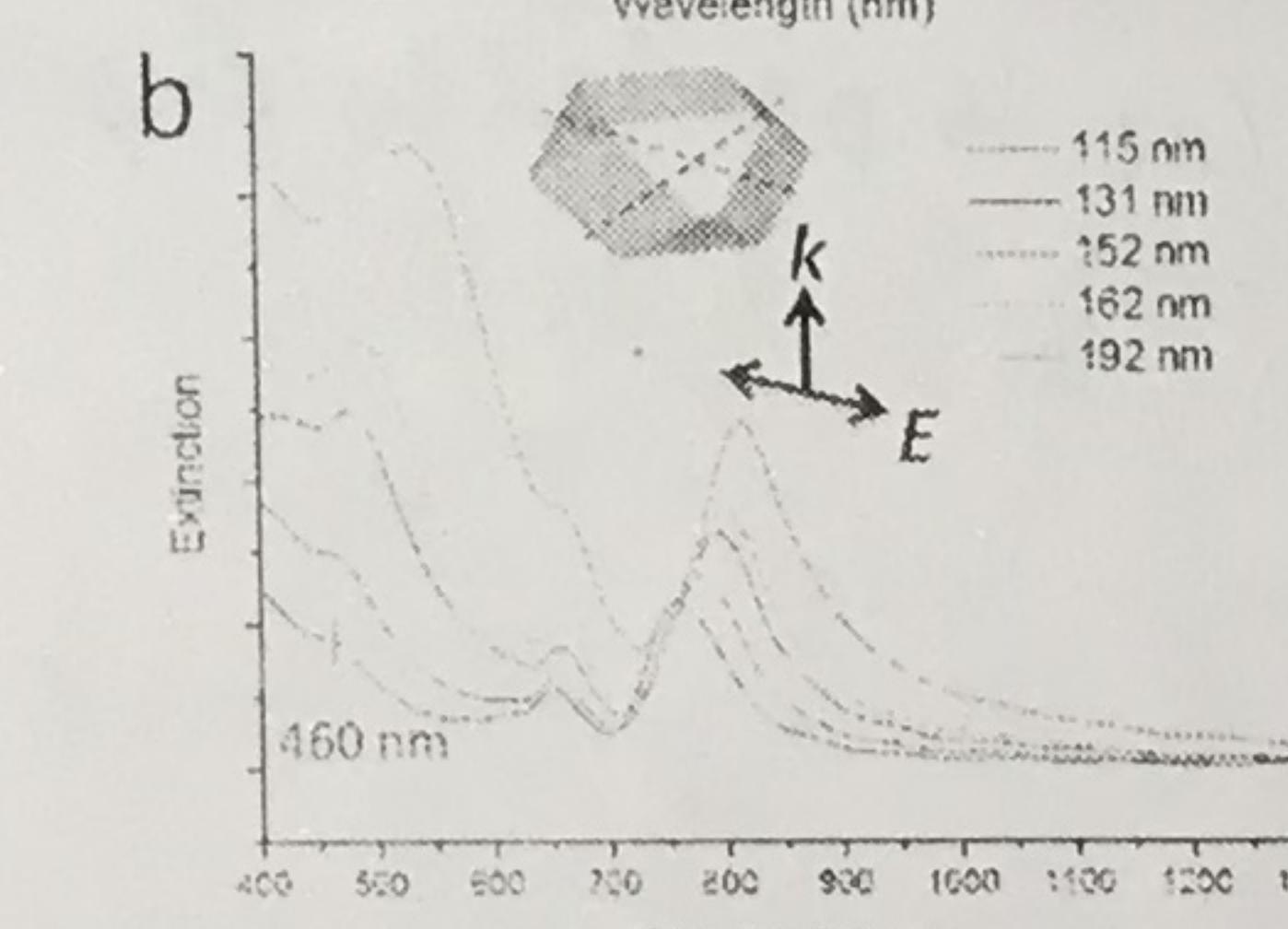


Figure 2 consists of three panels (a, b, c) showing extinction spectra and corresponding transmission electron microscopy (TEM) images.

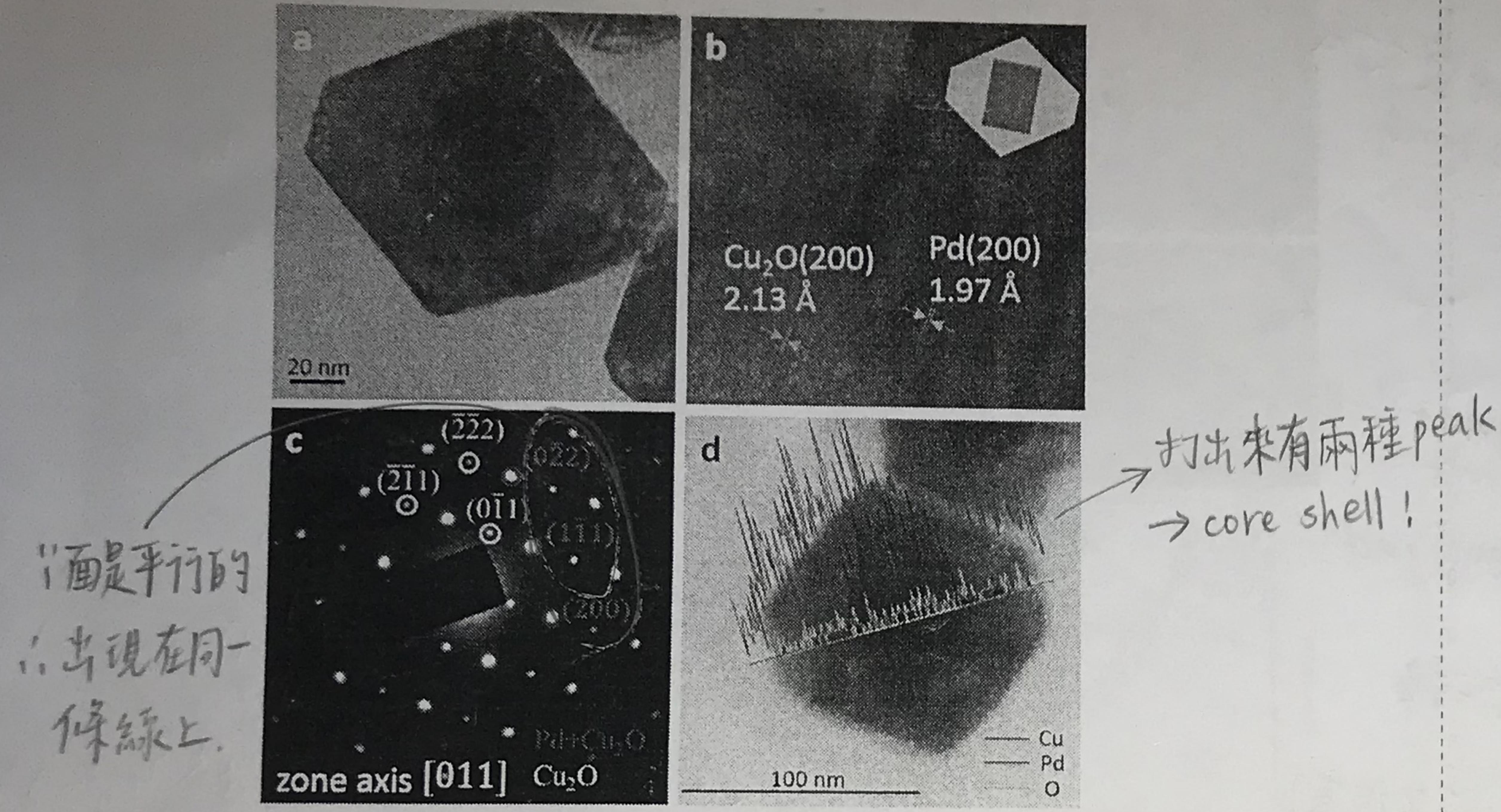
- Panel (a):** Shows extinction spectra for sample (110). The y-axis is labeled "Extinction (a. u.)" and the x-axis is "Wavelength (nm)" from 400 to 900 nm. Three curves are shown for different wavelengths: 122 nm (solid line), 140 nm (dashed line), and 183 nm (dash-dot line). The 122 nm curve has a peak at 490 nm and a shoulder at 499 nm. The 140 nm curve has a peak at 521 nm. The 183 nm curve has a peak at 694 nm. A small TEM image shows a square-shaped nanoparticle with a central dark region. Labels "(110)" and "RD" are present.
- Panel (b):** Shows extinction spectra for sample (488). The y-axis is labeled "Extinction (a. u.)" and the x-axis is "Wavelength (nm)" from 400 to 900 nm. Three curves are shown for different wavelengths: 126 nm (solid line), 155 nm (dashed line), and 196 nm (dash-dot line). The 126 nm curve has a peak at 501 nm. The 155 nm curve has a peak at 527 nm. The 196 nm curve has a peak at 721 nm. A small TEM image shows a square-shaped nanoparticle with a central dark region.
- Panel (c):** Shows extinction spectra for sample (500). The y-axis is labeled "Extinction (a. u.)" and the x-axis is "Wavelength (nm)" from 400 to 900 nm. Three curves are shown for different wavelengths: 86 nm (solid line), 103 nm (dashed line), and 119 nm (dash-dot line). The 86 nm curve has a peak at 500 nm. The 103 nm curve has a peak at 511 nm. The 119 nm curve has a peak at 533 nm. A small TEM image shows a square-shaped nanoparticle with a central dark region. Labels "(100)" and "RD" are present.

Au SPR band position differs by 47 nm from Au-Cu₂O rhombic dodecahedra to nanocubes. Here 35 nm octahedral Au cores were used.

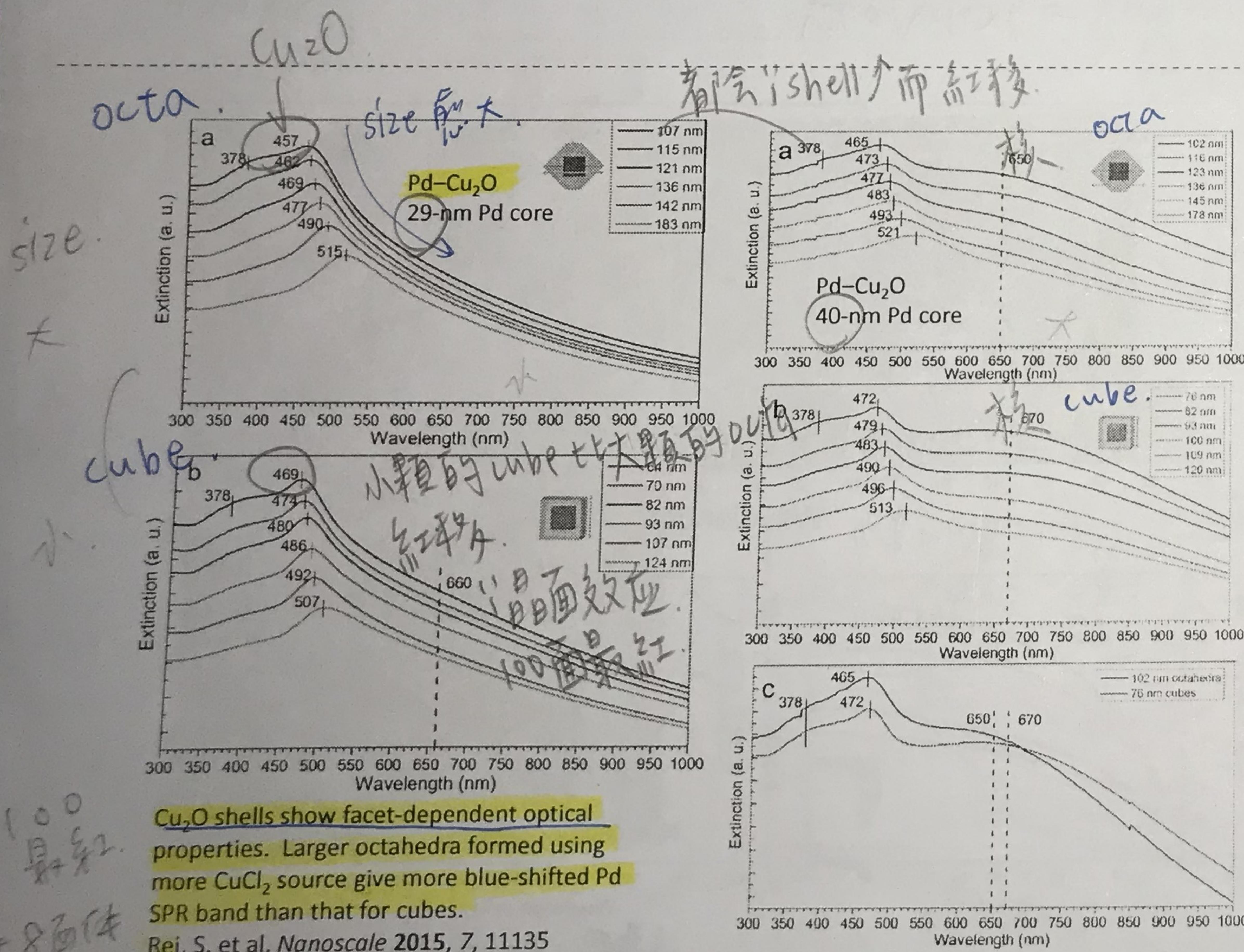
Hsu, S.-C.; Liu, S.-Y.; Wang, H.-J.; Huang, M. H.
Small 2015, 11, 195.

Huang, M. H.

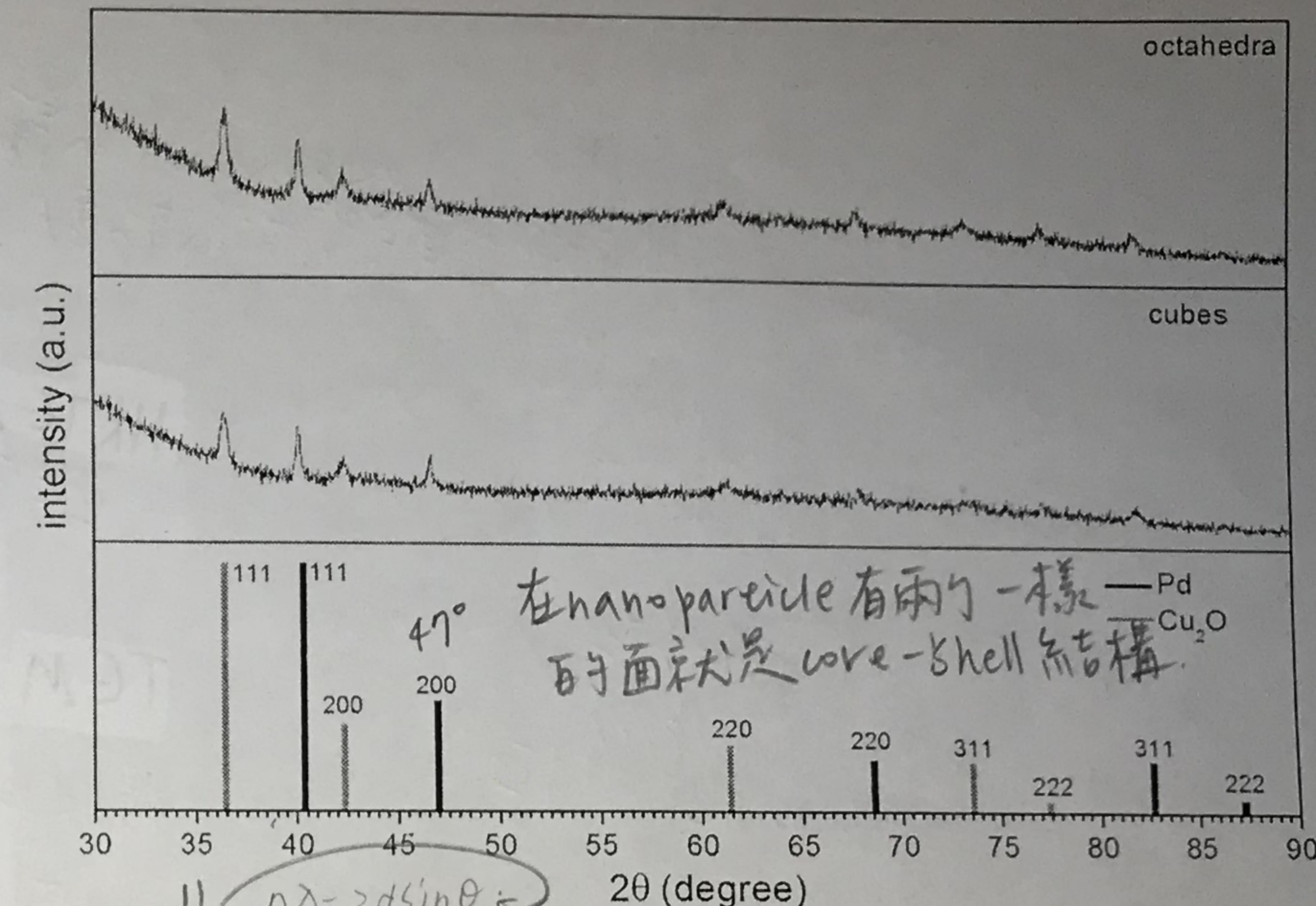
- * face-dependent optical effect



(a) TEM image, (b) HR-TEM image, (c) SAED pattern, and (d) EDS line scans of a Pd–Cu₂O core–shell octahedron.

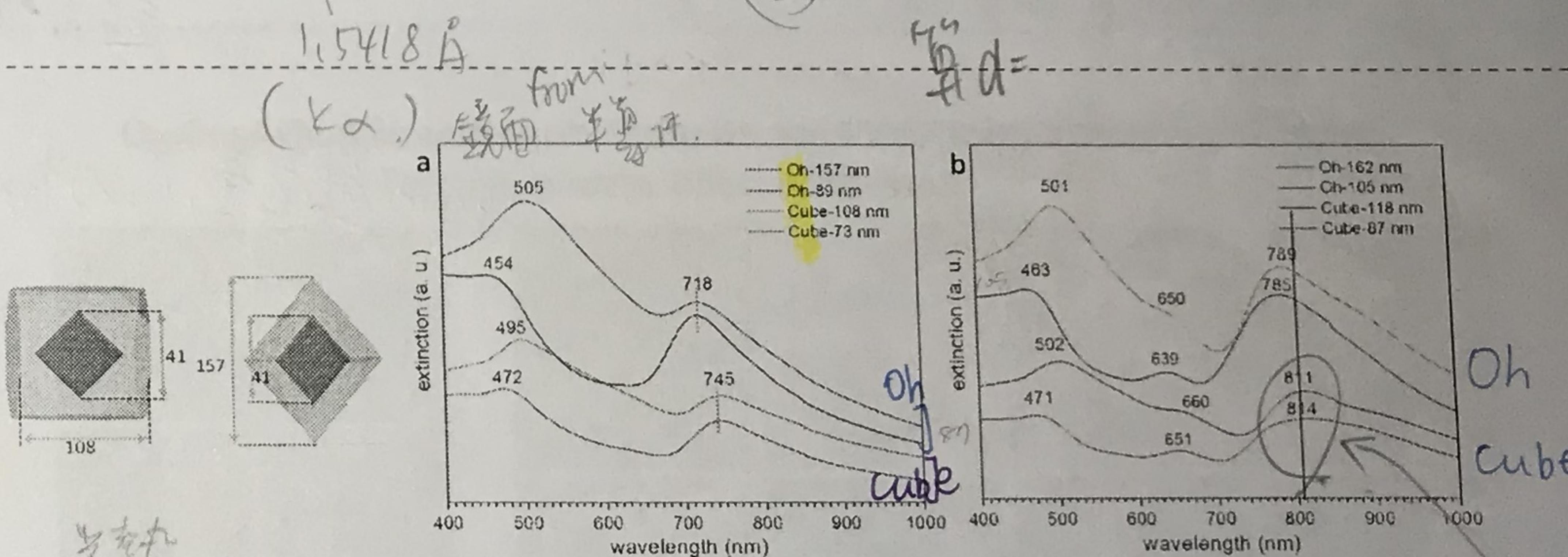


Cu₂O shells show facet-dependent optical properties. Larger octahedra formed using more CuCl₂ source give more blue-shifted Pd SPR band than that for cubes.

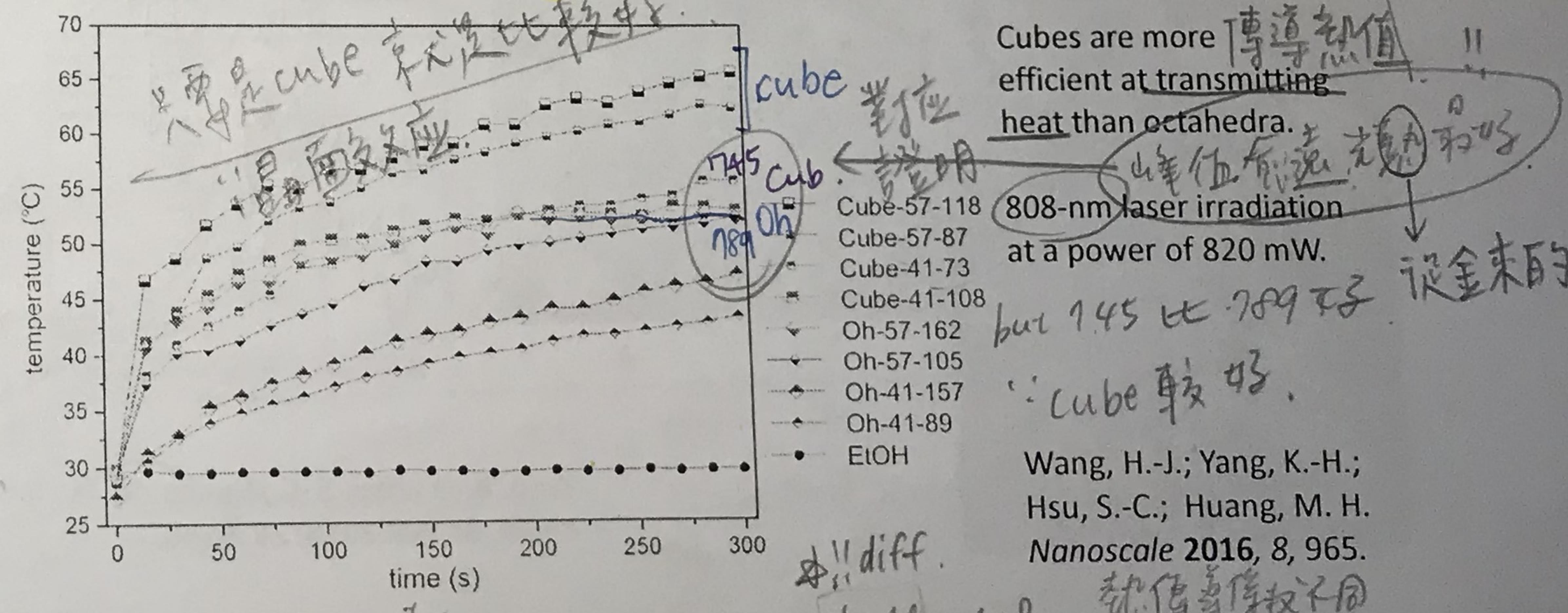


Representative XRD patterns of Pd–Cu₂O octahedra and nanocubes. Standard XRD patterns of Pd and Cu₂O are also provided.

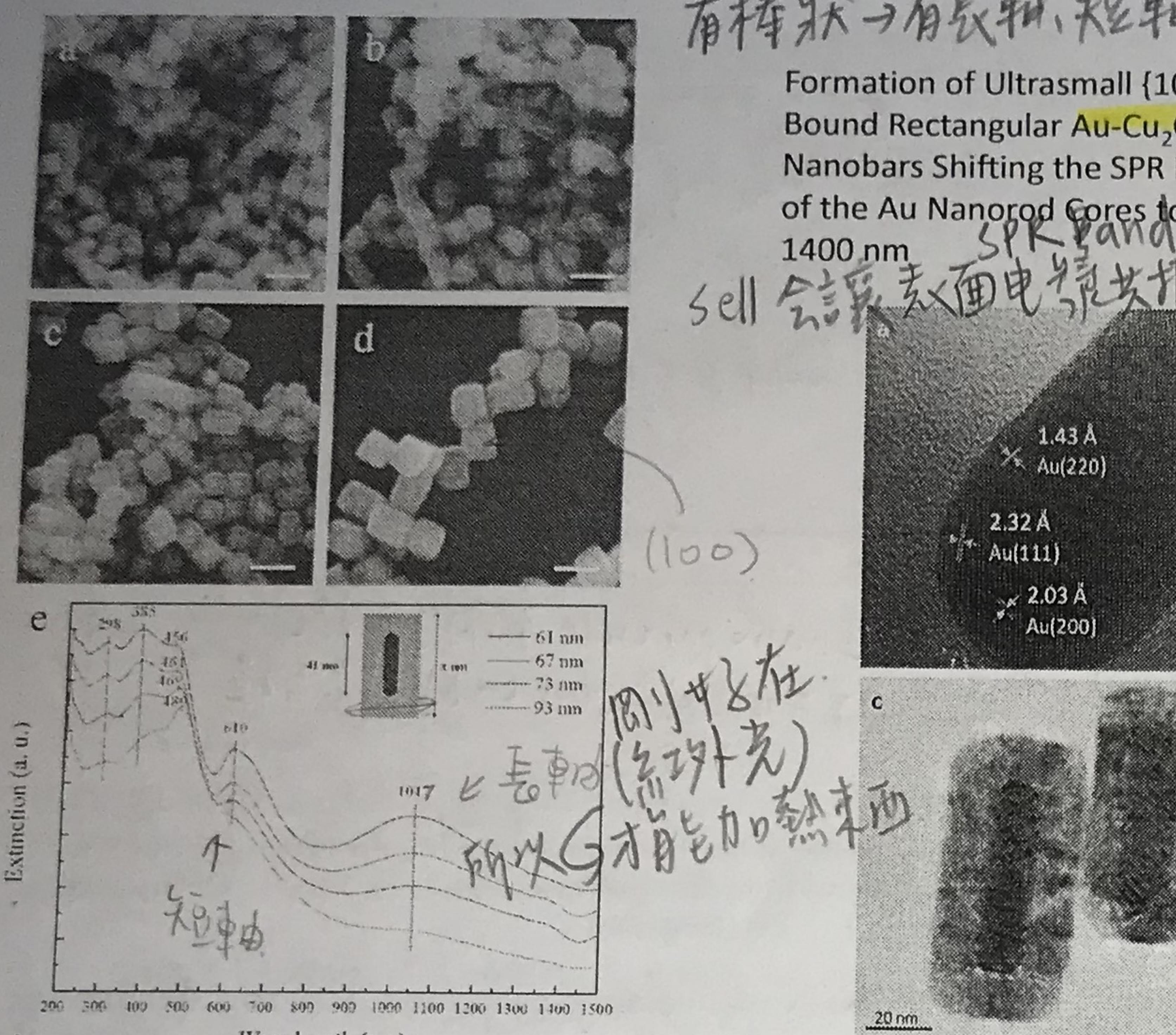
$$n \times 1.5418 = 2d \times \sin \theta \frac{4}{2}$$



Photothermal efficiency of Au–Cu₂O nanocrystals were found to be facet-dependent.

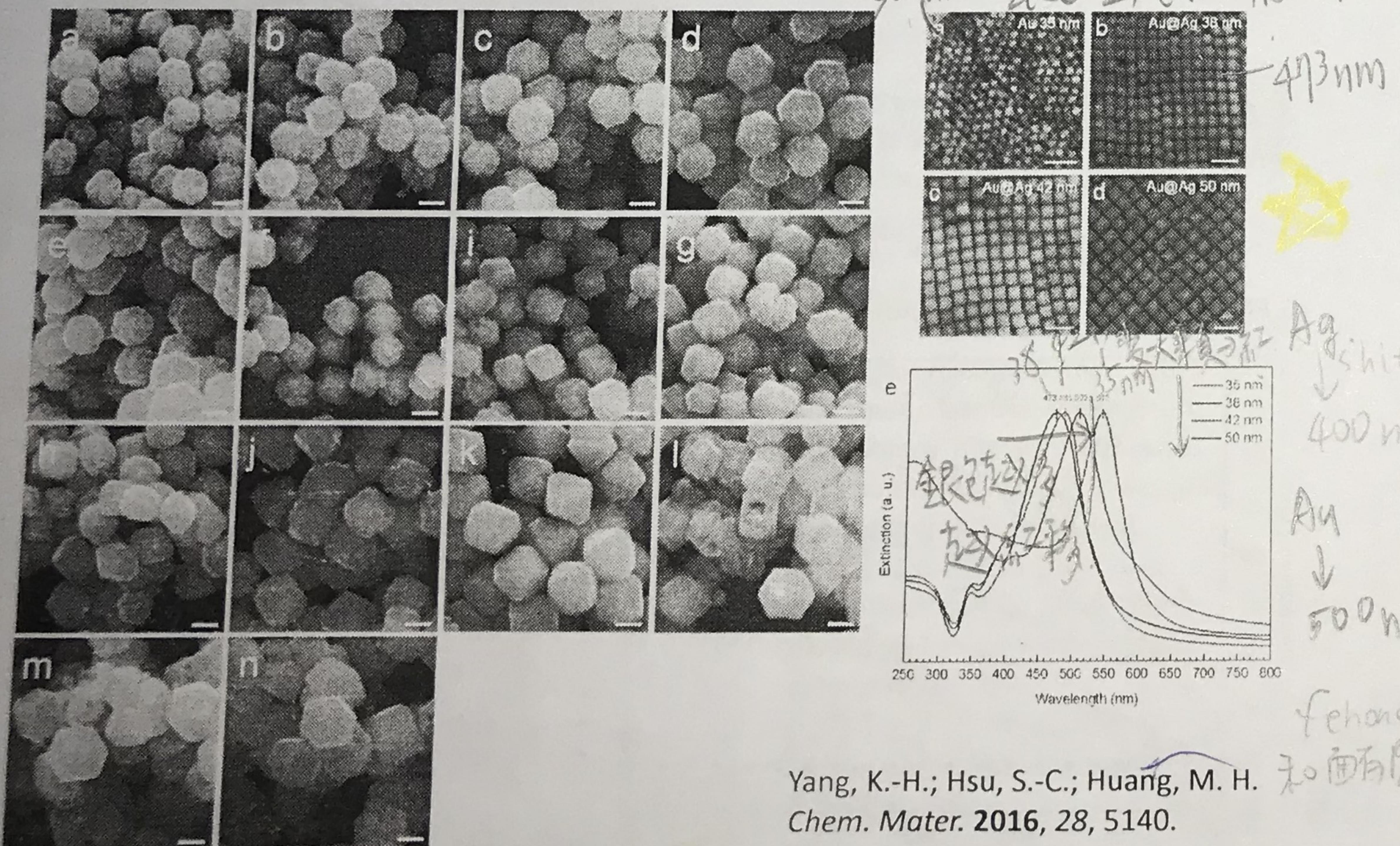


Wang, H.-J.; Yang, K.-H.;
Hsu, S.-C.; Huang, M. H.
Nanoscale **2016**, *8*, 965.

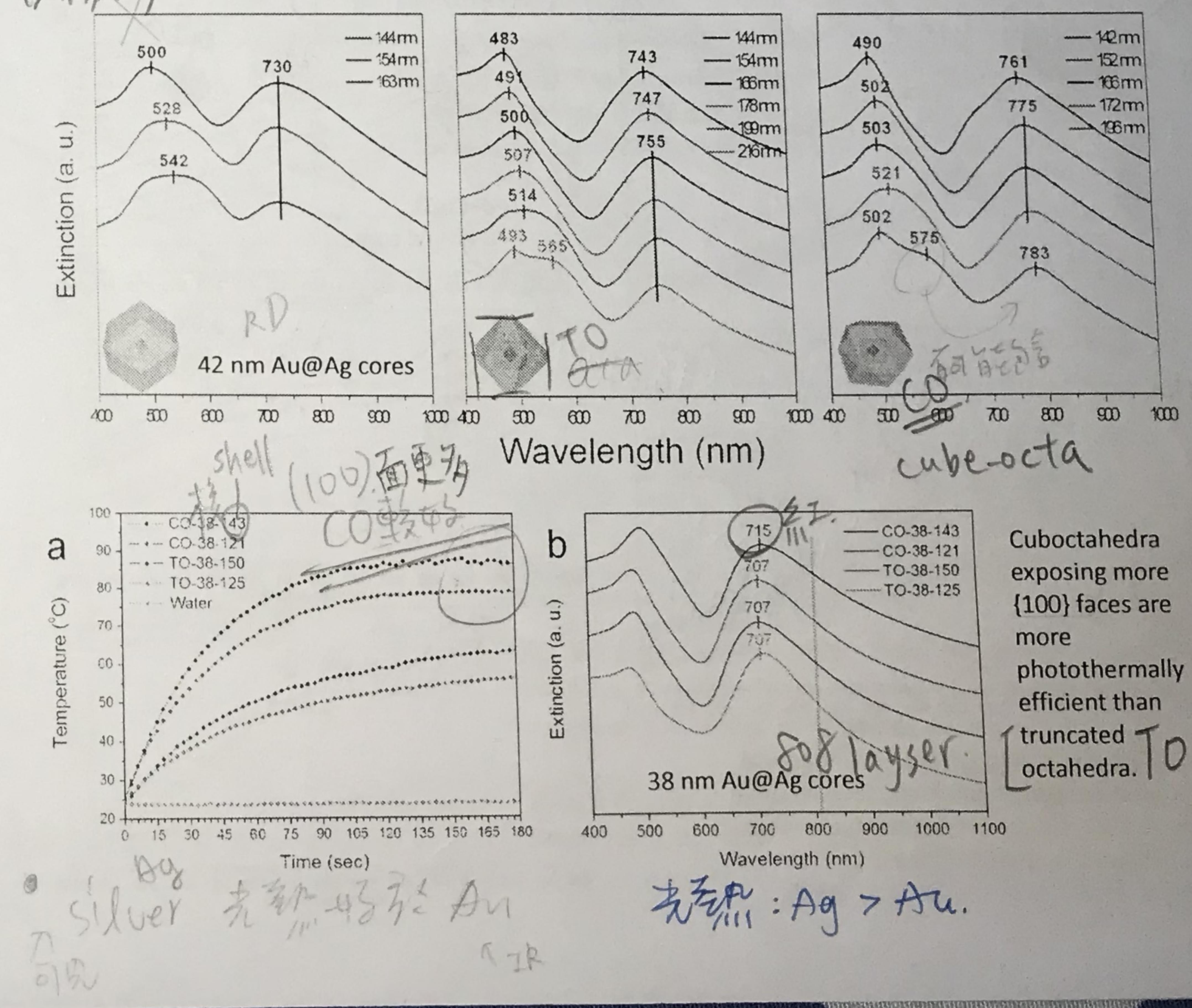
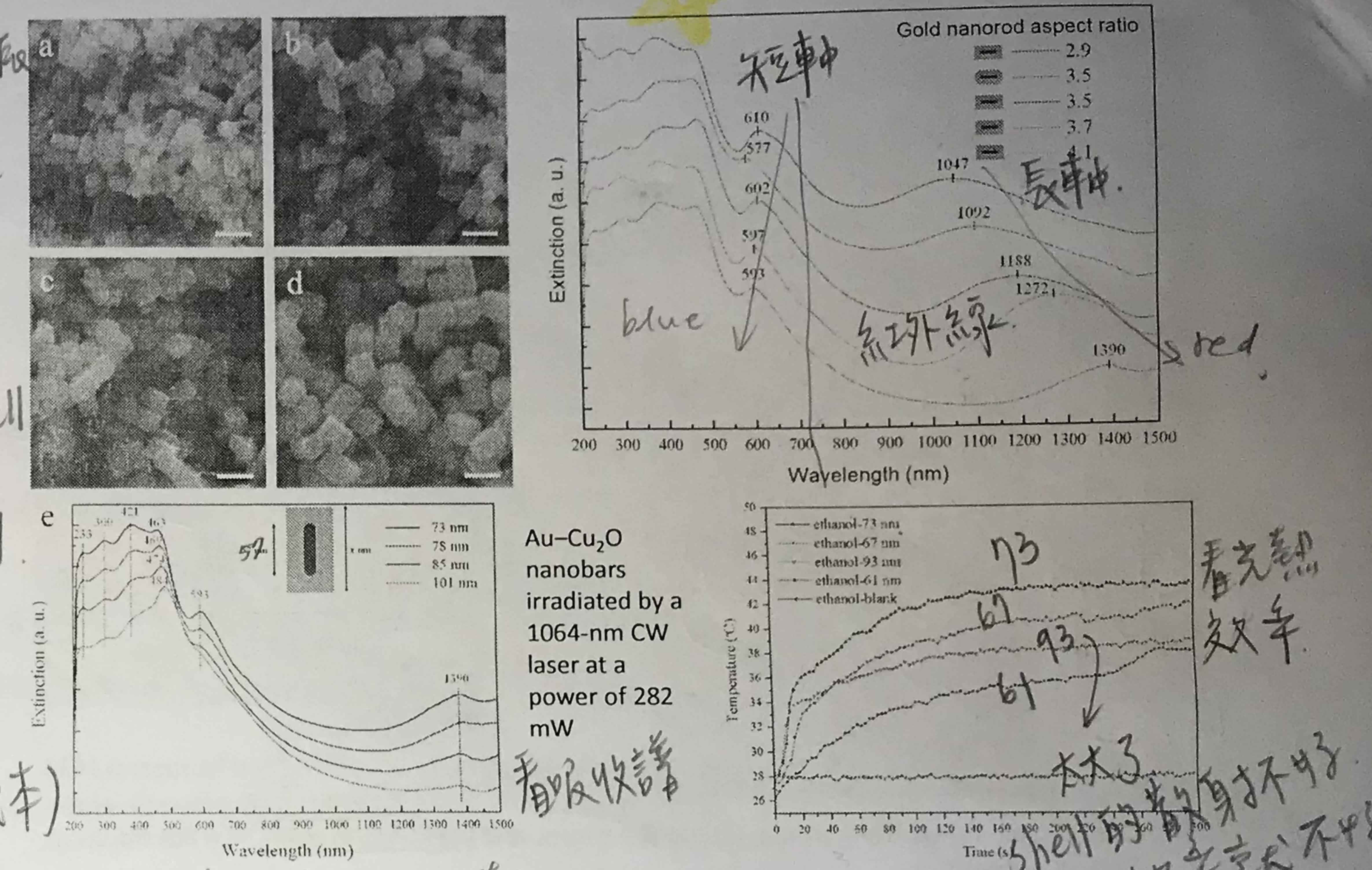


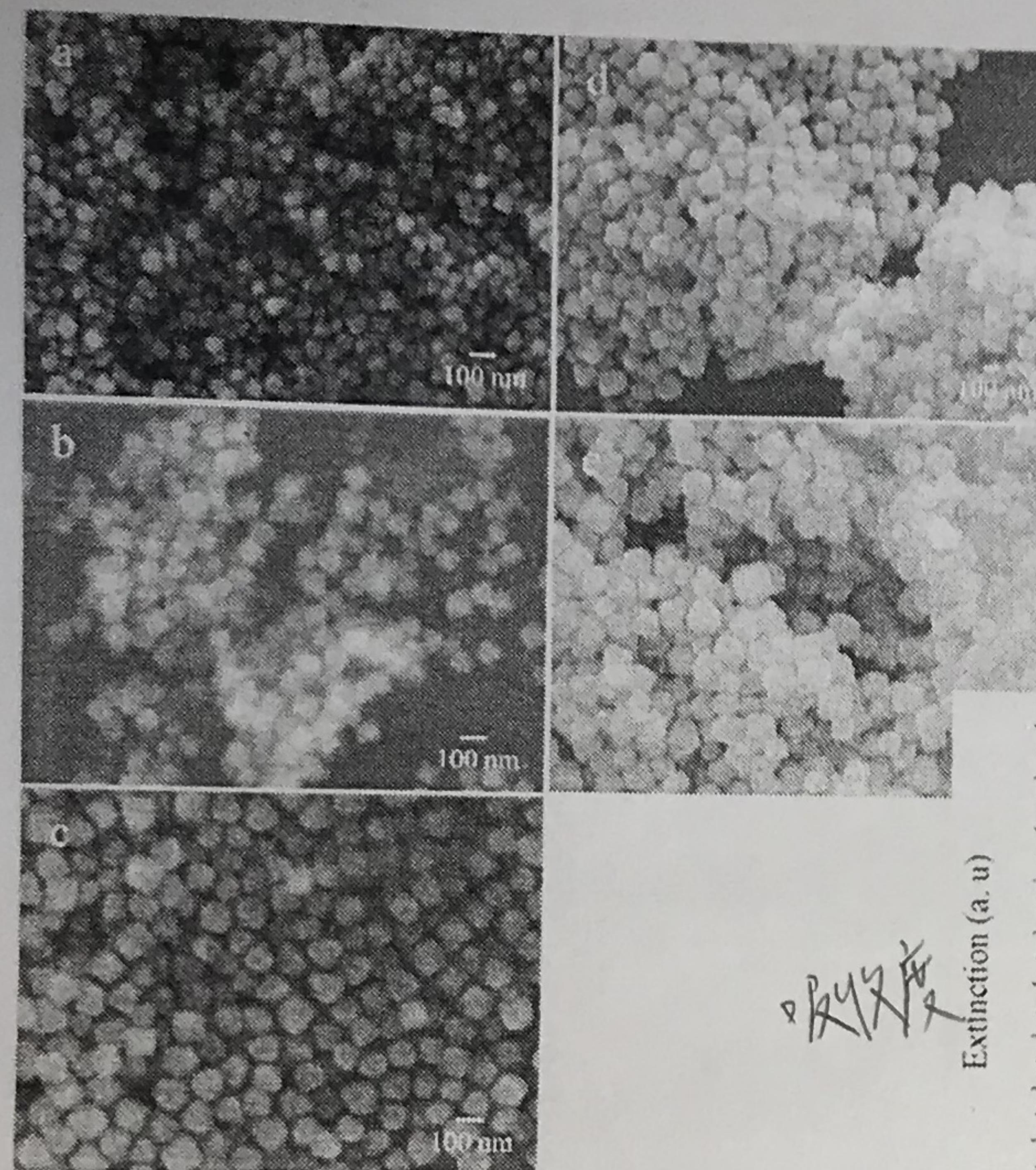
shift 趨勢 → 使之朝著紅端 red shift

Facet-Dependent Optical and Photothermal Properties of Au@Ag–Cu₂O Core–Shell Nanocrystals



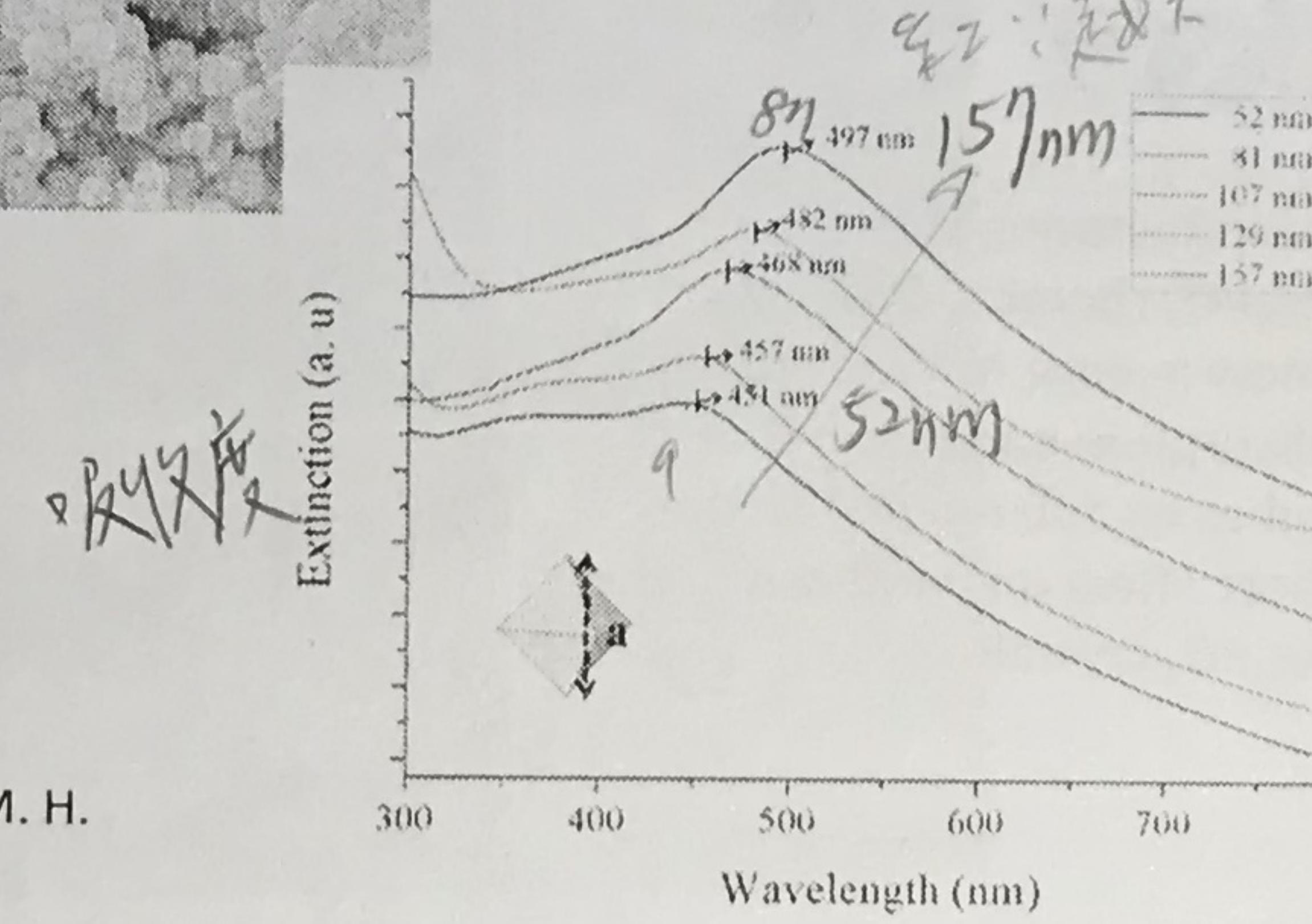
Yang, K.-H.; Hsu, S.-C.; Huang, M. H.
Chem. Mater. 2016, 28, 5140.





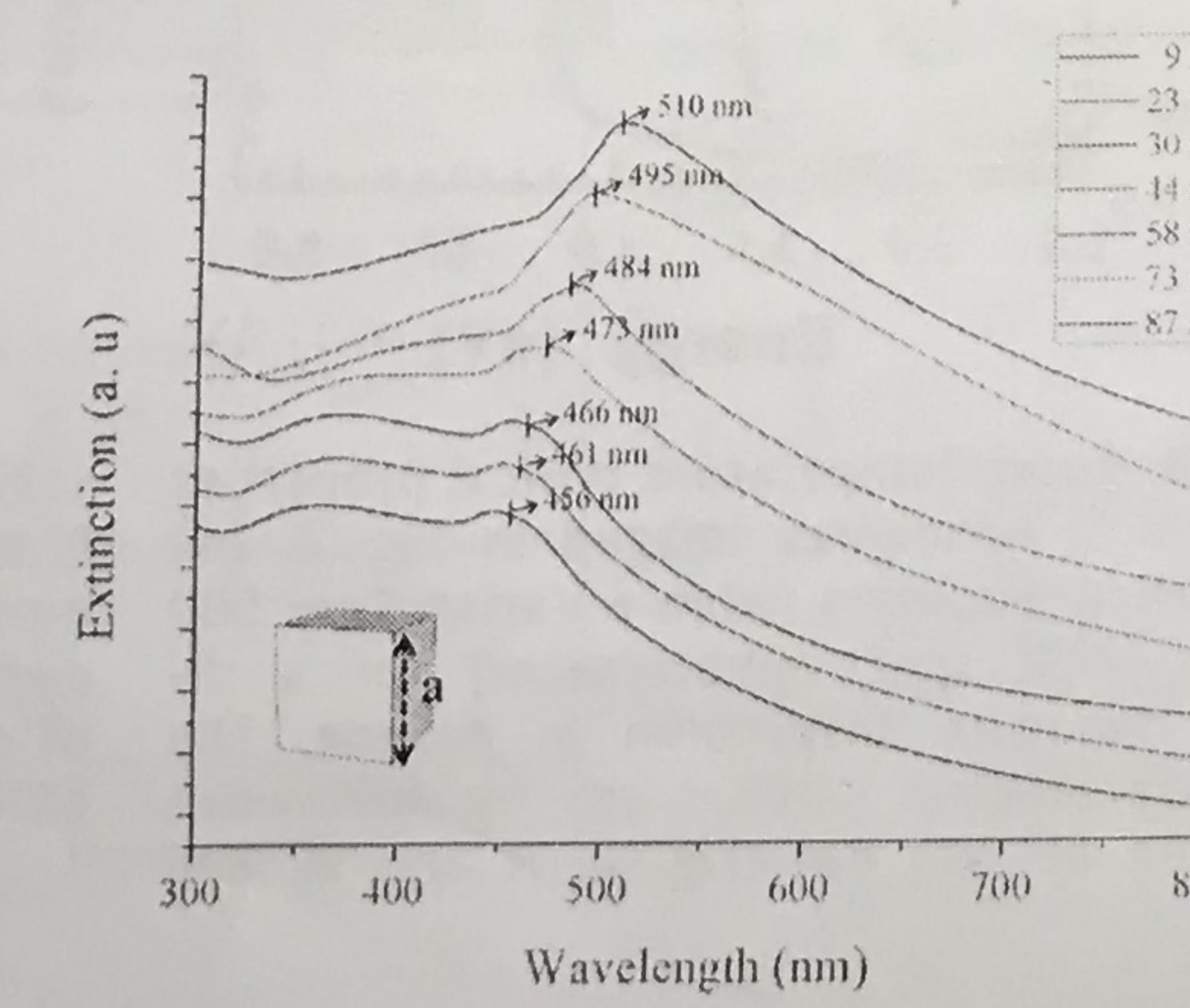
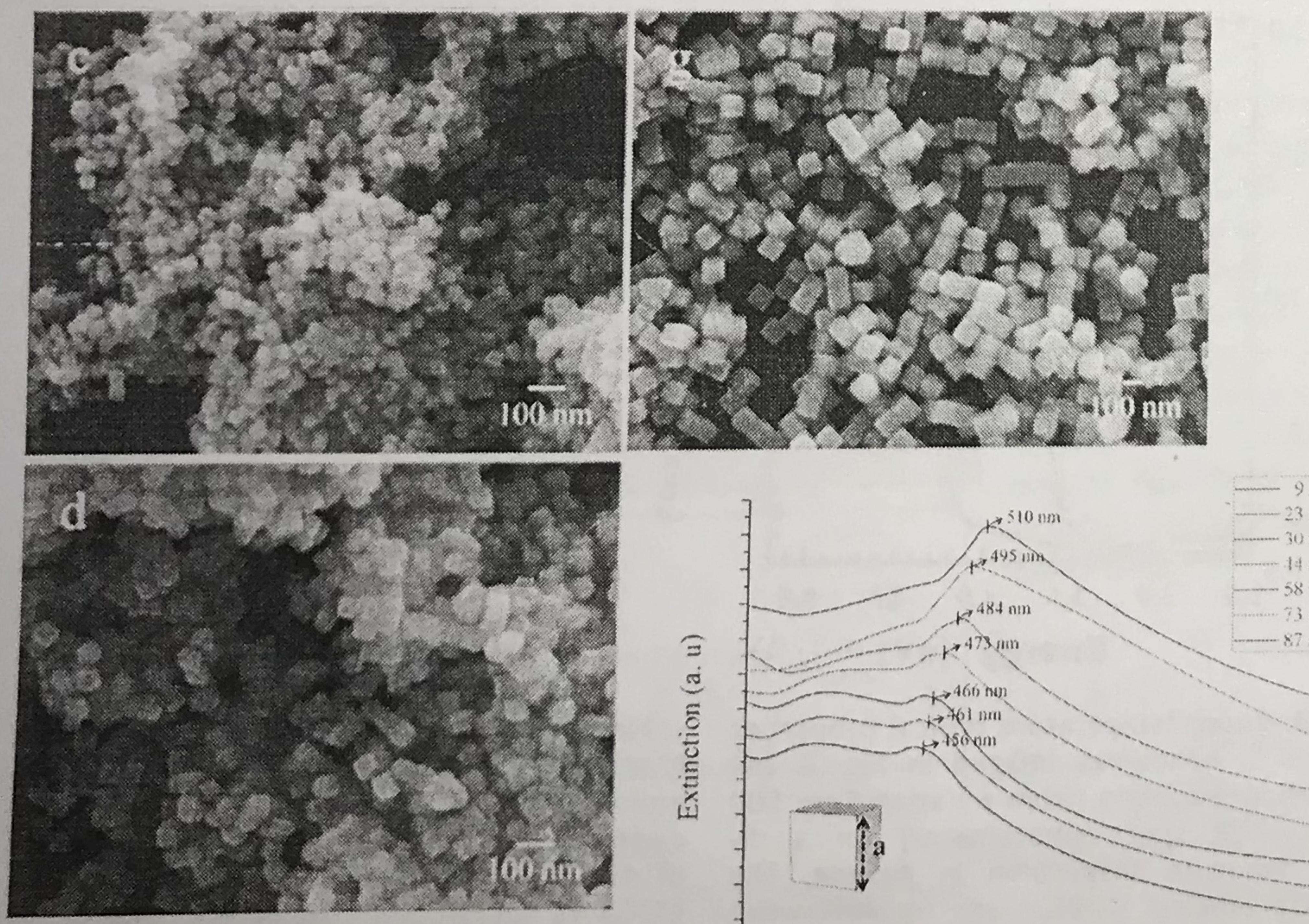
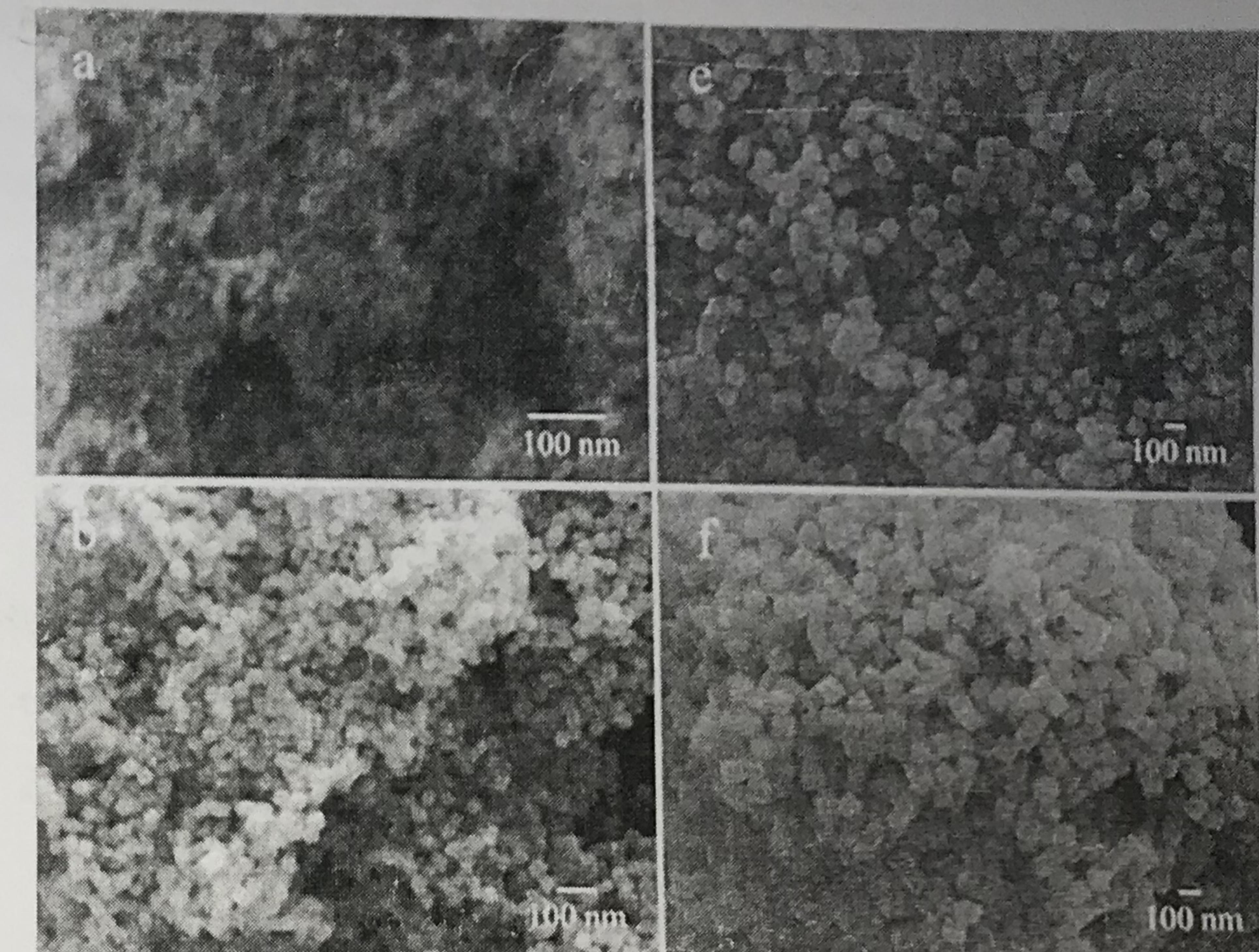
Small Cu_2O Octahedra

小顆和大顆有差別

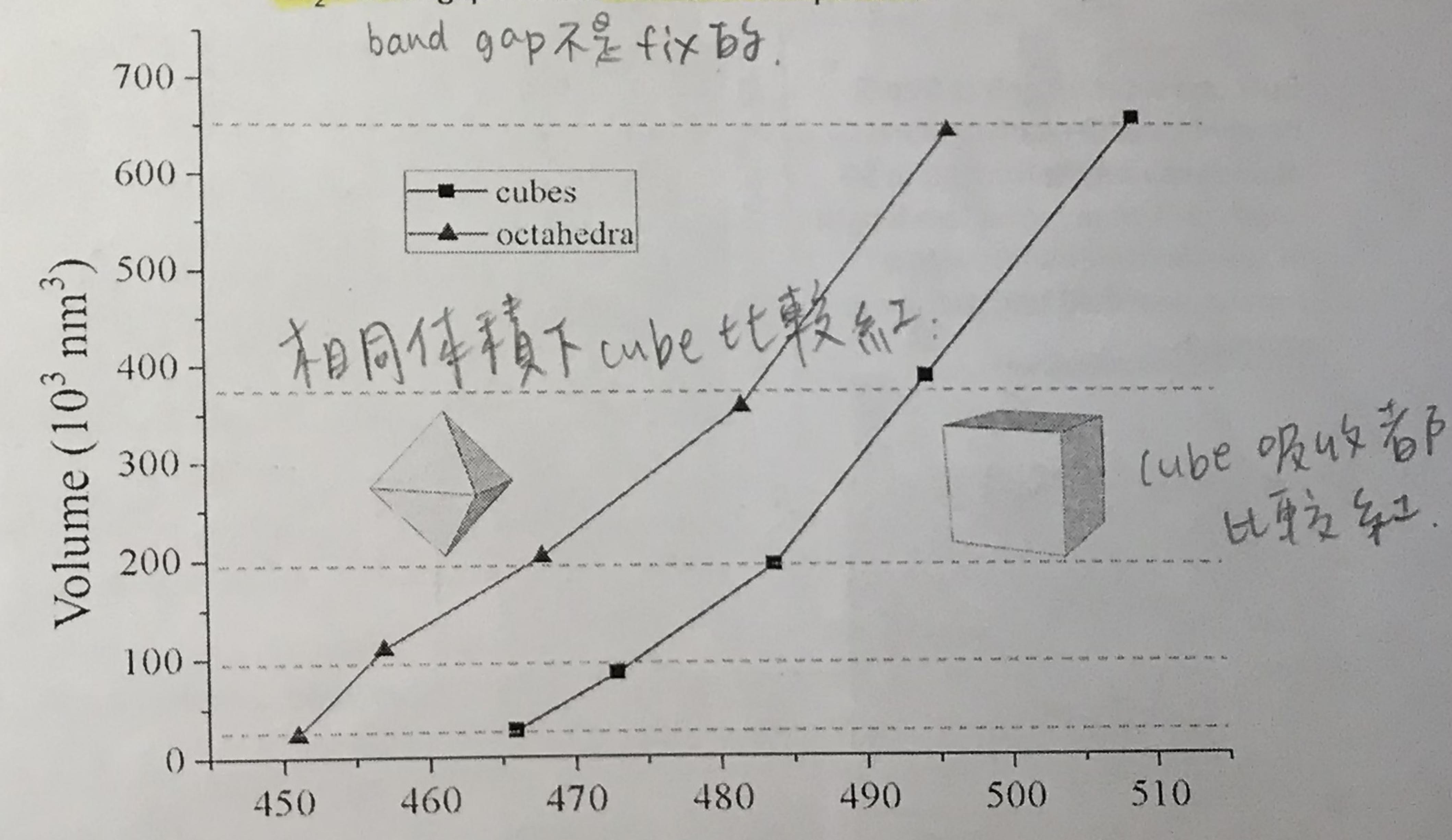


Ke, W.-H.; Hsia, C.-F.; Chen, Y.-J.; Huang, M. H.
Small 2016, 12, 3530.

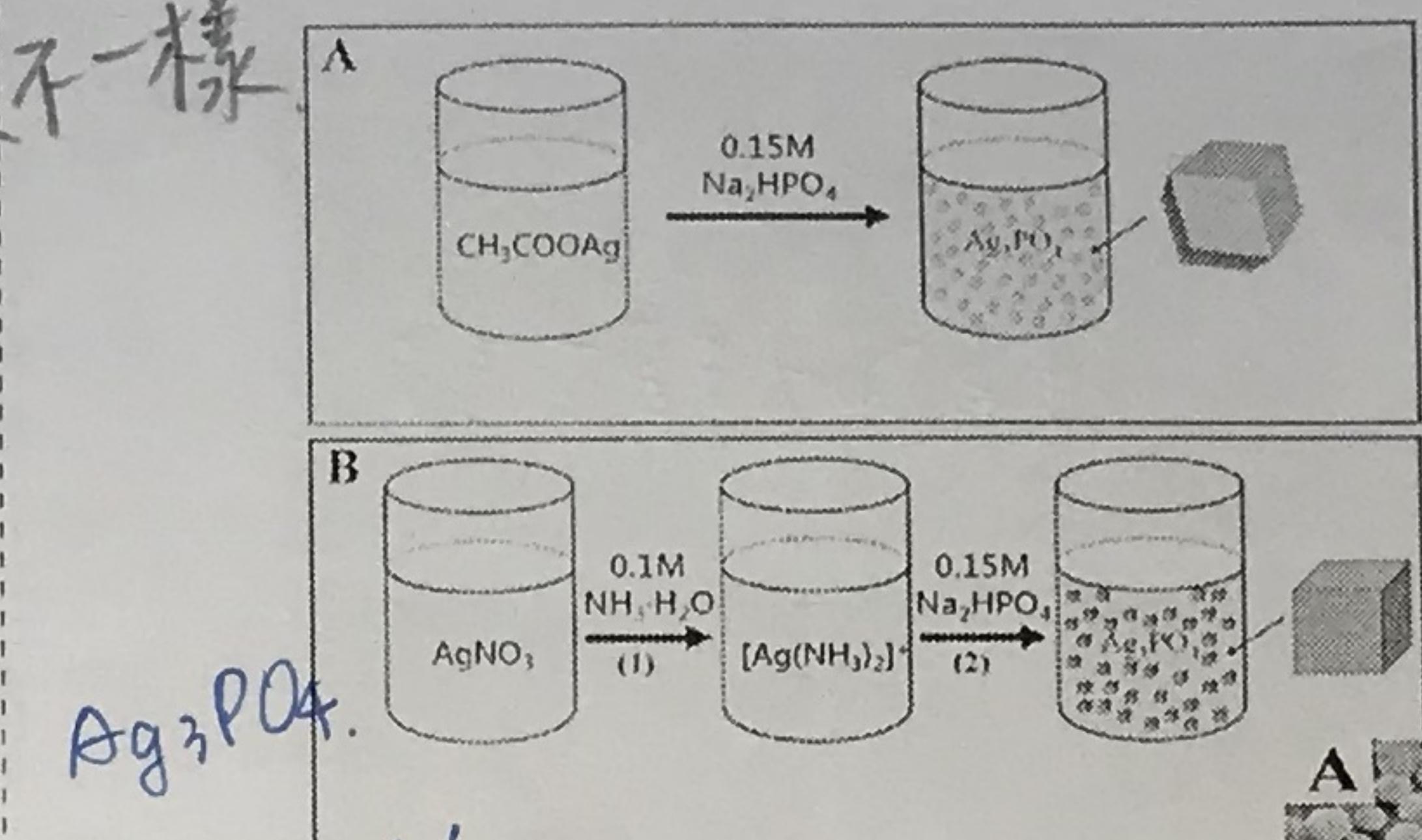
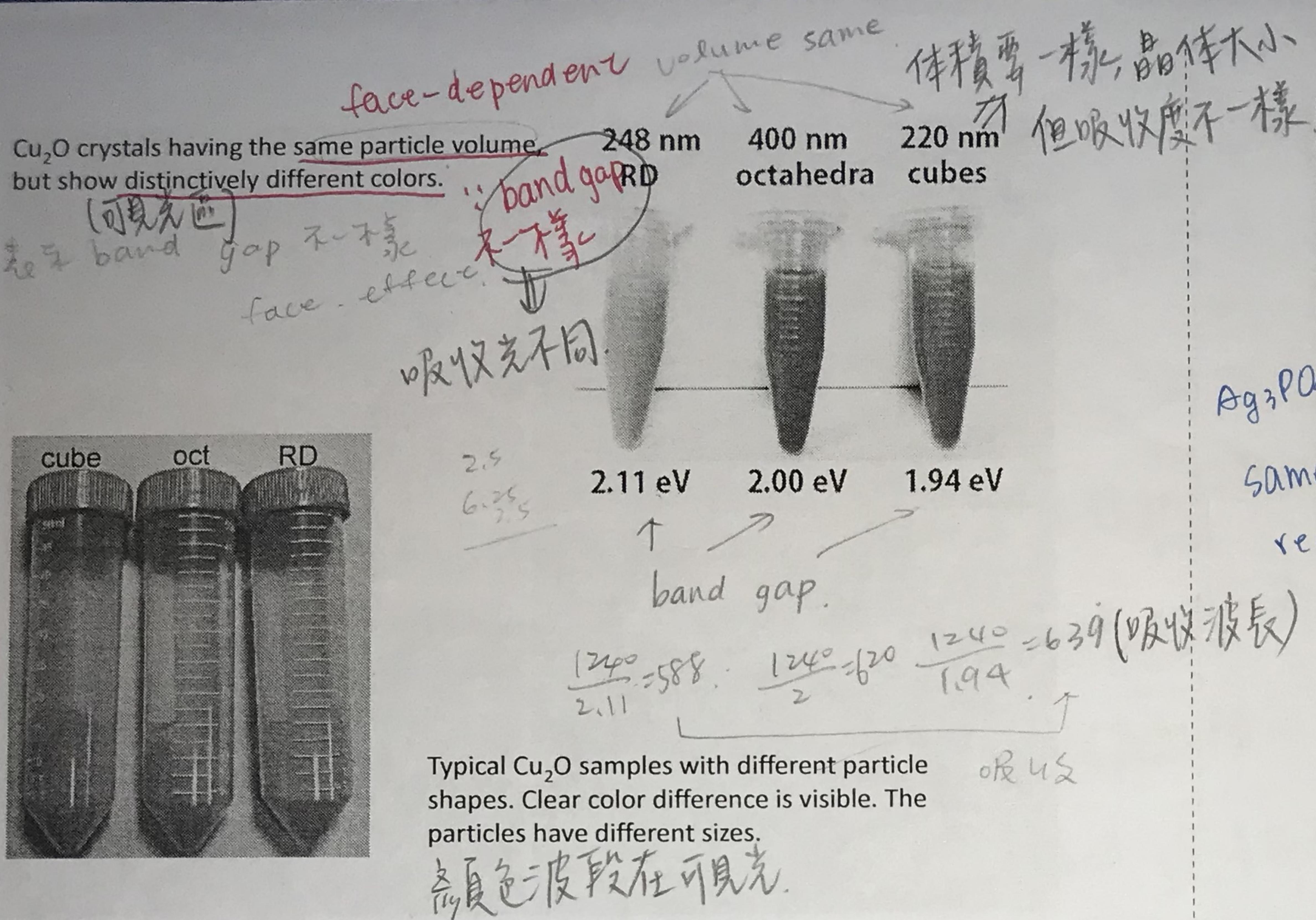
Figure 6.5 Two layers of close touching, and (b) with lines are visible



Synthesis of Ultrasmall Cu_2O Nanocubes and Octahedra with Tunable Sizes for Facet-Dependent Optical Property Examination
 Cu_2O band gap has size and facet components. no shape

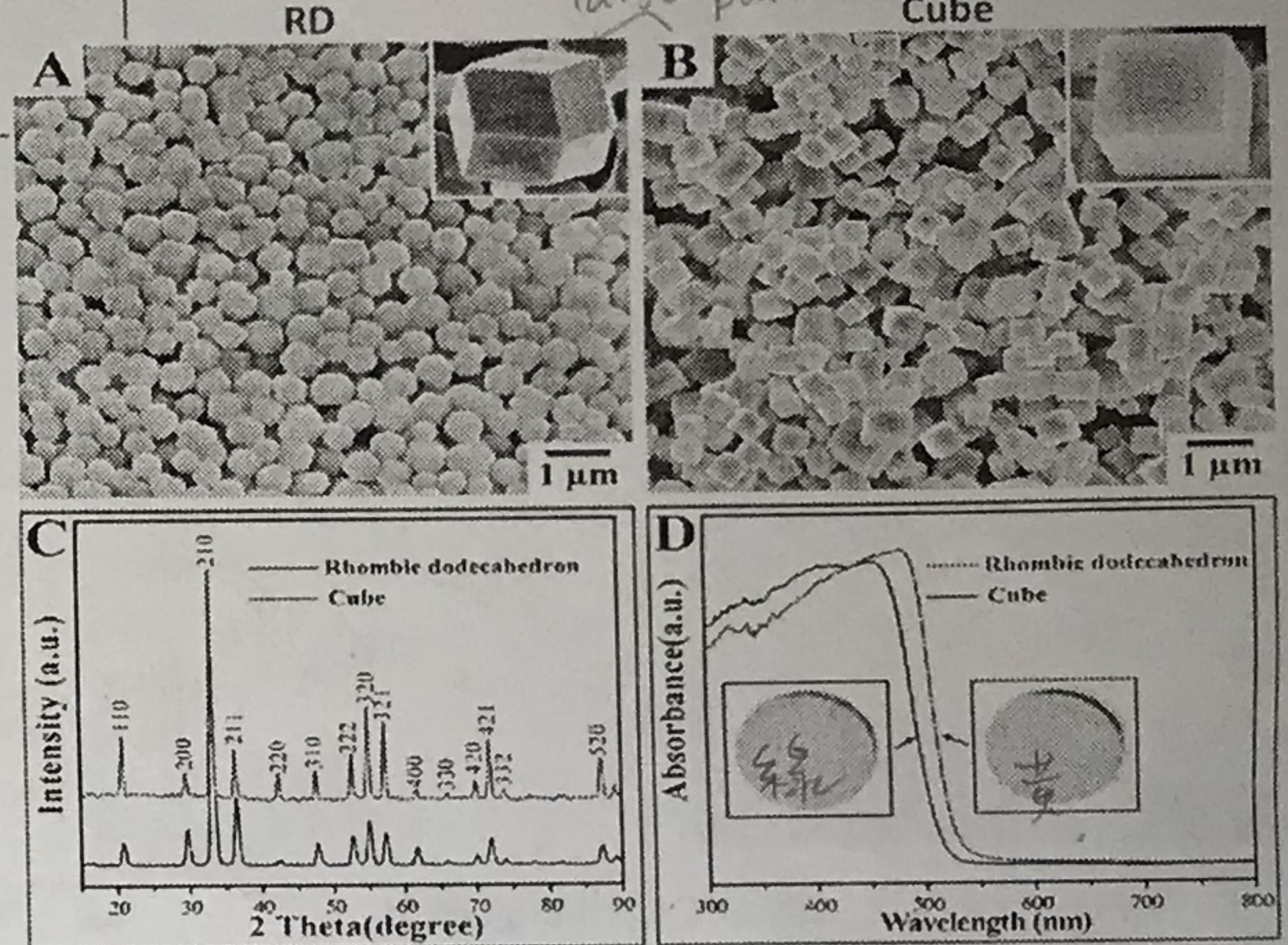


Ke, W.-H.; Hsia, C.-F.; Chen, Y.-J.;
Huang, M. H. *Small* 2016, 12, 3530.



Ag₃PO₄
 same V.
 red: RD > cube

Despite having similar sizes, Ag₃PO₄ rhombic dodecahedra show a more red-shifted absorption band than that of cubes by ~30 nm due to the facet effect on band gap of the Ag₃PO₄ crystals.



在石墨酸化銀 RD & Cube 紅移

small quantity quality

Band gap of Si = 1.1 eV (1127 nm)

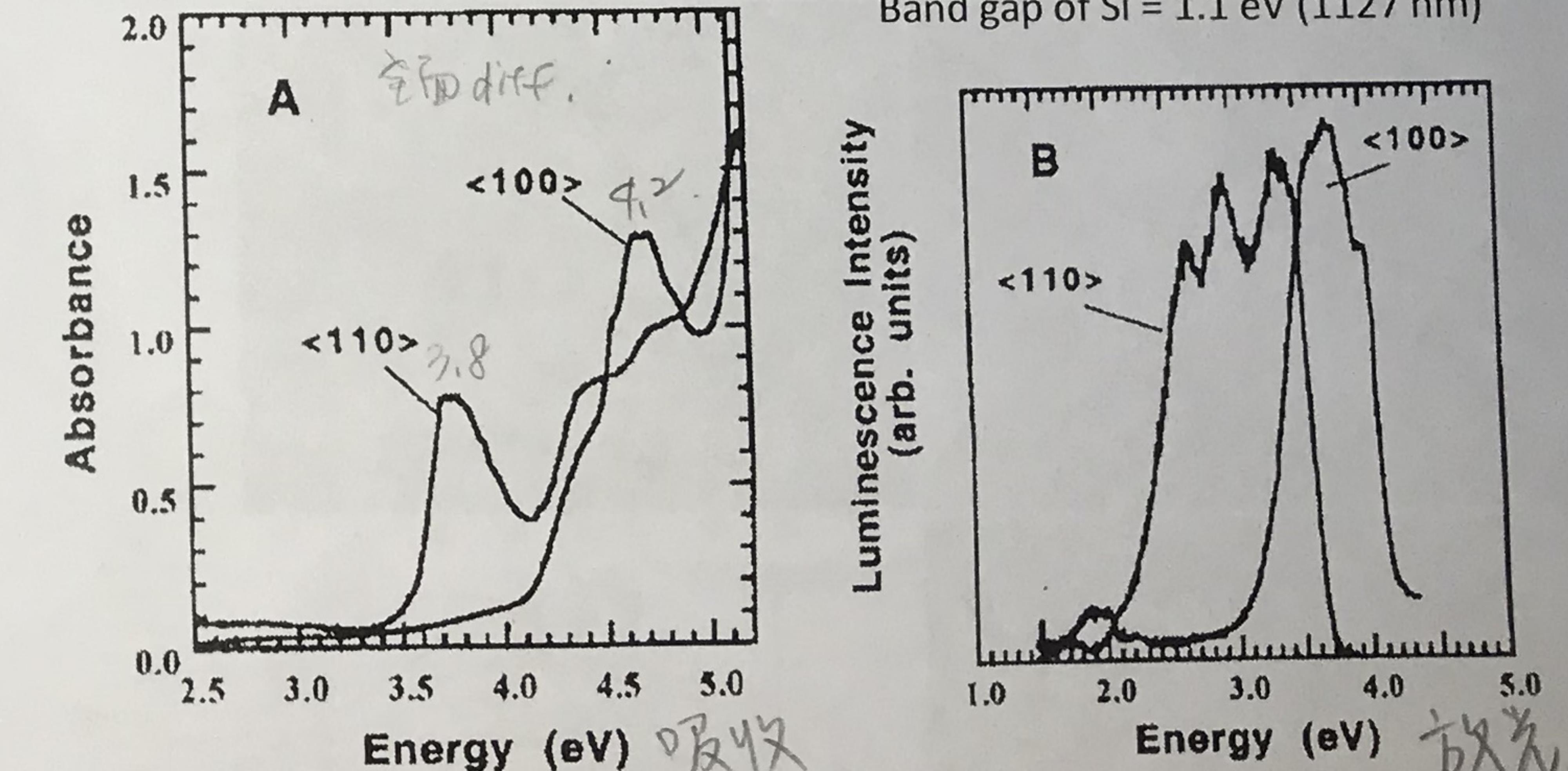
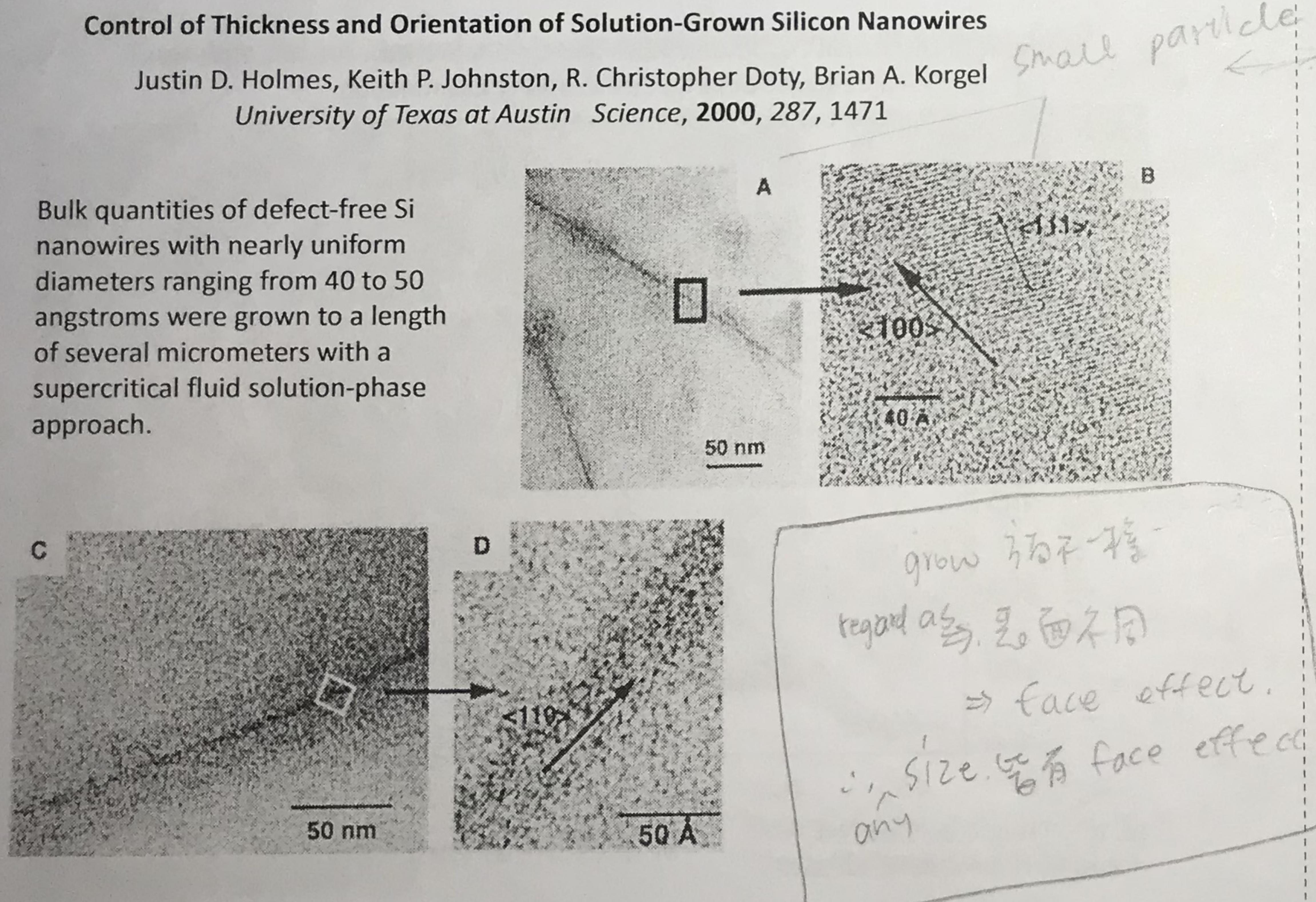


Fig. 3. Room-temperature optical properties of the Si nanowires imaged in Fig. 2. (A) Absorbance spectra (from a Varian Cary 500 UV-Vis-NIR spectrophotometer) for a dilute nanowire suspension in hexane. The spectra labeled <100> are for nanowires formed at 200 bar (Fig. 2, A and B) and

<110> at 270 bar (Fig. 2, C and D). (B) Photoluminescence spectra (from a SPEX Fluorolog-3 spectrophotometer) of nanowires dispersed in hexane with excitation energies of 4.46 eV (277 nm, <100>) and 4.12 eV (300 nm, <110>).

size ↓ ⇒ gap ↑

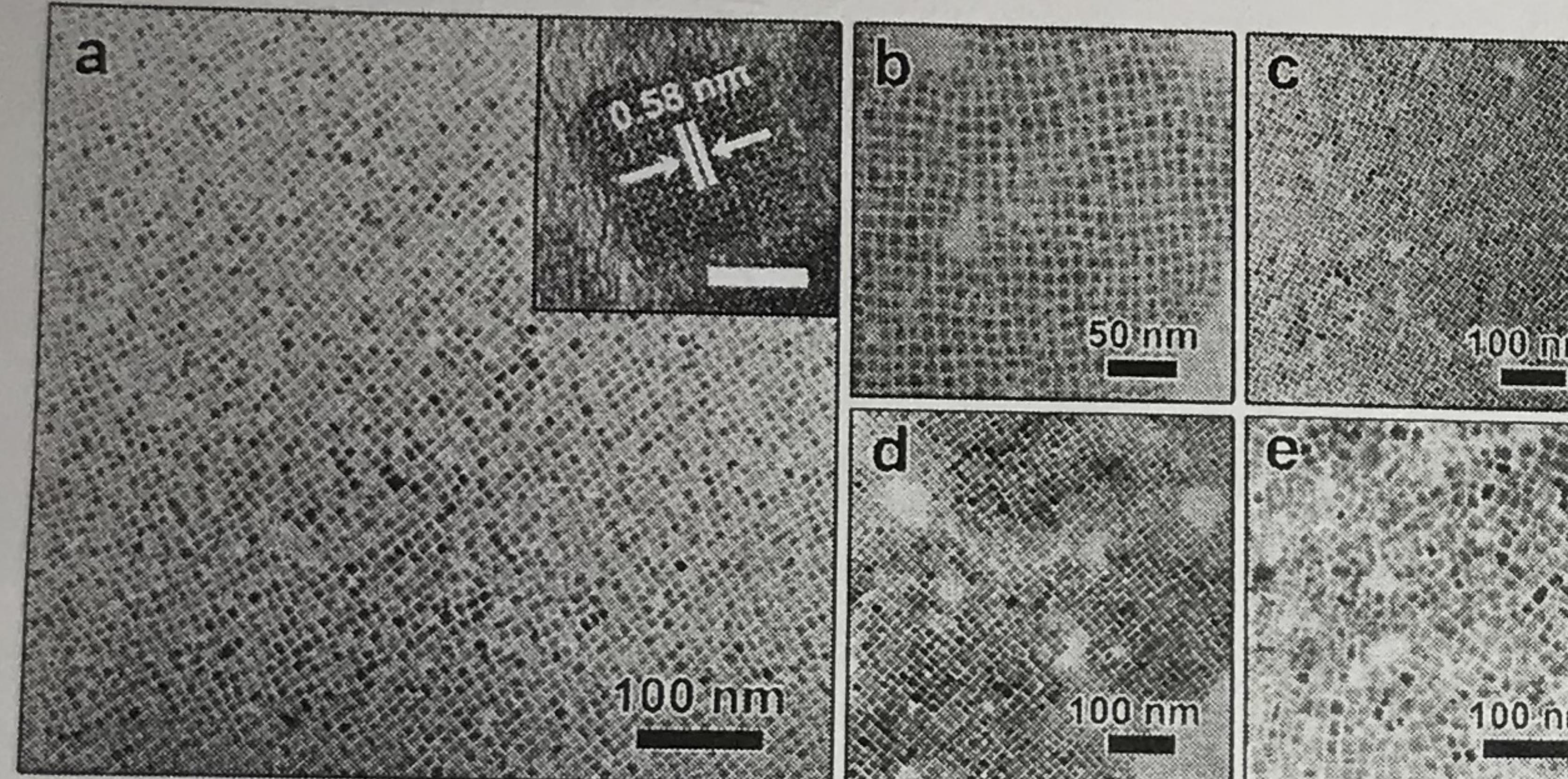


溶劑熱法

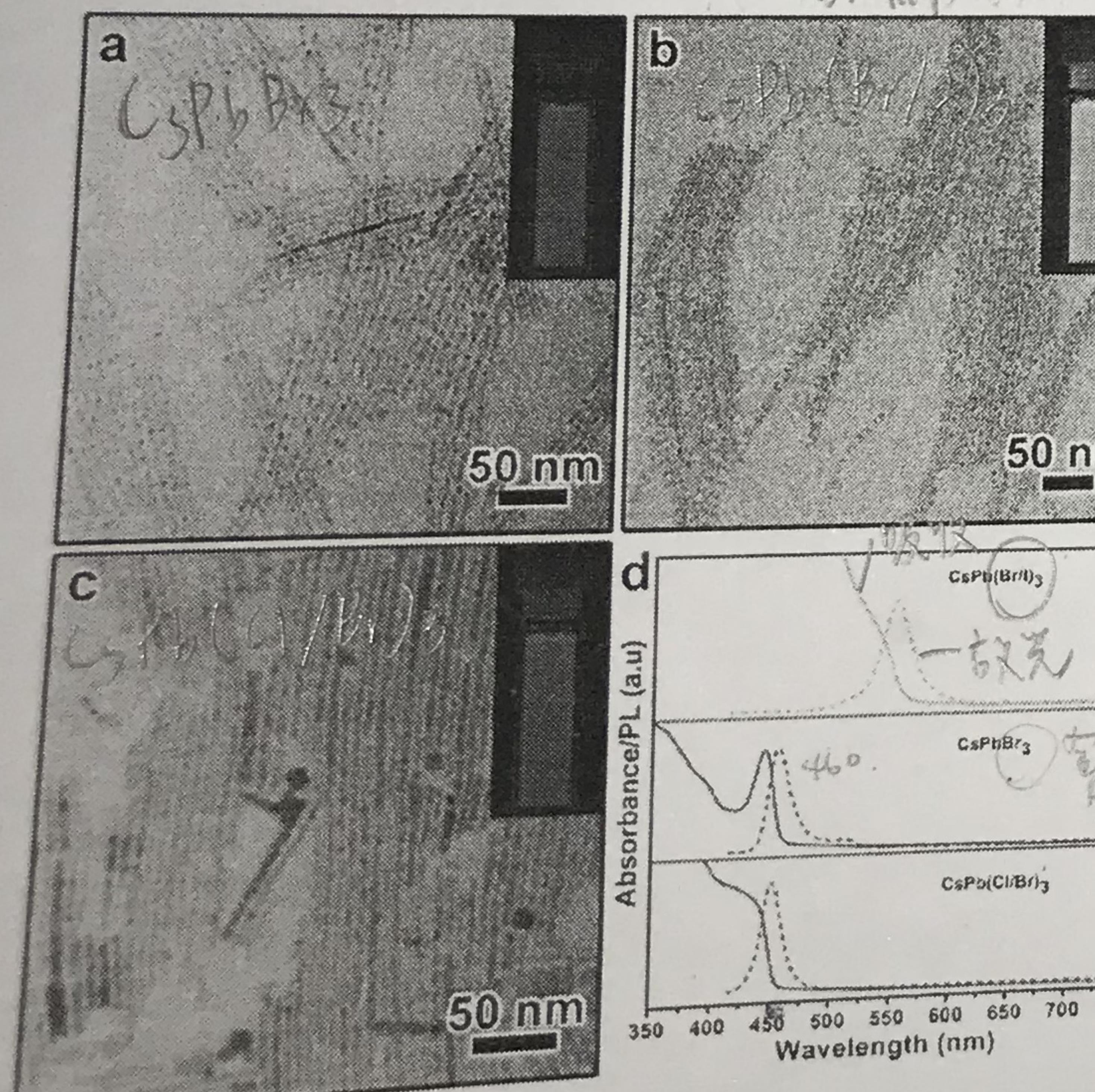
Solvothermal Synthesis of High-Quality All-Inorganic Cesium Lead Halide Perovskite Nanocrystals: From Nanocube to Ultrathin Nanowire

Adv. Funct. Mater. 2017, 1701121

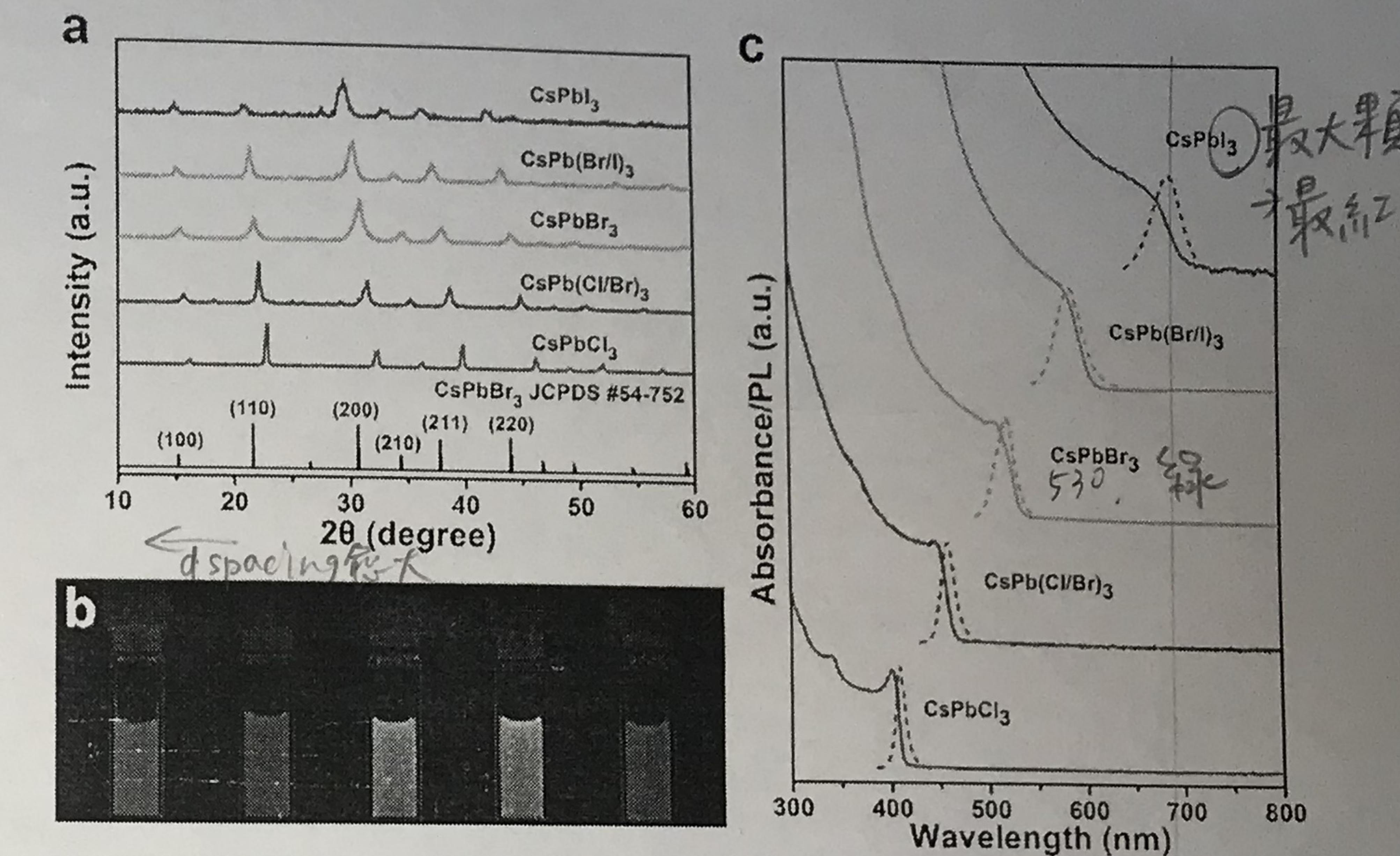
Uniform CsPbX_3 ($X = \text{Cl}, \text{Br}, \text{I}$, and mixed $\text{Cl}/\text{Br}, \text{Br}/\text{I}$) nanocrystals are obtained through a simple solvothermal method. In a typical experiment, cesium acetate (CsOAc) and lead halide (PbX_2) are mixed in a stainless autoclave containing 1-ODE, OA, and OAm. The autoclave is then placed in a rolling oven and heated to 160°C and maintained at that temperature for 30 min. The product is centrifuged and washed with hexane.



TEM images of a) CsPbBr_3 , b) CsPbCl_3 , c) $\text{CsPb}(\text{Cl}/\text{Br})_3$, d) $\text{CsPb}(\text{Br}/\text{I})_3$, and e) CsPbI_3 nanocrystals.

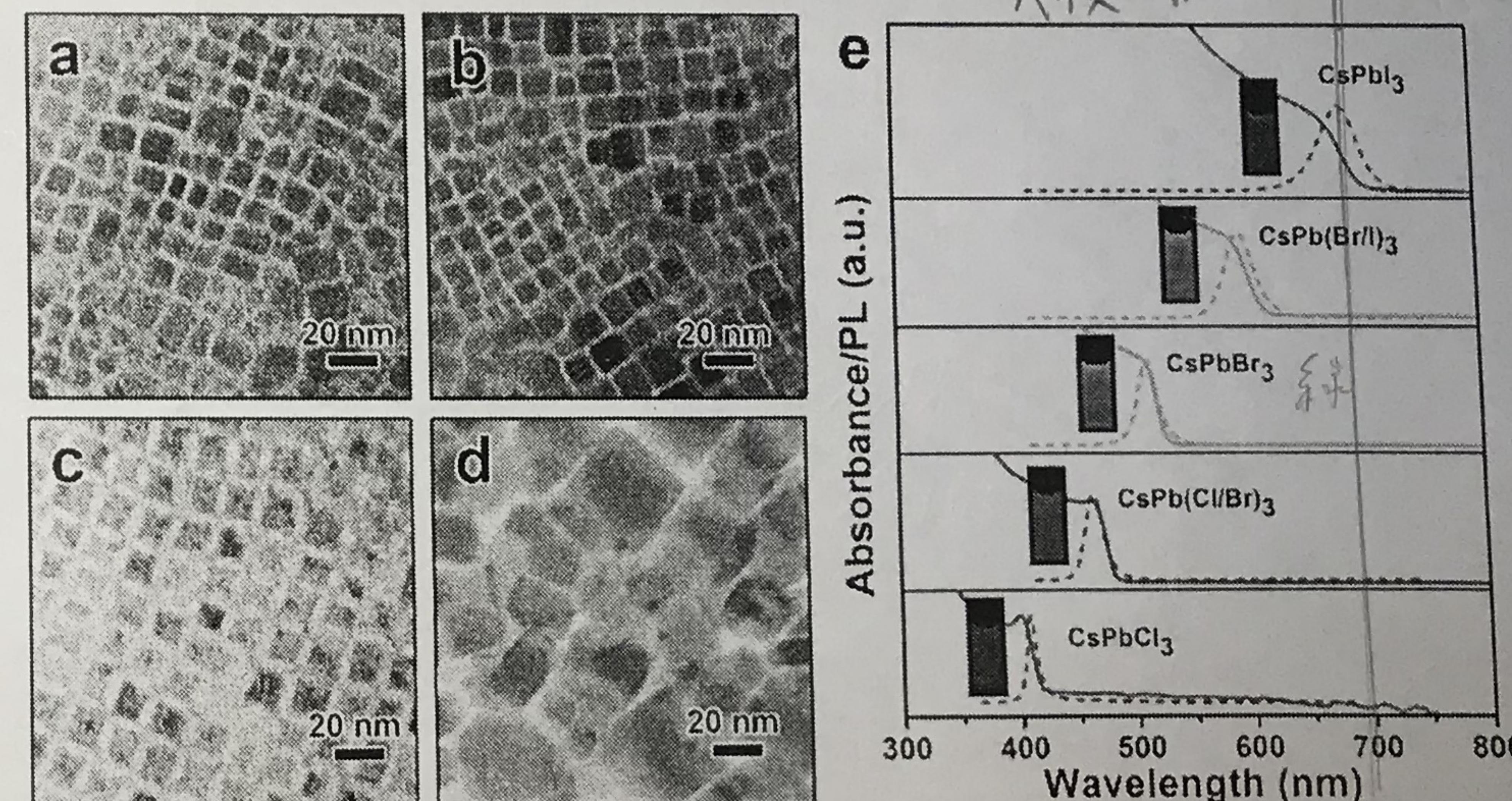


TEM images of ultrathin a) CsPbBr_3 , b) $\text{CsPb}(\text{Br}/\text{I})_3$, and c) $\text{CsPb}(\text{Cl}/\text{Br})_3$ nanowires. Insets show the bright emission color of colloidal CsPbX_3 solution in hexane under UV illumination ($\lambda = 365$ nm). d) UV-vis absorption and PL spectra of the as-prepared CsPbX_3 nanowires.



a) XRD patterns of typical ternary and mixed-halide nanocrystals. b) Digital photograph of colloidal CsPbX_3 nanocrystals ($X = \text{Cl}, \text{Br}, \text{I}$, and mixed $\text{Cl}/\text{Br}, \text{Br}/\text{I}$) solution in hexane under a UV (365 nm) lamp illumination. c) Typical UV-vis absorption (solid) and PL emission spectra (dash) of five samples

↓ Size effect. 放大也有 size effect.
大顆 → 紅移 → 量效應.



TEM images of CsPbX_3 nanocrystals: a) $\text{CsPb}(\text{Cl}/\text{Br})_3$, b) CsPbBr_3 , c) $\text{CsPb}(\text{Br}/\text{I})_3$, and d) CsPbI_3 , obtained from Cs_2CO_3 as the precursor. The insets are photograph of (a-d) in solution under UV light irradiation ($\lambda = 365$ nm). e) UV-vis absorption and PL spectra of the CsPbX_3 nanocrystals obtained by using Cs_2CO_3 as the precursor.

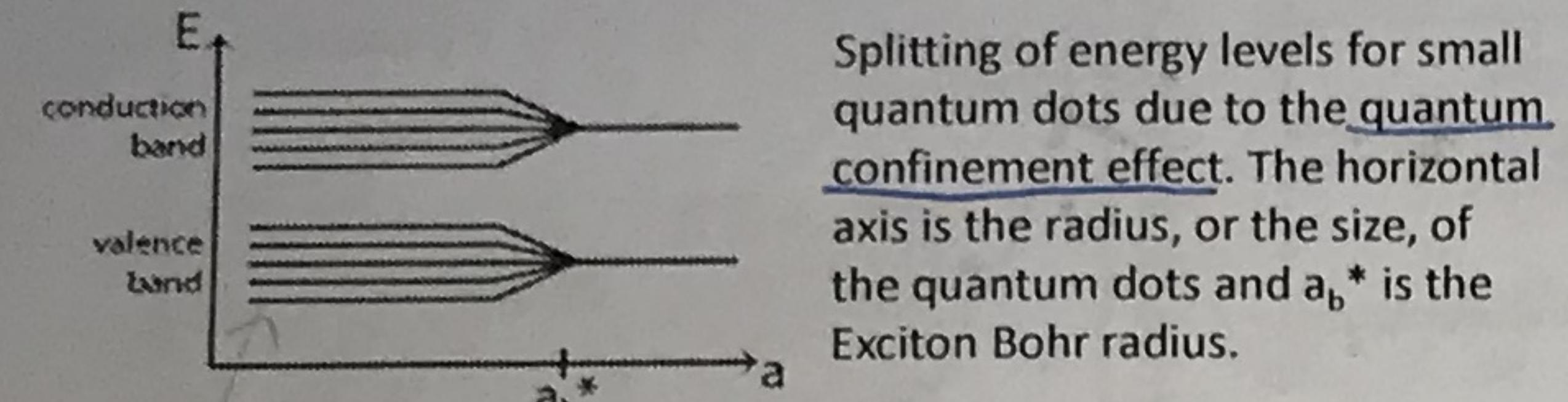
(a) with the spheres reduced so that connected octahedral holes are in

21日/1c

→ 比奈米粒子更小的半導體，其光學和電子特性與較大顆粒的特性不同
 QD 級示器 The general theory of semiconductor band structure \rightarrow $e^- + h^+ \rightarrow e^- + h^+$

Quantum dots (QD) are very small semiconductor particles, only several nanometres in size, so small that their optical and electronic properties differ from those of larger particles.

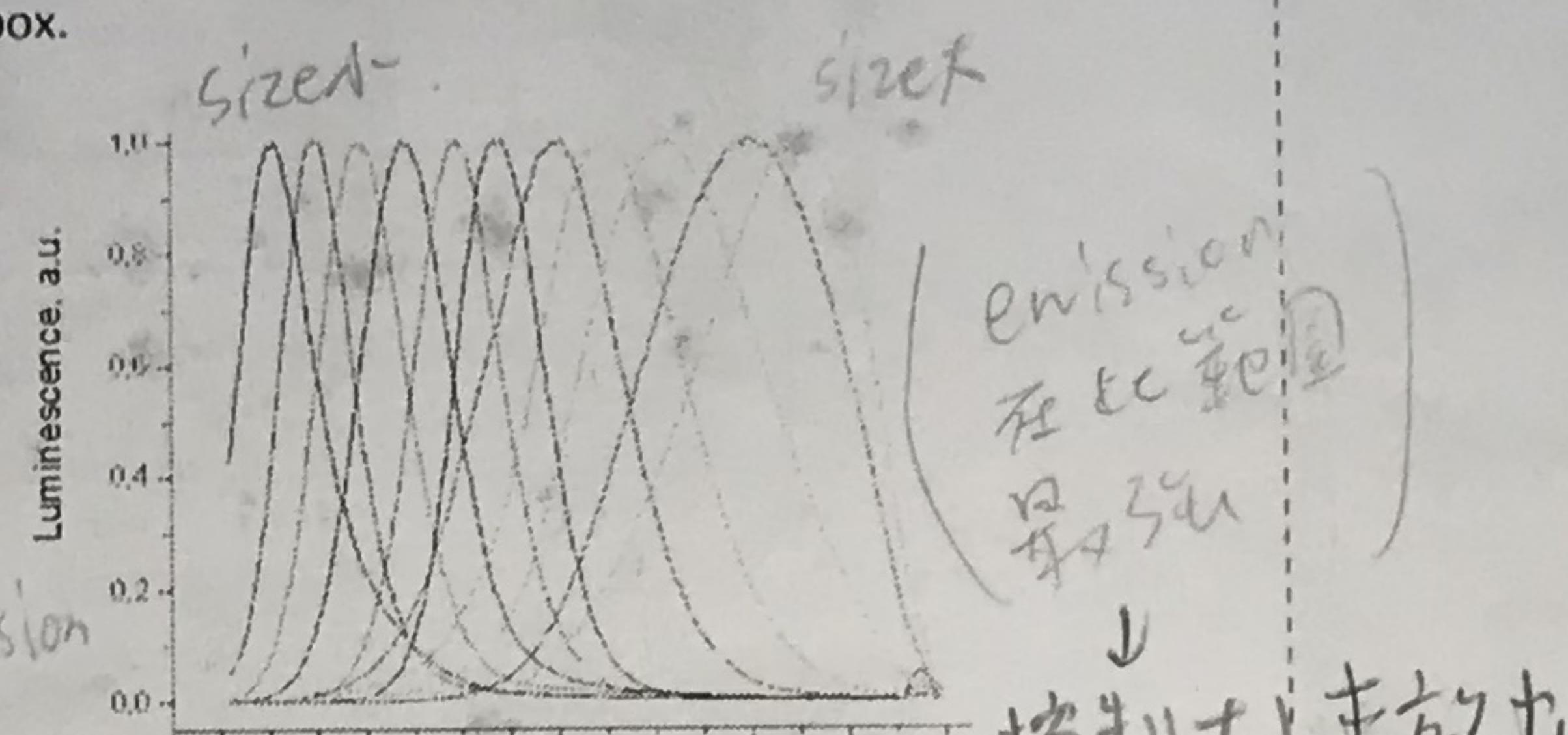
In a semiconductor crystallite whose size is smaller than twice the size of its exciton Bohr radius, the excitons are squeezed, leading to quantum confinement. The energy levels can then be predicted using the particle in a box model in which the energies of states depends on the length of the box.



看來像
分子。量子限幅效應。

Our idea

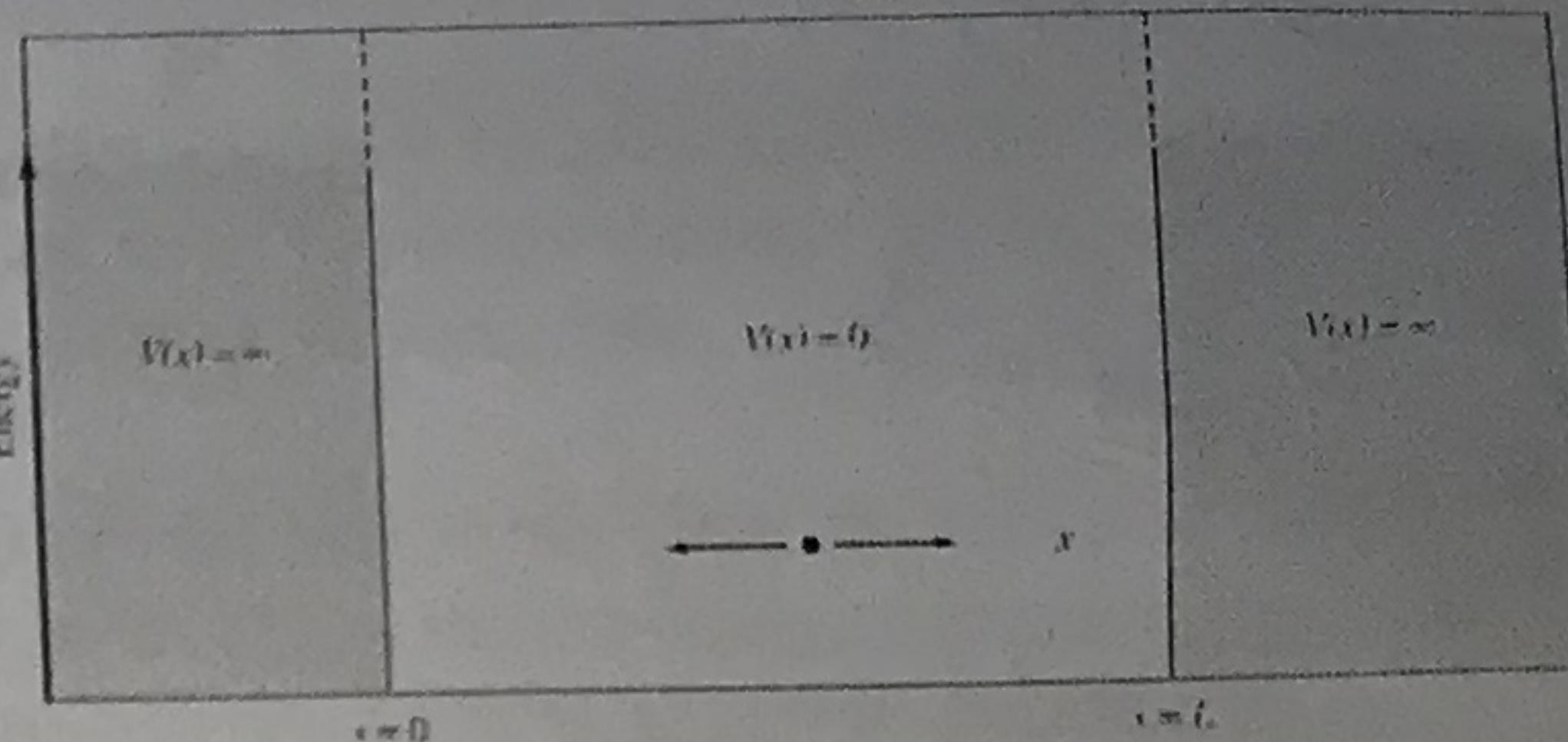
From our observations made on Cu_2O nanocrystals and those made by others on Ag_3PO_4 microcrystals (RD and cube absorption band positions differ by 30 nm), ultrathin Si nanowires (4-5 nm in diameter but different growth directions with very large absorption and emission band separation) and other examples, tunable absorption and emission bands can still be observed in nanoscale and sub-microscale semiconductor crystals. Facet effects are present from quantum dots to microcrystals because band gaps have size and facet components.



Fluorescence spectra of CdTe quantum dots of various sizes (1-7 nm). Different sized quantum dots emit different color light due to quantum confinement.

↓
控制未來放出
不同顏色。

Modified semiconductor band diagram



particle-in-a-box situation $E = \frac{n^2 h^2}{8mL^2}$
 可和晶效應有關聯。

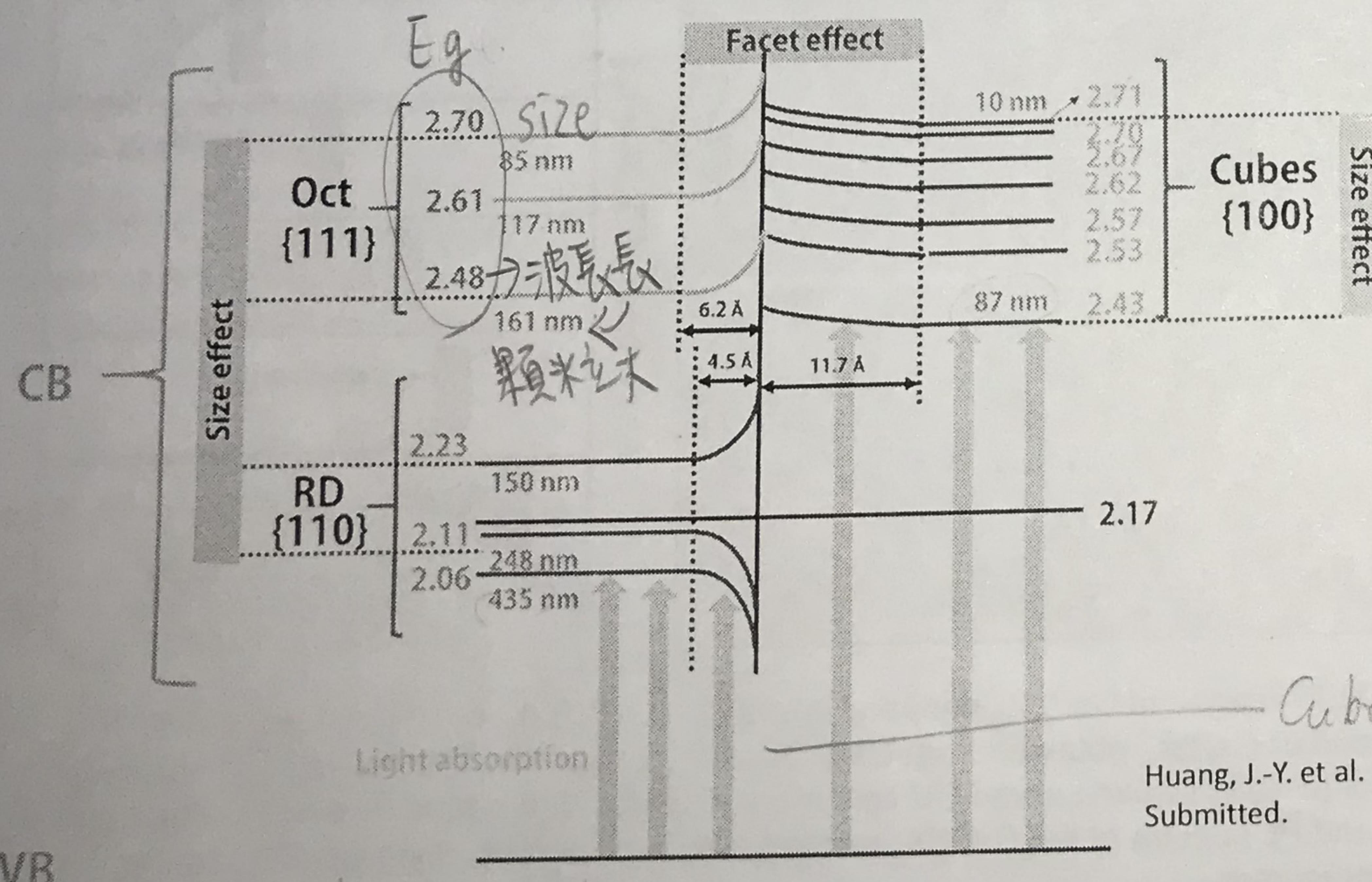
Band gap size is tunable from quantum dots (~2 nm) to nanocrystals beyond 200 nm

Facet effect added to the band gap to tune the band size or tune the degree of band bending

Eg: bulk吸收 + 表面吸收

固定...↑晶面效應影響 Eg
 → 影響半導體效率

Modified and General Band Diagram for Cu_2O Nanocrystals Incorporating Optical Size and Facet Effects



Huang, J.-Y. et al.
 Submitted.

Cube, if size 不同。

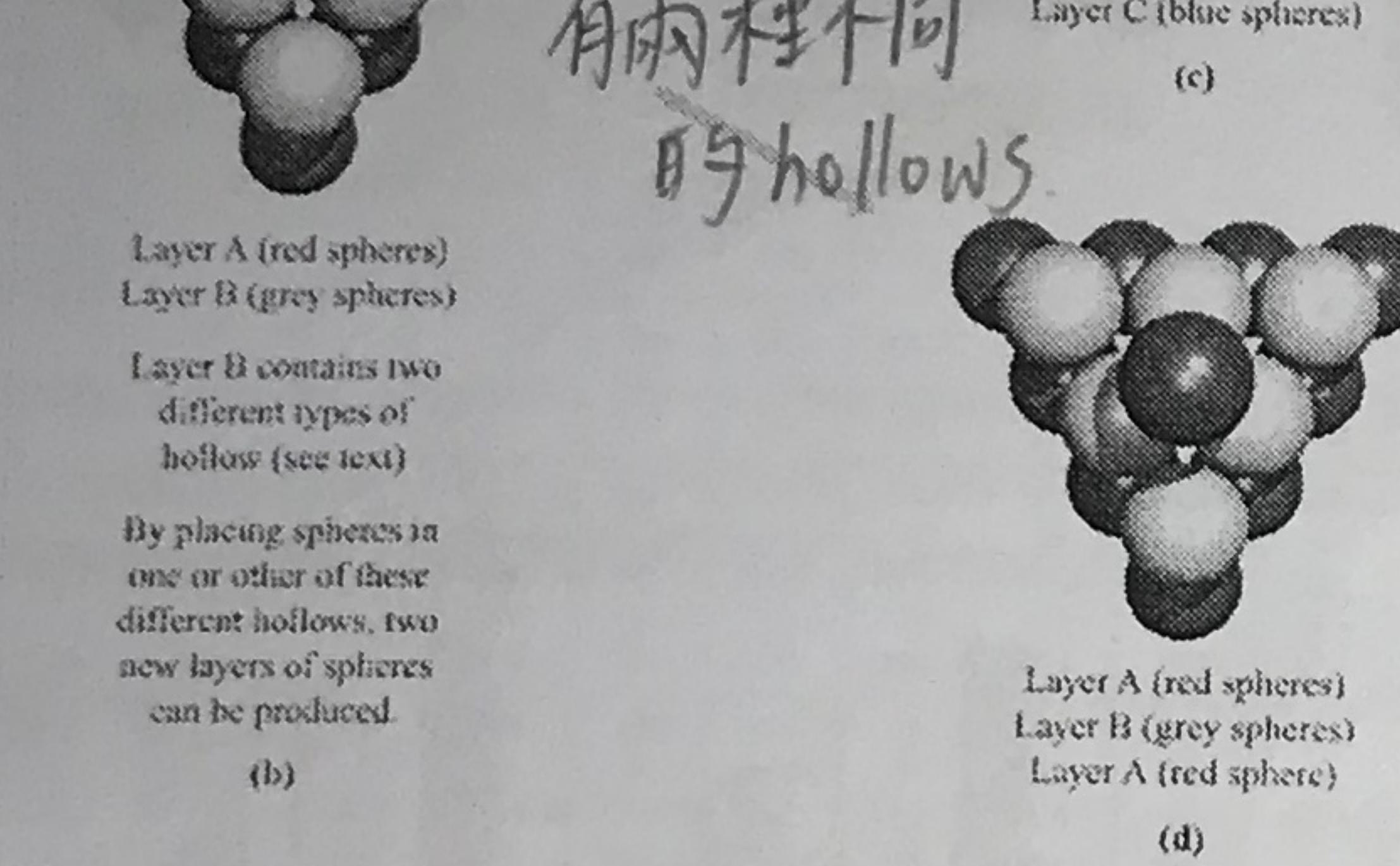
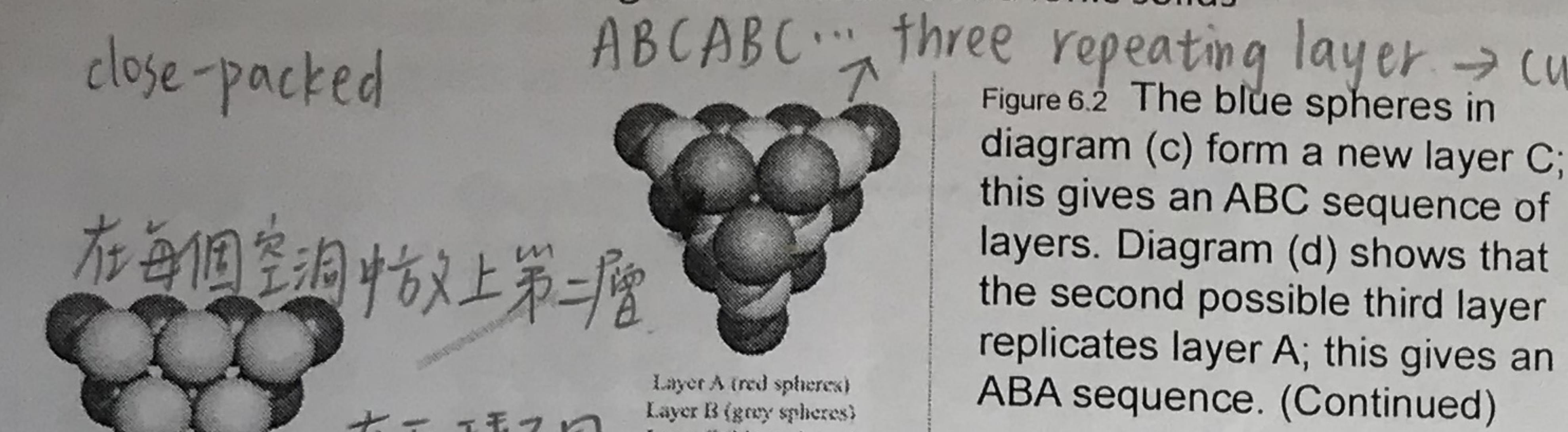
VB

band b6吸收

Packing of spheres 最密堆積 → 球體總體積占空間大小的比例 → 密度

Chapter 6 Structures and energetics of metallic and ionic solids

close-packed ABCABC... three repeating layer → cubic close-packing (ccp)



Layer A (red spheres)
Layer B (grey spheres)
Layer A (red sphere)

ABABAB...
two repeating layer.
→ hexagonal close-packing (hcp).

74% of the unit cell volume is occupied for a close-packed arrangement.

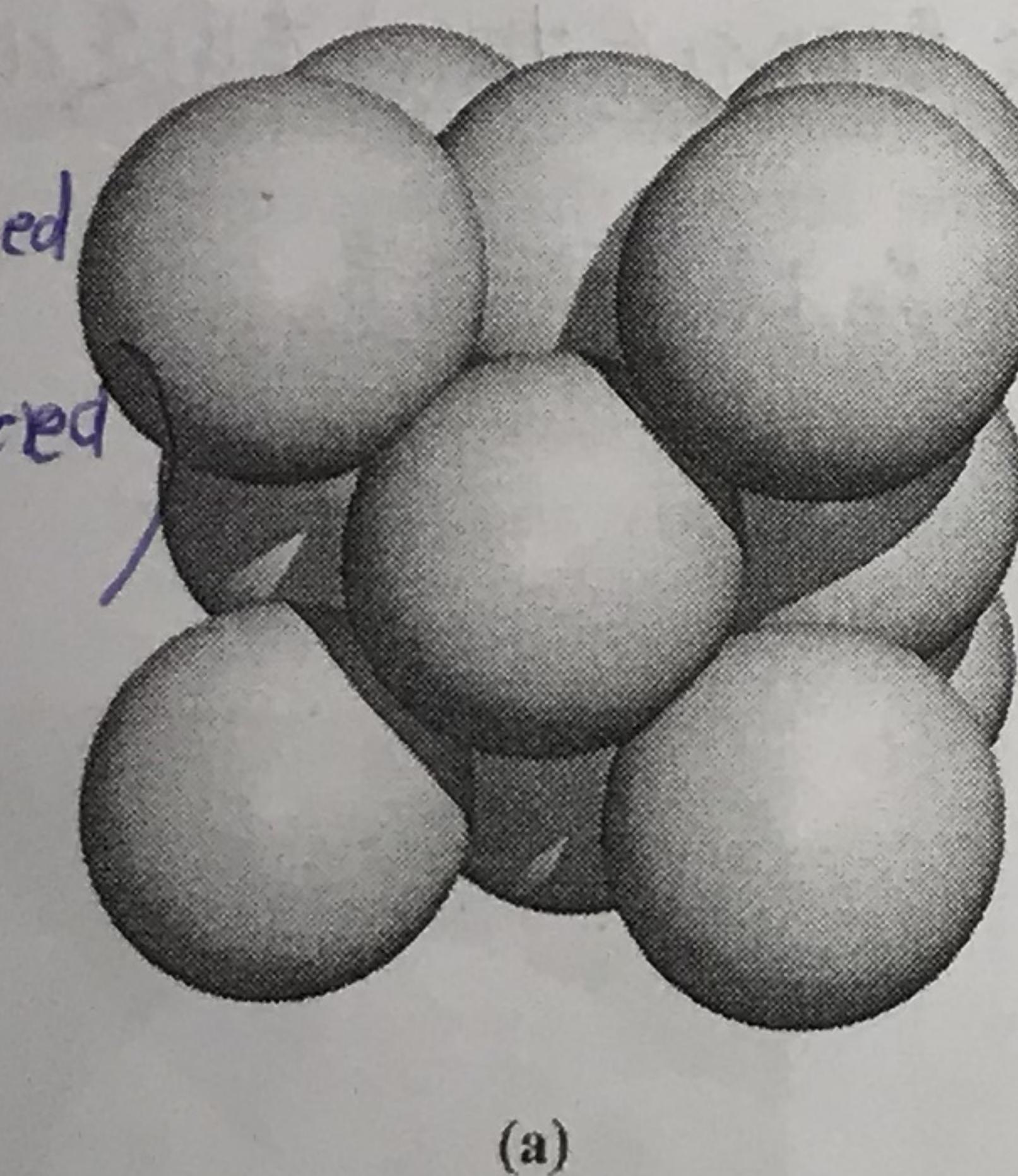


Figure 6.4 Unit cells of (a) a cubic close-packed (face-centred cubic) lattice and (b) a hexagonal close-packed (hcp) lattice.

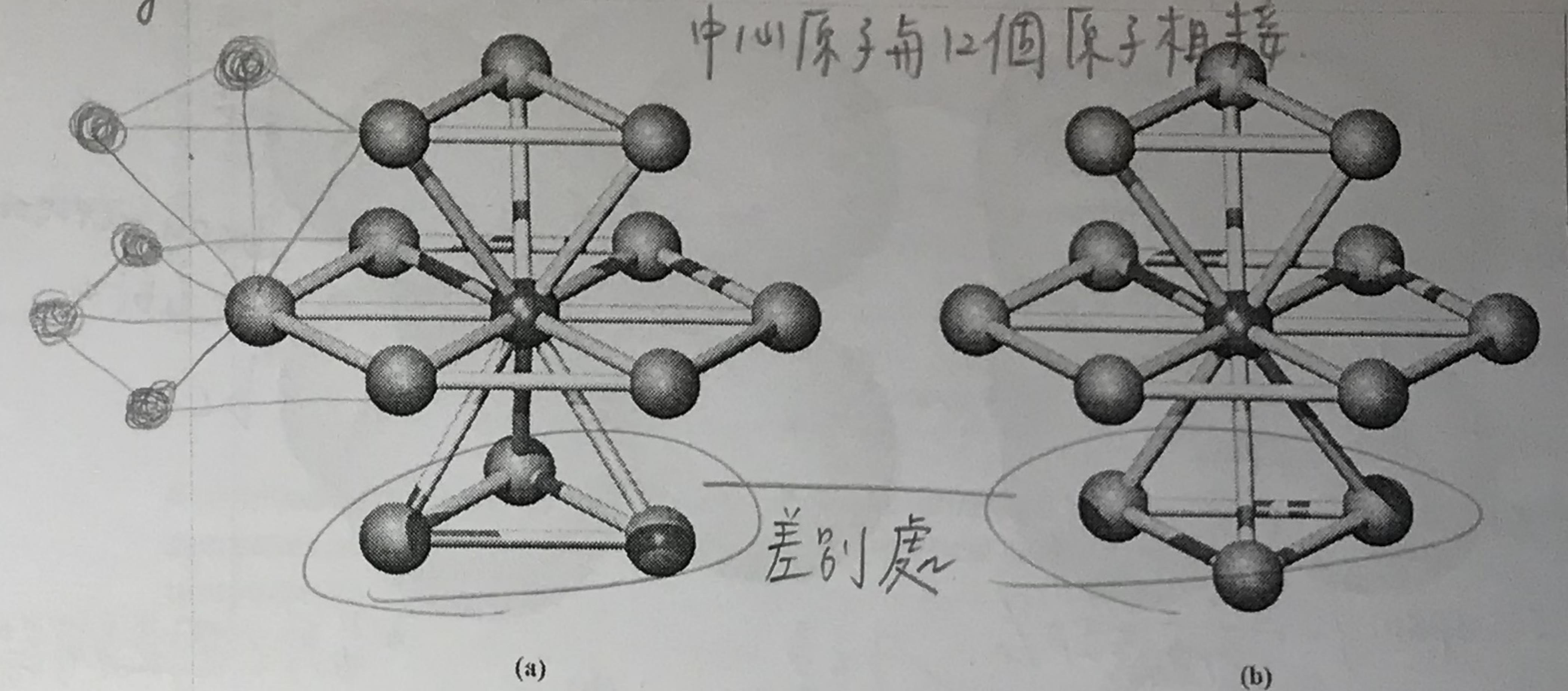
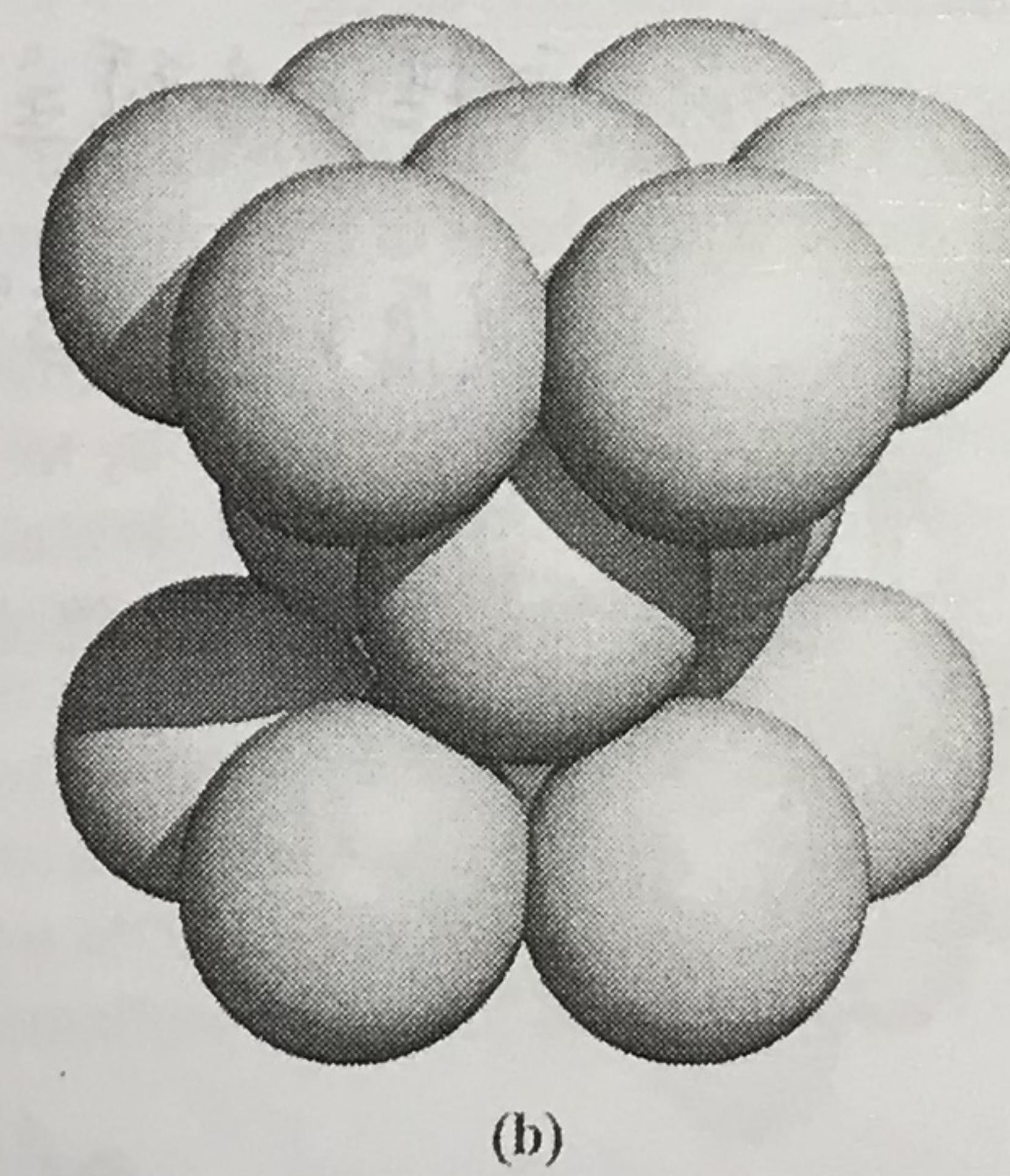


Figure 6.3 In both the (a) ABA and (b) ABC close-packed arrangements, the coordination number of each atom is 12.

Interstitial holes: close-packed structures contain octahedral and tetrahedral holes (or sites).

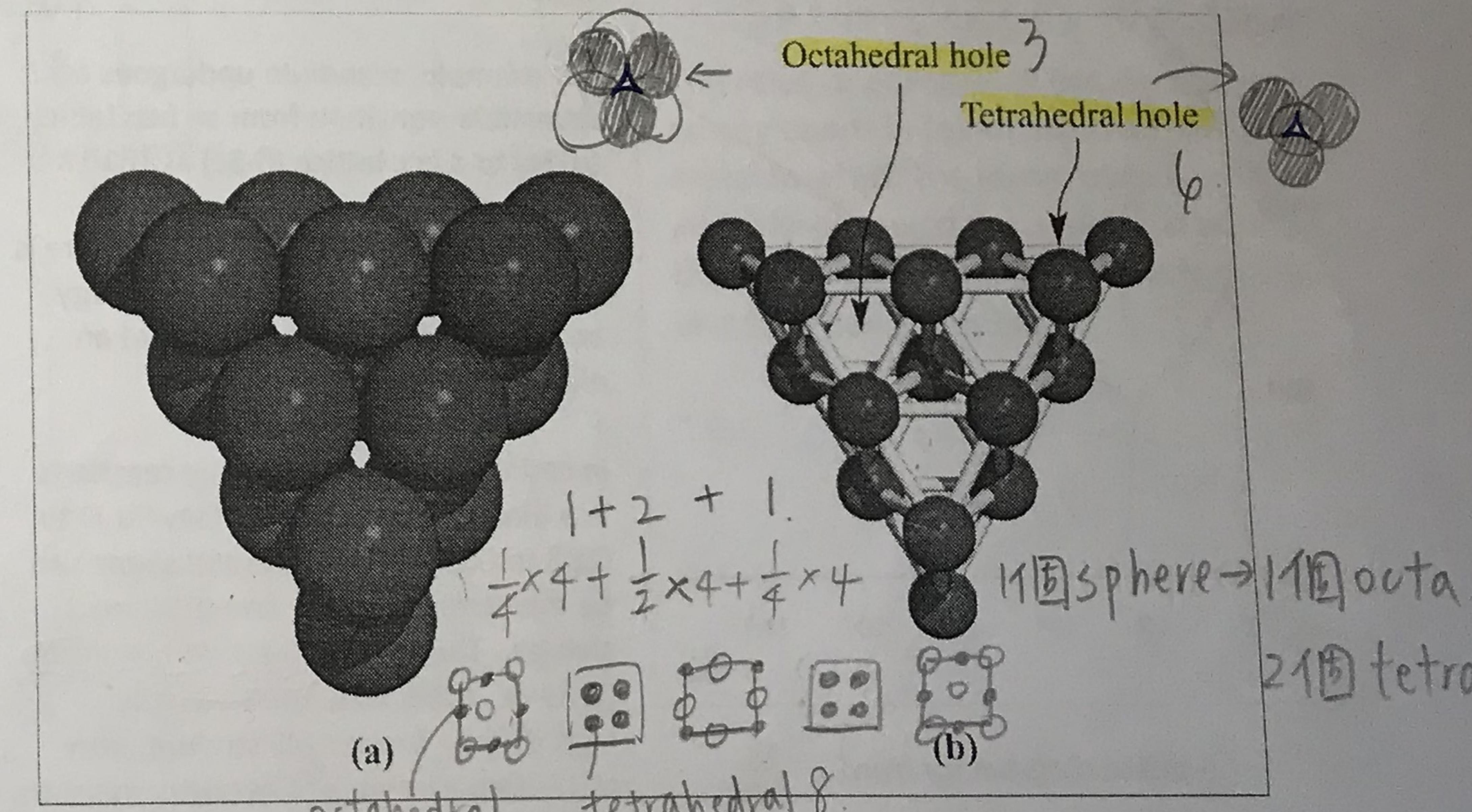


Figure 6.5 Two layers of close-packed atoms shown (a) with the spheres touching, and (b) with the sizes of the spheres reduced so that connectivity lines are visible. In (b), the tetrahedral and octahedral holes are indicated.

atoms are inertial enough
with a small enough compound

packing of sphere model 適用 $18A$, H_2 , $F_2 \rightarrow$ freely rotating
 $\text{ccp} \leftarrow \text{hcp}$ in the solid state.

Table 6.2 Structures (at 298 K), melting points (K) and values of the standard enthalpies of atomization of the metallic elements. $\blacklozenge = \text{hcp}$; $\bullet = \text{ccp}$ (fcc); $\blacksquare = \text{bcc}$.

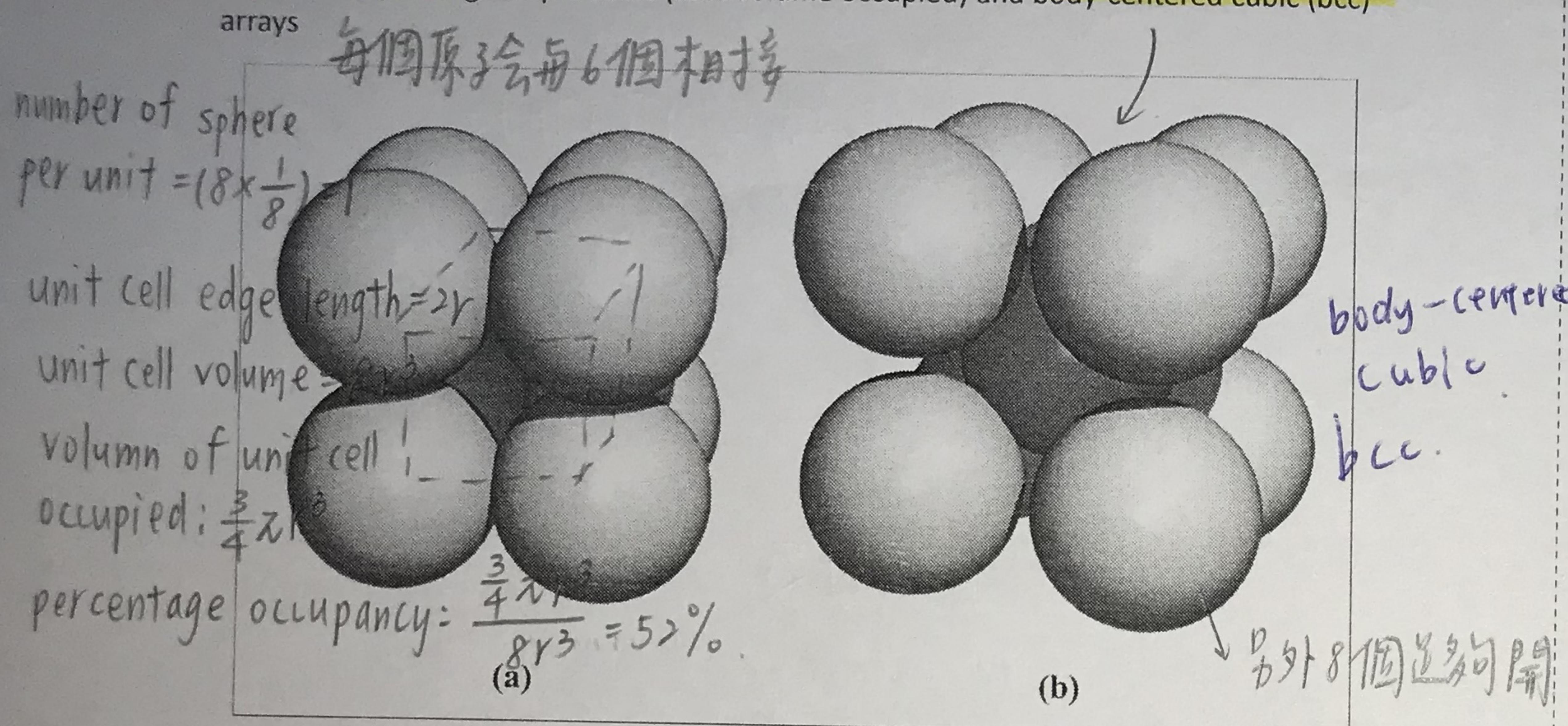


Figure 6.6 Unit cells of (a) a simple cubic lattice and (b) a body-centred cubic lattice.

	1	2	3	4	5	6	7	8	9	10	11	12	13	14	15
Li	●	Be	◆												
454	1560														
361	324														
187	112														
Na	●	Mg	◆												
371	923														
198	146														
191	160														
K	●	Ca	Sc	Tl	V	Cr	Mn	Fe	Co	Ni	Cu	Zn	Al		
337	1115	1814	1941	2183	2180	1519	1811	1768	1728	1358	693	303	933		
99	128	378	470	514	397	283	418	428	430	338	130	277	320		
235	197	164	147	135	129	137	126	125	128	137	137	153	143		
Rb	●	Sr	Y	Zr	Nb	Mo	Tc	Ru	Rb	Pd	Ag	Cd	In	Sn	
312	1040	1799	2128	2750	2896	2430	2607	2237	1828	1235	594	430	505		
82	163	423	699	721	658	677	651	556	377	285	112	243	307		
250	215	182	160	147	140	135	134	134	137	144	152	167	158		
Cs	●	Ba	La	Hf	Ta	W	Re	Os	Ir	Pt	Ag	Hg	Tl	Pb	Bi
301	1900	1193	2506	3290	3695	3459	3306	2719	2041	1337	234	577	600	544	
78	178	423	619	782	850	774	787	669	566	368	144	135	182	195	210
272	224	188	159	147	141	137	135	136	139	144	135	171	173	182	

See Fig. 15.3e and associated text.

liquid

Some metals are polymorphic and exhibit more than one structure depending upon T.P.

Metallic radii

The metallic radius is half of the distance between the nearest neighbor atoms in a solid state metal lattice, and is dependent upon coordination number. If the coordination decreases, r_{metal} also decreases.

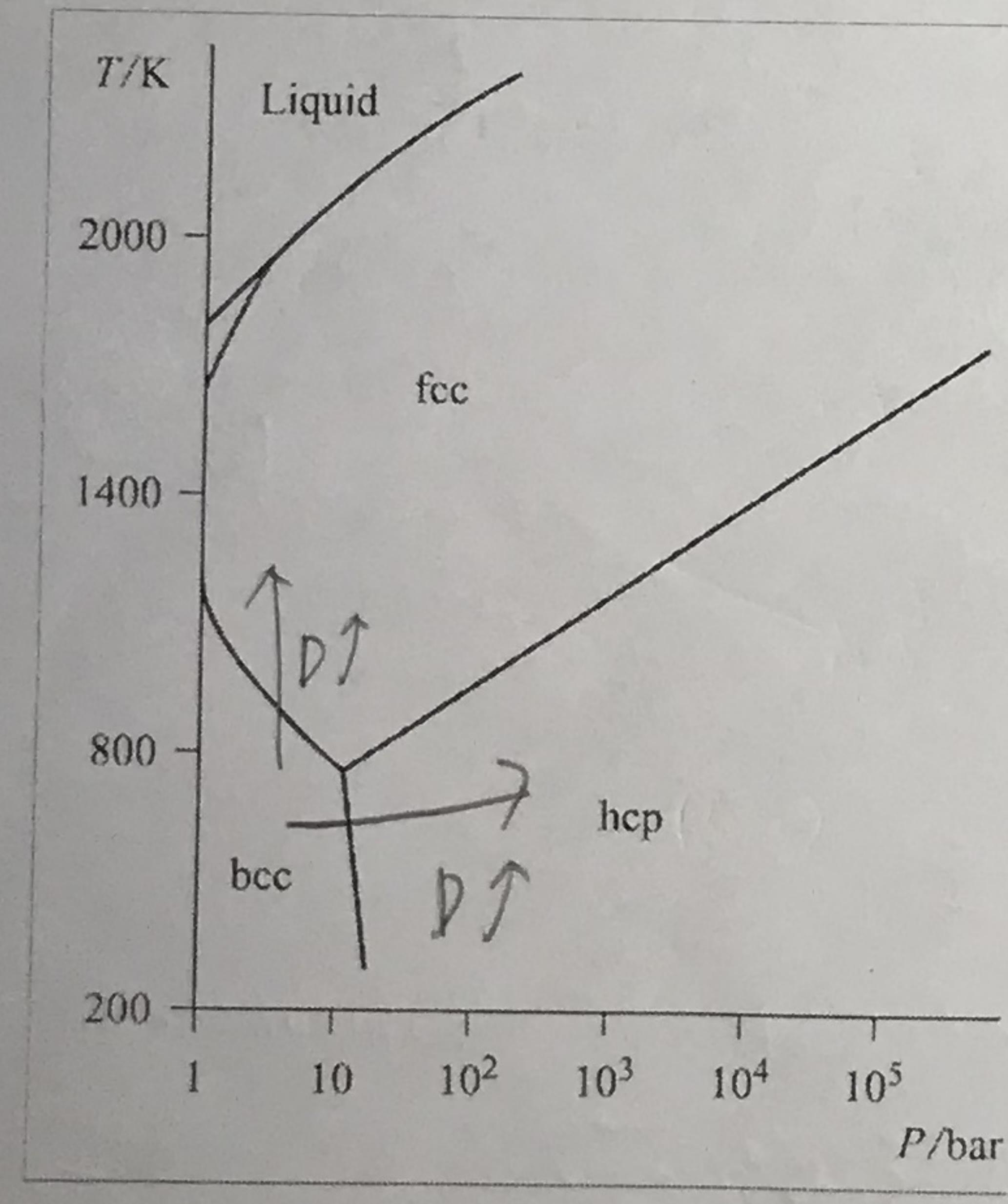
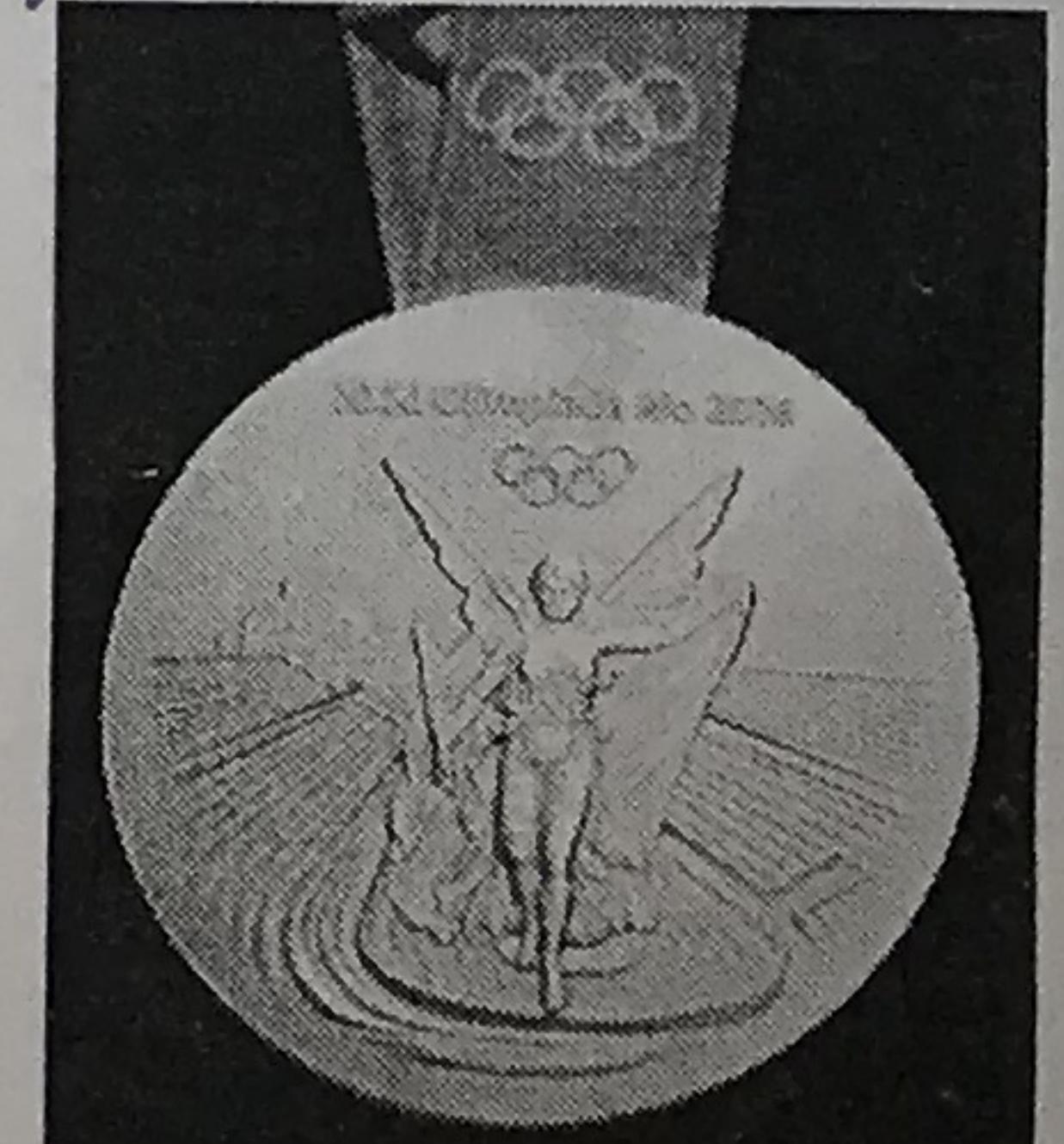
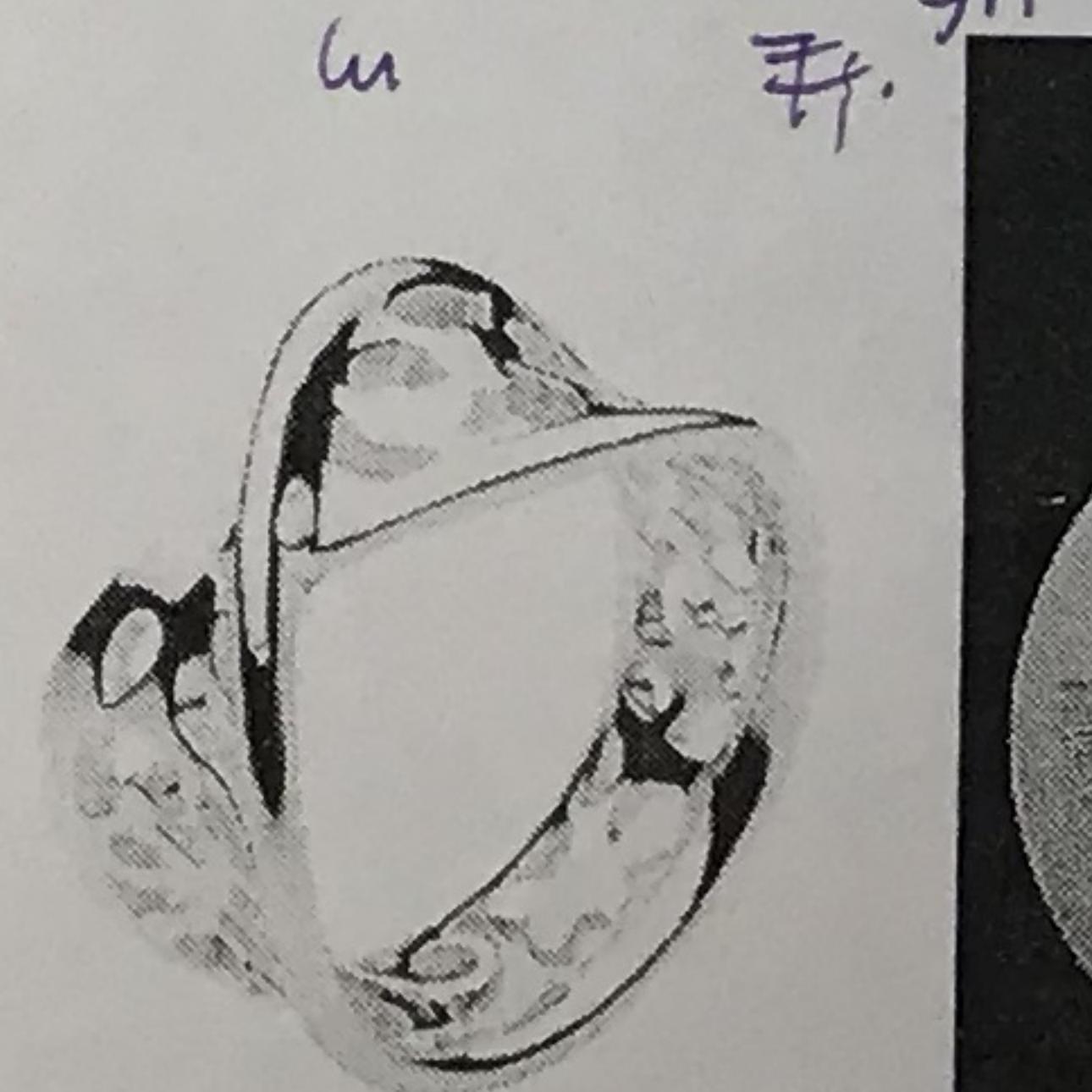
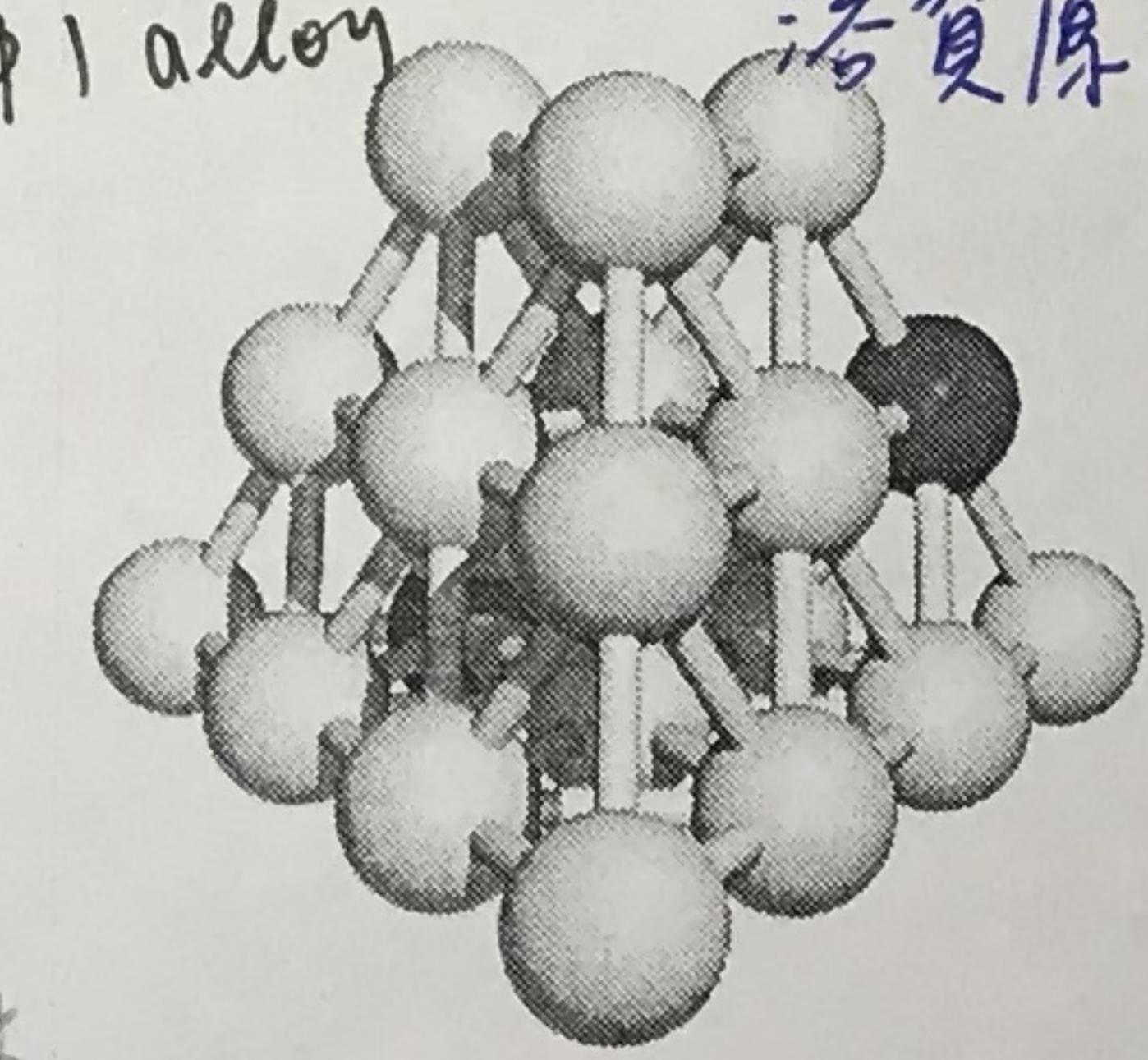
Type 1 全混合兩種或多種金屬或非金屬的化合物(沒有固定比例)

An alloy is an intimate mixture or a compound of two or more metals or non-metals. In a

Type 2, substitutional alloy atoms of the solute occupy sites in the lattice of the solvent metal.

其中 1 alloy 溶質原子佔據溶劑金屬晶格中的位置

Sterling silver is an alloy of silver containing 92.5% by weight of silver and 7.5% by weight of other metals, usually copper. Bronze is an alloy made of 88% copper and 12% tin.

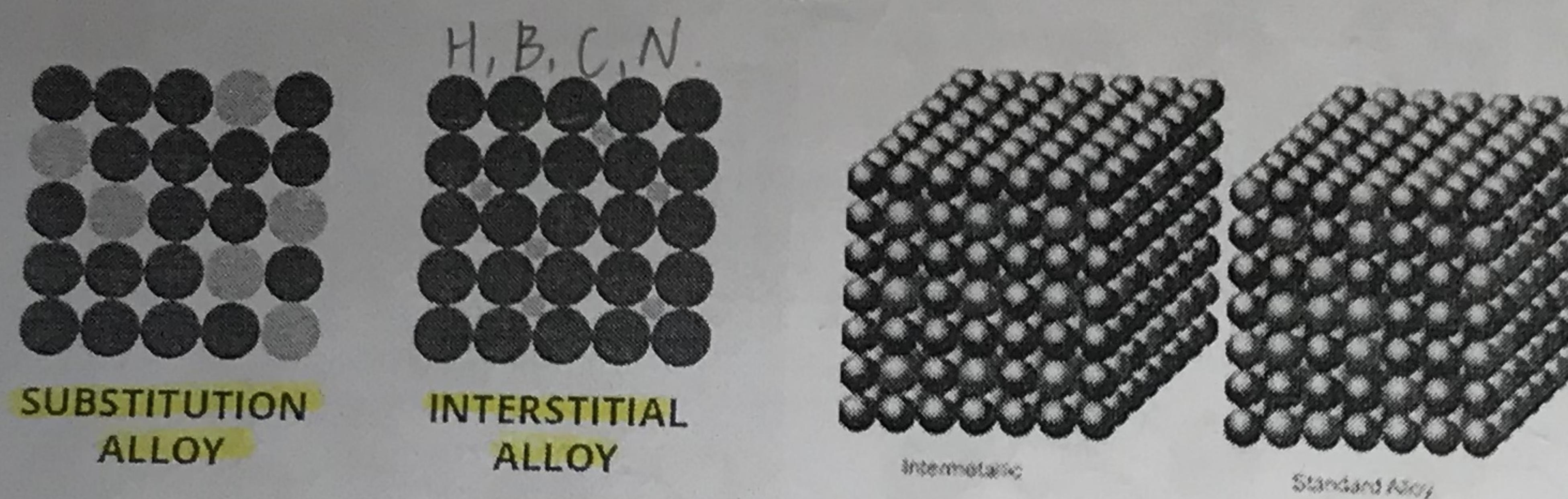


A phase diagram for iron (Fe).

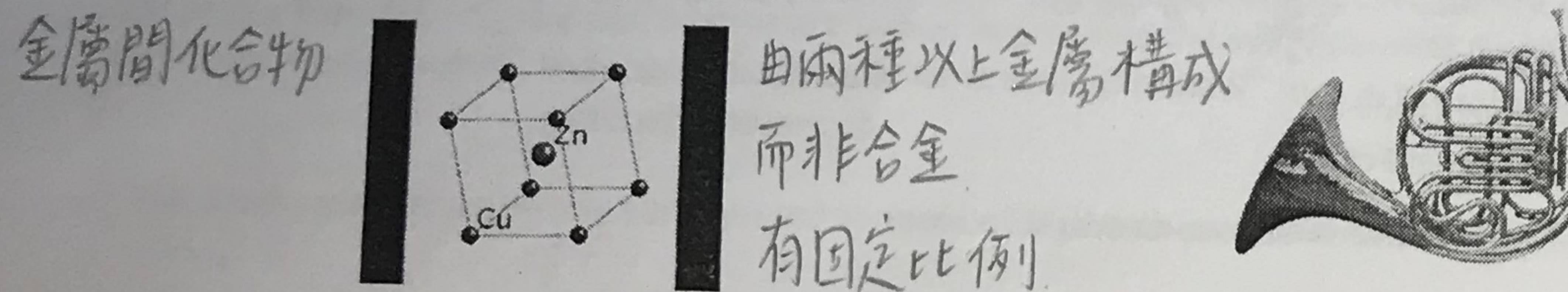
In cation and anion exchange reactions in a binary semiconductor (say Cu_2O to Cu_2S to CdS), the nanocrystal shape can be maintained despite compositional change. This is called pseudomorphism (Science 2016, 351, 1306-1310 by 吳欣倫等) – former MS student, now NCKU Department of Chemistry assistant professor

儘管成份發生變化
但仍然保持奈米晶體
形狀
相同的

An interstitial compound, or interstitial alloy, is a compound that is formed when an atom with a small enough radius sits in an interstitial "hole" in a metal lattice. Examples of small atoms are hydrogen, boron, carbon and nitrogen.



When melts of some metal mixtures solidify, the alloy formed may possess a definite structure type that is different from those of the pure metal. Such systems are classified as intermetallic compounds, e.g. β -brass, CuZn.

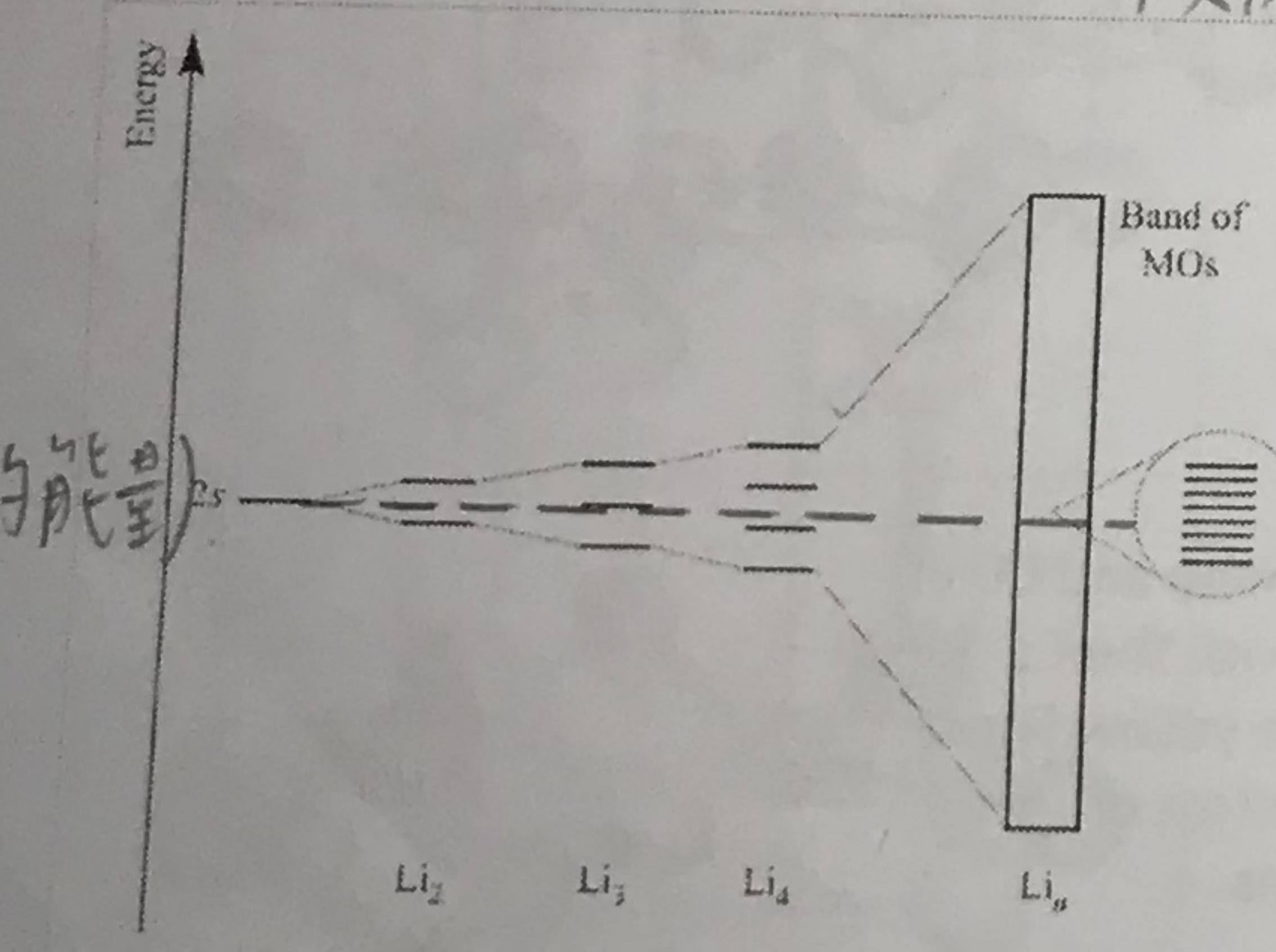


$$(Rm) \rightarrow R = \rho \frac{L}{A} \rightarrow m^2 \quad (\text{考慮長度與截面積})$$

Resistance (in Ω) = [resistivity (in $\Omega \text{ m}$) \times length of wire (in m)]/[cross-sectional area of wire (in m^2)]

Electrical conductivity (σ) is the inverse of resistivity (ρ). $\sigma = \frac{1}{\rho}$.

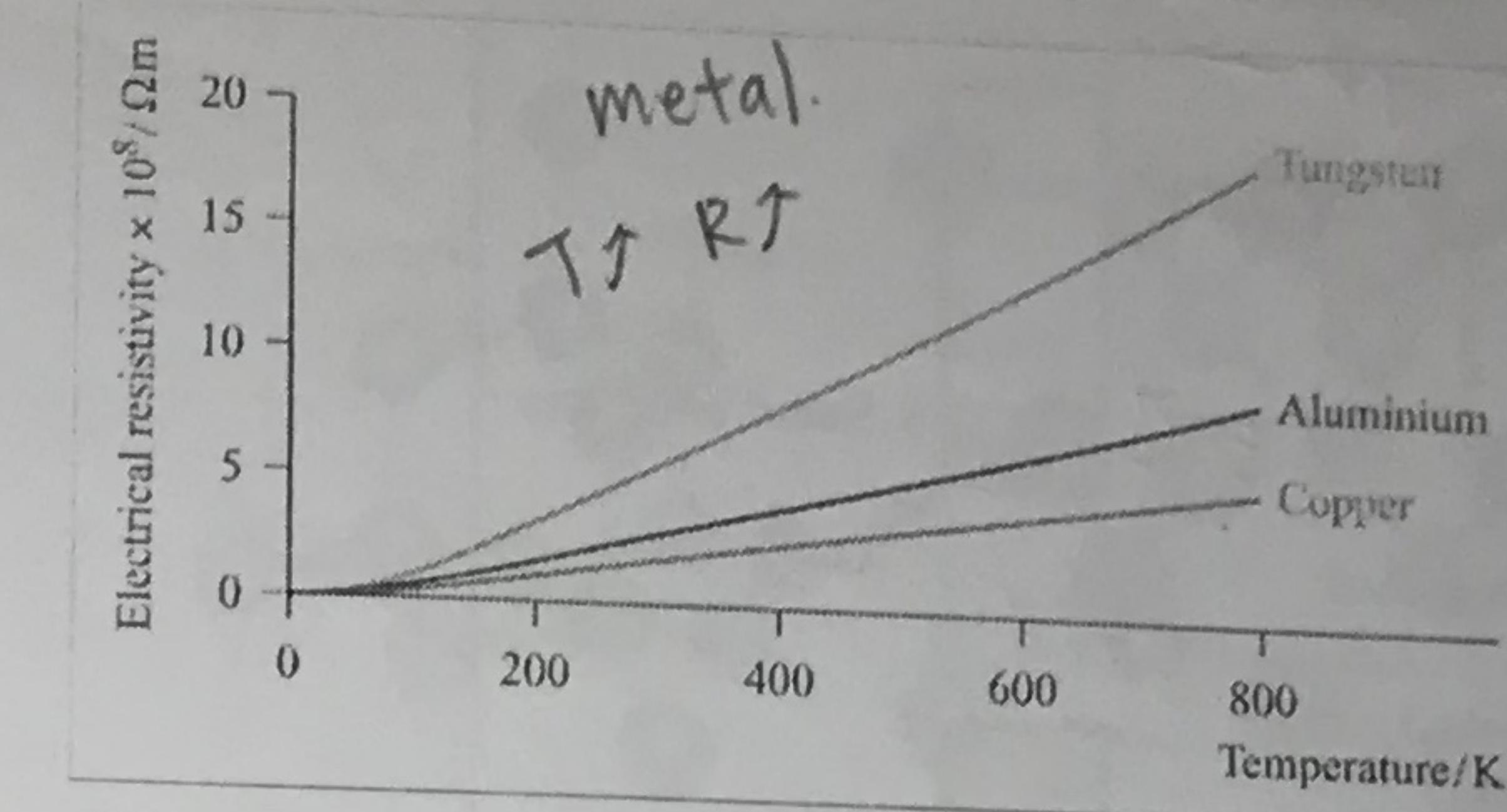
Band theory of metals and insulators



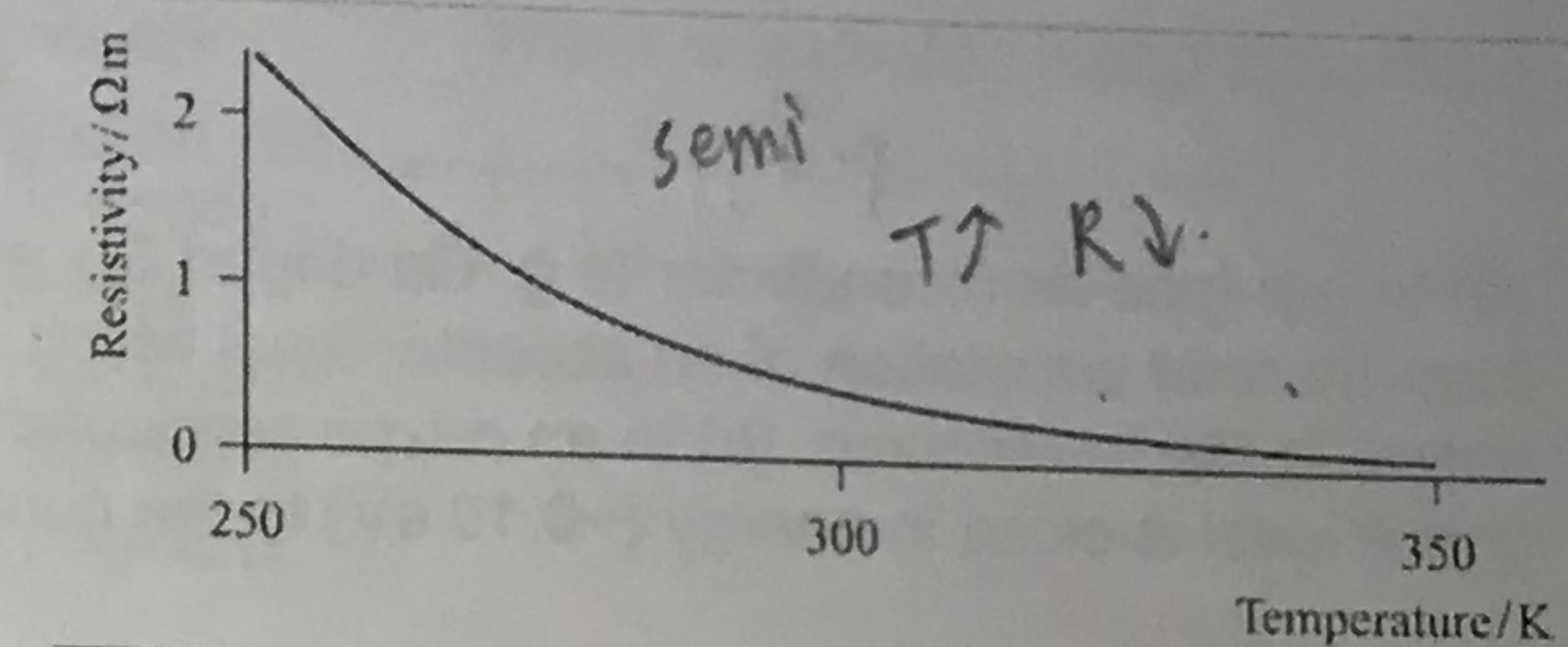
The interaction of two 2s atomic orbitals in Li_2 leads to the formation of two MOs. With three Li atoms, three MOs are formed, and so on. For Li_n , there are n molecular orbitals, but because the 2s atomic orbitals are all of the same energy, the energies of the MOs are very close together and constitute a band of orbitals.

產生交互作用的原子個數

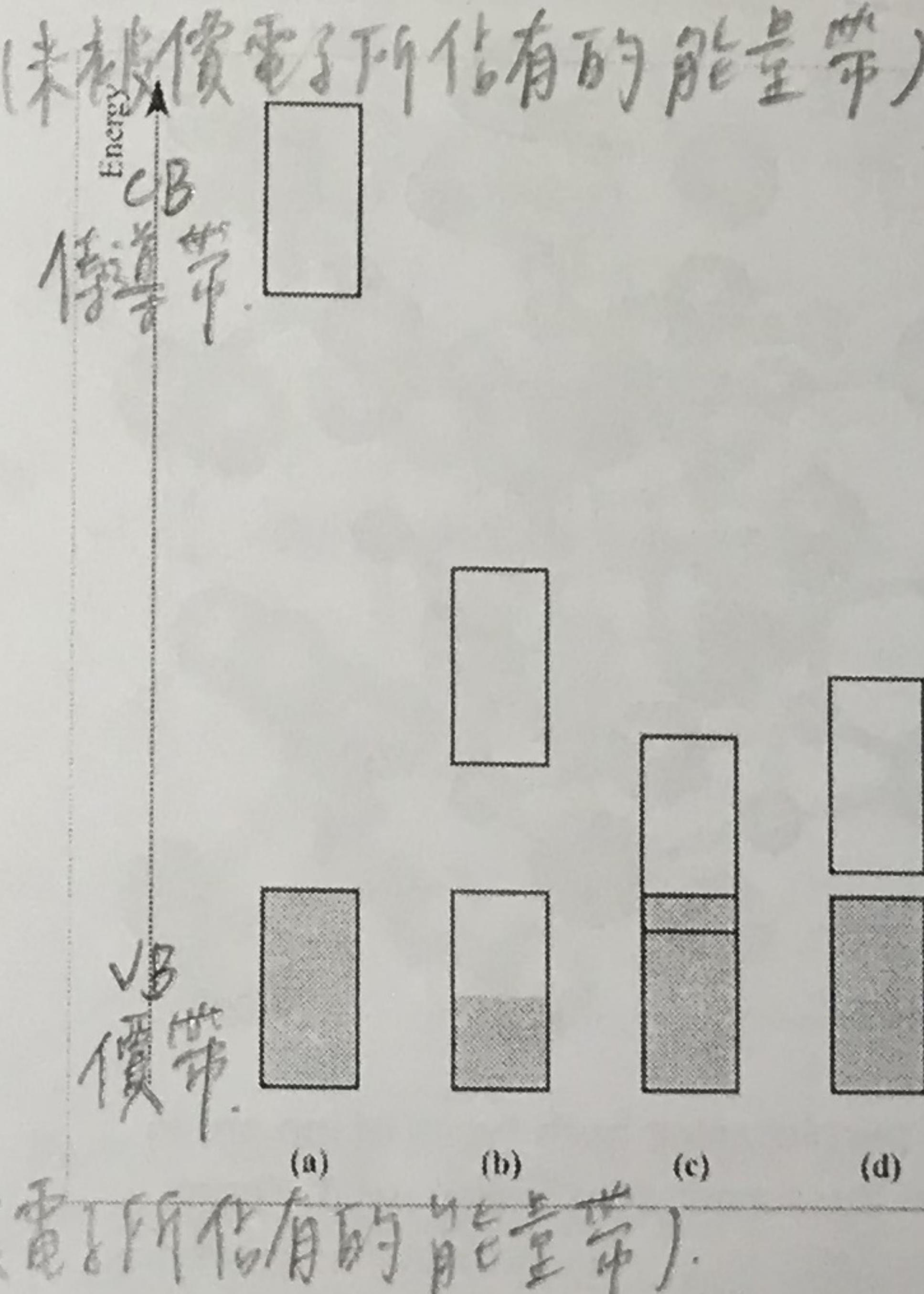
Bondings in metals and semiconductors



A metal is characterized by the fact that its electrical resistivity increases as the temperature increases, i.e. its electrical conductivity decreases as the temperature increases.

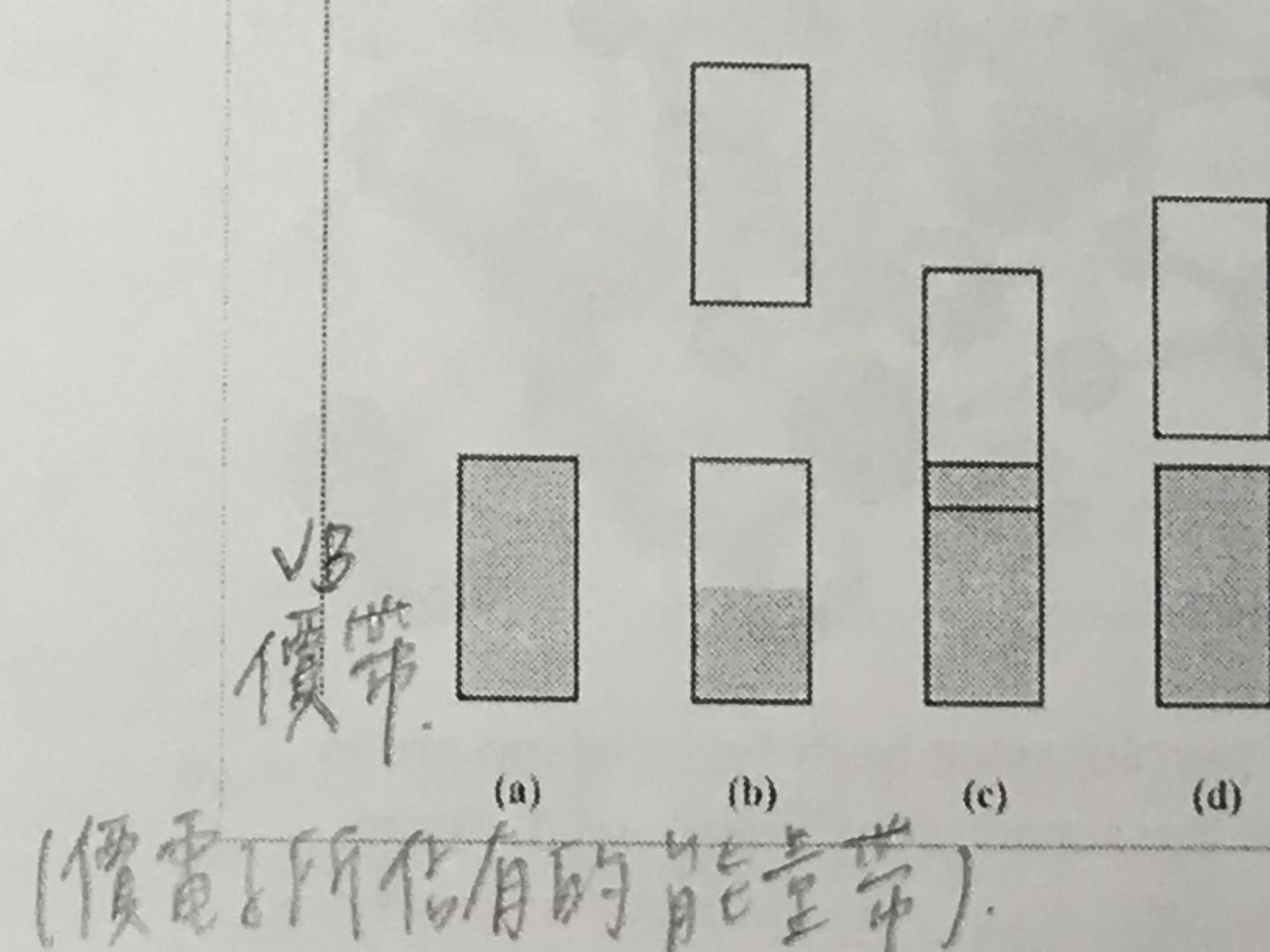


A semiconductor, such as germanium, is characterized by the fact that its electrical resistivity decreases as the temperature increases. Its electrical conductivity increases as the temperature increases.



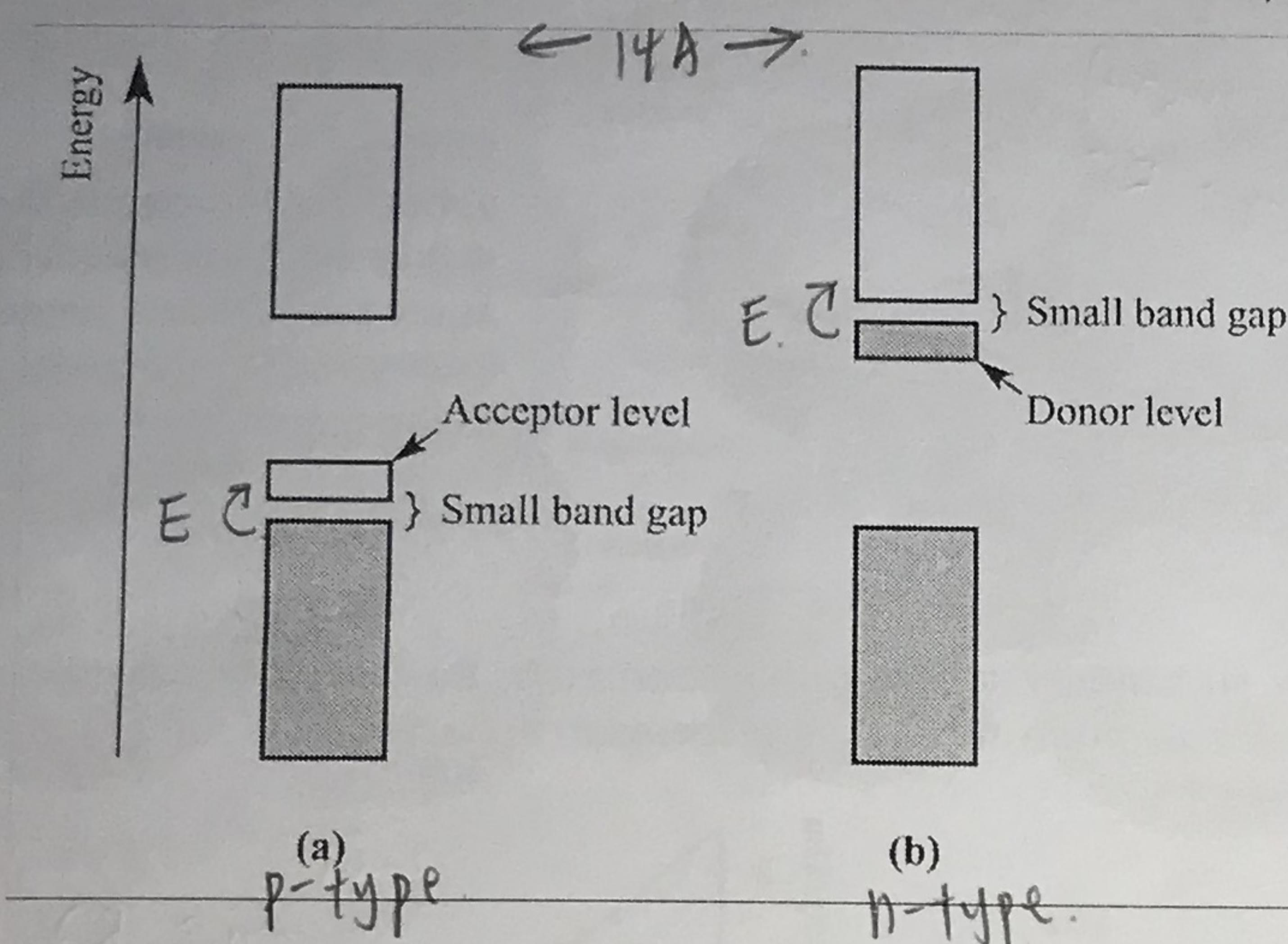
The relative energies of occupied and empty bands in (a) an insulator, (b) a metal in which the lower band is only partially occupied, (c) a metal in which the occupied and empty bands overlap, and (d) a semiconductor.

The Fermi level.

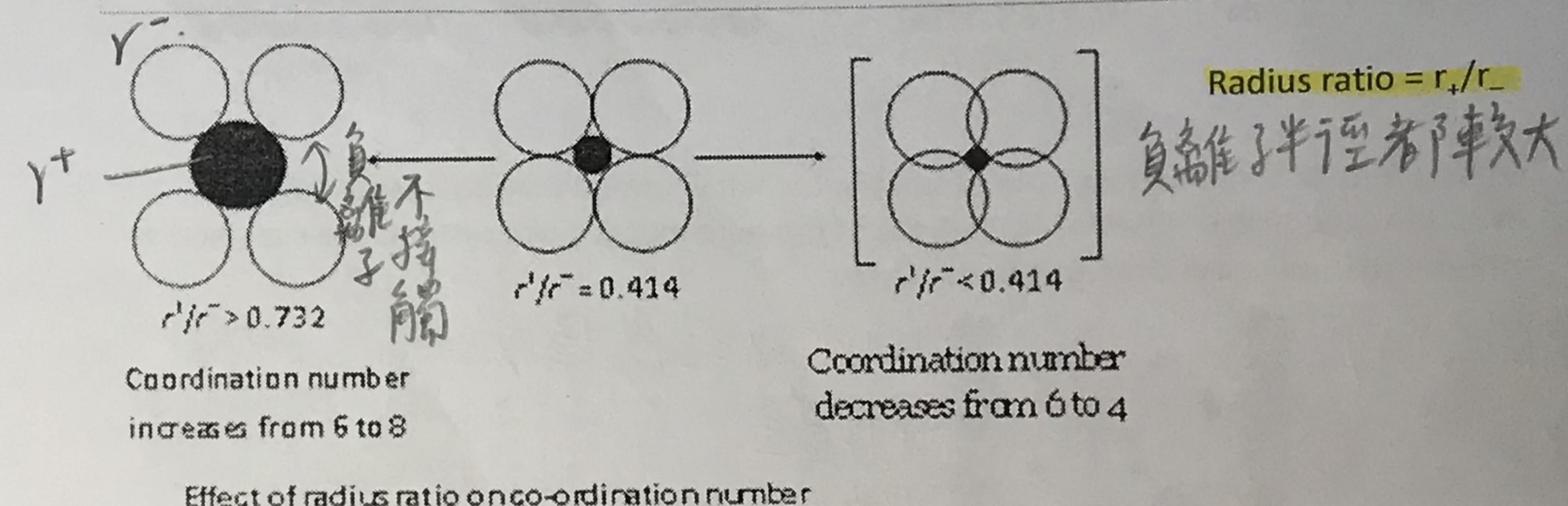
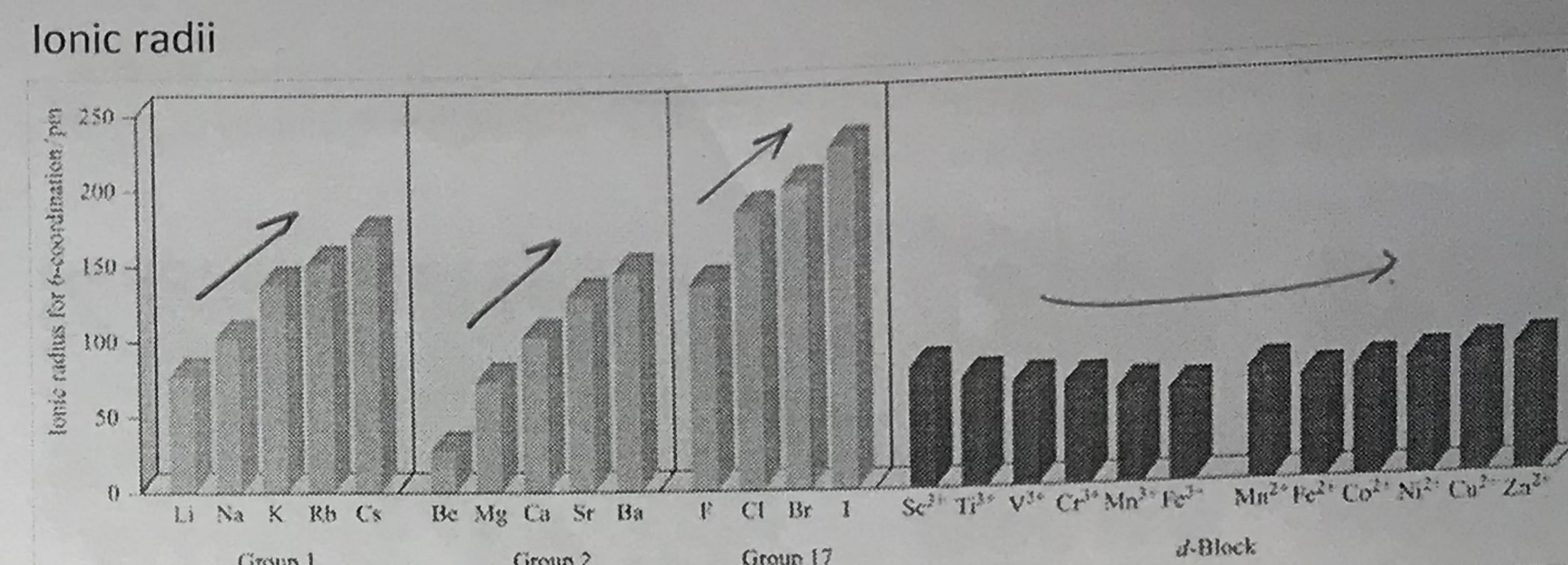


If a material behaves as a semiconductor without the addition of dopants, it is an intrinsic semiconductor.

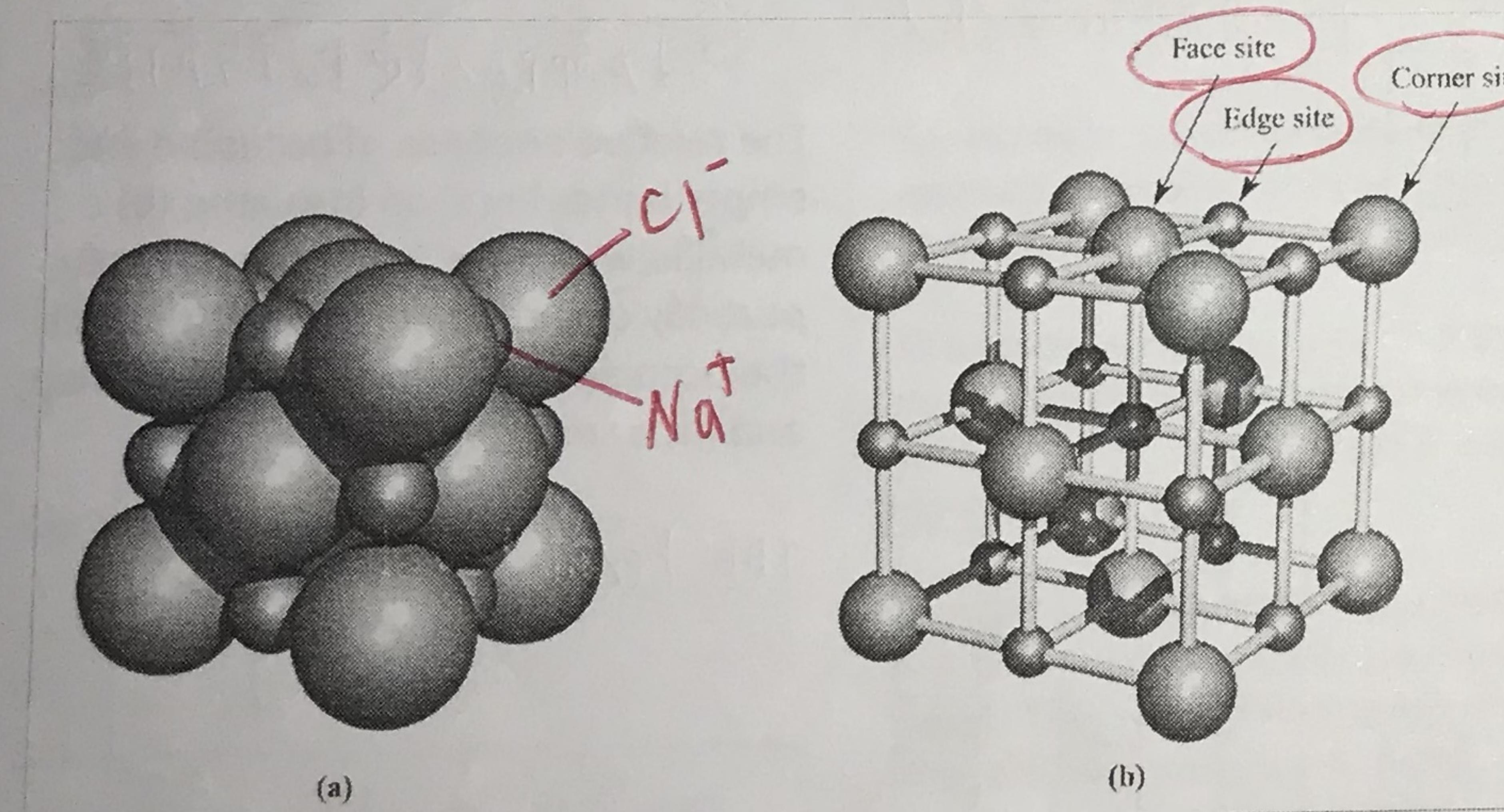
Extrinsic (*n*- and *p*-type) semiconductors contain dopants; a dopant is an impurity introduced into a semiconductor in minute amounts to enhance its electrical conductivity.



(a) In a *p*-type semiconductor (e.g. Ga-doped Si), electrical conductivity arises from thermal population of an acceptor level which leaves vacancies (positive holes) in the lower band. (b) In an *n*-type semiconductor (e.g. As-doped Si), a donor level is close in energy (~0.10 eV) to the conduction band.

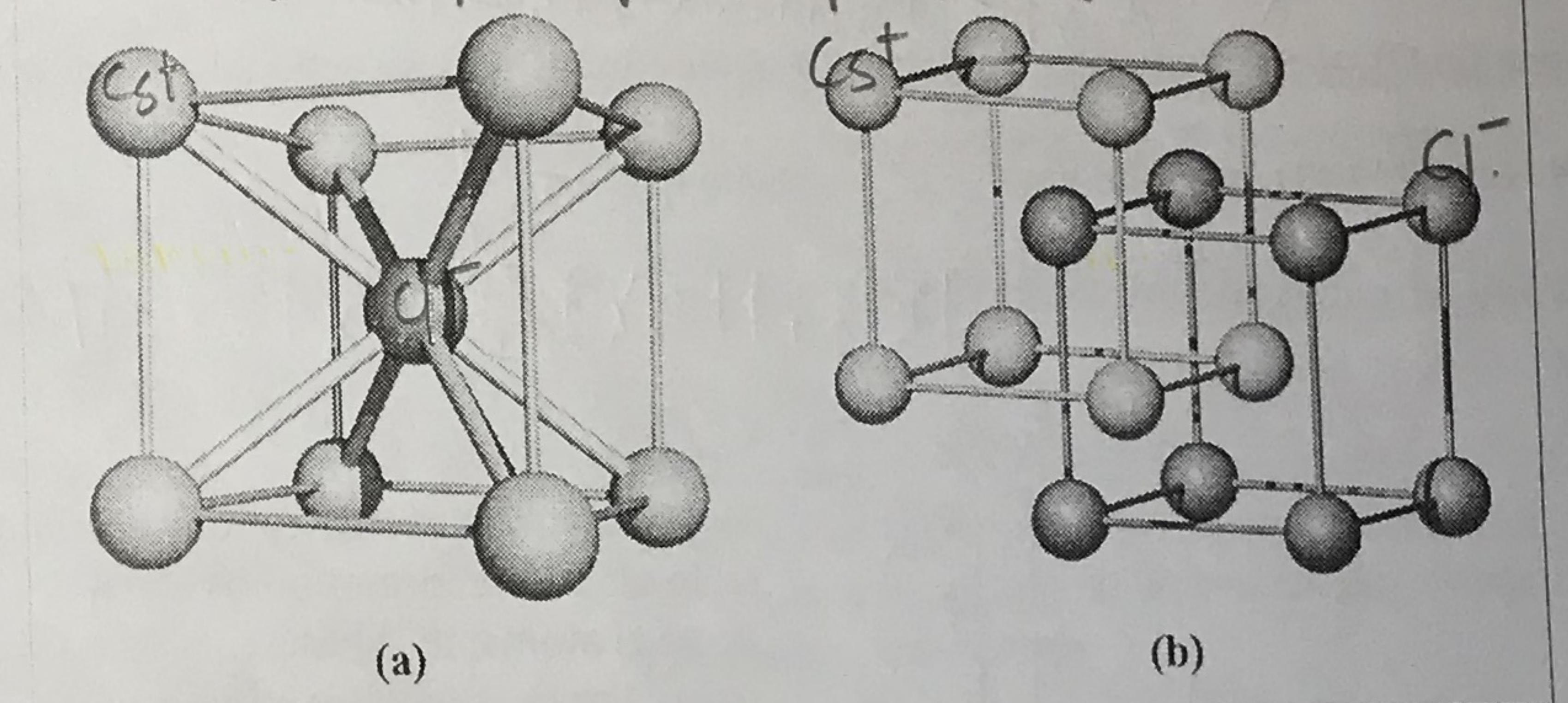


Ionic lattices
The rock salt (NaCl) structure type



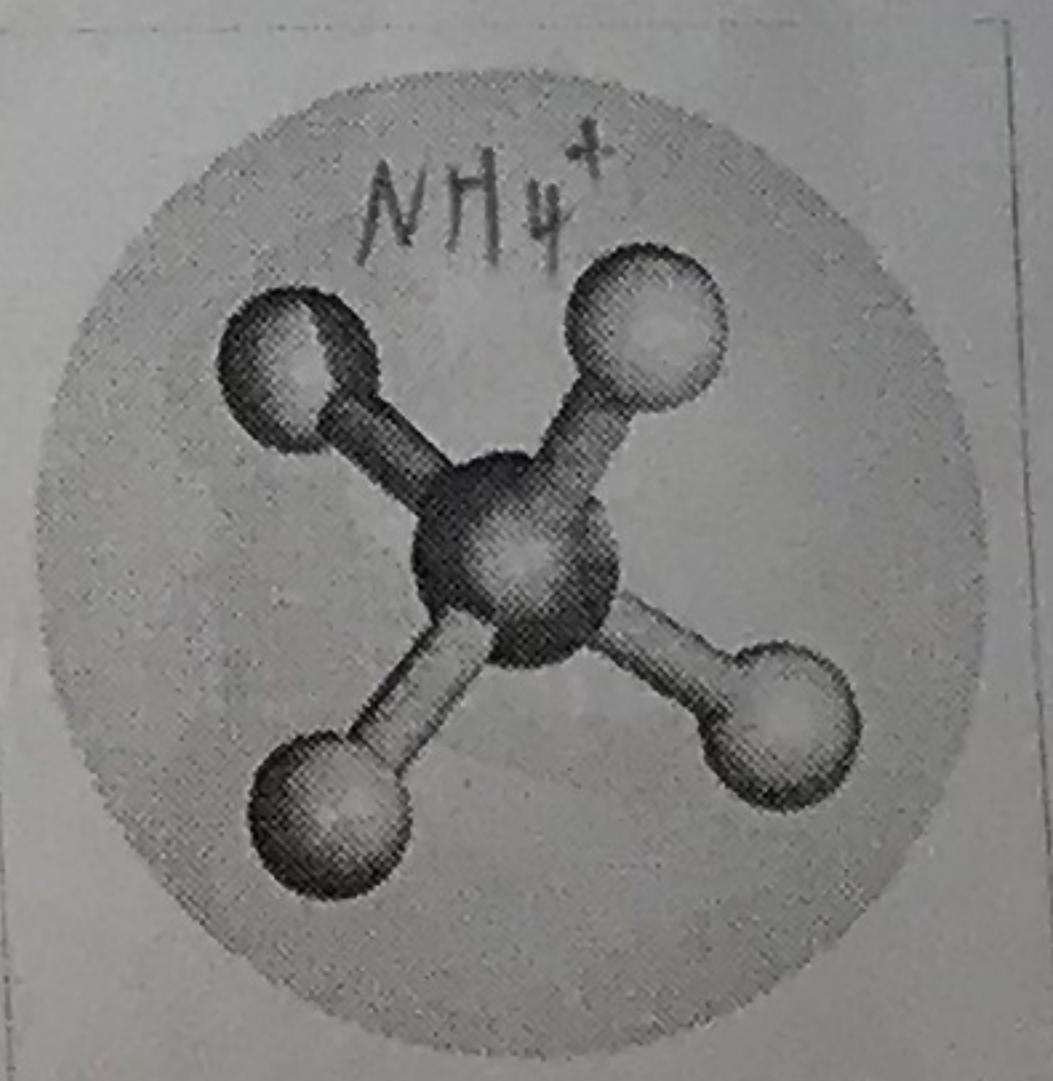
The Cl⁻ ions are shown in green and the Na⁺ ions in purple; since both types of ion are in equivalent environments, a unit cell with Na⁺ ions in the corner sites is also valid. There are four types of site in the unit cell: central (not labelled), face, edge and corner positions.

指不管中心原子是哪個皆可 $\text{CsCl} = \text{NH}_4\text{Cl} = \text{NH}_3\text{Br}$



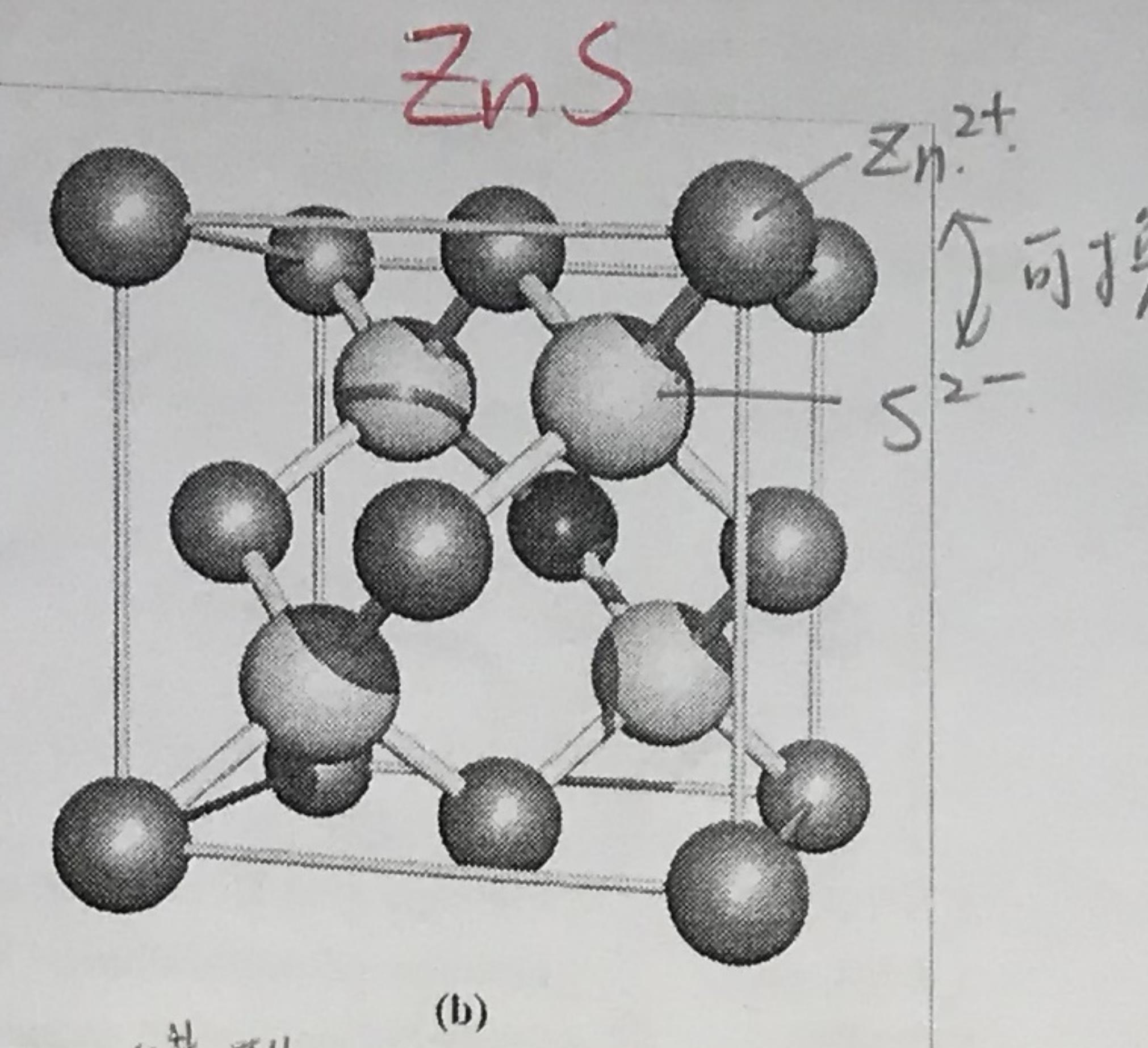
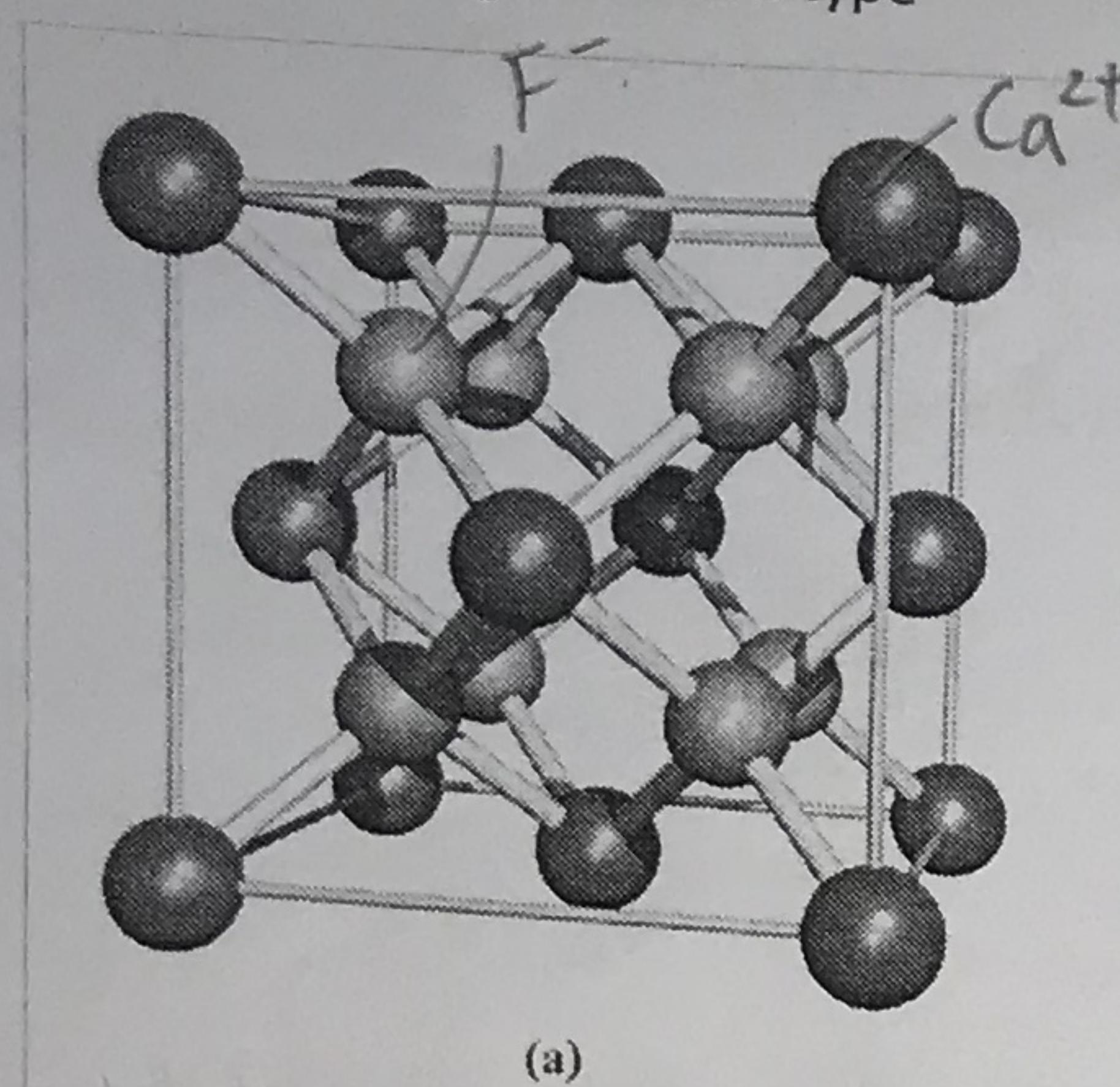
- (a) The unit cell of CsCl; Cs⁺ ions are shown in yellow and Cl⁻ in green, but the unit cell could also be drawn with the Cs⁺ ion in the central site. The unit cell is defined by the yellow lines.
 (b) One way to describe the CsCl structure is in terms of interpenetrating cubic units of Cs⁺ and Cl⁻ ions.

NH₄Cl and NH₃Br possess CsCl structure. The [NH₄]⁺ ion can be treated as a sphere in descriptions of solid state lattices; some other ions (e.g. [BF₄]⁻, [PF₆]⁻) can be treated similarly.



CaF_2

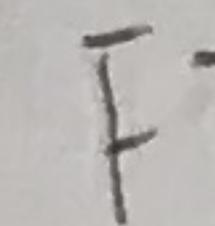
The fluorite (CaF_2) structure type



構型: zinc blende

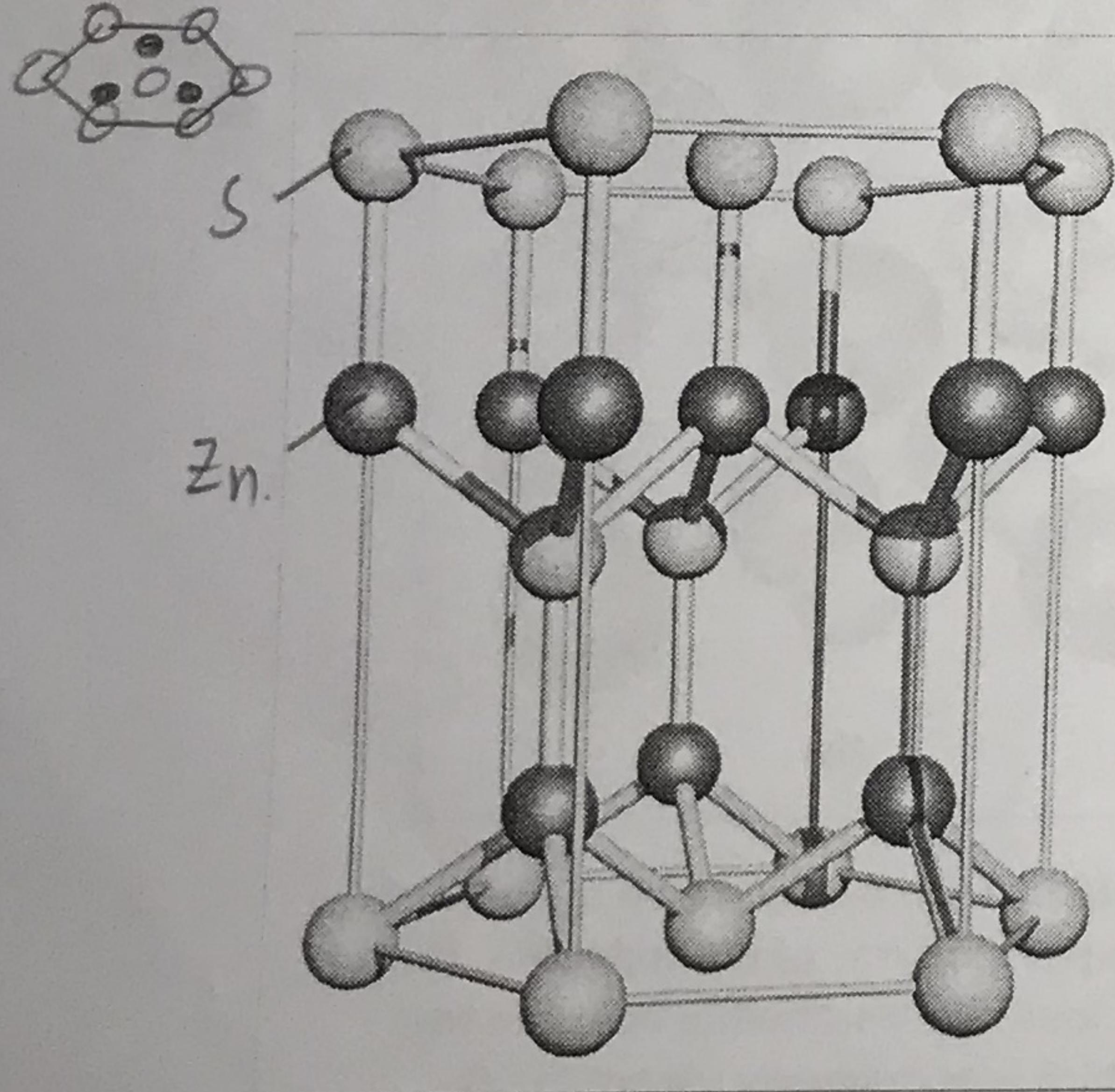
(a) The unit cell of CaF_2 ; the Ca^{2+} ions are shown in red and the F^- ions in green. (b) The unit cell of zinc blende (ZnS); the zinc centres are shown in grey and the sulfur centres in yellow. Both sites are equivalent, and the unit cell could be drawn with the S^{2-} ions in the grey sites.

The antifluorite structure has a compound formula of M_2X with cations in all 8 tetrahedral sites.



Wurtzite ZnS

The wurtzite (ZnS) structure



同質異形体

Three unit cells of wurtzite (a second polymorph of ZnS) define a hexagonal prism; the Zn^{2+} ions are shown in grey and the S^{2-} ions in yellow. Both ions are tetrahedrally sited and an alternative unit cell could be drawn by interchanging the ion positions.

六方密堆积

Ti⁴⁺在畸变形的八面体中

The unit cell of rutile (one polymorph of TiO_2). Colour code: Ti, silver; O, red.

Ti^{4+} 的配位数 = 6

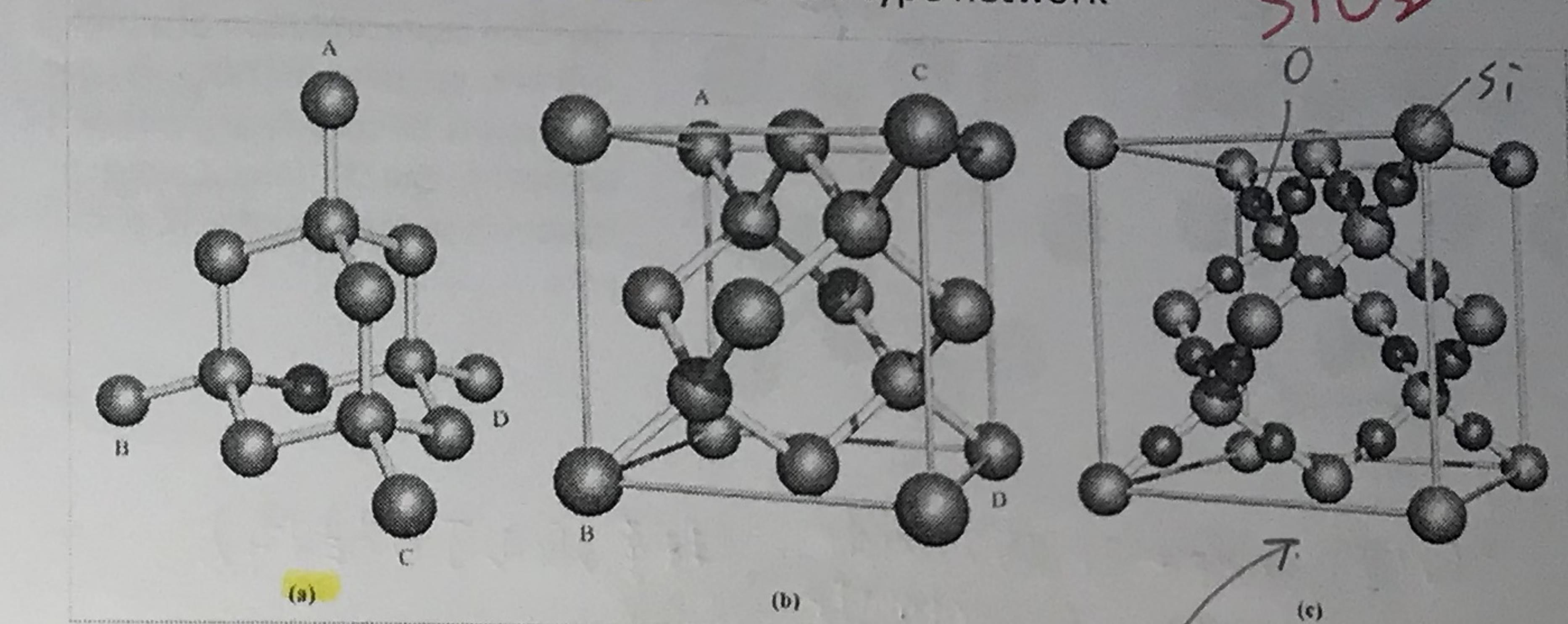
O^{2-} 有3个 Ti^{4+} 配位

每個晶胞中: 27 Ti^{4+}

45 O^{2-}

coordination number { cation: 4
anion: 4 }

The zinc blende (ZnS) structure: a diamond-type network



SiO_2

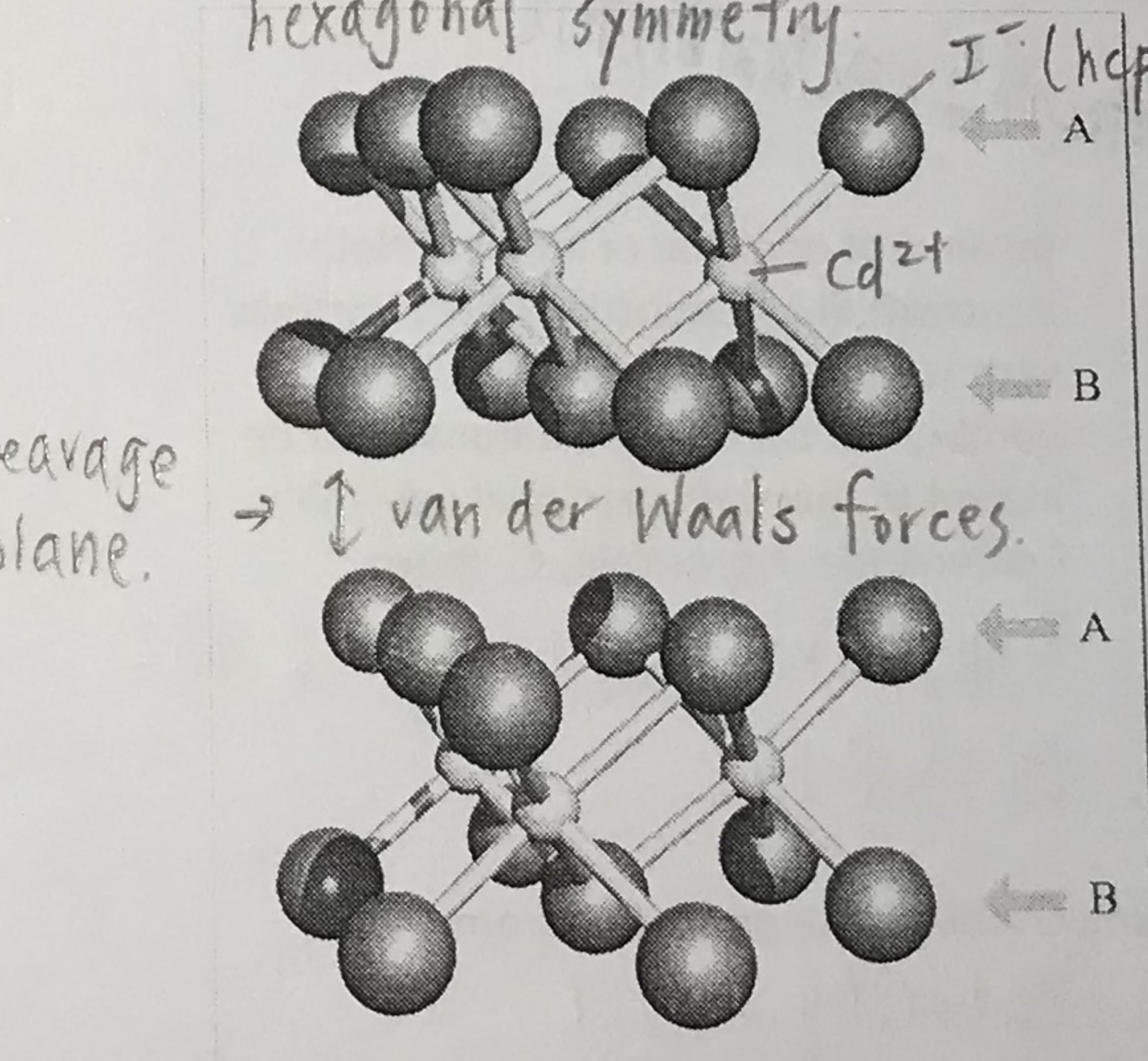
The β -cristobalite (SiO_2) structure

(a) A typical representation of the diamond structure. (b) Reorientation of the network shown in (a) provides a representation that can be compared with the unit cell of zinc blende (Fig. 6.19b); the atom labels correspond to those in diagram (a). This structure type is also adopted by Si, Ge and α -Sn. (c) The unit cell of β -cristobalite, SiO_2 ; colour code: Si, purple; O, red.

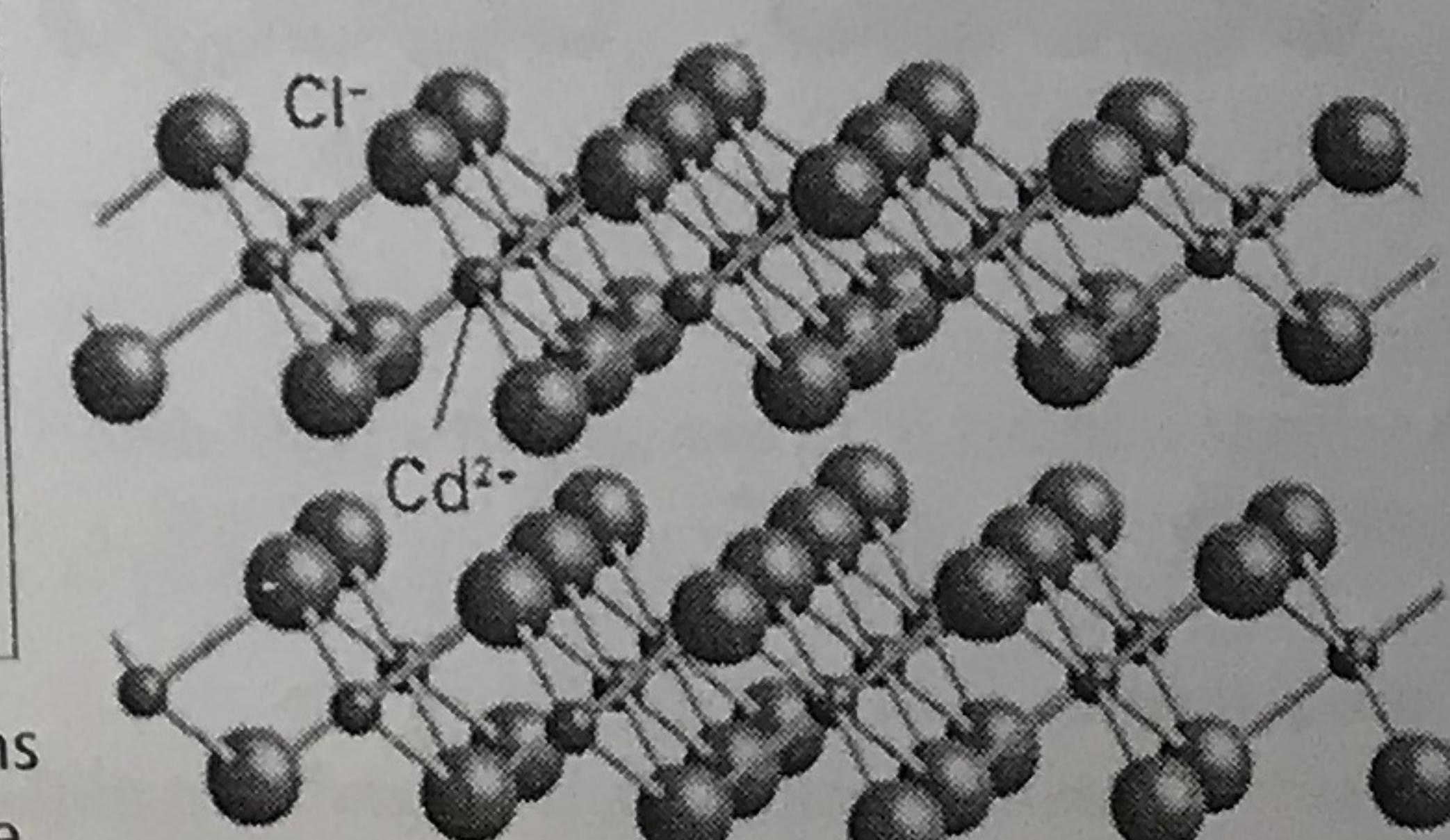
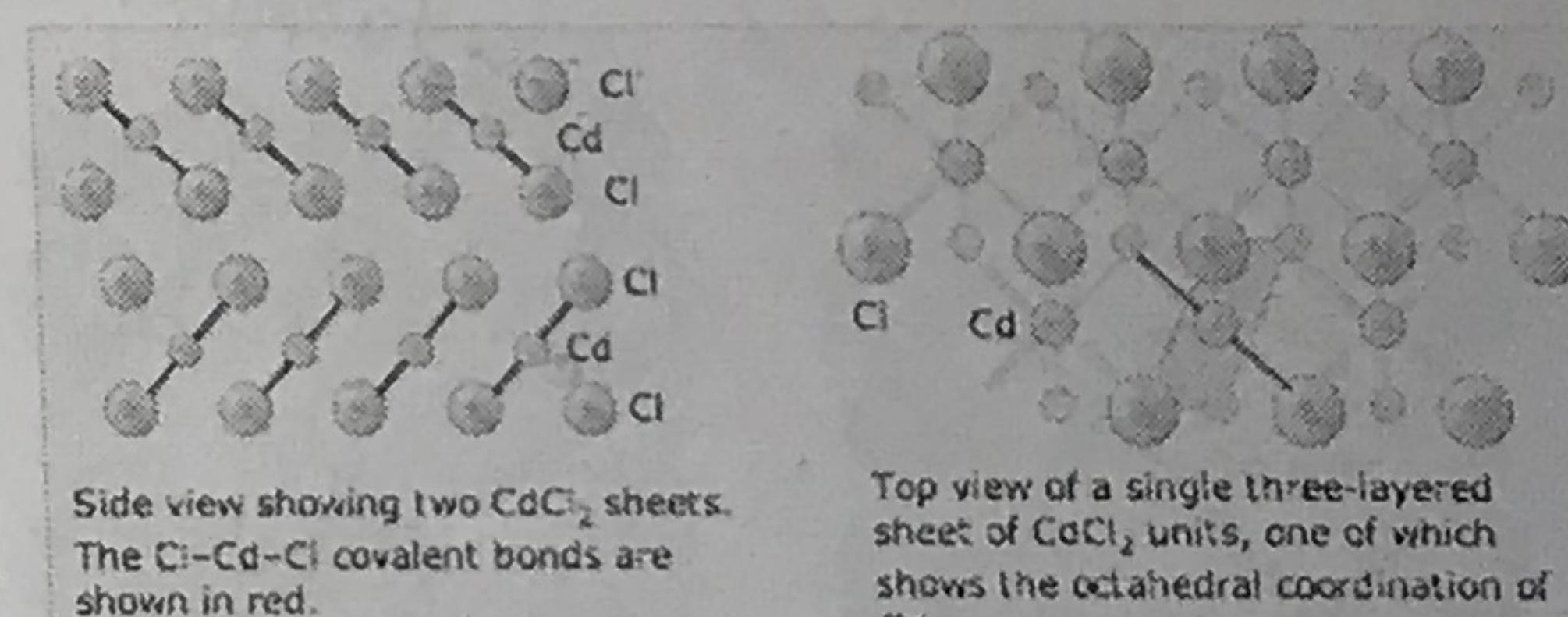
$\text{CdI}_2 / \text{CdCl}_2$

$\rightarrow \text{I}^-$ hcp 構排列, Cd^{2+} 填入所有 octahedral hole.

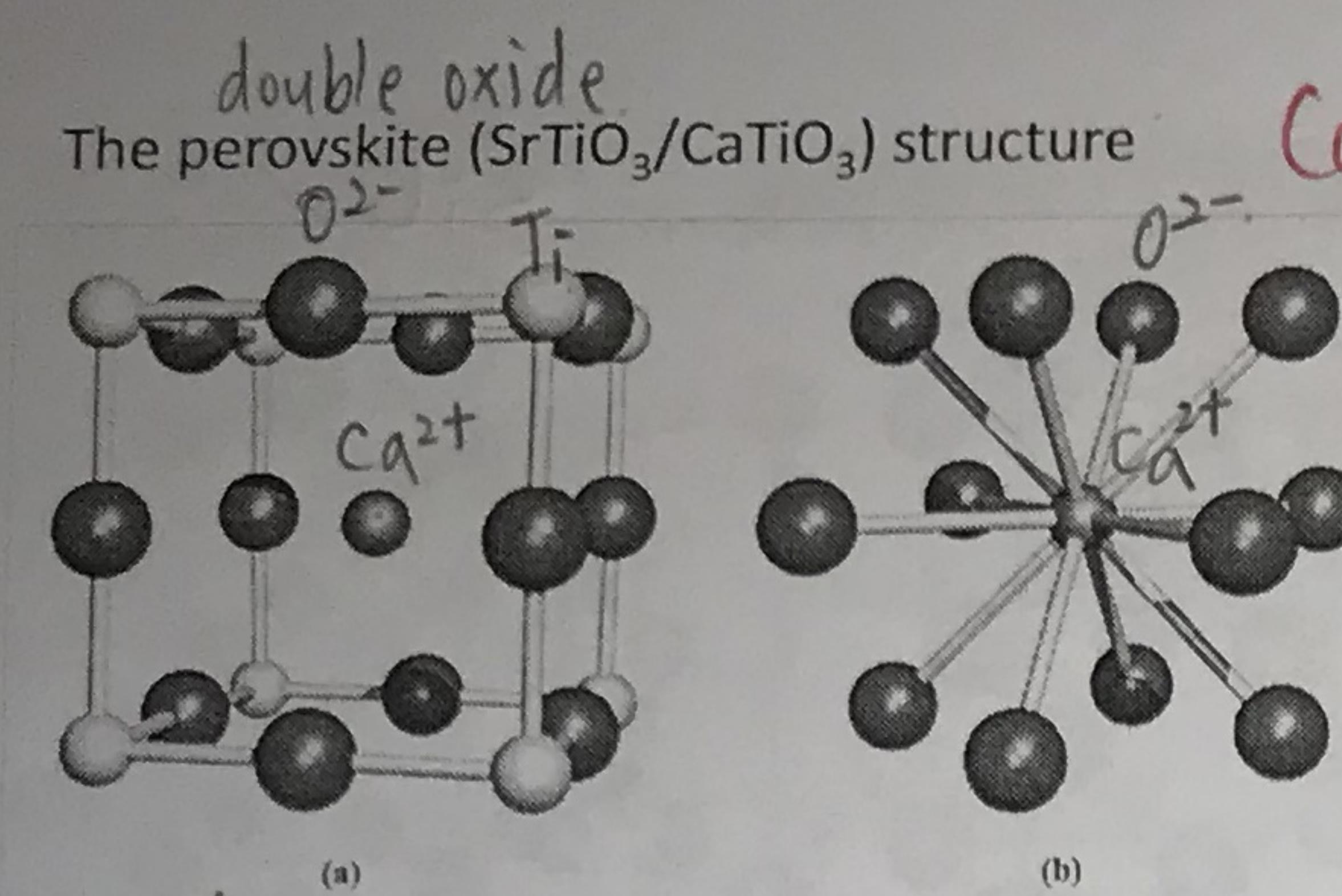
CdI_2 and CdCl_2 : layer structure hexagonal symmetry.



The structure of CdCl_2 is related to CdI_2 layer structure but with the Cl^- ions in a cubic close-packed arrangement.



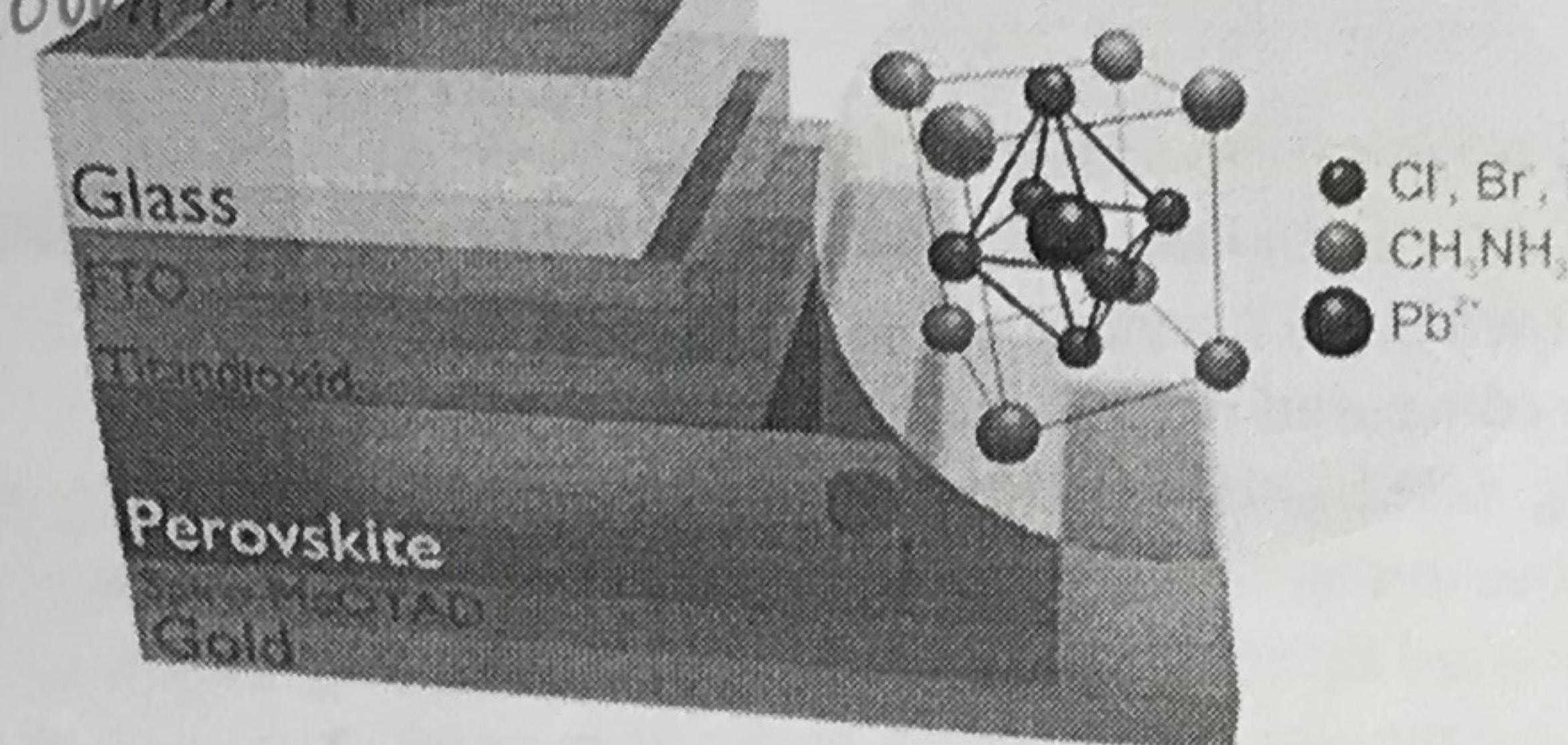
Parts of two layers of the CdI_2 lattice; Cd^{2+} ions are shown in pale grey and I^- ions in gold. The I^- ions are arranged in an hcp array. Each AB layer is electrically neutral and only weak van der Waals forces operate between the layers.



(a) One representation of a unit cell of perovskite (CaTiO_3); (b) the Ca^{2+} ion is 12-coordinate with respect to the O^{2-} ions. Colour code: Ca, purple; O, red; Ti, pale grey.

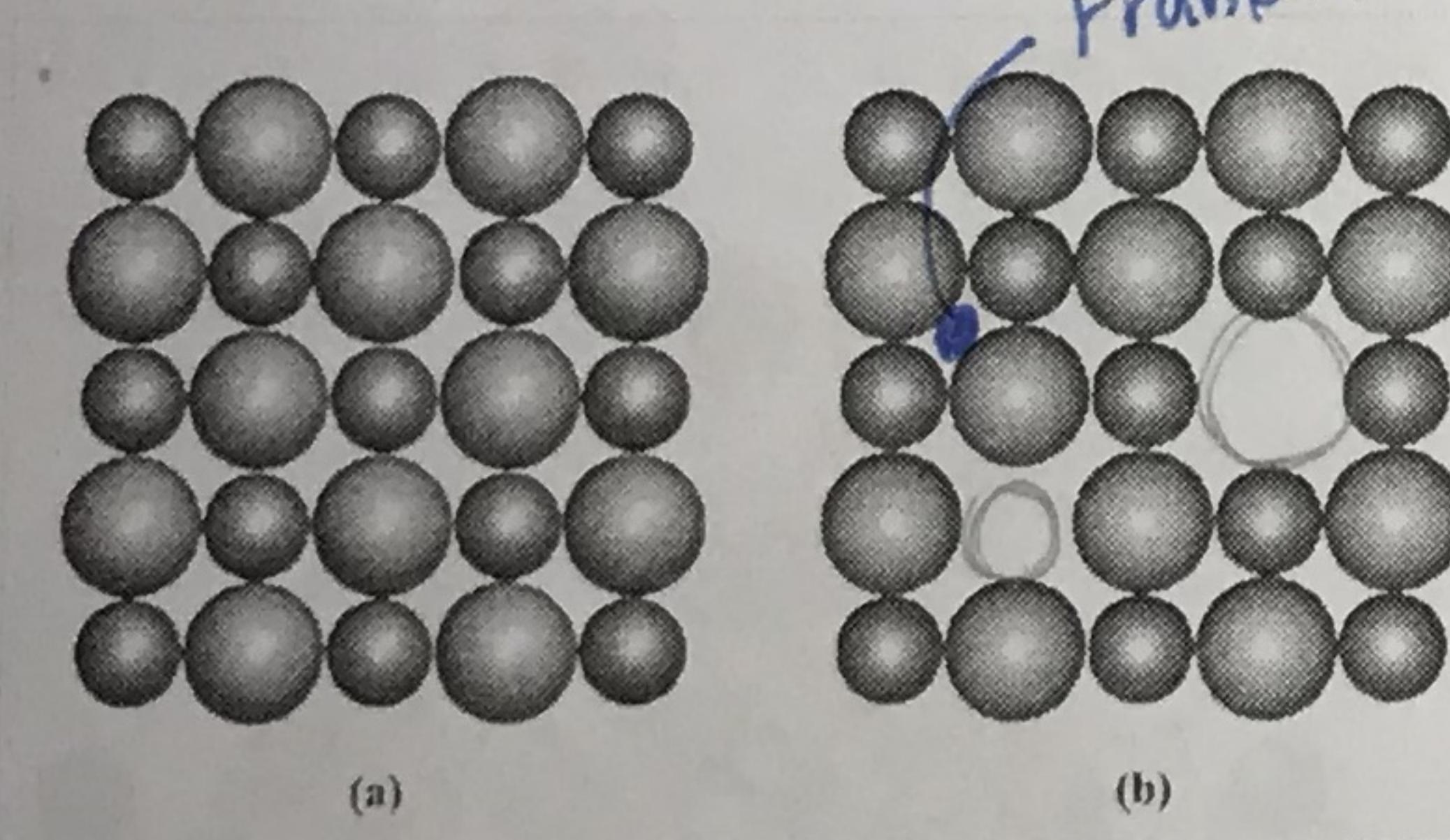
$\downarrow \text{Ca(II) oxide} + \text{Ti(IV) oxide}$ (含有 BRnTiO 相接)
12 coordinate 6 coordinate

Perovskite solar cells
 $\text{CH}_3\text{NH}_3\text{PbX}_3$



Please remember that in reality, ionic solids are formed from metal ions solvated in water or other solvents, rather than from gaseous ionic states.

Defects in solid state lattices



(a) Part of one face of an ideal NaCl structure. (b) A Schottky defect involves vacant cation and anion sites; equal numbers of cations and anions must be absent to maintain electrical neutrality. Colour code: Na, purple; Cl, green.

要維持相同數量的正負價才能維持電中性。

Schottky defect

A Schottky defect is an example of a point defect in a crystal lattice and arises from vacant lattice sites.

每個 vacancy 都是獨立的 Schottky defect.

Frankel defect

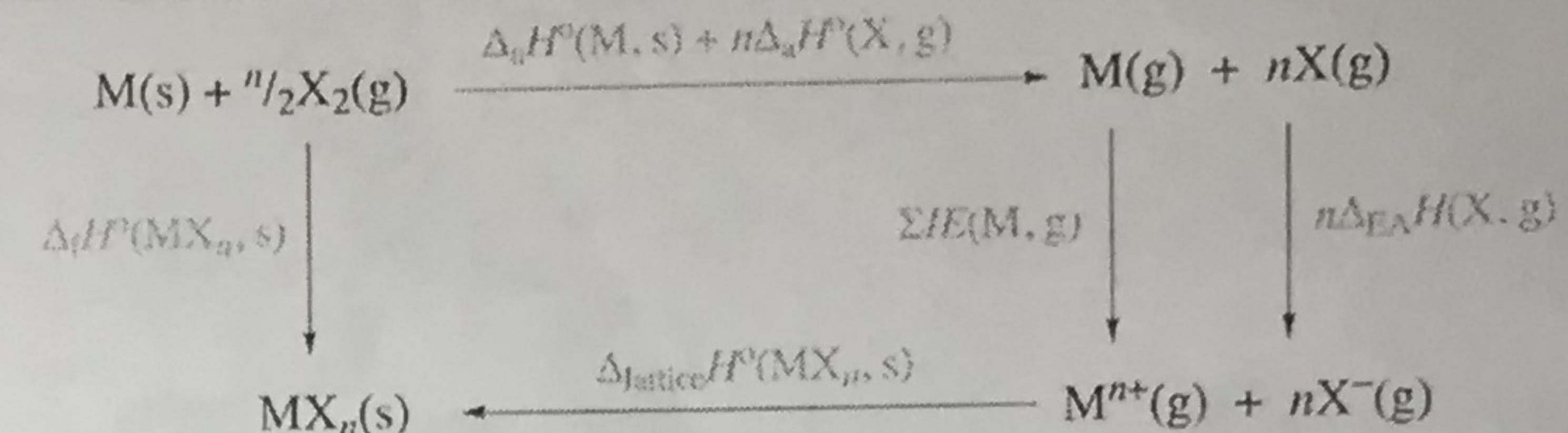
晶格密度減小

In ionic lattices in which there is a significant difference in size between the cation and anion, the smaller ion may occupy a site that is vacant in the ideal lattice. This is a Frenkel defect and does not affect the stoichiometry or electrical neutrality of the compound.

原子(離子)離開自己的格架而成為間隙原子。

Lattice energy

The lattice energy of a crystalline solid is usually defined as the energy of formation of the crystal from infinitely-separated ions and as such is invariably negative. In the case of NaCl , the lattice energy is the energy released by the reaction

$$\text{Na}^+(\text{g}) + \text{Cl}^-(\text{g}) \rightarrow \text{NaCl}(\text{s}), \text{ which would amount to } -786 \text{ kJ/mol.}$$


$\Delta_a H^\circ(\text{M, s})$ = Enthalpy of atomization of metal M

$\Delta_a H^\circ(\text{X, g})$ = Enthalpy of atomization of X

$\Sigma IE(\text{M, g})$ = Sum of the ionization energies for the processes $\text{M(g)} \rightarrow \text{M}^+(\text{g}) \rightarrow \text{M}^{2+}(\text{g}) \dots \rightarrow \text{M}^{n+}(\text{g})$

$\Delta_{EA} H^\circ(\text{X, g})$ = Enthalpy change associated with the attachment of an electron

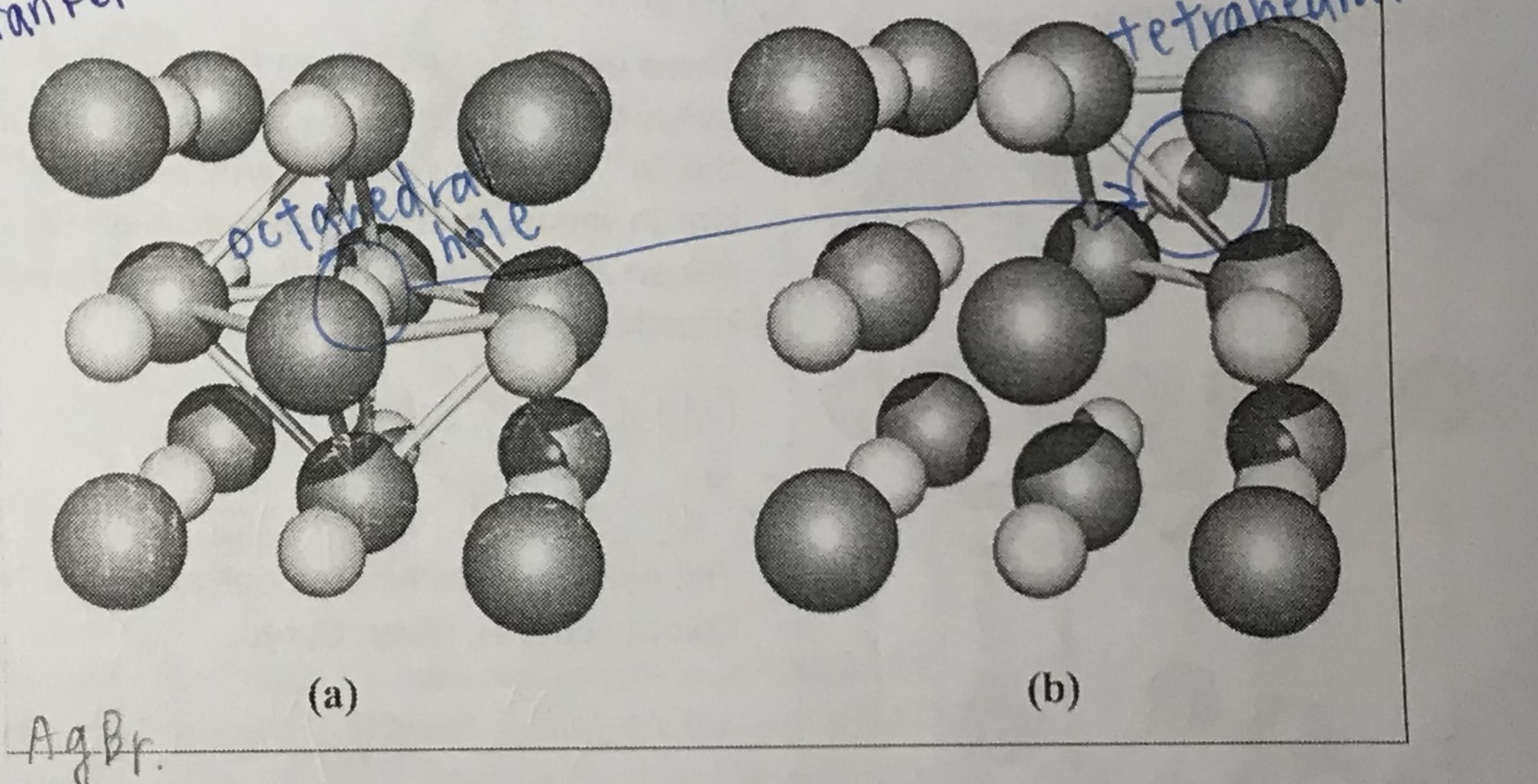
$\Delta_f H^\circ(\text{MX}_n, \text{s})$ = Standard enthalpy of formation

$\Delta_{lattice} H^\circ(\text{MX}_n, \text{s})$ = Lattice enthalpy change (see text)

A Born–Haber thermochemical cycle for the formation of a salt MX_n . This gives an enthalpy change associated with the formation of the ionic lattice MX_n .

$$\begin{aligned} \Delta_f H^\circ(\text{MX}_n, \text{s}) &= \Delta_a H^\circ(\text{M, s}) + n\Delta_a H^\circ(\text{X, g}) + \Sigma IE(\text{M, g}) + n\Delta_{EA} H^\circ(\text{X, g}) \\ &\quad + \Delta_{lattice} H^\circ(\text{MX}_n, \text{s}) \end{aligned}$$

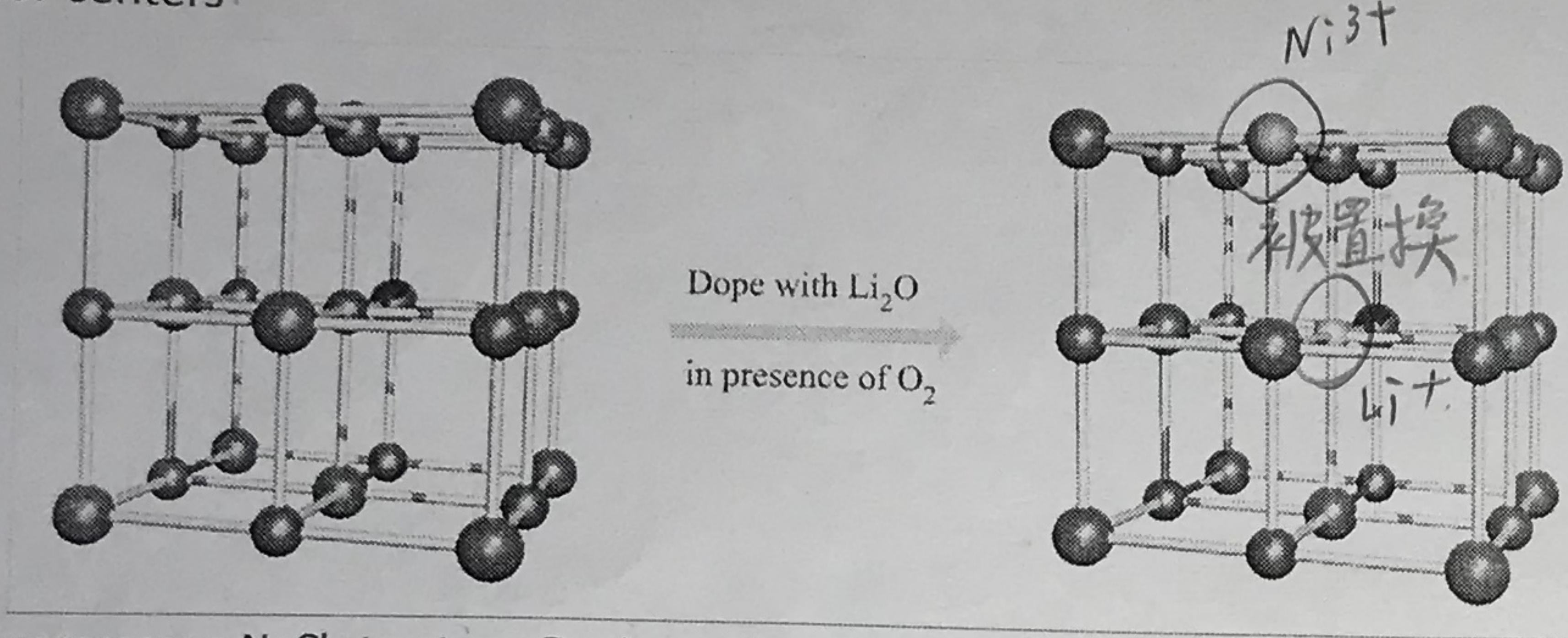
Frankel defect



Silver bromide adopts a NaCl structure. (a) An ideal lattice can be described in terms of Ag^+ ions occupying octahedral holes in a cubic close-packed array of bromide ions. (b) A Frenkel defect in AgBr involves the migration of Ag^+ ions into tetrahedral holes; in the diagram, one Ag^+ ion occupies a tetrahedral hole which was originally vacant in (a), leaving the central octahedral hole empty. Colour code: Ag, pale grey; Br, gold.

Non-stoichiometric compounds 組成中各類原子的相對數目不能用小的整數比表示
Many defects result in a compound being non-stoichiometric. Metal oxides and sulfides are particularly prone to non-stoichiometric defects. For example, Fe_{1-x}O ($0.04 < x < 0.11$). Some $\text{Fe}^{(III)}$ ions are present to counter what would otherwise be a charge imbalance caused by $\text{Fe}^{(II)}$ vacancies. Fe_{1-x}O . ($0.04 < x < 0.11$)

Color centers.



NiO possesses a NaCl structure. Doping with Li_2O in the presence of air/ O_2 results in the replacement of a Ni^{2+} centre (blue) with a Li^+ ion (yellow), and the oxidation of one Ni^{2+} to a Ni^{3+} centre (green). Oxide ions are shown in red. Excitation and subsequent relaxation of the trapped electron results in the emission of radiation in the visible region. The electron center is known as an F-center.

可在小範圍內運動
而保持基本結構不變
但會造成物理性質改變。
(ex:導電性).

hexagonal close-packed (hcp) lattice.

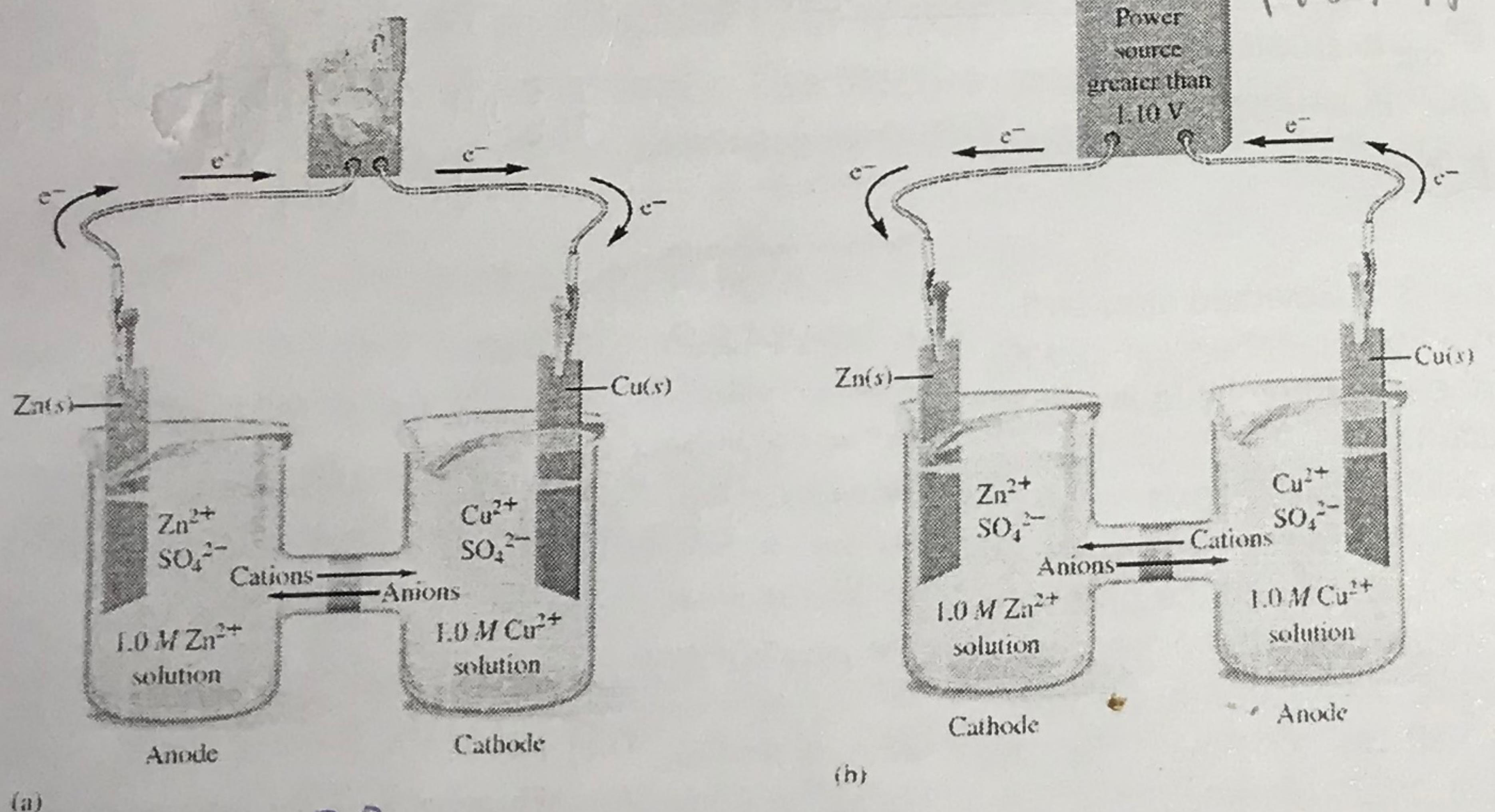
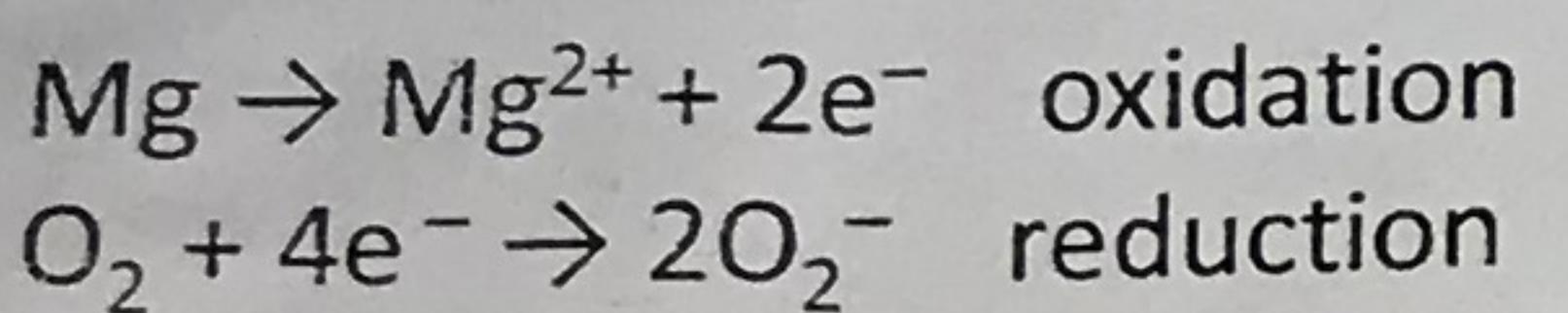
Figure 6.5 Two layers of close-packed atoms shown (a) with the spheres touching, and (b) with the sizes of the spheres reduced so that connectivity lines are visible. In (b), the tetrahedral and octahedral holes are indicated.

Chapter 8 Reduction and Oxidation

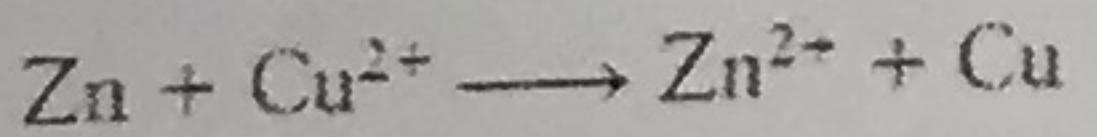
正價還原
An oxidation-reduction (redox) reaction involves a transfer of electrons from the reducing agent to the oxidizing agent and that oxidation involves a loss of electrons (an increase in oxidation number) and reduction involves a gain of electrons (a decrease in oxidation number).

Oxidation refers to gaining oxygen, losing hydrogen or losing one or more electrons. Reduction refers to losing oxygen, gaining hydrogen or gaining one or more electrons.

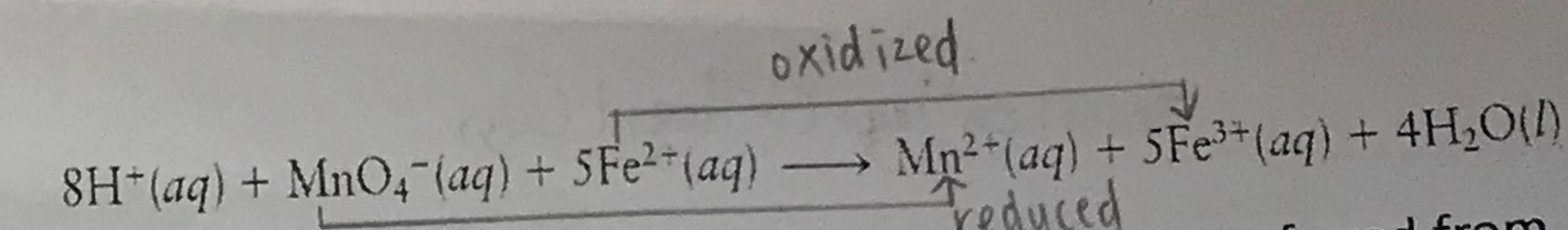
$2\text{Mg} + \text{O}_2 \rightarrow 2\text{MgO}$ Here magnesium is oxidized, while oxygen is reduced. Magnesium acts as the reducing agent or reductant, while O_2 acts as the oxidizing agent or oxidant.



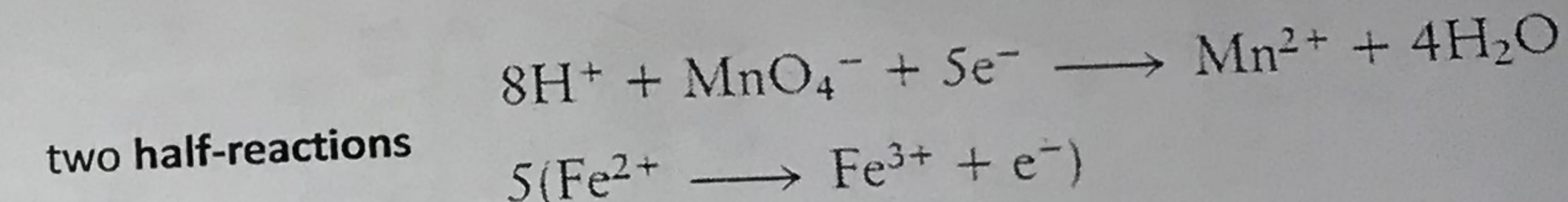
(a) A standard galvanic cell based on the spontaneous reaction.



(b) A standard electrolytic cell. A power source forces the opposite reaction.



Fe²⁺ is oxidized and MnO₄⁻ is reduced; electrons are transferred from Fe²⁺ (the reducing agent) to MnO₄⁻ (the oxidizing agent).



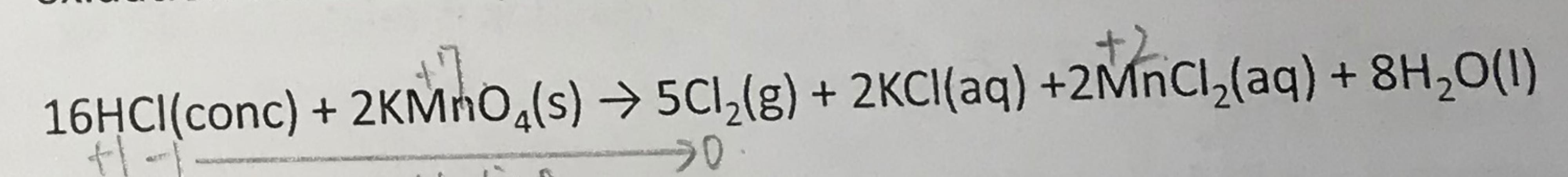
(伏打电池)
In a galvanic cell, a spontaneous redox reaction occurs and generates an electrical current. 氧化还原反应 → 電子流

(雷电池)
In an electrolytic cell, the passage of an electrical current through an electrolyte causes a chemical reaction to occur.

電解質 → 電子流 → 化学反应

氧化
Oxidation states can be assigned to each atom of an element in a compound. The oxidation state of an element is taken to be zero, irrespective of whether the element exists as atoms (e.g. Ne), molecules (e.g. O₂, P₄) or an infinite lattice (e.g. Si). In H₂O₂, the oxidation state of each O atom is -1.

An oxidation process is accompanied by an increase in the oxidation state of the element involved; conversely, a decrease in the oxidation state corresponds to a reduction step.



+1 -1 → 0 oxidation

Here the oxidation state of Cl in HCl is -1, and in Cl₂ is 0; the change indicates an oxidation step. In KMnO₄, the oxidation state of Mn is +7, while in MnCl₂ it is +2, i.e. [MnO₄]⁻ is reduced to Mn²⁺.

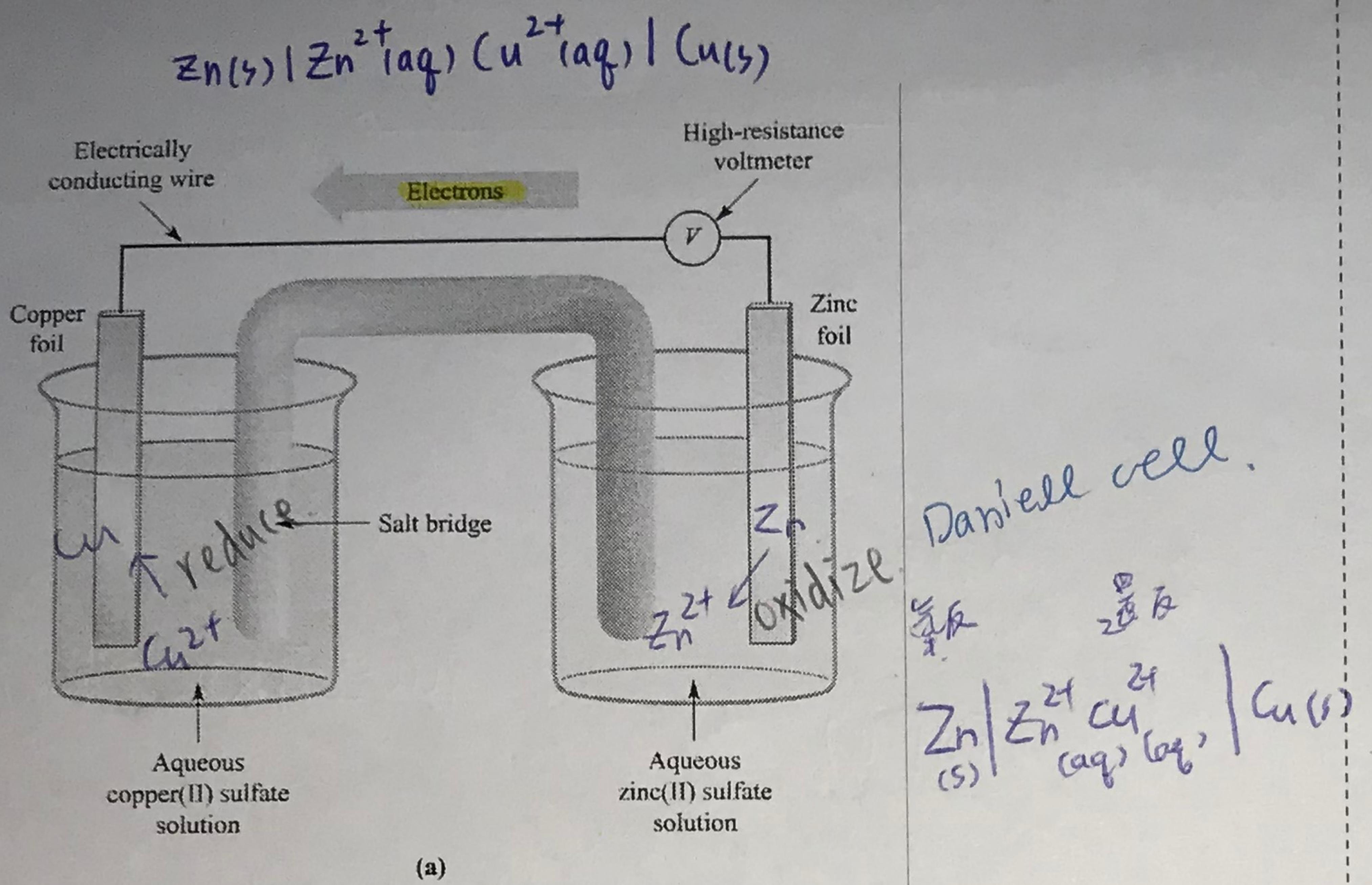


Figure 8.1 (a) A representation of the **Daniell cell**. In the left-hand cell, Cu^{2+} ions are reduced to copper metal, and in the right-hand cell, zinc metal is oxidized to Zn^{2+} ions. The cell diagram is written as: $Zn(s) | Zn^{2+}(aq) | Cu^{2+}(aq) | Cu(s)$.

Standard conditions for an electrochemical cell are defined as follows: **標準狀態下的條件**:

- unit activity for each component in the cell (for dilute solutions, activity is approximated to concentration);
- the pressure of any gaseous component is **1 bar**;
- a solid component is in its standard state;
- the temperature is **298 K**.

→ **K 和 ΔG° 的關係式**

The equilibrium constant, K , for the cell reaction is related to ΔG° by

$$\Delta G^\circ = -RT \ln K = -zFE$$

and $\ln K = zFE^\circ_{\text{cell}}/RT$

where $R = 8.314 \text{ J K}^{-1} \text{ mol}^{-1}$

$$\Delta G^\circ = -1 \times 96485 \times 0.6 \approx -60 \text{ kJ/mol}$$

For $z = 1$, a value of $E^\circ_{\text{cell}} = 0.6 \text{ V}$ corresponds to a value of $\Delta G^\circ \sim -60 \text{ kJ mol}^{-1}$ and $K \sim 10^{10}$ at 298 K, i.e. this indicates a thermodynamically favorable cell reaction, one that will tend towards completion.

$$57891 = RT \ln K \\ \ln K = 23,366 \\ K = e^{23,366} \sim 10^{10}$$

The Daniell cell is an example of a **galvanic cell**. In this type of electrochemical cell, electrical work is done **by the system**. The potential difference, E_{cell} , between the two half-cells can be measured (in volts, V) on a voltmeter in the circuit (Fig. 8.1a) and the value of E_{cell} is related to the change in Gibbs energy for the cell reaction.

Equation 8.9 gives this relationship under standard conditions, where E°_{cell} is the standard cell potential

$$\Delta G^\circ = -zFE^\circ_{\text{cell}} \quad (8.9)$$

where F = Faraday constant = 96485 C mol^{-1} ; z (or n) = number of moles of electrons transferred per mole of reaction; ΔG° is in J mol^{-1} ; E°_{cell} is in volts.

$$\text{庫侖 (C)} \times \text{電壓 (V)} = W (\text{J})$$

For a **thermodynamic favorable** cell reaction:

- E°_{cell} is positive;
- ΔG° is negative
- $K > 1$.

有含 OH^- 者則使用 $E^\circ_{[\text{OH}^-]=1}/V$ 的標準

Table 8.1 Selected standard reduction potentials (at 298 K); further data are listed in Appendix 11. The

concentration of each substance in aqueous solution is 1 mol dm^{-3} and the pressure of a gaseous component is 1 bar (10^5 Pa). Note that where the half-cell contains $[\text{OH}^-]$, the value of E° refers to $[\text{OH}^-] = 1 \text{ mol dm}^{-3}$, and the notation $E^\circ_{[\text{OH}^-]=1}$ should be used (see Box 8.1).

Reduction half-equation	E° or $E^\circ_{[\text{OH}^-]=1}/V$
$\text{Li}^+(aq) + e^- \rightleftharpoons \text{Li}(s)$	-3.04
$\text{K}^+(aq) + e^- \rightleftharpoons \text{K}(s)$	-2.93
$\text{Ca}^{2+}(aq) + 2e^- \rightleftharpoons \text{Ca}(s)$	-2.87
$\text{Na}^+(aq) + e^- \rightleftharpoons \text{Na}(s)$	-2.71
$\text{Mg}^{2+}(aq) + 2e^- \rightleftharpoons \text{Mg}(s)$	-2.37
$\text{Al}^{3+}(aq) + 3e^- \rightleftharpoons \text{Al}(s)$	-1.66
$\text{Mn}^{2+}(aq) + 2e^- \rightleftharpoons \text{Mn}(s)$	-1.19
$\text{Zn}^{2+}(aq) + 2e^- \rightleftharpoons \text{Zn}(s)$	-0.76
$\text{Fe}^{2+}(aq) + 2e^- \rightleftharpoons \text{Fe}(s)$	-0.44
$\text{Cr}^{3+}(aq) + e^- \rightleftharpoons \text{Cr}^{2+}(aq)$	-0.41
$\text{Fe}^{3+}(aq) + 3e^- \rightleftharpoons \text{Fe}(s)$	-0.04
$2\text{H}^+(aq, 1 \text{ mol dm}^{-3}) + 2e^- \rightleftharpoons \text{H}_2(g, 1 \text{ bar})$	0 → 0.
$\text{Cu}^{2+}(aq) + e^- \rightleftharpoons \text{Cu}^+(aq)$	+0.15
$\text{AgCl}(s) + e^- \rightleftharpoons \text{Ag}(s) + \text{Cl}^-(aq)$	+0.22

¹bpy = 2,2'-bipyridine; phen = 1,10-phenanthroline (see Table 7.7).

Reduction half-equation	E° or $E^\circ_{[\text{OH}^-]=1}/V$
$\text{Cu}^{2+}(\text{aq}) + 2\text{e}^- \rightarrow \text{Cu}(\text{s})$	+0.34
$[\text{Fe}(\text{CN})_6]^{4-}(\text{aq}) + \text{e}^- \rightarrow [\text{Fe}(\text{CN})_6]^{3-}(\text{aq})$	+0.36
$\text{O}_2(\text{g}) + 2\text{H}_2\text{O}(\text{l}) + 4\text{e}^- \rightarrow 4[\text{OH}]^-(\text{aq})$	+0.40
$\text{I}_2(\text{aq}) + 2\text{e}^- \rightarrow 2\text{I}^-(\text{aq})$	+0.54
$\text{Fe}^{3+}(\text{aq}) + \text{e}^- \rightarrow \text{Fe}^{2+}(\text{aq})$	+0.77
$\text{Ag}^+(\text{aq}) + \text{e}^- \rightarrow \text{Ag}(\text{s})$	+0.80
$[\text{Fe}(\text{bpy})_3]^{3+}(\text{aq}) + \text{e}^- \rightarrow [\text{Fe}(\text{bpy})_3]^{2+}(\text{aq})^\dagger$	+1.03
$\text{Br}_2(\text{aq}) + 2\text{e}^- \rightarrow 2\text{Br}^-(\text{aq})$	+1.09
$[\text{Fe}(\text{phen})_3]^{3+}(\text{aq}) + \text{e}^- \rightarrow [\text{Fe}(\text{phen})_3]^{2+}(\text{aq})^\dagger$	+1.12
$\text{O}_2(\text{g}) + 4\text{H}^+(\text{aq}) + 4\text{e}^- \rightarrow 2\text{H}_2\text{O}(\text{l})$	+1.23
$[\text{Cr}_2\text{O}_7]^{2-}(\text{aq}) + 14\text{H}^+(\text{aq}) + 6\text{e}^- \rightarrow 2\text{Cr}^{3+}(\text{aq}) + 7\text{H}_2\text{O}(\text{l})$	+1.33
$\text{Cl}_2(\text{aq}) + 2\text{e}^- \rightarrow 2\text{Cl}^-(\text{aq})$	+1.36
$[\text{MnO}_4]^{-}(\text{aq}) + 8\text{H}^+(\text{aq}) + 5\text{e}^- \rightarrow \text{Mn}^{2+}(\text{aq}) + 4\text{H}_2\text{O}(\text{l})$	+1.51
$\text{Co}^{3+}(\text{aq}) + \text{e}^- \rightarrow \text{Co}^{2+}(\text{aq})$	+1.92
$[\text{S}_2\text{O}_8]^{2-}(\text{aq}) + 2\text{e}^- \rightarrow 2[\text{SO}_4]^{2-}(\text{aq})$	+2.01
$\text{F}_2(\text{aq}) + 2\text{e}^- \rightarrow 2\text{F}^-(\text{aq})$	+2.87

[†]bipy = 2,2'-bipyridine; phen = 1,10-phenanthroline (see Table 7.7).

$$E = E^\circ - \frac{RT}{zF} \times \ln(Q)$$

Consider a Zn^{2+}/Zn half-cell (at 298 K) in which $[\text{Zn}^{2+}] = 0.10 \text{ mol dm}^{-3}$, i.e. non-standard conditions. The Nernst equation shows how the reduction potential varies with the concentrations of the species present.

$$E = E^\circ - (RT/zF) \times \{\ln ([\text{reduced form}]/[\text{oxidized form}])\}$$

where $R = \text{molar gas constant} = 8.314 \text{ J K}^{-1} \text{ mol}^{-1}$

$T = \text{temperature in K}$

$F = \text{Faraday constant} = 96\,485 \text{ C mol}^{-1}$

$z = \text{number of electrons transferred}$

$$E = E^\circ - \frac{0.0591}{n} \log(Q) \quad \text{at } 25^\circ\text{C}$$

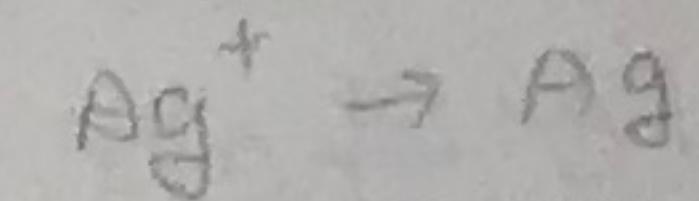
Application of the Nernst equation to the Zn^{2+}/Zn half-cell ($E^\circ = -0.76 \text{ V}$) gives $E = -0.79 \text{ V}$ for $[\text{Zn}^{2+}] = 0.10 \text{ mol dm}^{-3}$. The more negative value of E , corresponding to a more positive ΔG , signifies that it is more difficult to reduce Zn^{2+} at the lower concentration.

濃度愈小，愈難還原 Zn^{2+} ($-E \rightarrow +G$)

Solution pH also has a strong effect on E and ΔG , when H^+ or OH^- enters the equation under examination. See page 252.

Table 11.1 Standard Reduction Potentials at 25°C (298 K) for Many Common Half-reactions

Half-reaction	E° (V)	Half-reaction	E° (V)
$\text{F}_2 + 2\text{e}^- \rightarrow 2\text{F}^-$	2.87	$\text{O}_2 + 2\text{H}_2\text{O} + 4\text{e}^- \rightarrow 4\text{OH}^-$	0.40
$\text{Ag}^{2+} + \text{e}^- \rightarrow \text{Ag}^+$	1.99	$\text{Cu}^{2+} + 2\text{e}^- \rightarrow \text{Cu}$	0.34
$\text{Co}^{3+} + \text{e}^- \rightarrow \text{Co}^{2+}$	1.82	$\text{Hg}_2\text{Cl}_2 + 2\text{e}^- \rightarrow 2\text{Hg} + 2\text{Cl}^-$	0.27
$\text{H}_2\text{O}_2 + 2\text{H}^+ + 2\text{e}^- \rightarrow 2\text{H}_2\text{O}$	1.78	$\text{AgCl} + \text{e}^- \rightarrow \text{Ag} + \text{Cl}^-$	0.22
$\text{Ce}^{4+} + \text{e}^- \rightarrow \text{Ce}^{3+}$	1.70	$\text{SO}_4^{2-} + 4\text{H}^+ + 2\text{e}^- \rightarrow \text{H}_2\text{SO}_3 + \text{H}_2\text{O}$	0.20
$\text{PbO}_2 + 4\text{H}^+ + \text{SO}_4^{2-} + 2\text{e}^- \rightarrow \text{PbSO}_4 + 2\text{H}_2\text{O}$	1.69	$\text{Cu}^{2+} + \text{e}^- \rightarrow \text{Cu}^+$	0.16
$\text{MnO}_4^- + 4\text{H}^+ + 3\text{e}^- \rightarrow \text{MnO}_2 + 2\text{H}_2\text{O}$	1.68	$2\text{H}^+ + 2\text{e}^- \rightarrow \text{H}_2$	0.00
$\text{IO}_3^- + 2\text{H}^+ + 2\text{e}^- \rightarrow \text{IO}_3^- + \text{H}_2\text{O}$	1.60	$\text{Fe}^{3+} + 3\text{e}^- \rightarrow \text{Fe}$	-0.036
$\text{MnO}_4^- + 8\text{H}^+ + 5\text{e}^- \rightarrow \text{Mn}^{2+} + 4\text{H}_2\text{O}$	1.51	$\text{pb}^{2+} + 2\text{e}^- \rightarrow \text{pb}$	-0.13
$\text{Au}^{3+} + 3\text{e}^- \rightarrow \text{Au}$	1.50	$\text{Sn}^{2+} + 2\text{e}^- \rightarrow \text{Sn}$	-0.14
$\text{PbO}_2 + 4\text{H}^+ + 2\text{e}^- \rightarrow \text{Pb}^{2+} + 2\text{H}_2\text{O}$	1.46	$\text{Ni}^{2+} + 2\text{e}^- \rightarrow \text{Ni}$	-0.23
$\text{Cl}_2 + 2\text{e}^- \rightarrow 2\text{Cl}^-$	1.36	$\text{PbSO}_4 + 2\text{e}^- \rightarrow \text{Pb} + \text{SO}_4^{2-}$	-0.35
$\text{Cr}_2\text{O}_7^{2-} + 14\text{H}^+ + 6\text{e}^- \rightarrow 2\text{Cr}^{3+} + 7\text{H}_2\text{O}$	1.33	$\text{Cd}^{2+} + 2\text{e}^- \rightarrow \text{Cd}$	-0.40
$\text{O}_2 + 4\text{H}^+ + 4\text{e}^- \rightarrow 2\text{H}_2\text{O}$	1.23	$\text{Fe}^{2+} + 2\text{e}^- \rightarrow \text{Fe}$	-0.44
$\text{MnO}_2 + 4\text{H}^+ + 2\text{e}^- \rightarrow \text{Mn}^{2+} + 2\text{H}_2\text{O}$	1.21	$\text{Cr}^{3+} + \text{e}^- \rightarrow \text{Cr}^{2+}$	-0.50
$\text{IO}_3^- + 6\text{H}^+ + 5\text{e}^- \rightarrow \frac{1}{2}\text{I}_2 + 3\text{H}_2\text{O}$	1.20	$\text{Cr}^{3+} + 3\text{e}^- \rightarrow \text{Cr}$	-0.73
$\text{Br}_2 + 2\text{e}^- \rightarrow 2\text{Br}^-$	1.09	$\text{Zn}^{2+} + 2\text{e}^- \rightarrow \text{Zn}$	-0.76
$\text{VO}_2^+ + 2\text{H}^+ + \text{e}^- \rightarrow \text{VO}^{2+} + \text{H}_2\text{O}$	1.00	$2\text{H}_2\text{O} + 2\text{e}^- \rightarrow \text{H}_2 + 2\text{OH}^-$	-0.83
$\text{AuCl}_4^- + 3\text{e}^- \rightarrow \text{Au} + 4\text{Cl}^-$	0.99	$\text{Mn}^{2+} + 2\text{e}^- \rightarrow \text{Mn}$	-1.18
$\text{NO}_3^- + 4\text{H}^+ + 3\text{e}^- \rightarrow \text{NO} + 2\text{H}_2\text{O}$	0.96	$\text{Al}^{3+} + 3\text{e}^- \rightarrow \text{Al}$	-1.66
$\text{ClO}_2 + \text{e}^- \rightarrow \text{ClO}_2^-$	0.954	$\text{H}_2 + 2\text{e}^- \rightarrow 2\text{H}^-$	-2.23
$2\text{Hg}^{2+} + 2\text{e}^- \rightarrow \text{Hg}_2^{2+}$	0.91	$\text{Mg}^{2+} + 2\text{e}^- \rightarrow \text{Mg}$	-2.37
$\text{Ag}^+ + \text{e}^- \rightarrow \text{Ag}$	0.80	$\text{La}^{3+} + 3\text{e}^- \rightarrow \text{La}$	-2.71
$\text{Hg}_2^{2+} + 2\text{e}^- \rightarrow 2\text{Hg}$	0.80	$\text{Na}^+ + \text{e}^- \rightarrow \text{Na}$	-2.76
$\text{Fe}^{3+} + \text{e}^- \rightarrow \text{Fe}^{2+}$	0.77	$\text{Ca}^{2+} + 2\text{e}^- \rightarrow \text{Ca}$	-2.90
$\text{O}_2 + 2\text{H}^+ + 2\text{e}^- \rightarrow \text{H}_2\text{O}_2$	0.68	$\text{Ba}^{2+} + 2\text{e}^- \rightarrow \text{Ba}$	-2.92
$\text{MnO}_4^- + \text{e}^- \rightarrow \text{MnO}_4^{2-}$	0.56	$\text{K}^+ + \text{e}^- \rightarrow \text{K}$	-3.05
$\text{I}_2 + 2\text{e}^- \rightarrow 2\text{I}^-$	0.54	$\text{Li}^+ + \text{e}^- \rightarrow \text{Li}$	
$\text{Cu}^+ + \text{e}^- \rightarrow \text{Cu}$	0.52		

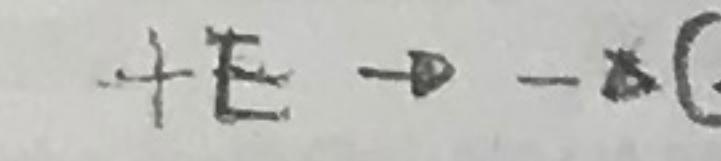


The effect of complex formation or precipitation on M^{2+}/M reduction potential

$$E = E^\circ - \frac{RT}{zF} \times \ln \left(\frac{P_{\text{gas}}}{P_{\text{std}}} \right)$$

Half-cells involving silver halides

Under standard conditions, Ag^+ ions are reduced to Ag , but if the concentration of Ag^+ is lowered, application of the Nernst equation shows that the reduction potential becomes less positive (i.e. ΔG is less negative). Consequently, reduction of Ag^+ to Ag becomes less easy.



$$\text{Ag}^+(\text{aq}) + \text{e}^- \rightarrow \text{Ag}(\text{s}) \quad E^\circ = +0.80 \text{ V} \quad \Delta G^\circ = -77.2 \text{ kJ per mole of Ag} \quad (8.29)$$

A lower concentration of Ag^+ ions can be achieved by dilution of the aqueous solution, but it can also be brought about by removal of Ag^+ ions from solution by the formation of a stable complex or by precipitation of a sparingly soluble salt.

Consider the formation of AgCl for which $K_{\text{sp}} = 1.77 \times 10^{-10}$.

$$\text{AgCl}(\text{s}) \rightleftharpoons \text{Ag}^+(\text{aq}) + \text{Cl}^-(\text{aq}) \quad \Delta G^\circ = +55.6 \text{ kJ per mole of AgCl} \quad \Delta G^\circ = -RT \ln K$$

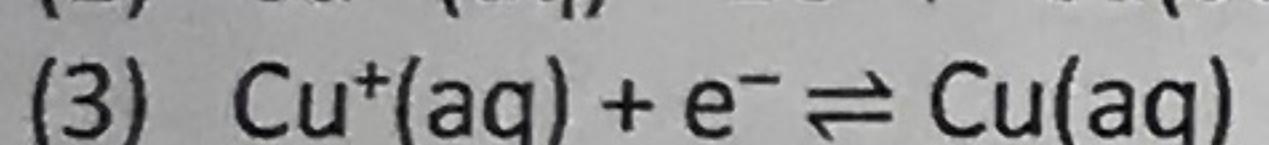
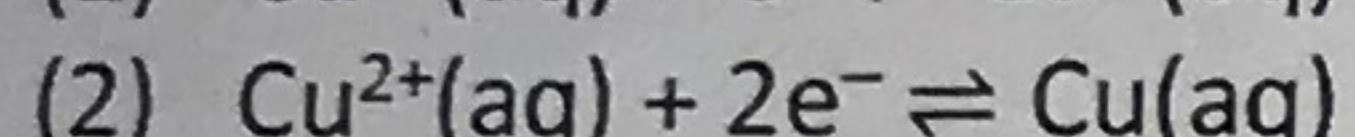
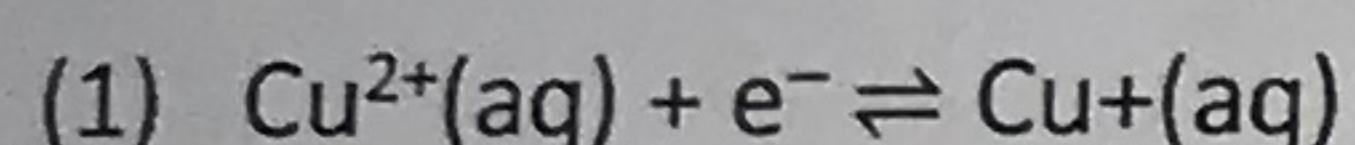
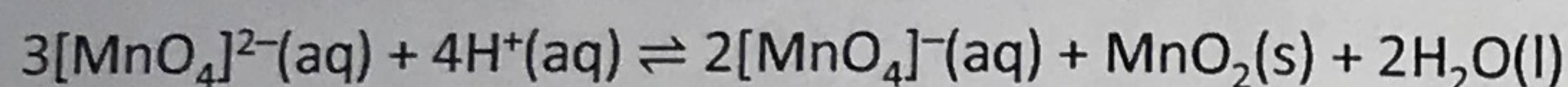
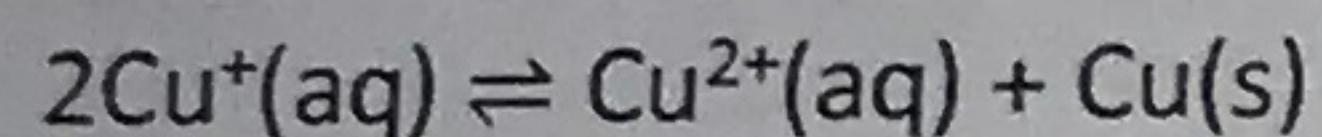
$$\text{AgCl}(\text{s}) + \text{e}^- \rightarrow \text{Ag}(\text{aq}) + \text{Cl}^-(\text{aq}) \quad E^\circ = +0.22 \text{ V} \quad \Delta G^\circ = -21.6 \text{ kJ per mole of AgCl} \quad (8.31)$$

The difference in the value of E° for half-reactions 8.29 and 8.31 indicates that it is less easy to reduce $\text{Ag}(\text{l})$ in the form of solid AgCl than as hydrated Ag^+ .

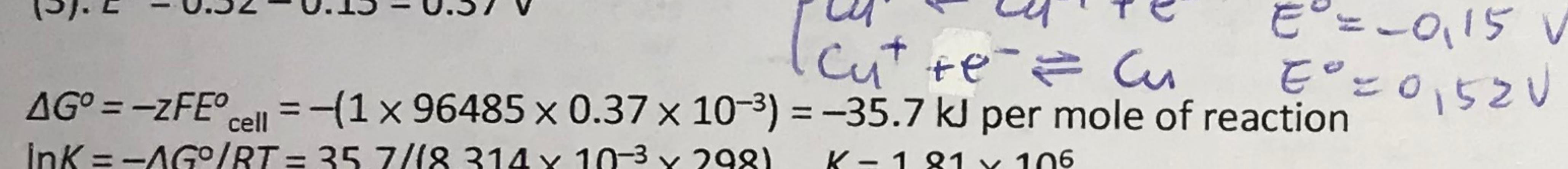
By precipitation $\Rightarrow \Delta G$ less negative \Rightarrow less easy to reduce $\text{Ag}(\text{l})$

Disproportionation 不均化反應 自身氧化還原

Some redox reactions involve disproportionation.



The disproportionation of Cu(I) is the result of combining half-reactions (1) and (3). $E^\circ = 0.52 - 0.15 = 0.37 \text{ V}$



$$\Delta G^\circ = -zFE^\circ_{\text{cell}} = -(1 \times 96485 \times 0.37 \times 10^{-3}) = -35.7 \text{ kJ per mole of reaction}$$

$$\ln K = -\Delta G^\circ/RT = 35.7/(8.314 \times 10^{-3} \times 298) \quad K = 1.81 \times 10^6$$

The value indicates that disproportionation is thermodynamically favorable.

Cu⁺ can be stabilized by forming CuCl or [Cu(CN)₄]³⁻.

E°_{cell} is positive
 ΔG° is negative
 $K > 1$

產生 diff particle shape:

反應環境相同之下：前體物

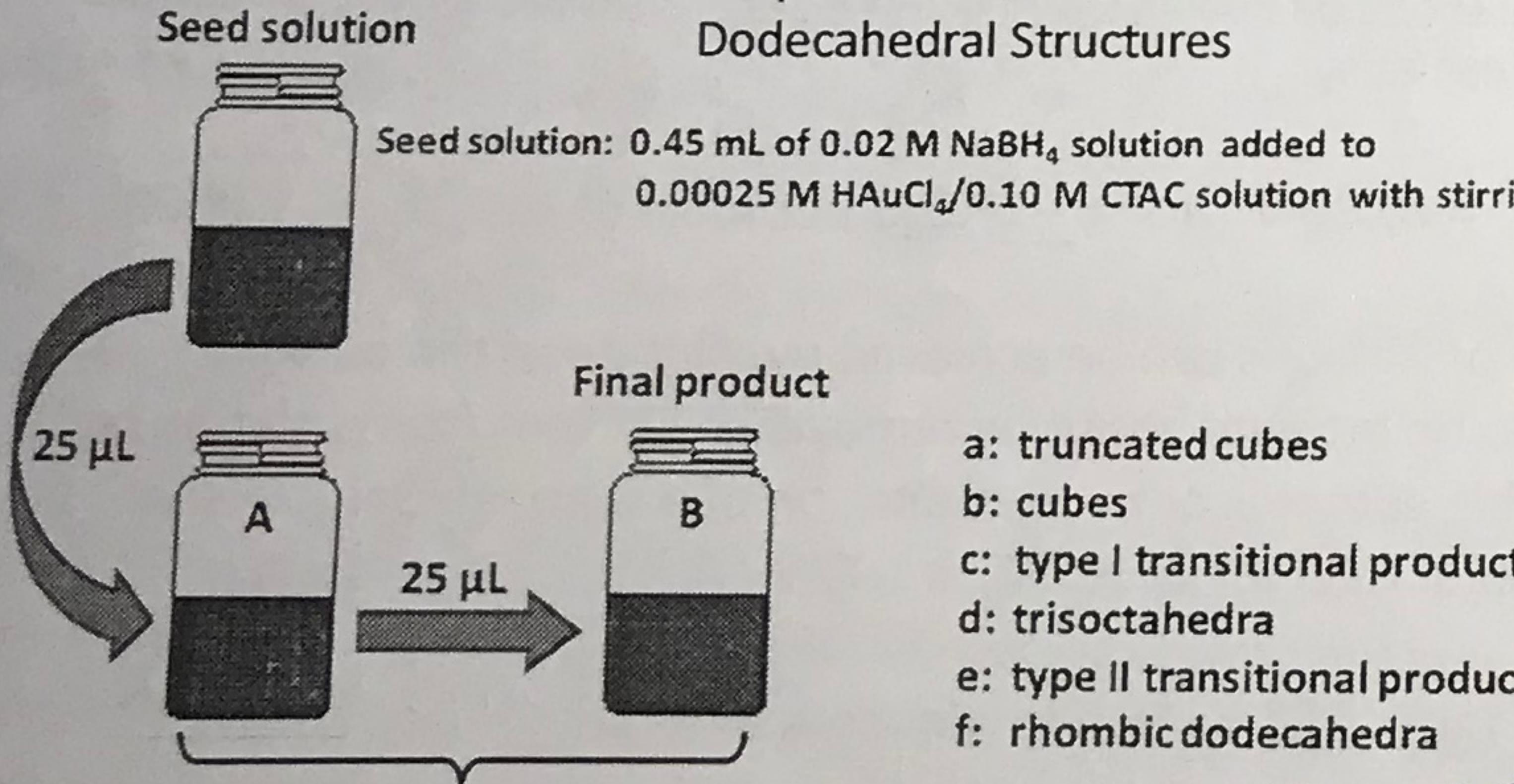
① 調整還原劑的量

Reaction conditions can be same, but adjusting the amount of reducing agent, or tuning the metal precursor through halide ligand exchange, tunes the reduction potential of the precursor. This leads to different particle shapes.

metal precursor through halide ligand exchange 改變 precursor 的還原電位

Seed-Mediated Synthesis of Au Nanocrystals with Systematic Shape Evolution from Cubic to Trisoctahedral and Rhombic Dodecahedral Structures

(用 iodine ligand 取代 some chloride ligands)



	(0.01 M)	(0.01 M)	10 mL total volume
a	0.32 g CTAC + 9640 μL H ₂ O + 250 μL HAuCl ₄ + 10 μL NaBr	75 μL AA	Scale bar: 50 nm
b	0.32 g CTAC + 9625 μL H ₂ O + 250 μL HAuCl ₄ + 10 μL NaBr	90 μL AA	
c	0.32 g CTAC + 9615 μL H ₂ O + 250 μL HAuCl ₄ + 10 μL NaBr	100 μL AA	
d	0.32 g CTAC + 9605 μL H ₂ O + 250 μL HAuCl ₄ + 10 μL NaBr	110 μL AA	
e	0.32 g CTAC + 9590 μL H ₂ O + 250 μL HAuCl ₄ + 10 μL NaBr	125 μL AA	
f	0.32 g CTAC + 9565 μL H ₂ O + 250 μL HAuCl ₄ + 10 μL NaBr	150 μL AA	

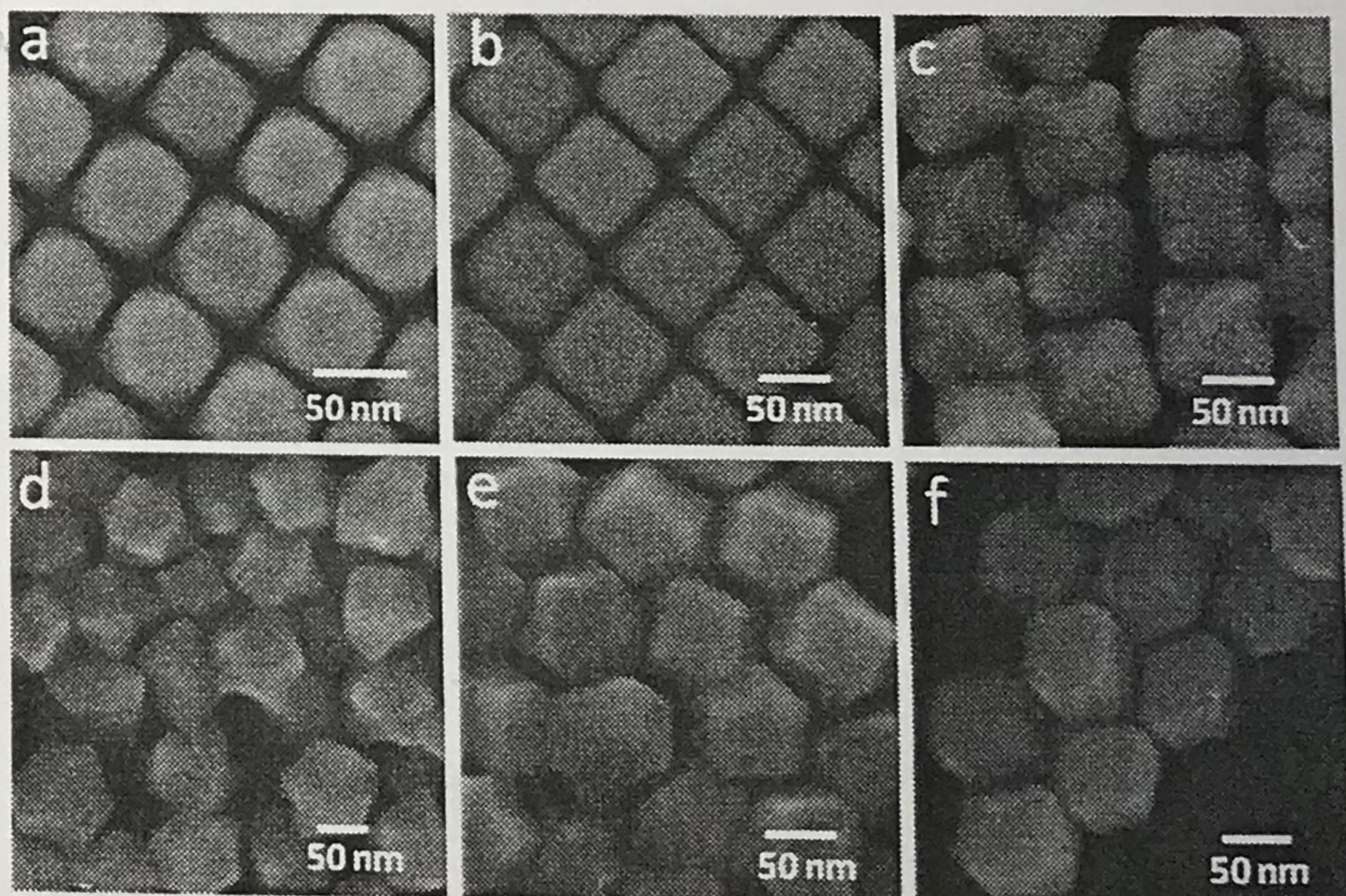
① 還原劑種類一樣，濃度不一樣

Knowing that reduction of Ag⁺ ions from, say AgNO₃, and AgCl are different in reduction potential, it does not help when it comes to synthesis of Ag particles with shape control. In fact, shape control is vital to metal and semiconductor nanocrystals/microcrystals, because the exposed surfaces have great influence on the properties of the materials such as their (catalytic, electrical, and optical properties). We should examine real problems to see the relevance of what we have learned in inorganic chemistry.

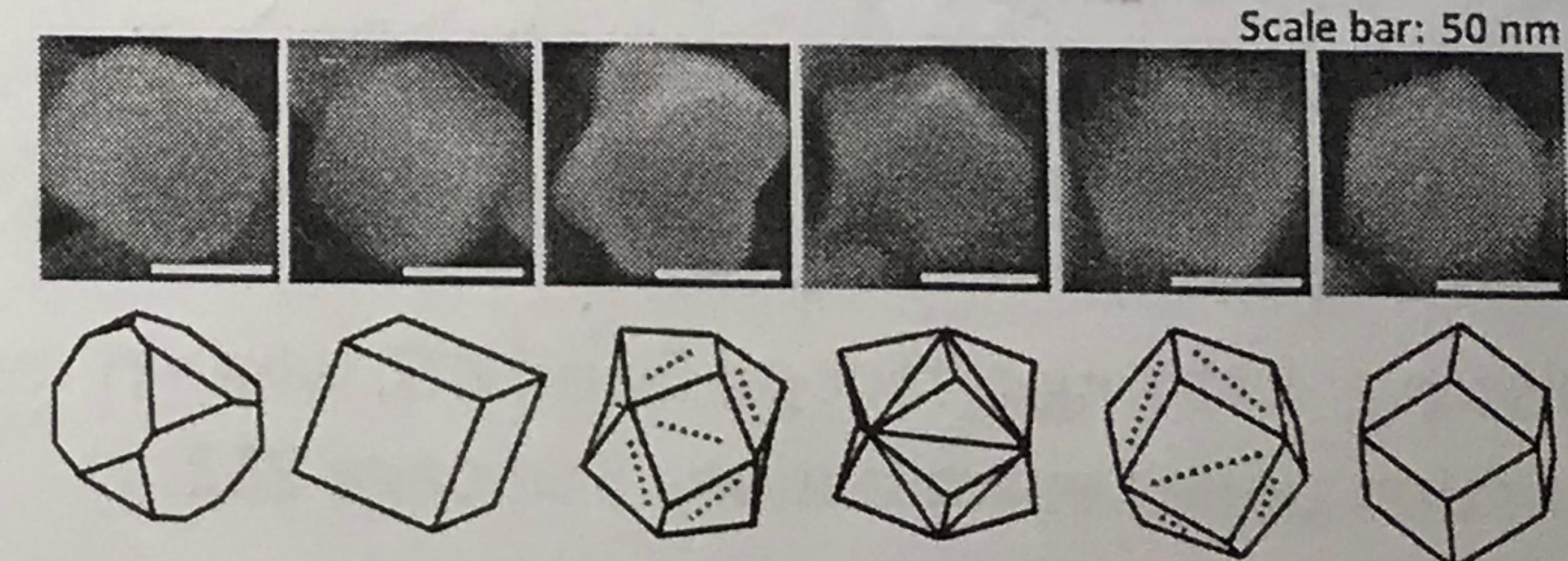
↓ 光學性質

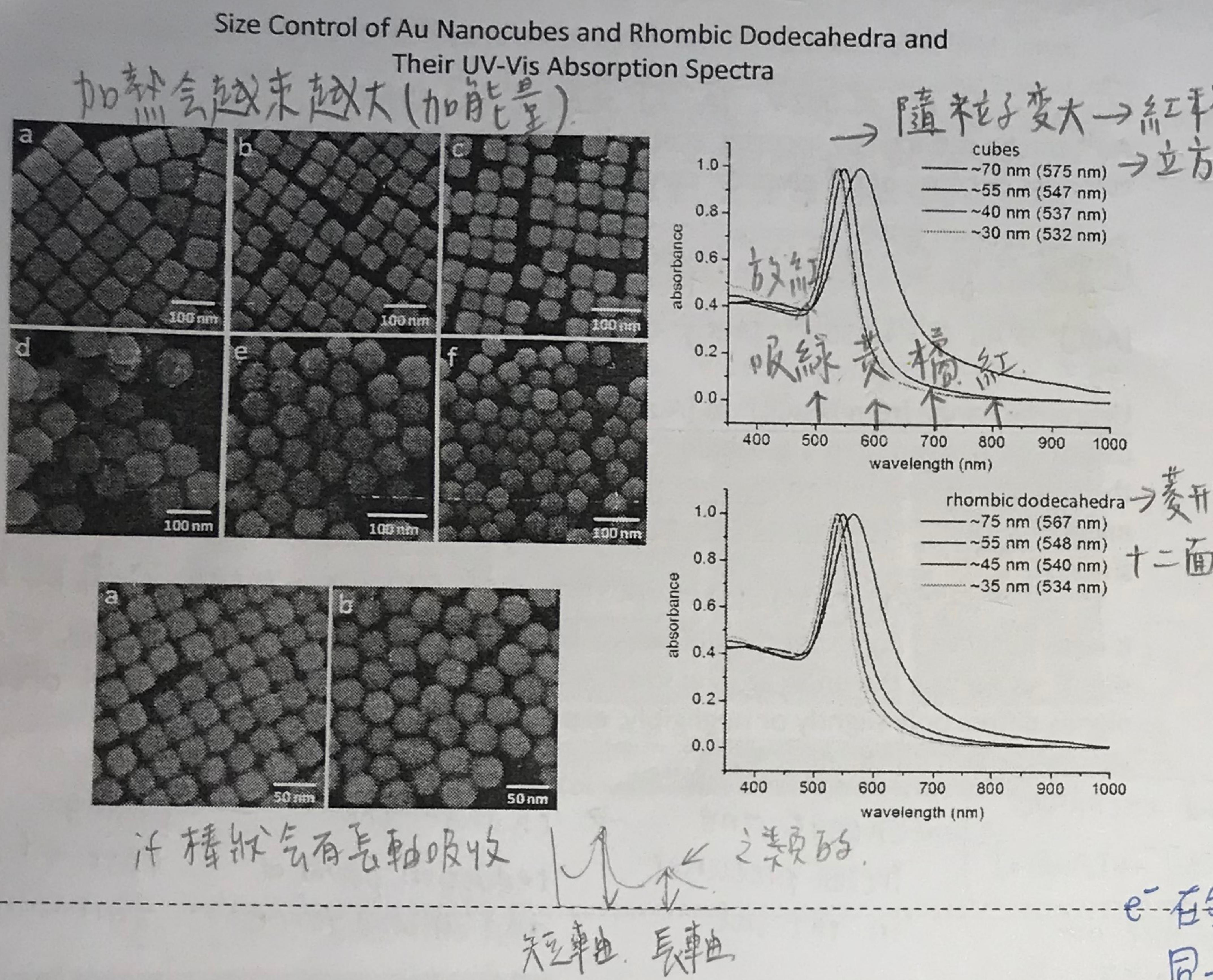
In the synthesis of noble metal (such as Au, Ag, and Pd) and Cu₂O nanoparticles with a series of shape evolution, we have found consistently that tuning the reaction rate (or reduction rate) enables the formation of different particle shapes.

- For noble metal (Au, Ag, Pd) and Cu₂O nanoparticles
 → 變 reaction rate (or reduction rate) → 半導體的 nanoparticle.
 可使成為不同形狀 ⇌ ligand exchange.

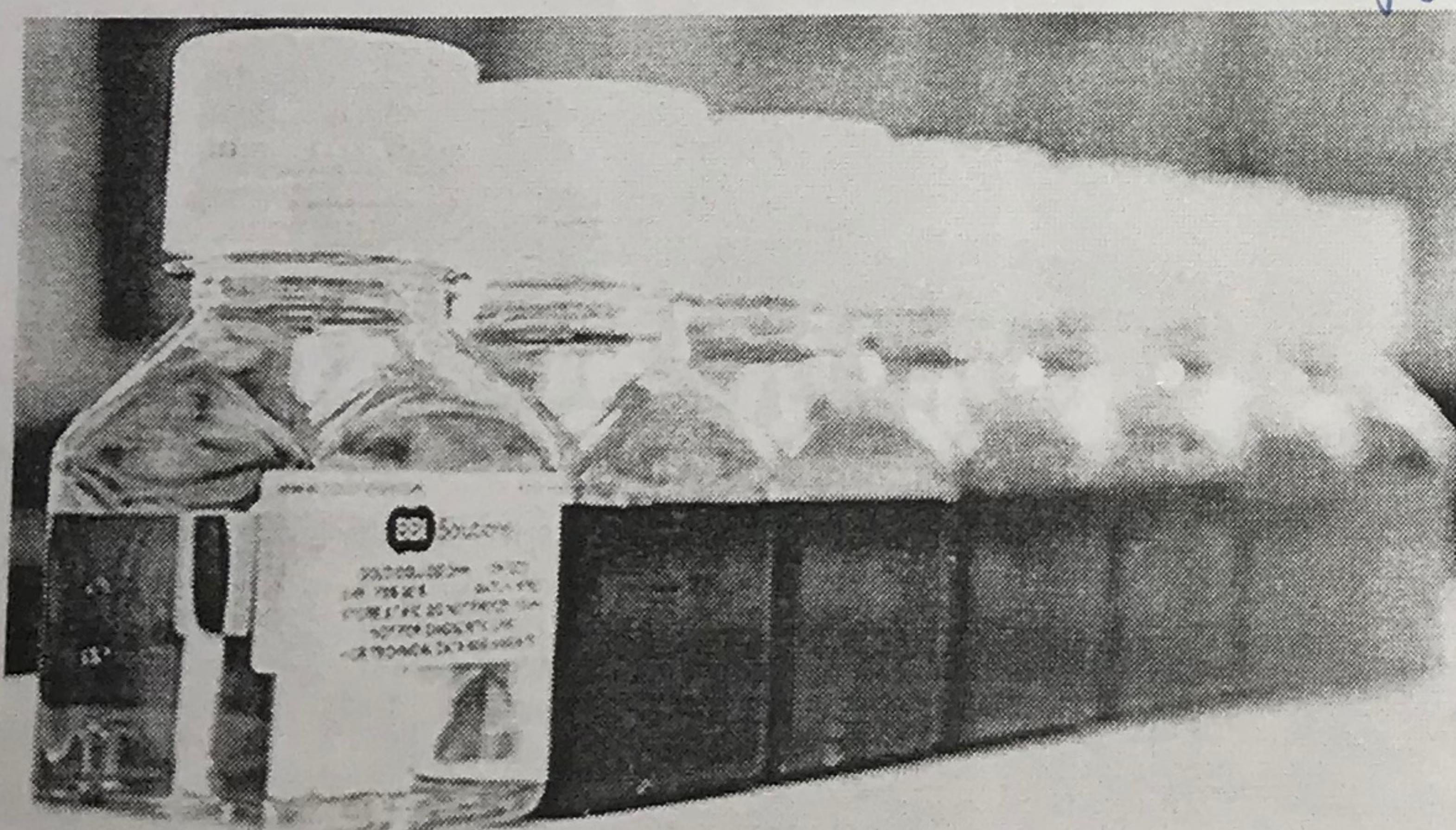


- a. Truncated cubes
- b. Cubes
- c. Type I transitional particles
- d. Trisoctahedra with {221} surfaces
- e. Type II transitional particles
- f. Rhombic dodecahedra



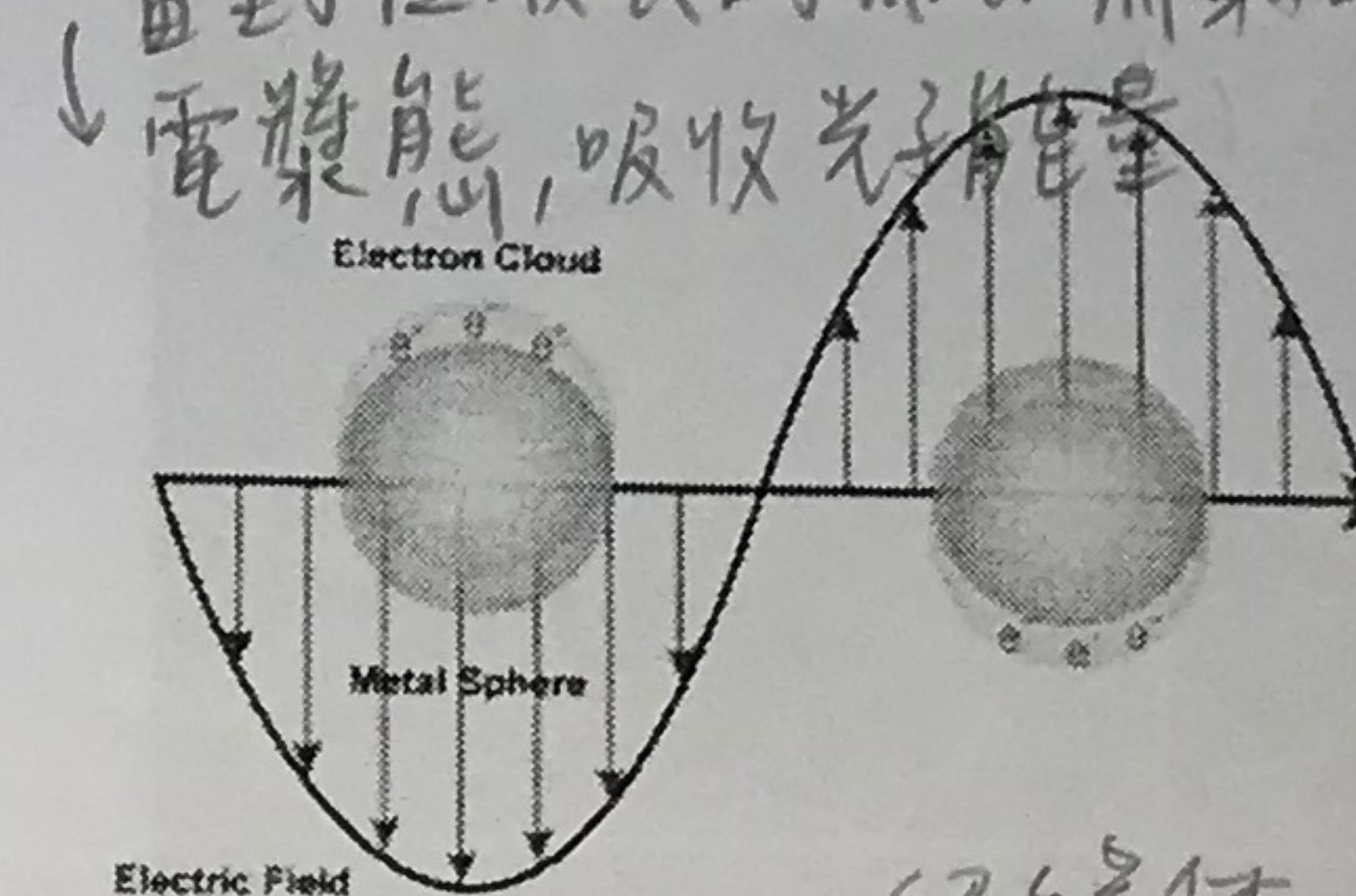


Gold Colloid 20nm / 40nm /
60nm / 80nm
• Type: Gold
Nanoparticles
• Applications: Lateral
Flow Life Science
Amount
20ml
Shipping
Ambient
£144.43



* 用 iodine ligand 取代
some chloride ligands
可改變 particle shape.
(保持 reducing agent
相同的量)

表面電漿共振 → 受到 size 和面影影響而看見不同吸收 red/blue shift
當對應波長的 laser 照射時，表面的 e- 會受電場振動影響，能量上升



SPR
The colors of metallic nanoparticles dispersed in a dielectric medium (low conductivity such as water) are dominated by localized surface plasmon resonance (表面電漿共振) absorption, the collective coherent oscillation of electrons at the metal-dielectric interface. Light impinging on metallic particles causes optical excitation of their electrons in the valence band.

光的激發

電場

電子雲

光子

吸收

散射

反射

透射

吸收

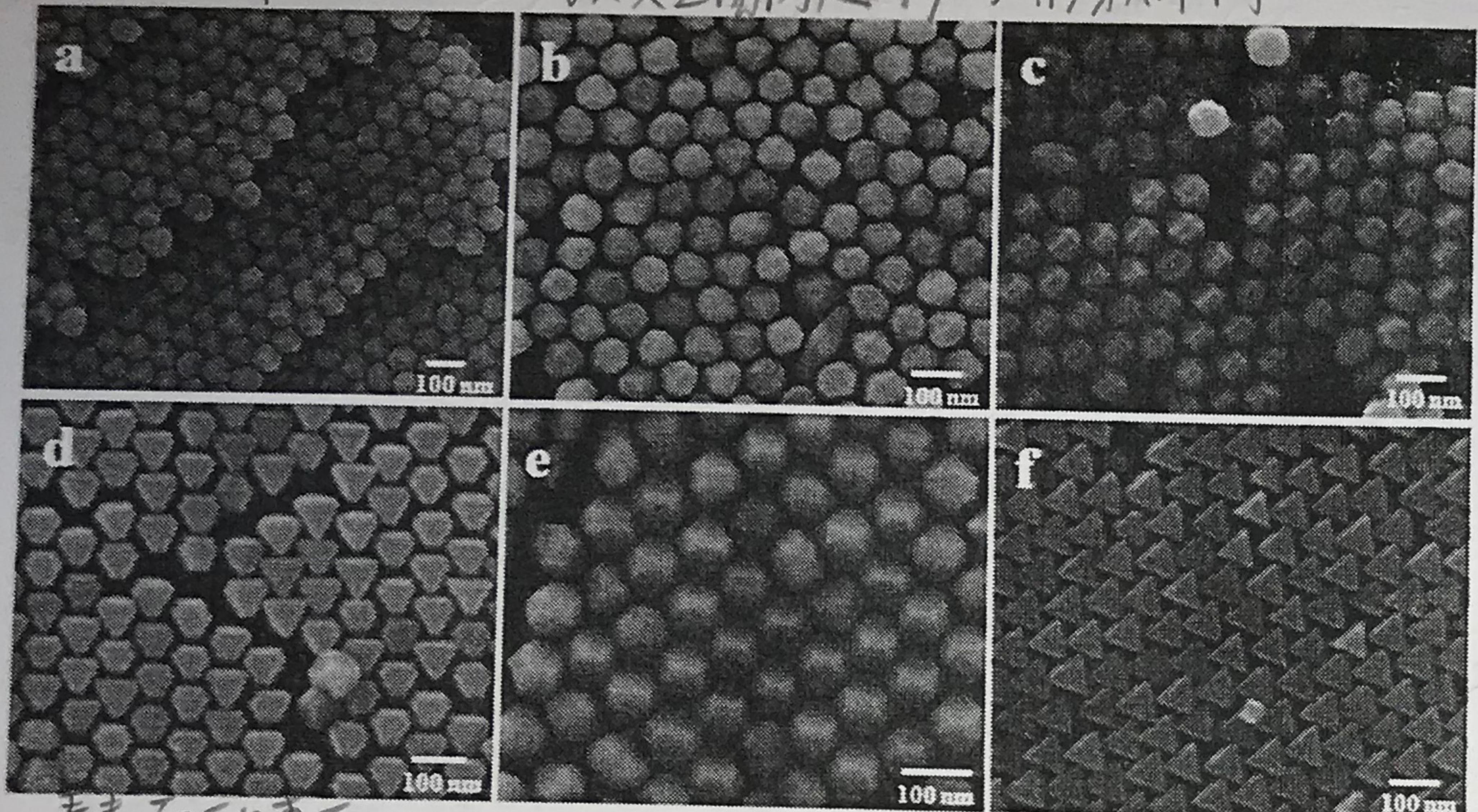
散射

反射

K1

RD.

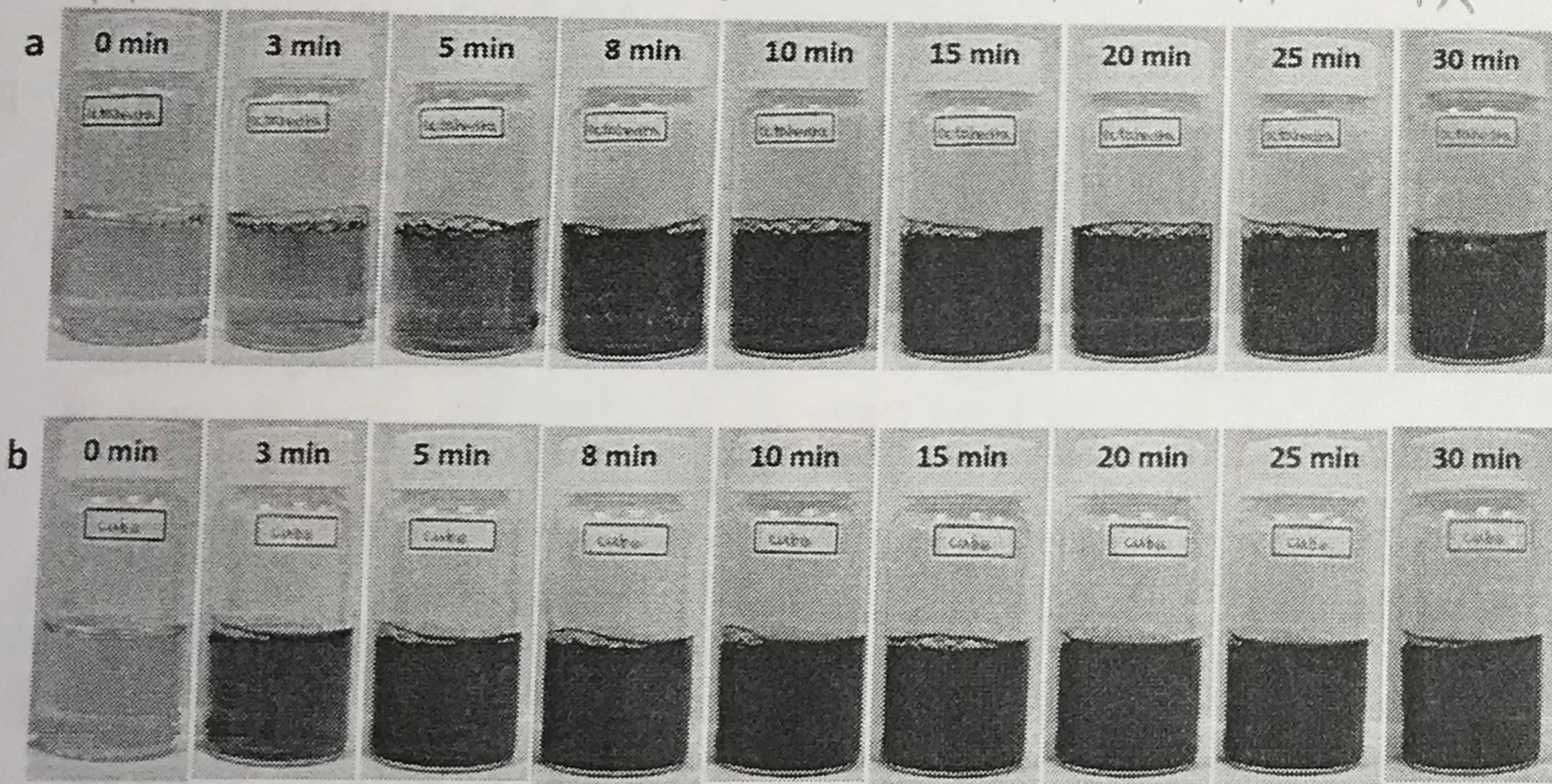
改變金屬前驅物→形狀不同



看表面的东西

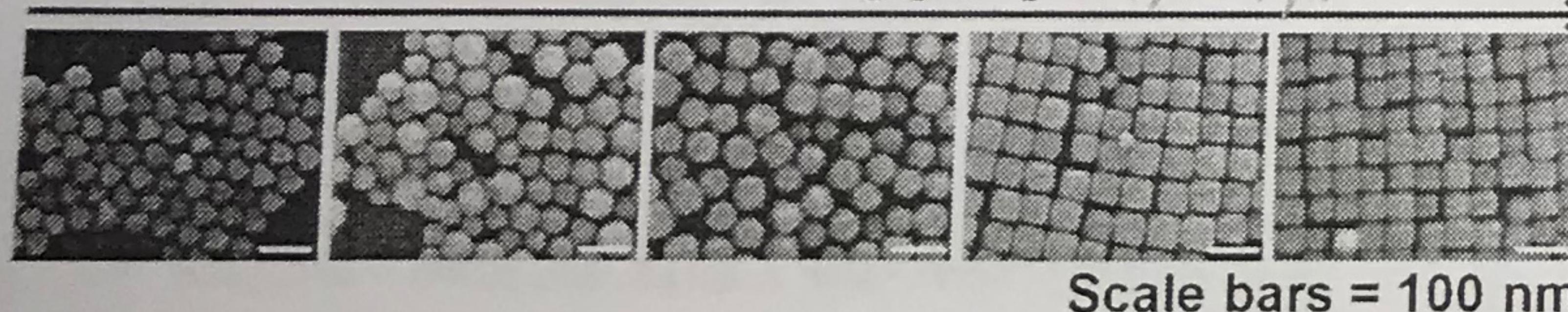
SEM images of the gold nanocrystals synthesized by progressively increasing the amount of KI added. (a) Rhombic dodecahedra. (b) Rhombicuboctahedra. (c) Edge- and corner-truncated octahedra. (d, e) Corner-truncated octahedra self-assembled into two different orientations. (f) Octahedra.

煮越久越来越大颗(但颜色不同),粒子越来越小颗



Photographs of the solutions taken during the synthesis of (a) Pd octahedra and (b) nanocubes.

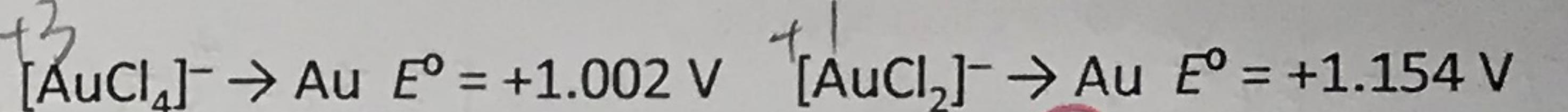
Increasing [KBr] 改變形狀



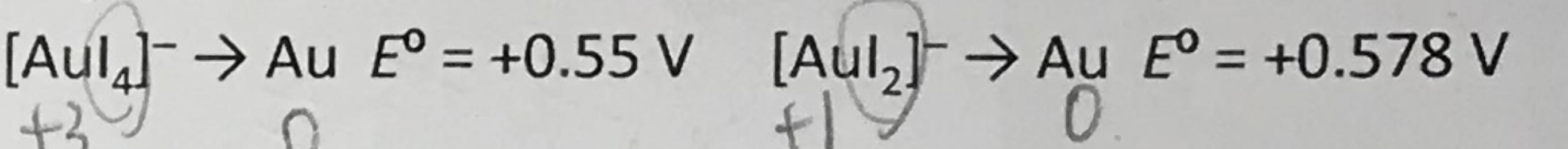
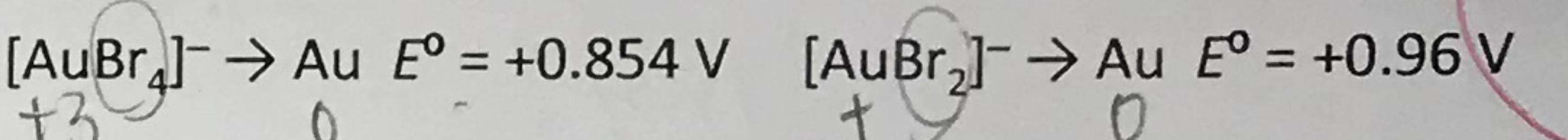
Langmuir 2015,
31, 6538

Scale bars = 100 nm

改變不同 ligand → 不同還原電位 → 不同形狀



Au^{3+} can be reduced by ascorbic acid to Au^+ , making the precursor solution colorless because of d^{10} electron configuration of gold.



單域全滿

colorless

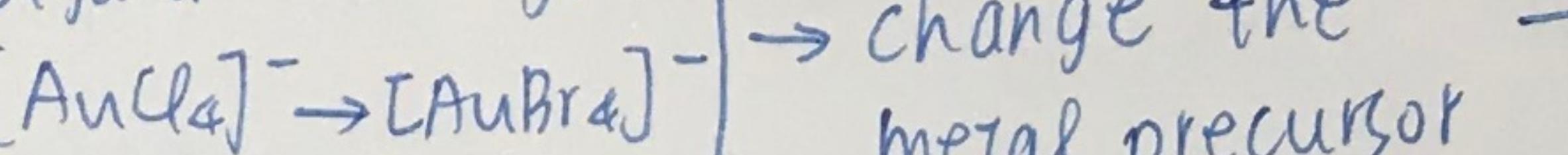
界面活性劑

Ligand exchange from $[\text{AuCl}_4]^-$ to $[\text{AuBr}_4]^-$ in the presence of surfactant cetyltrimethylammonium bromide (CTAB) or KI changes the metal precursors in the solution, which in turn changes the reduction potential and driving force and, consequently, rate of particle formation giving rise to different particle shapes.

* 形狀 particles exposing diff surface planes 需的能量

It is important to note that the difference in the reaction conditions can be very slight, suggesting the energetics in forming particles exposing different surface planes differs only slightly or negligibly, explaining why a mixture of particle shapes is often produced.

Ligand exchange.

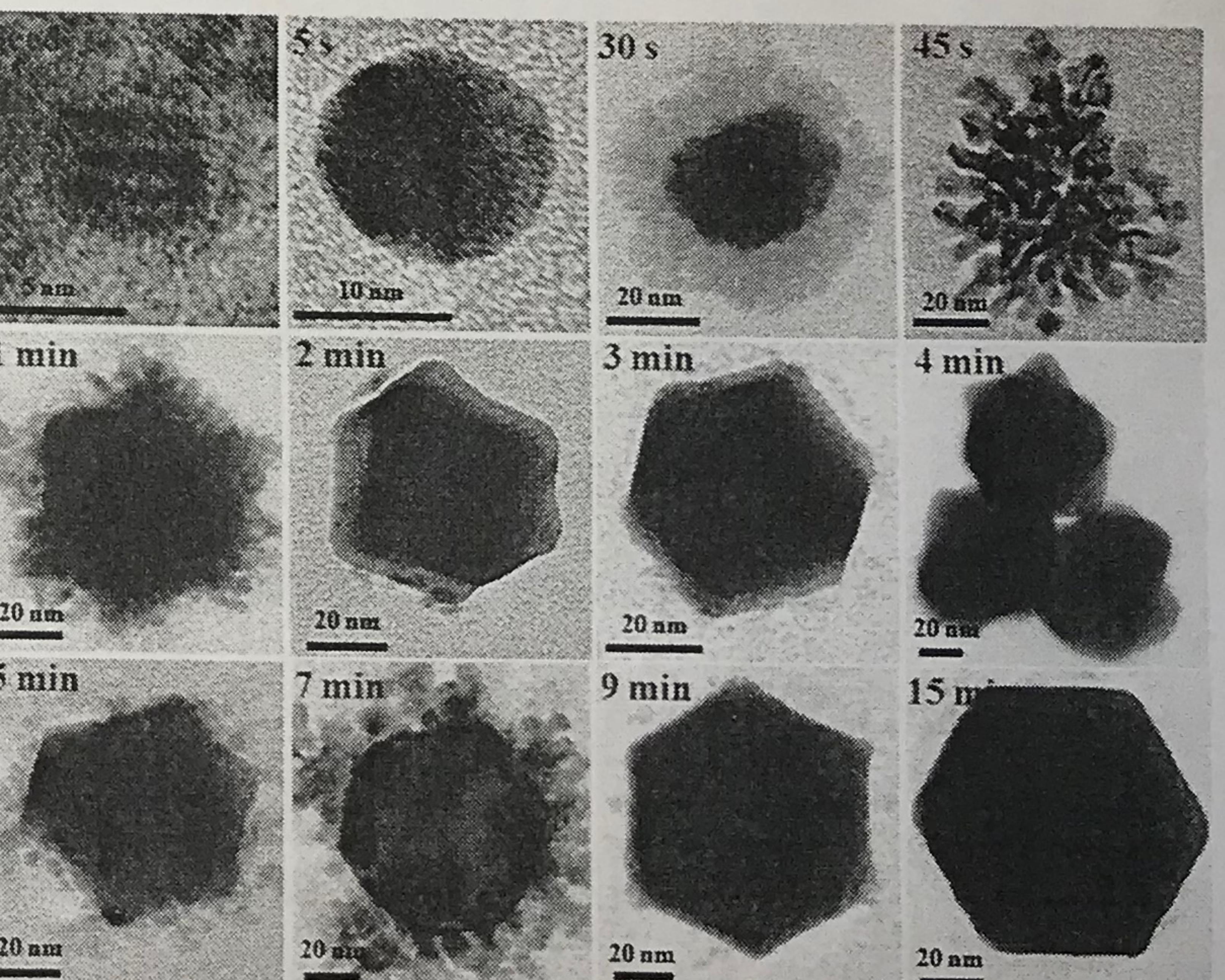


in presence of
CTAB or KI

→ change the metal precursor → change the reduction potential and driving force → change the rate of particle formation

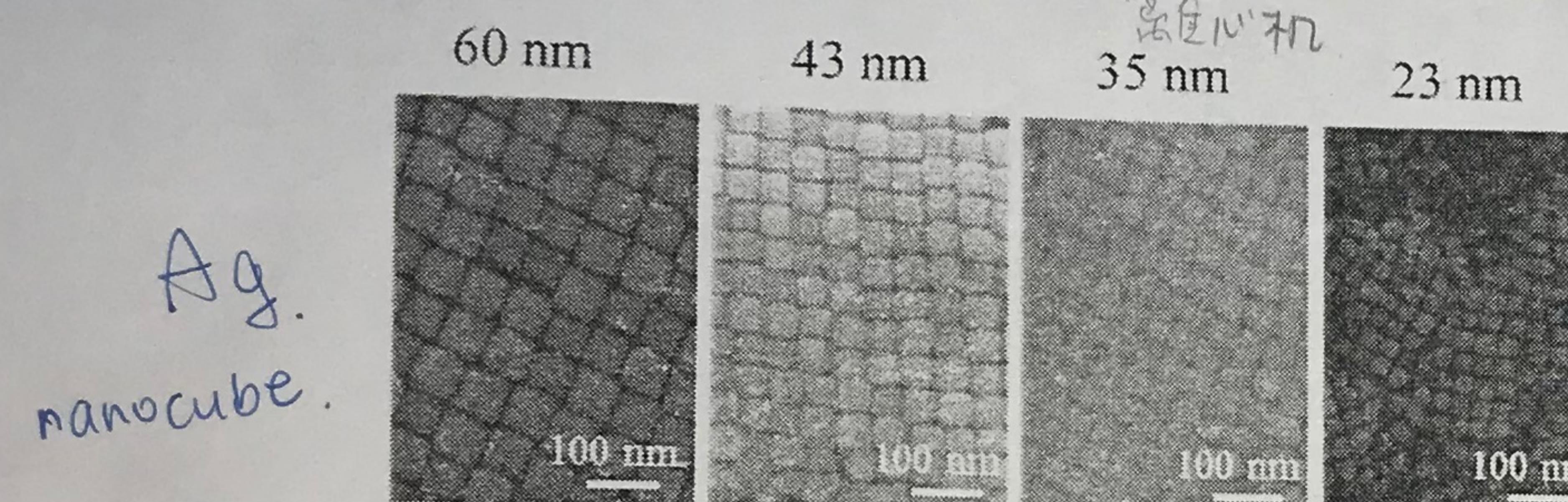
↓ give diff particle sh

Intermediate Structures Observed in the Growth of Octahedral Au Nanocrystals



Ag(nanocube)
to tune Ag(nanocube). Next,
add to vials. Next,
0.1 M CF_3COOAg sol
in a water bath at 60°C.
the solution was still

詞語 小瓶
在相同時間，不同濃度下粒子大小不同。
To tune Ag nanocube size, different volumes of deionized water and CTAC were added to vials. Next, 50, 100, 300, and 1000 μL of the seed solution and 100 μL of 0.1 M CF_3COOAg solution were introduced to each vial. The capped vial was kept in a water bath at 60 $^{\circ}\text{C}$ for 20 min. Then ascorbic acid solution was added and the solution was stirred in the capped vial for 1.5 h at 60 $^{\circ}\text{C}$. After the reaction was finished, the particles were collected by centrifugation at 9000 rpm for 10 min to obtain silver nanocubes. Please note that heating is necessary because AgCl is being reduced to Ag with a standard reduction potential of just 0.22 V instead of 0.80 V for Ag^+ to Ag.

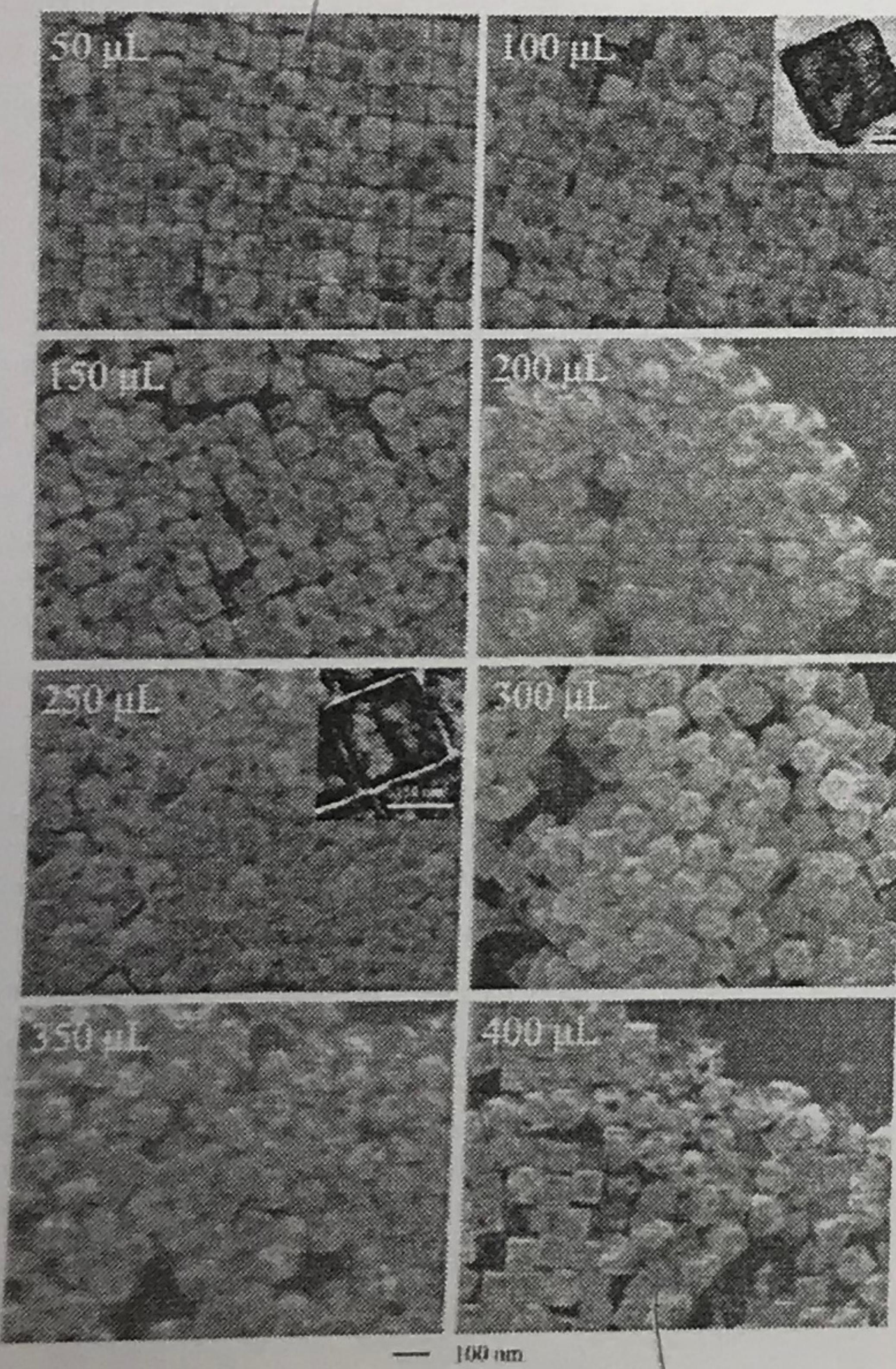


Chem.-Eur. J.
2016, 22, 2326

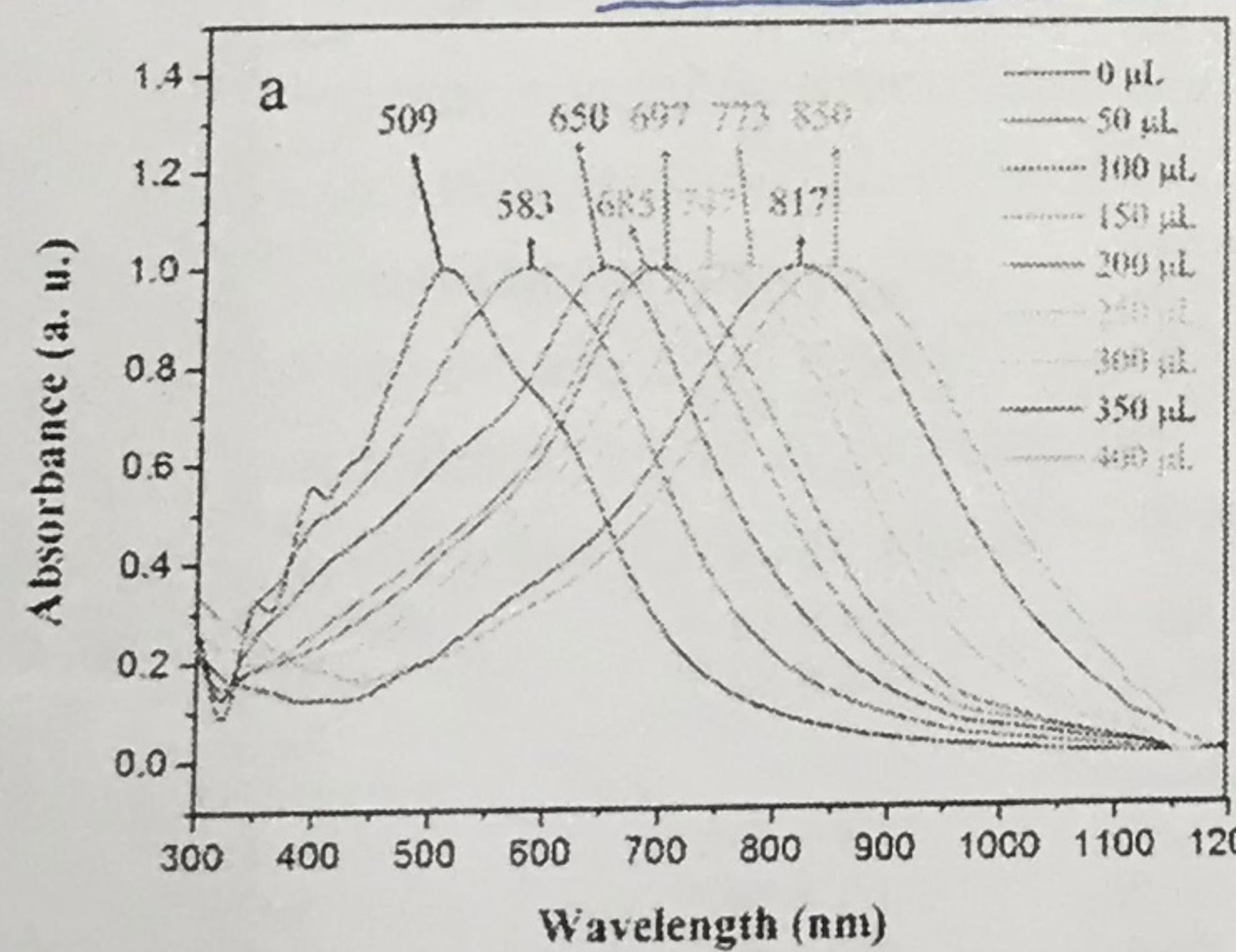
Increasing the volume of seed solution

size ↓

實心銀被金取代出來。

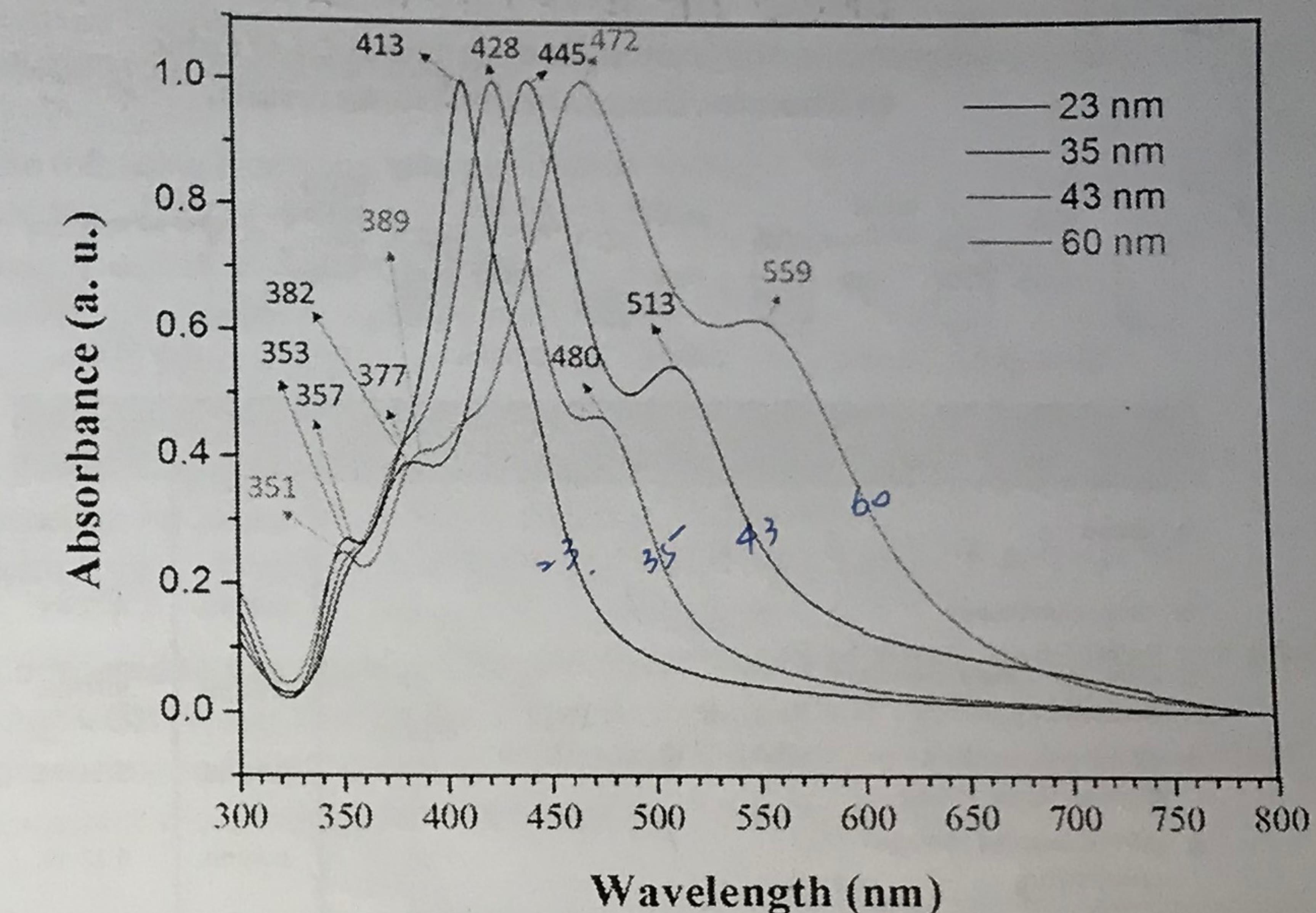


SEM images of Au nanocages obtained by adding 50–400 mL of 0.001 M HAuCl_4 solution to a solution containing 70 nm Ag nanocubes. The HAuCl_4 solution volumes added are labeled. Au replaces Ag because it has a higher standard reduction potential.



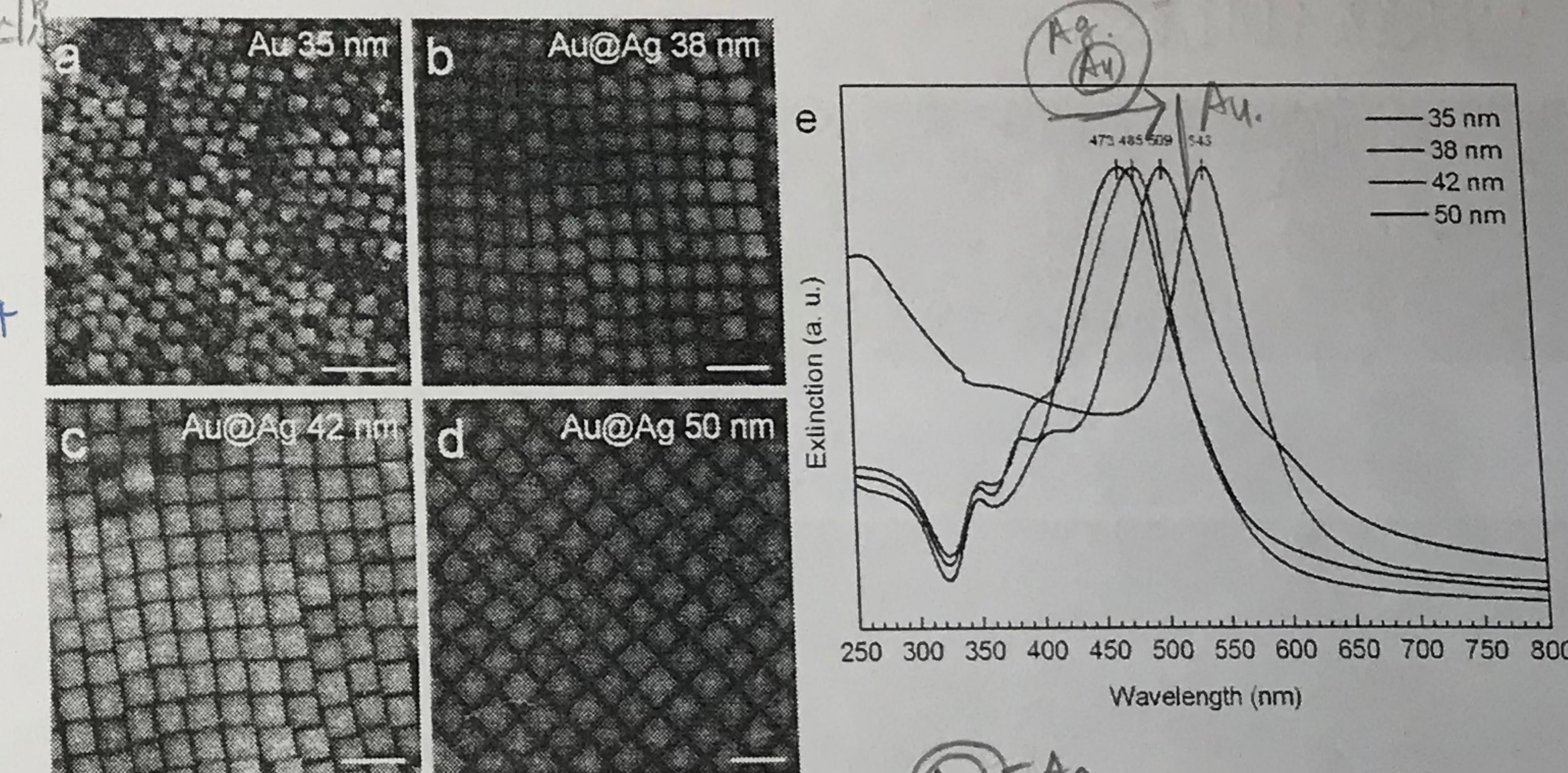
As the nanocages become thinner, their SPR absorption band red-shifts progressively.

金本身吸收金較銀紅移。



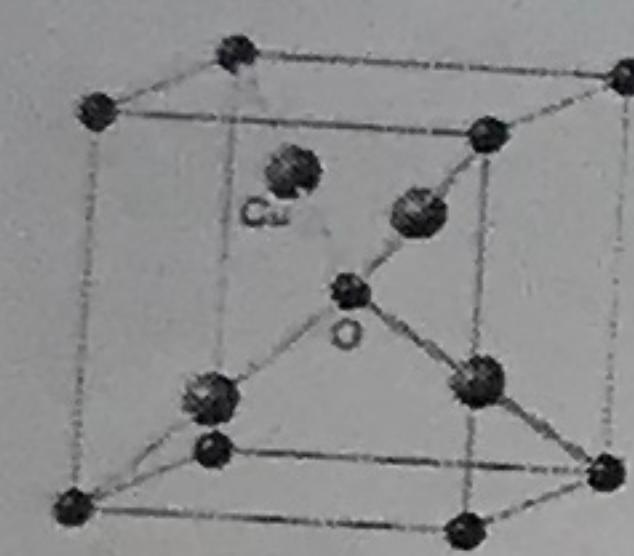
Normalized UV-vis absorption spectra of the synthesized Ag nanocube samples with tunable sizes.

size ↑ → red shift.



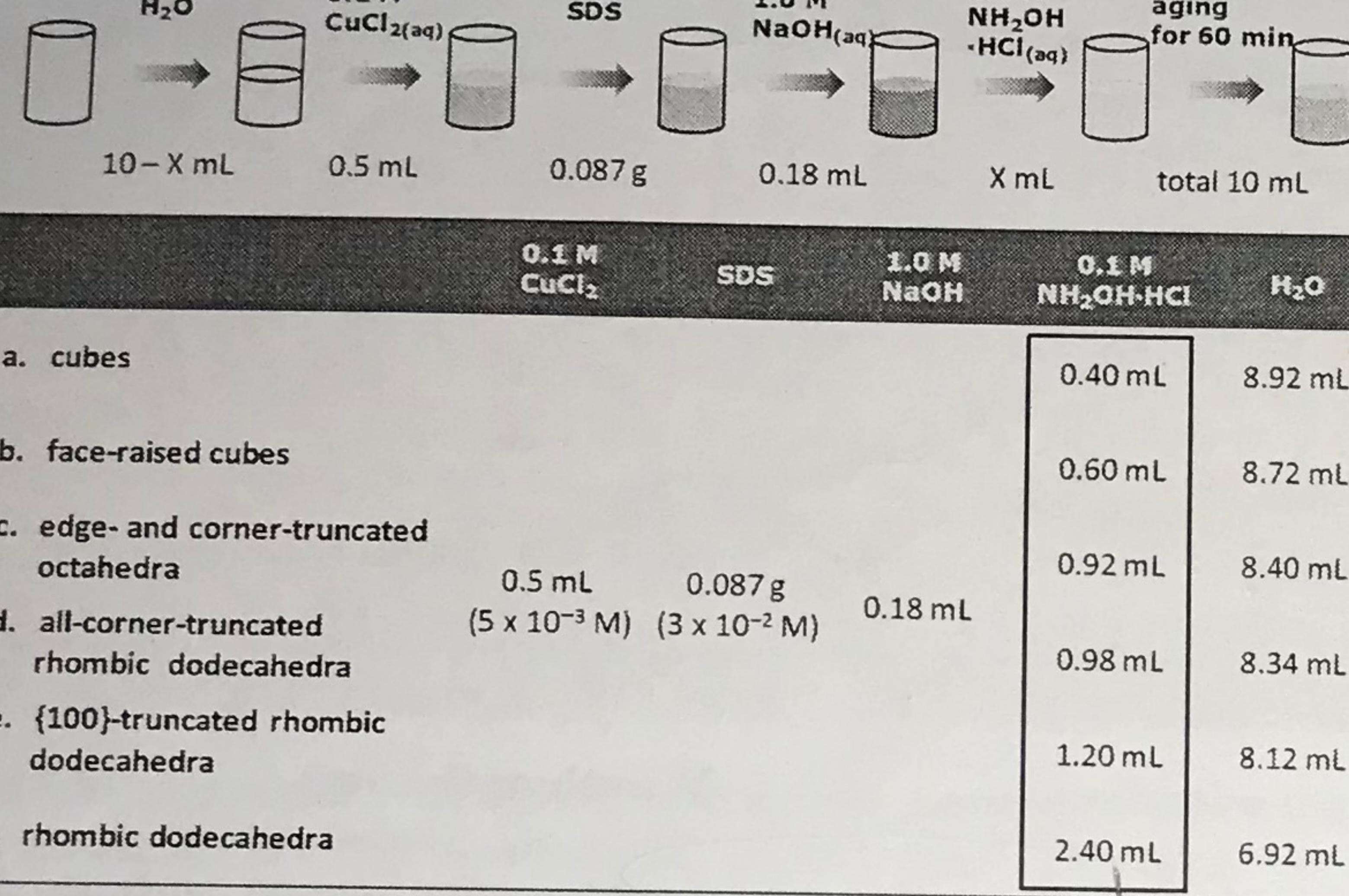
Using 35 nm octahedral Au nanoparticles as cores for Ag shell growth, initially there is a large blue-shift of the LSPR absorption band, followed by progressive red-shift as the Ag shell thickness increases.

Yang, K.-H.; Hsu, S.-C.; Huang, M. H.
Chem. Mater. 2016, 28, 5140.



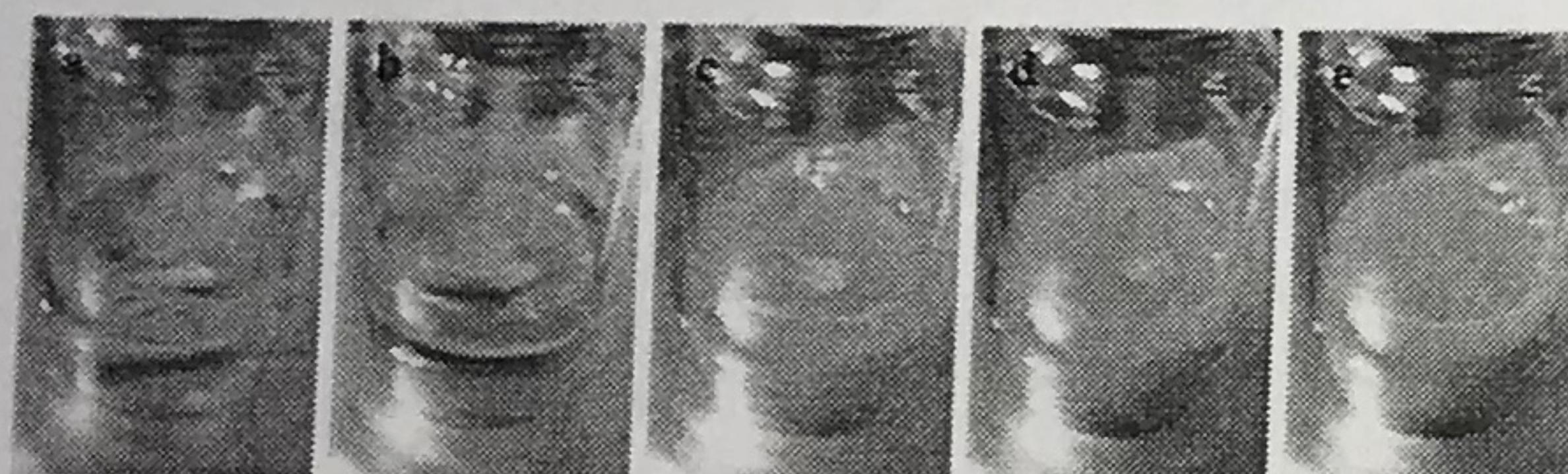
合成菱形十二面体的氧化亞銅(有半導體的性質)

Synthesis of Rhombic Dodecahedral Cu_2O Cubic to Rhombic Dodecahedral Nanocrystals



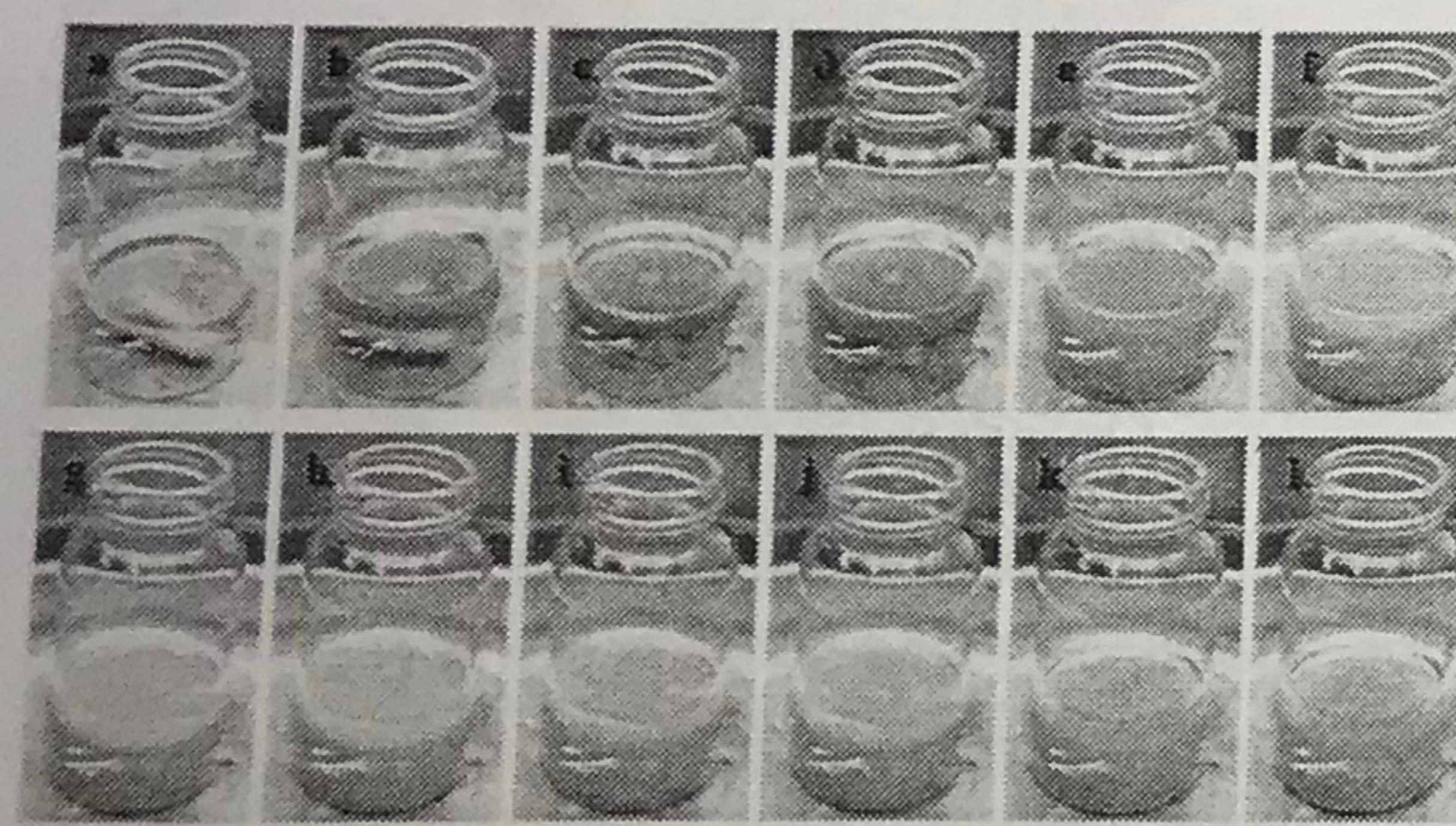
Huang, W.-C.; Lyu, L.-M.; Yang, Y.-C.; Huang, M. H. J. Am. Chem. Soc. 2012, 134, 1261

越大顆不同顏色



Photographs of the solution in the synthesis of Cu_2O nanocubes.

(a) Immediately after adding NaOH to the mixture of CuCl_2 and SDS aqueous solution, blue $\text{Cu}(\text{OH})_2$ formed. (b) 3 s, (c) 10 s, (d) 20 s, and (e) 40 s after adding $\text{NH}_2\text{OH}\cdot\text{HCl}$ to start crystal growth.

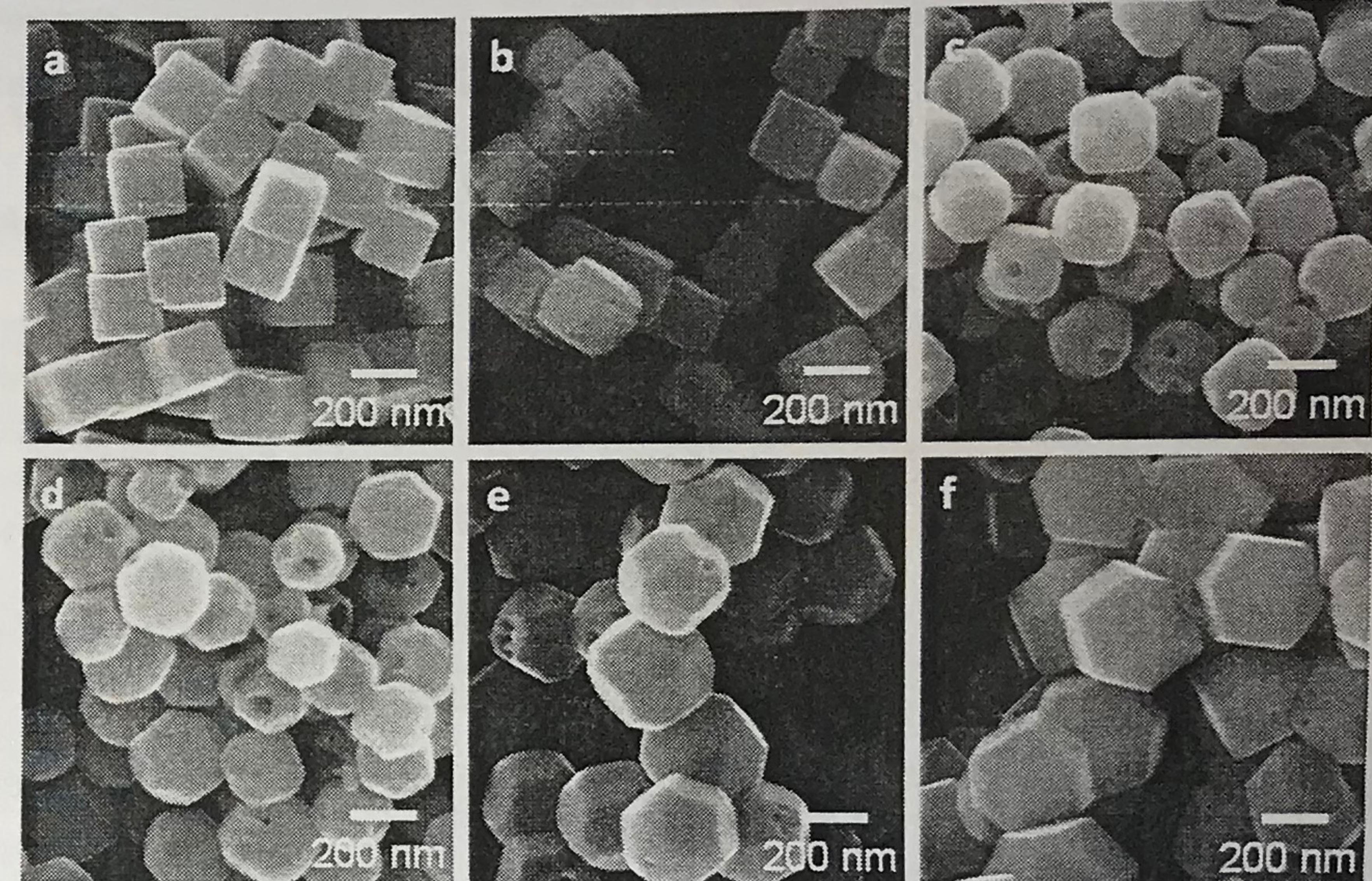
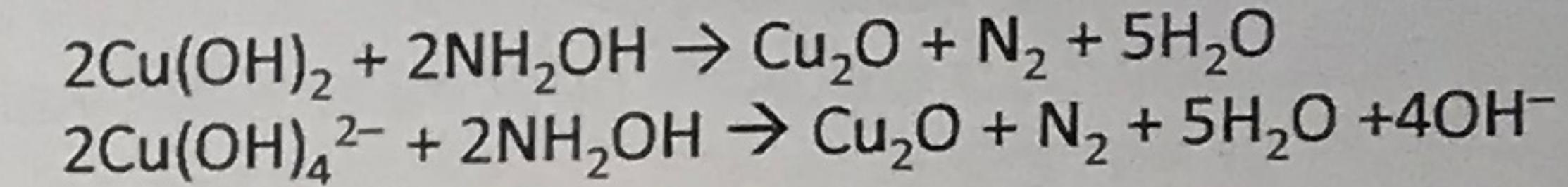


Photographs of the solution in the synthesis of Cu_2O rhombic dodecahedra. (a) Immediately after adding NaOH to the mixture of CuCl_2 and SDS solution, (b) 3 s, (c) 30 sec, (d) 1 min, (e) 3 min, (f) 5 min, (g) 8 min, (h) 10 min, (i) 20 min, (j) 30 min, (k) 45 min, and (l) 60 min after adding $\text{NH}_2\text{OH}\cdot\text{HCl}$.

☆ Rhombic dodecahedra are formed at a much slower rate than that of cubes.

ΔG 不同 \rightarrow driving force 不同

NaOH was added before the introduction of $\text{NH}_2\text{OH}\cdot\text{HCl}$ to form $\text{Cu}(\text{OH})_2$ and $\text{Cu}(\text{OH})_4^{2-}$ species first.



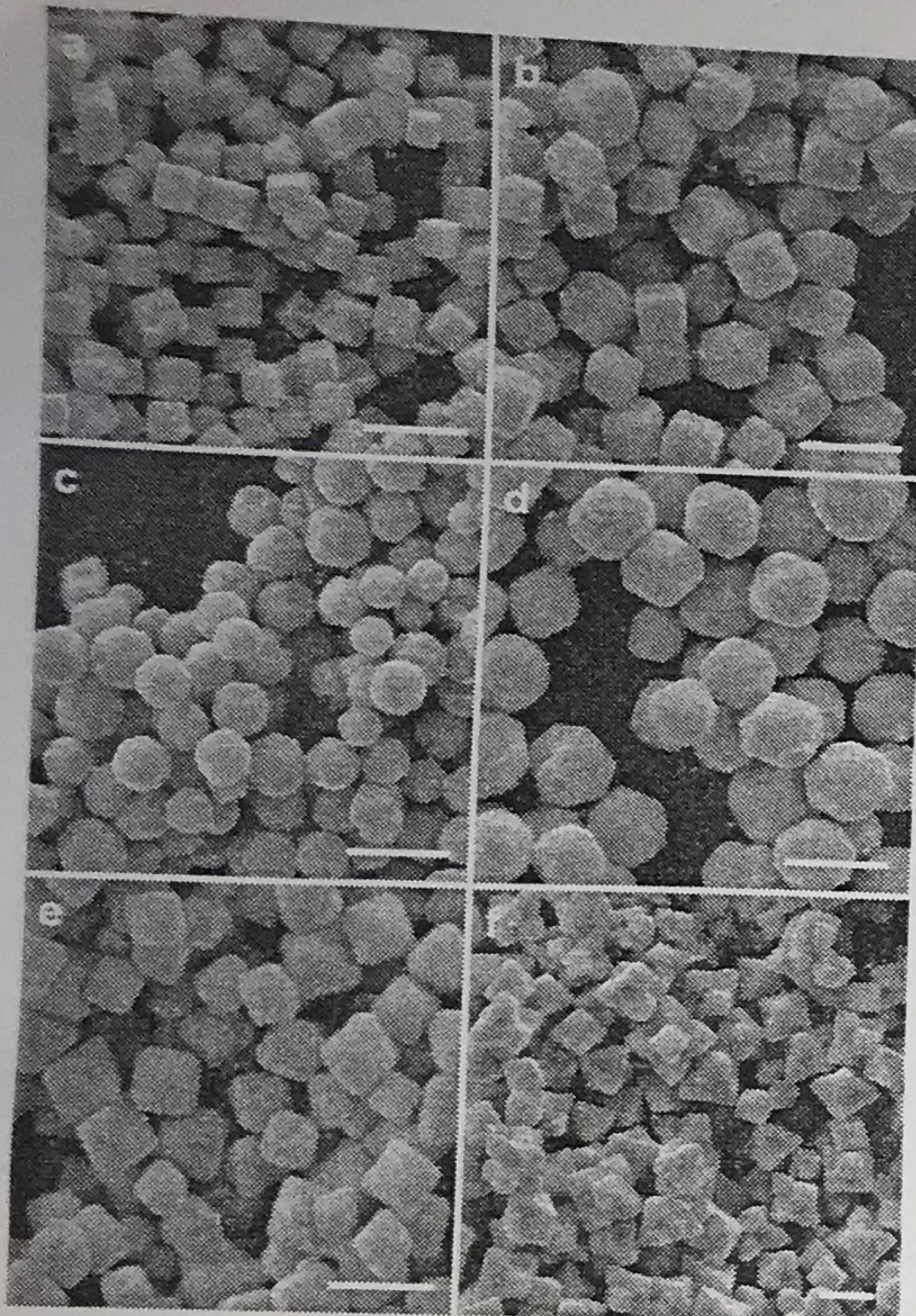
還原劑的量不同

造成不同形狀

Table 8.5
 K_{sp} Values at 25°C for Common Ionic Solids

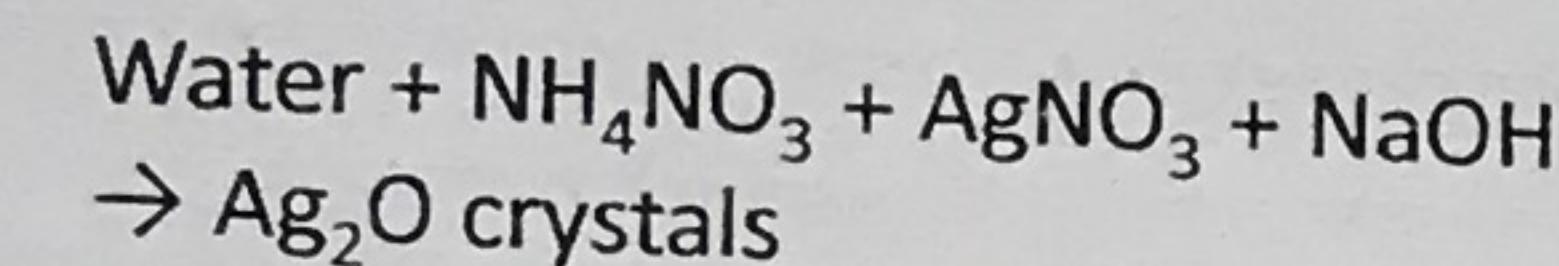
Ionic Solid	K_{sp} (at 25°C)	Ionic Solid	K_{sp} (at 25°C)	Ionic Solid	K_{sp} (at 25°C)
Fluorides		Chlorides		Bromides	
BaF_2	2.4×10^{-5}	PbCl_2	1.6×10^{-5}	PbBr_2	4.6×10^{-6}
MgF_2	6.4×10^{-9}	AgCl	1.6×10^{-10}	AgBr	5.0×10^{-13}
PbF_2	4×10^{-8}	Hg_2Cl_2^*	1.1×10^{-18}	Hg_2Br_2^*	1.3×10^{-22}
SrF_2	7.9×10^{-10}				
CaF_2	4.0×10^{-15}				
Carbonates					
NiCO_3	1.4×10^{-7}	CaCO_3	8.7×10^{-9}	MnCO_3	8.8×10^{-11}
BaCO_3	1.6×10^{-9}	SrCO_3	7×10^{-10}	FeCO_3	2.1×10^{-11}
SrCO_3		CdCO_3		Ag_2CO_3	8.1×10^{-12}
CuCO_3	2.5×10^{-10}	PbCO_3	1.5×10^{-15}	CdCO_3	5.2×10^{-12}
ZnCO_3	2×10^{-10}	MgCO_3	1×10^{-15}	MgCO_3	1×10^{-15}
		Hg_2CO_3^*	9.0×10^{-15}	Hg_2CO_3^*	9.0×10^{-15}
Sulfides					
MnCO_3		PbS		CoS	
FeCO_3		ZnS		SnS	
Ag_2CO_3		CdS		CdS	
CdCO_3		PbS		PbS	
Iodides					
PbI_2	1.4×10^{-8}	AgI	1.5×10^{-10}	Hg_2I_2^*	4.5×10^{-29}
AgI					
Hg_2I_2^*					
Hydroxides					
$\text{Ba}(\text{OH})_2$	5.0×10^{-3}	$\text{Sr}(\text{OH})_2$	3.2×10^{-4}	$\text{Ca}(\text{OH})_2$	1.3×10^{-6}
AgOH	2.0×10^{-8}	$\text{Mg}(\text{OH})_2$	8.9×10^{-12}	AgOH	2.0×10^{-8}
$\text{Mg}(\text{OH})_2$		$\text{Mn}(\text{OH})_2$		$\text{Cd}(\text{OH})_2$	
		$\text{Pb}(\text{OH})_2$		$\text{Pb}(\text{OH})_2$	
Sulfates					
CaSO_4	6.1×10^{-5}	Ag_2SO_4	1.2×10^{-5}	$\text{Sr}_3(\text{PO}_4)_2$	1×10^{-41}
Ag_2SO_4		Sr_5SO_4		$\text{Ca}_3(\text{PO}_4)_2$	1.3×10^{-32}
Sr_5SO_4	3.2×10^{-7}	PbSO_4	1.3×10^{-8}	$\text{Ba}_3(\text{PO}_4)_2$	6×10^{-39}
PbSO_4		BaSO_4	1.5×10^{-9}	$\text{Pb}_3(\text{PO}_4)_2$	1×10^{-54}
Chromates					
SrCrO_4	3.6×10^{-5}				

*Contains Hg_2^{2+} ions. $K_{sp} = [\text{Hg}_2^{2+}][\text{X}^-]^2$ for Hg_2X_2 salts.



Synthesis of Ag_2O Crystals with Systematic Shape Evolution

Ag_2O has the same crystal structure as that of Cu_2O .

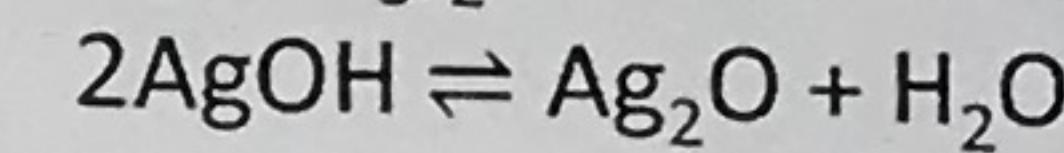
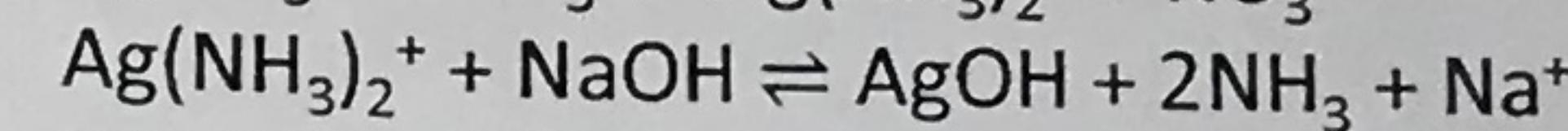
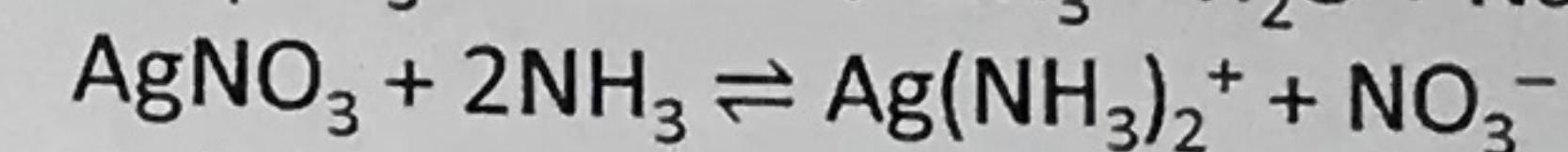
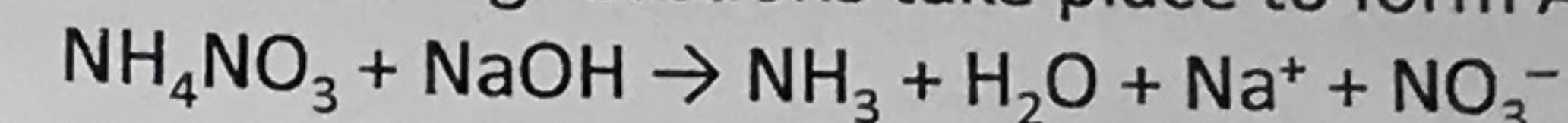


- a. Cubes
- b. Edge- and corner-truncated cubes
- c. Rhombicuboctahedra
- d. Edge- and corner-truncated octahedra
- e. Octahedra
- f. Hexapods

Lyu, L.-M.; Wang, W.-C.; Huang, M. H.
Chem. Eur. J. 2010, 16, 14167

An aqueous mixture of AgNO_3 , NH_4NO_3 , and NaOH was prepared with fixed molar ratios of the reagents. Formation of $\text{Ag}(\text{NH}_3)_2^+$ complex ions can control the reaction rate and allow the growth of nanocrystals with excellent shape control.

The following reactions take place to form Ag_2O :



Equation 3 as written has an equilibrium constant K of 2.94 (inverse of the reaction $\text{AgOH} + 2\text{NH}_3 + \text{Na}^+ \rightleftharpoons \text{Ag}(\text{NH}_3)_2^+ + \text{NaOH}$ with $K = K_{sp}$ of $\text{AgOH} \times K_f$ of $\text{Ag}(\text{NH}_3)_2^+$ = $(2.0 \times 10^{-8}) \times (1.7 \times 10^7) = 0.34$).

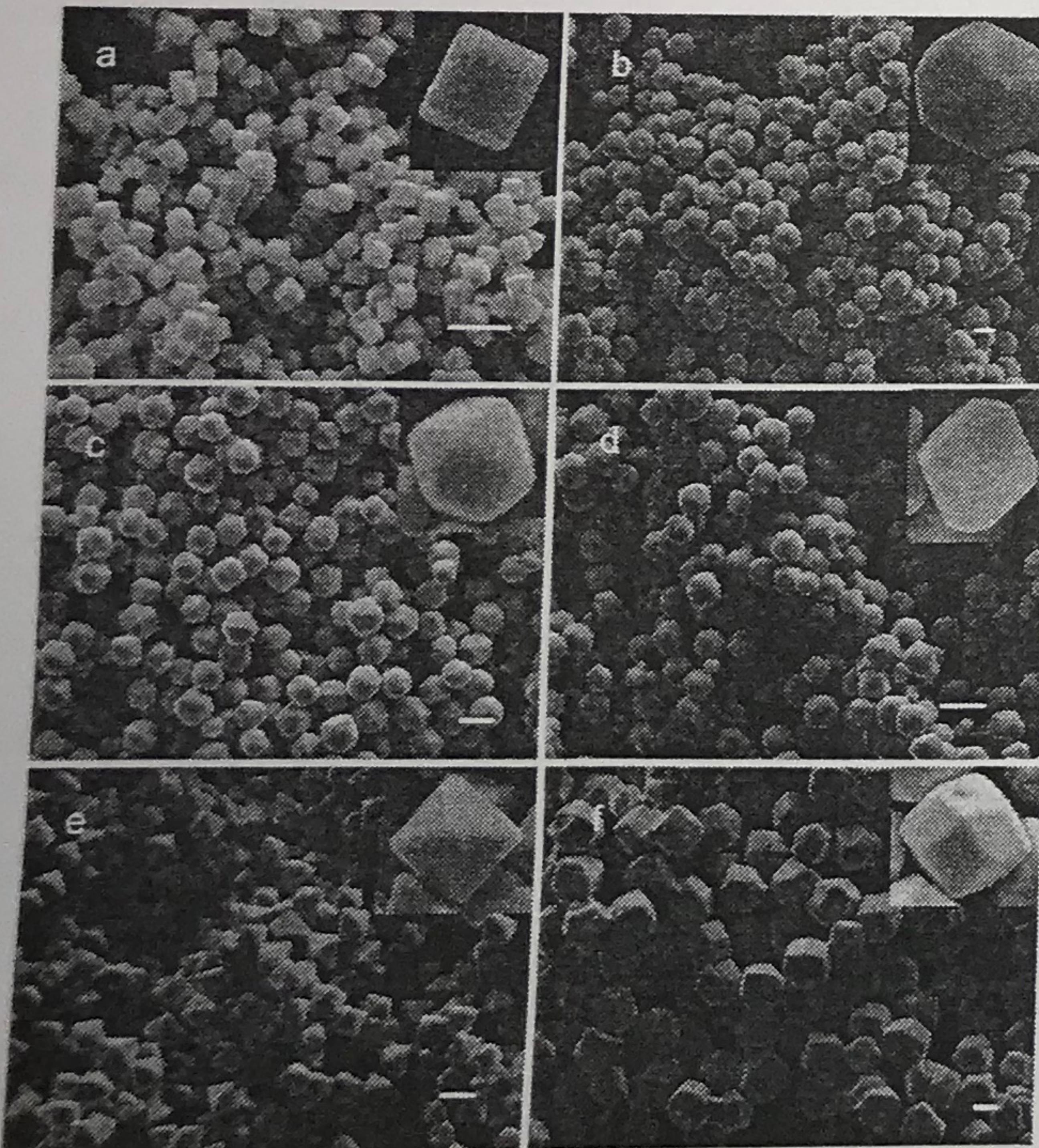
Compared to the value of K for the direct mixing of AgNO_3 and NaOH at 5×10^7 ($\text{Ag}^+ + \text{OH}^- \rightleftharpoons \text{AgOH}$ with $K = 1/K_{sp}$), formation of the $\text{Ag}(\text{NH}_3)_2^+$ species can drastically reduce the rate of rapid growth of AgOH and thus Ag_2O to achieve excellent morphology control of the Ag_2O nanocrystals.

* For crystal growth by a precipitation reaction, lowering the equilibrium constant to product formation is the key to particle shape control. $\Delta G^\circ = -RT \ln K$. Lowering K also reduces ΔG° , the driving force for product formation.

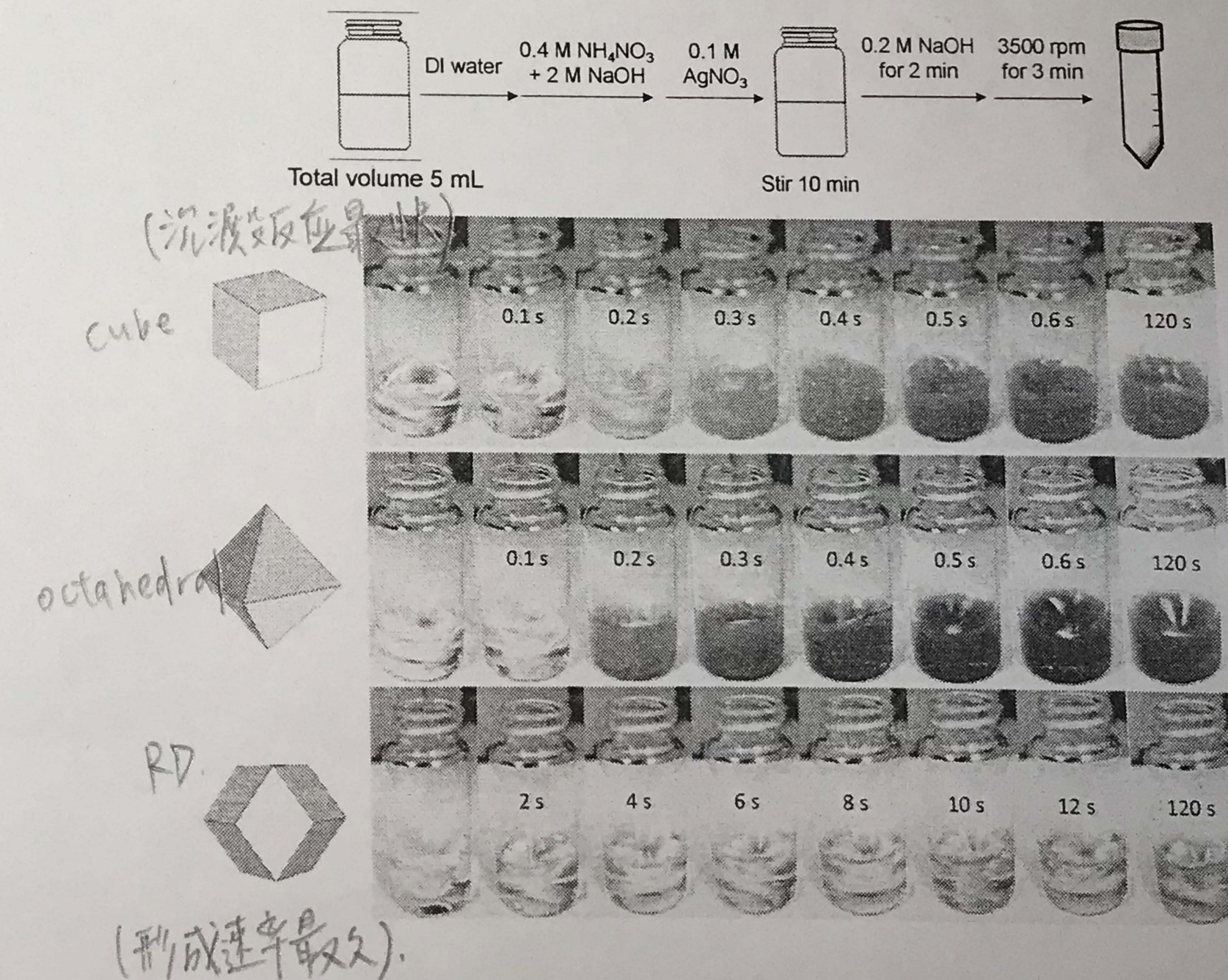
driving force

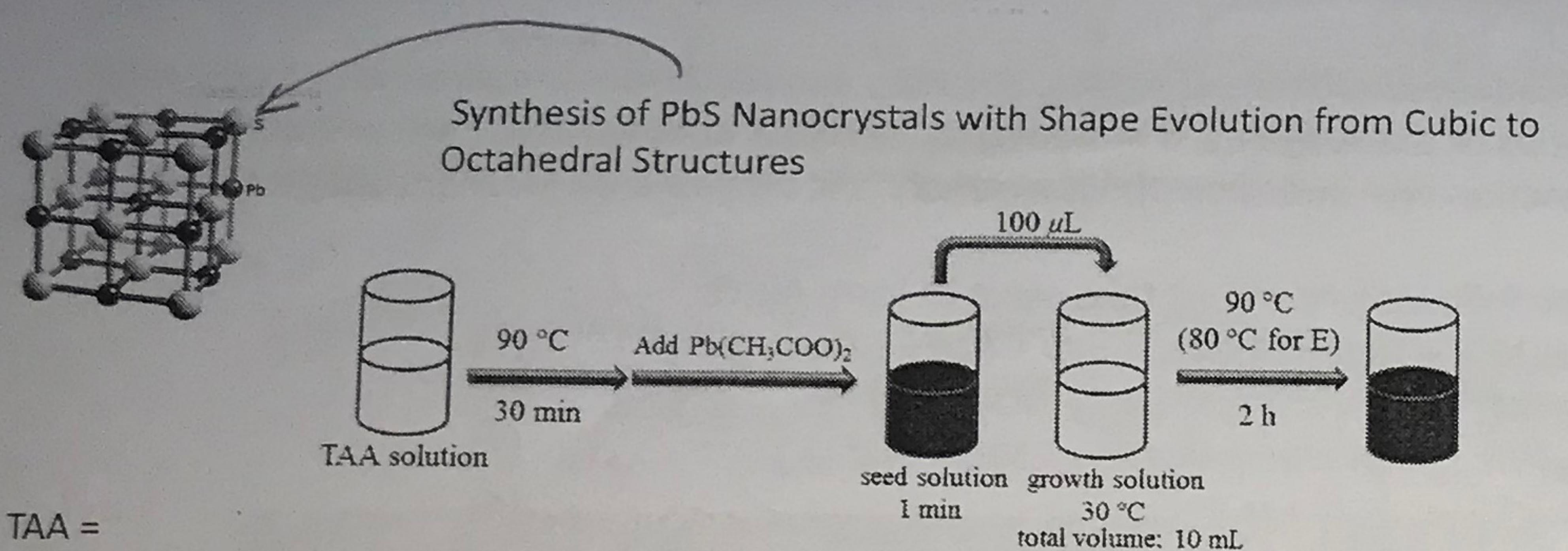
Synthesis of diverse Ag_2O crystals and their facet-dependent photocatalytic activity examination

ACS Appl. Mater. Interfaces 2016, 8, 19672



SEM images of (a) cubic, (b) great rhombicuboctahedral, (c) cuboctahedral, (d) corner-truncated octahedral, (e) octahedral, and (f) rhombic dodecahedral Ag_2O crystals. All scale bars are equal to 1 μm .





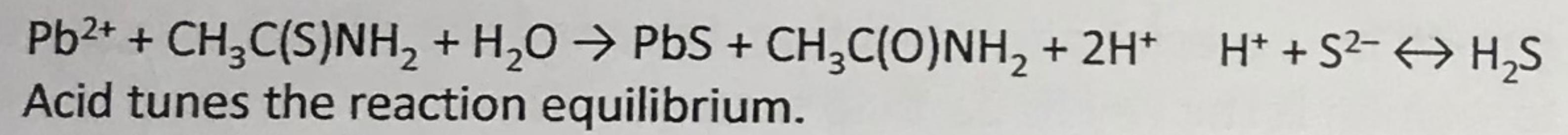
TAA =
thioacetamide

CH

seed solution			
	0.1 M $\text{Pb}(\text{CH}_3\text{COO})_2$	TAA	Total Volume
	200 μL	0.0756 g (0.1 M)	10 mL

growth solution					
	CTAB	DI water	0.1 M $\text{Pb}(\text{CH}_3\text{COO})_2$	1.0 M HNO_3	0.1 M TAA
A		4.65 mL			5.0 mL (0.05 M)
B		6.15 mL			3.5 mL (0.035 M)
C	0.01 g (0.0027 M)	6.45 mL	200 μL (0.002 M)	50 μL (0.005 M)	3.2 mL (0.032 M)
D		7.15 mL			2.5 mL (0.025 M)
E		9.65 mL			0.04 g (0.053 M)

(A) cubes (B) truncated cubes (C) cuboctahedra (D) octahedra (E) truncated octahedra



Wu, J.-K.; Lyu, L.-M.; Liao, C.-W.; Wang, Y.-N.; Huang, M. H. *Chem.-Eur. J.* 2012, 18, 14473

改变TAA浓度
不同形状

